TRANSPORTATION RESEARCH RECORD 733

Mechanics of Track Support, Piles, and Geotechnical Data

TRANSPORTATION RESEARCH BOARD

COMMISSION ON SOCIOTECHNICAL SYSTEMS
NATIONAL RESEARCH COUNCIL

NATIONAL ACADEMY OF SCIENCES
WASHINGTON, D.C. 1979

Transportation Research Record 733
Price $5.80
Edited for TRB by Frances Zwanzig

modes
1 highway transportation
3 rail transportation

subject areas
61 soil exploration and classification
62 soil foundations
63 soil and rock mechanics

Transportation Research Board publications are available by ordering directly from the board. They may also be obtained on a regular basis through organizational or individual supporting membership in the board; members or library subscribers are eligible for substantial discounts. For further information, write to the Transportation Research Board, National Academy of Sciences, 2101 Constitution Avenue, N.W., Washington, D.C. 20418.

Library of Congress Cataloging in Publication Data
National Research Council. Transportation Research Board.
Mechanics of track support, piles, and geotechnical data.

(Transportation research record; 733)
Reports prepared for the 58th annual meeting of the Transportation Research Board.
1. Soil mechanics–Addresseses, essays, lectures. 2. Roads–Subgrades–Addresses, essays, lectures. 3. Railroads–Track–Foundations–Addresses, essays, lectures.
I. Title. II. Series.
TE7.H5 no. 733 [TA710] 380.5s [625.1'22]
ISBN 0-309-02988-0 ISSN 0361-1981 80-13046

Sponsorship of the Papers in This Transportation Research Record

GROUP 2–DESIGN AND CONSTRUCTION OF TRANSPORTATION FACILITIES
Eldon J. Yoder, Purdue University, chairman

General Design Section
Lester A. Herr, Federal Highway Administration, chairman

Committee on Compaction
Charles M. Higgins, Louisiana State Department of Transportation and Development, chairman
Mehmet C. Anday, Marvin L. Byington, Robert C. Deen, J. M. Hoover, Eugene Y. Huang, Ernest Jonas, James E. Kelly, Charles Dabney Lamb, William B. O'Sullivan, John R. Sallberg, J. Chris Schwarzhoff, Charles H. Shepard, Donald Ray Snethen, Robert J. Weaver

Committee on Soil-Bituminous Stabilization
Jon A. Epps, Texas A&M University, chairman
David D. Currin, Jack N. Dybalski, K. P. George, J. M. Hoover, Edwin H. Jones, Larry L. Kole, Sidney Mintzer, Raymond K. Moore, James A. Scherocman, Charles G. Schmitz, Leonard J. Stern, B. A. Vallerga, Thomas D. White, Anwar E. Z. Wissa, Walter H. Zimpfer

Committee on Chemical Stabilization of Soil and Rock
Hassan A. Sultan, University of Arizona, chairman
Kandiah Arulanandan, William D. Bingham, Gerald H. Brandt, Robert C. Deen, Conan P. Furber, Edward D. Graf, Charles M. Higgins, James K. Mitchell, Thomas M. Petry, C. K. Shen, Andrew Sluz, Wilfred W. Wong

Committee on Foundations of Bridges and Other Structures
Clyde N. Laughter, Wisconsin Department of Transportation, chairman
Arnold Aronowitz, Micahael Bozozuk, Bernard E. Butler, W. Dale Carney, Harry M. Coyle, Gerald F. Dalquist, M. T. Davisson, Bengt H. Fellenius, Frank M. Fuller, G. G. Goble, Richard J. Goettle III, Stanley Gordon, Stanley Haas, Hal W. Hunt, Philip Keene, G. A. Leonards, Alex Rutka, Richard J. Suedkamp, Aleksandar S. Vesic, John L. Walkinshaw, James Doyle Webb, William J. Williams

Committee on Mechanics of Earth Masses and Layered Systems
Harvey E. Wahls, North Carolina State University, chairman
Dimitri Athanasiou-Grivas, Walter R. Barker, Richard D. Barksdale, Jerry C. Chang, John T. Christian, Michael I. Darter, Umakant Dash, Chandrakant S. Desai, Raymond R. Fox, Milton E. Harr, Gerald P. Raymond, Robert L. Schiffman, Robert D. Stoll, William G. Weber, Jr., T. H. Wu

Committee on Subsurface Drainage
George W. Ring III, Federal Highway Administration, chairman
Charles C. Calhoun, Jr., Robert G. Carroll, Jr., Harry R. Cedergren, Charles J. Churilla, Allen L. Cox, Barry J. Dempsey, Edward N. Eiland, Gary L. Klinedinst, Arthur O. Kruse, Alfred W. Maner, Glen L. Martin, Edward M. Masterson, Lyndon H. Moore, Lyle K. Moulton, Russell B. Preuit, Jr., Hallas H. Ridgeway, Travis W. Smith, William D. Trolinger, Walter C. Waidelich, Clayton E. Warner, David C. Wyant, Thomas F. Zimmie

Committee on Exploration and Classification of Earth Materials
Robert B. Johnson, Colorado State University, chairman
Carl D. Ealy, Martin C. Everitt, Edward A. Fernau, William Bryan Greene, Robert K. H. Ho, Frank L. Jagodits, Gene O. Johnson, Robert D. Krebs, Donald E. McCormack, Frank R. Perchalski, Alex Rutka, Robert L. Schuster, J. Chris Schwarzhoff, Robert B. Sennett, Andrew Sluz, Sam I. Thornton, J. Allan Tice, Gilbert Wilson

Committee on Soil and Rock Properties
William F. Brumund, Golder Associates, chairman
Samuel P. Clemence, Carl D. Ealy, Richard E. Goodman, James P. Gould, Ernest Jonas, T. Cameron Kenney, Charles C. Ladd, G. A. Leonards, C. William Lovell, John D. Nelson, Douglas R. Piteau, Gerald P. Raymond, Robert L. Schiffman, Hassan A. Sultan, William D. Trolinger, David J. Varnes, J. Lawrence Von Thun, Harvey E. Wahls, John L. Walkinshaw, T. H. Wu.

Committee on Physicochemical Phenomena in Soils
Joakim G. Laguros, University of Oklahoma, chairman
Kandiah Arulanandan, Gerald H. Brandt, Turgut Demirel, George R. Glenn, Charles A. Moore, Edward Belk Perry, Gilbert L. Roderick, Dwight A. Sangrey, Scott Stephen Smith, Hans F. Winterkorn

Committee on Engineering Geology
Robert L. Schuster, U. S. Geological Survey, chairman
Robert C. Deen, Martin C. Everitt, Leonard H. Guilbeau, Robert B. Johnson, Marvin L. McCauley, Adrian Pelzner, David L. Royster, Dwight A. Sangrey, Robert B. Sennett, Berke L. Thompson, J. Allan Tice, A. Keith Turner, Frank W. Wilson

John W. Guinnee, Transportation Research Board staff

Sponsorship is indicated by a footnote at the end of each report. The organizational units and officers and members are as of December 31, 1978.

Contents

Three-Dimensional Analysis of Rail Track Structure

David J. Turcke and Gerald P. Raymond, Department of Civil Engineering, Queen's University, Kingston, Ontario

A three-dimensional finite-element model of a railway track structure that includes rails, ties, and ballast is described. The material properties used for the cohesionless ballast and subballast are obtained from triaxial tests. A nonlinear, incremental numerical procedure based on a bicubical-spline stress-strain approximation is being developed for use in the finite-element analysis. At present, the program is capable of linear analysis only. The behavior of the track structure under static loading is predicted by using the linear analysis. Comparison is made between different ballast geometries on both typical sand and clay subgrades. The results show the potential value of a nonlinear analysis.

The increased speeds, higher traffic densities, and larger and heavier cars now being used on railroads have led to new requirements for improved stability and durability of rail track support. The impact of research and development in the area of track structure design and maintenance could be large; the costs associated with the replacement and upkeep of railroad fills are estimated to be about $100 million/year for Canadian railroads alone. A large portion of this cost is due to geotechnical problems.

To reduce these costs, the rail track structure must be improved so as to minimize both live-load deformations and permanent settlements. The solution to this problem depends on a large number of variables. These include, for example, the density, grading, and type of ballast; the shape of the particles; the dimensions of various layers; the water content in the lower layers; the type of subgrade; tie spacing; rail weight; and the magnitude and speed of wheel loads.

One approach to better understanding of the behavior of the rail track structure is the use of sophisticated analytical techniques to model the structure. This provides the engineer with a means of studying various maintenance techniques that affect the behavior of the track system.

FINITE-ELEMENT MODEL

To effectively model the behavior of ballast and foundation material requires the use of techniques that include the effects of the stress-path dependence and nonlinearity of the continuum and of its lack of ability to sustain tension.

This paper presents the first steps of a three-dimensional finite-element program—analysis of rail track structure—that is being developed (at present, only a linear model has been completed). The program described here, however, provides the user with a family of isoparametric hexahedral and pentahedral elements that are of sufficient complexity to simulate the anticipated displacements and stress fields from multidirectional static loading. Specifically, as shown in Figure 1, the program includes 8- and 20-nodal hexahedrons and 6- and 15-nodal pentahedrons.

The major properties programmed to characterize the behavior of the soil material are its stress-path dependence and its lack of ability to sustain tension. The soil elements used include ballast, subballast, and subgrade material. In addition, the elements representing the track ties may be taken as nonlinear in both tension and compression.

The first feature being incorporated—the stress-path dependence—requires an iterative step-by-step numerical procedure. The necessary constitutive relations are obtained by modeling the triaxial test results for various confining pressures by the use of bicubical splines (1). The stress or strain paths are then determined by three-dimensional interpolation. In the current program, each set of experimental discrete data for a particular confining pressure is first smoothed by the method of least squares and then approximated by a cubic spline curve (F_i) as shown in Figure 2. Given this function,

$$F_i = f(\sigma_1 - \sigma_3, \epsilon_1) \qquad (i = 1, 2, 3, \ldots, n) \tag{1}$$

where n = number of different confining pressures σ_3^i, the partial derivatives $(\partial F_i/\partial \epsilon_1)$ are taken at points corresponding to ϵ_{1k}, $k = 1, 2, 3, \ldots,$ m and denoted by $F_{i,k}$) where m = user-selected number of prescribed points in the ϵ_1 direction. (It should be noted that m need not have the same value as the number of experimental readings; once the spline F_i is known, the spacing on the ϵ_1 axis can be chosen arbitrarily.)

In the next step, the cubic splines are formulated in the σ_3 direction to give the set of functions

$$G_k = f(\sigma_1 - \sigma_3, \sigma_3) \tag{2}$$

and their derivatives $\partial G_k/\partial \sigma_3$ (or $G_{k,i}$). The last member of the vector [Note: in this paper, vector quantities are designated by asterisks]

$$\sigma_s^* = \{\sigma_s, \sigma_{s,\epsilon}, \sigma_{s,p}, \sigma_{s,\epsilon,p}\} \tag{3}$$

where

$$\sigma_s = \sigma_1 - \sigma_3,$$
$$p = \sigma_3,$$
$$\sigma_{s,\epsilon} = F_{i,k}, \text{ and}$$
$$\sigma_{s,p} = G_{k,i}$$

required for interpolation over the rectangular mesh, as shown in Figure 2, is then obtained by calculating the first derivatives of ϵ_1 in the σ_3 direction. Given all the vectors σ_{sik}^*, the complete bicubical spline (S) is defined as shown in Figure 2, and the tangent modulus $(E_t = \partial S/\partial \epsilon_1)$ can be calculated for any σ_3 and ϵ_1.

The second feature requires modeling the lack of ability of the ballast to sustain tension. An iterative, no-tension technique by Zienkiewica and others (2) is used for this purpose. This technique is as follows:

1. If certain tensile principal stresses have developed, they are eliminated without permitting any point in the structure to displace. Then, to satisfy overall equilibrium, restraining forces equivalent to the tensile principal stresses are evaluated element by element and temporarily applied to the structure.
2. These fictitious restraining forces are then removed by applying equal but opposite nodal forces. The structure is then reanalyzed to determine any remaining tensile stresses. If these are still greater than a certain limit, steps 1 and 2 are repeated.

In summary, the overall procedure for the j th step is as follows:

1. A small load increment is imposed, and the displacements and stresses are computed by using the tangent Young's moduli $E_{t,j-1}$.
2. All tensile stresses in the ballast are eliminated.
3. From the total stress-strain level reached, the new $E_{t,j}$ is calculated element by element by using the bicubic spline S, and the new global stiffness matrix for the structure is then computed.
4. If the total number of increments has not been reached, repeat steps 1-3; otherwise, stop.

The finite-element computer program being developed will be able to calculate the contact stresses. The theory used to obtain the contact stresses is as follows: If the external load acting on the tie is denoted by Q^*, the contact stress by $p(x, y)$, the equivalent force vector to p by P^*, the stiffness matrix of the tie (or an arbitrary body in contact for that matter) by K_1^*, and the stiffness matrix of the track bed by K_2^*, then the stiffness equations for the tie and the track bed separately are

$$Q^* - P^* = K_1^* \times \{w_1^*, w_{1_c}^*\} \tag{4}$$

Figure 1. Family of three-dimensional elements.

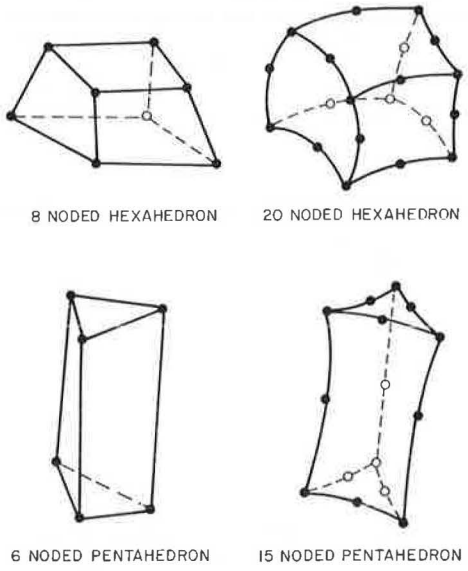

Figure 2. Determination of stress-strain surface by use of cubic spline.

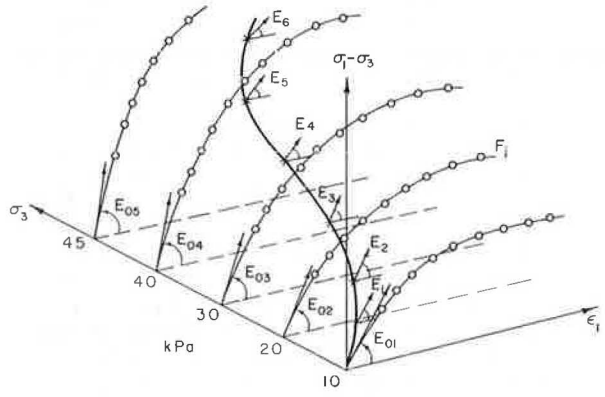

and

$$P^* = K_2^* \{w_{2_c}^*, w_2^*\}^T \tag{5}$$

where

w_1^*, w_d^* = displacements of the tie and the track bed, respectively, and
$w_{1_c}^*, w_{2_c}^*$ = corresponding displacements of the contact area.

The total structural system is then

$$Q^* = (K_1^* + K_2^*) \{w_1^*, w_{1_c}^* = w_{2_c}^*, w_2^*\}^T \tag{6}$$

Once this system is solved, the nodal forces (P^*) equivalent to the contact pressure can be calculated by using Equation 5. The contact stress [$p(x, y)$] can then be determined by using the principle of equivalent work

$$P^* \times w_{1_c}^{*T} = \int_A p(x,y) \times v(x,y) dA \tag{7}$$

where $v(x, y)$ = deflection of the contact area. If $p(x, y)$ is approximated by the same shape-function row matrix N as $v(x, y)$, then, because $v(x, y) = N^* v^{*T}$, $p(x, y) = N^* p^T$. Therefore,

$$P^* \times w_{1_c}^{*T} = p \int_A N^{*T} \times N^* \times dA \times v^{*T} \tag{7a}$$

and, by using the compatibility condition that

$$w_{1_c}^{*T} = v^{*T}$$

Equation 7a becomes

$$P^* = p^* \times M^* \tag{7b}$$

where

$$M^* = \int_A N^{*T} \times N^* dA$$

and thus $p^* = M^{*-1} \times P$ and finally $p(x, y) = N^* \times p^T$, which represents the continuous contact stress function.

Equation 6 holds for the bonded contact between the tie and the ballast. However, field results, as well as a simple observation of an actual rail track, show that the track bed does not settle uniformly. Settlements underneath the rail and under the tie ends are greater than those under the central portion of the tie. This is well known by railroad companies, because failure to maintain the track causes the ties to break along the track centerline. A currently used practical solution to this problem is to leave the central portion of the ballast bed uncompacted and compact only the ballast under the rails. This solution, however, does not appear to be the most efficient one. Uneven settlements due to uneven compaction cause separation of the contact between a tie and the ballast. Mathematically, this means that the contact contour is not known and is dependent on the relative stiffnesses of the tie and the ballast foundation. Although the tie stiffness is fairly constant, the stiffness of the ballast is dependent on the local density and varies across the track bed. Thus, in Equation 6, $w_{1_c}^*$ is not equal to $w_{2_c}^*$ everywhere under the tie. However, the approximate contact contour can be determined by iterative analysis. In such an analysis,

the contact between the tie and the ballast is determined by a step-by-step procedure for all the contact points that transmit tensile bonding forces. As has been shown by Svec (3), this method is simple and usually converges quickly. The only care required is that the contact area must be reduced by a logical procedure so that contact islands are not created.

A few useful additional features of this program should be mentioned. First, because the boundary conditions are imposed at the elemental level before the assembly of the total K_1^* and K_2^* stiffness matrices takes place, the total number of equations is reduced by up to 40 percent, depending on the mesh and boundary conditions. Second, the half band of these matrices are further divided and stored on a disk pack; direct access files are used for the assembly and sequential files are used for solving. Third, the advanced solver program developed by Wilson and others (4) was used in the program.

MATHEMATICAL MODEL FOR EXAMPLES

The finite-element model shown in Figure 3 was used to investigate various effects on the response of a linear elastic soil. This model is based on Canadian main-line railroad practice, which involves the use of 68-kg/m (136-lb/yd) continuous welded rail on 150-mm (6-in) deep by 200-mm (8-in) wide by 2.44-m (8.0-ft) long ties at 500-mm (20-in) center-to-center spacing. The ballast and subballast depths were varied from model to model; however, the shoulder at the top of the tie was taken as 150 mm, and the side slope of the ballast was fixed at a horizontal to vertical ratio of 2:1. Because only vertical loading was investigated, the ballast elements above the base of the ties were omitted to reduce computer computation time and charges.

The simulated loading was that of a series of E60 Cooper locomotives that has three axle bogies on adjoining locomotives spaced at approximately 8.2 m (27 ft) center to center. To reduce the amount of computation, mirror vertical faces (or shearless vertical planes) were assumed below the central axle of the bogie, below the coupler between two locomotives, and along the centerline of the track. Because the model requires that the loads be applied at nodes, the dimensions were modified where necessary so that the loads were approximately correctly positioned. The axle load for an E60 Cooper locomotive was taken as 287 kN (64 500 lbf). In addition, the effect of a bogie having a single axle at the same loading was investigated.

The elastic properties of the soil, which were taken as constant, are given below (1 MPa = 145 lbf/in^2).

Material	E (MPa)	ν
Rail	206 897	
Tie	11 724	0.30
Ballast	300	0.45
Subballast	100	0.45
Sand subgrade	100	0.45
Clay subgrade	20	0.45

Figure 3. Finite-element track model.

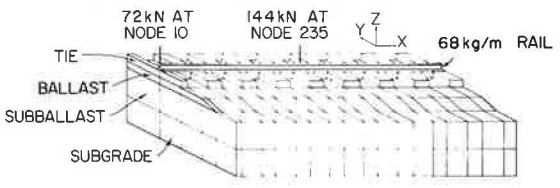

The various track support sections analyzed are given below (1 mm = 0.039 in).

Case	Ballast Depth (mm)	Subballast Depth (including sand subgrade) (mm)	Clay Subgrade Depth (mm)
1	150	1200	0
2	300	600	900
3	300	300	900
4	300	150	900
5	450	600	900
6	450	1200	0
7	300	750	900
8	450	750	900

COMPARISON OF EFFECTS OF SINGLE-AXLE LOAD AND THREE-AXLE BOGIE

The effects of a single-axle load versus a three-axle bogie were compared by using the finite-element model shown in Figure 3 and the ballast and subgrade depths shown above for cases 1, 2, 5, 7, and 8. The increase in vertical stress and displacement caused by the three axles at the tie-ballast interface below the rail and the central axle and the increase in horizontal displacement at the subballast-subgrade interface are given below (the locations chosen are points of the maximum value).

	Increase (%)		
Case	Vertical Stress at Node 9	Vertical Displacement at Node 9	Horizontal Displacement at Node 7
1	30	18	55
2	37	43	62
5	29	41	56
7	34	41	53
8	28	42	65

From case 1, which is the only one involving a sand subgrade, it can be seen that the increase in vertical deformation is the least of all the cases considered. This agrees with the simple theory normally used of a beam on an elastic foundation (i.e., constant coefficient of subgrade reaction), where an increasing coefficient of subgrade reaction causes a decrease in axle or wheel interaction. Figure 4 shows the vertical displacement across the loaded centerline section, which again demonstrates that the increased deflection due to axle interaction is small.

The horizontal displacements across the loaded centerline section for case 1 are shown in Figure 5. It is apparent that the effect of adding two outer axles is to reduce the longitudinal deformations in the direction of the rails near the central load and thus increase the lateral deformations perpendicular to the rail. It can be seen that the increase in lateral deformations of about 50 percent are general across the whole section.

When the subgrade is soft clay, the vertical deformations are increased (as would be expected by the low coefficient of subgrade reaction used in the beam-on-elastic-foundation theory because the effect of axle interaction is increased). The uniformity of the vertical- and lateral-deformation increases are demonstrated on the central cross-sections by the results obtained for case 2 (see Figures 6 and 7). As noted, the magnitude of the differences on a clay subgrade (Figure 6) are greater than those on sand (Figure 4). The percentage increases of the lateral deformations are similar, although the magnitudes are obviously greater for the clay subgrade.

Figure 4. Transverse vertical deformation below central tie: case 1.

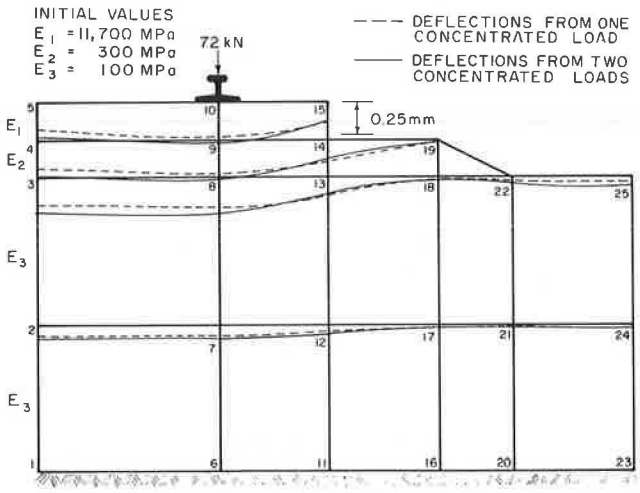

Figure 5. Transverse horizontal deformation below central tie: case 1.

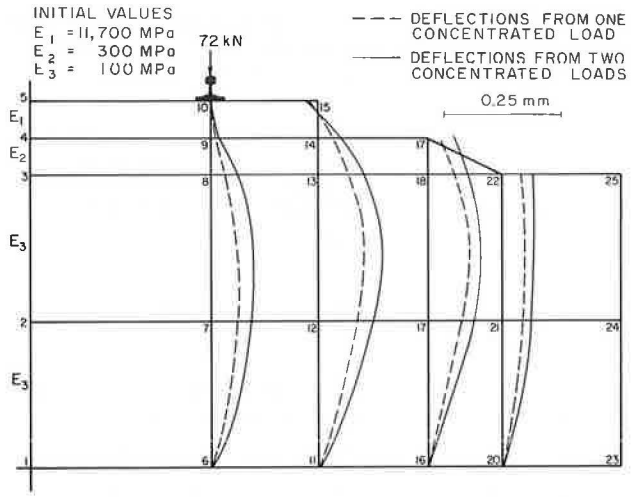

Figure 6. Transverse vertical deformation below central tie: case 2.

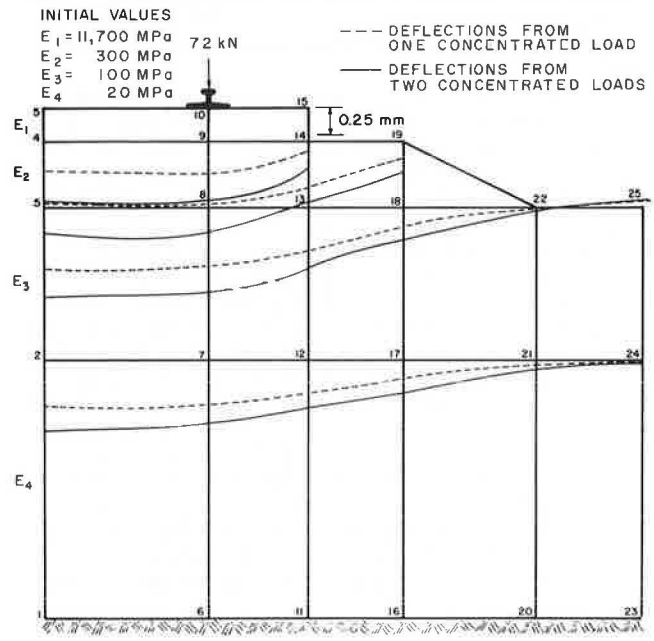

Figure 7. Transverse horizontal deformation below central tie: case 2.

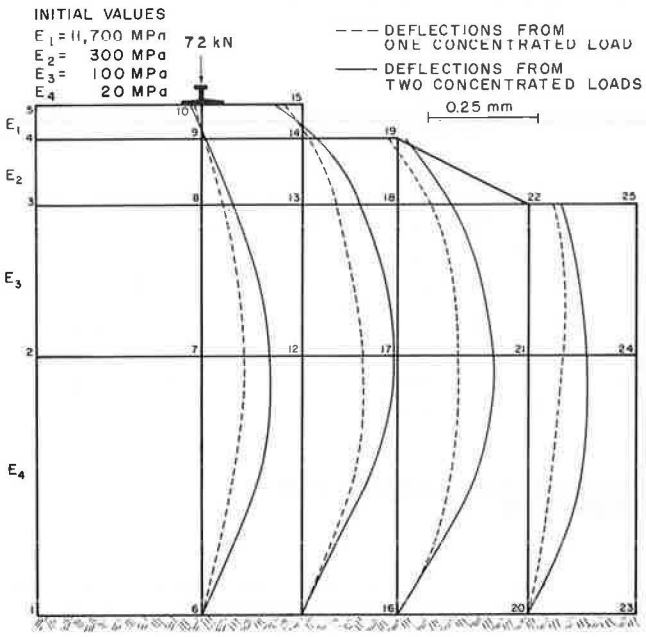

COMPARISON OF EFFECTS OF DIFFERENT DEPTHS OF SUBBALLAST ABOVE CLAY

The comparison of the results of cases 2, 3, and 4 allows a direct measure of the effect of increases in subballast (or ballast) depth above a clay subgrade, assuming no change due to confinement or decrease in shear stress in the clay properties. The effect of added granular cover under these conditions is negligible, as demonstrated by the vertical settlements below the rail vertical section (see Figure 8). However, in a real situation, it is to be expected that the elastic properties of a clay subgrade would change as the confinement and shear stresses changed. As shown in Figure 9, which illustrates the change in resilient modulus obtained by Raymond and others (5) for a triaxial sample of clay at a confining pressure of 35 kPa (5 lbf/in^2), there is considerable change in resilient modulus as the stress difference changes. In addition, added granular depth will also increase the confining pressure. (These effects will warrant investigation when the nonlinear portion of the program is available, as will consideration of the decrease in shear stress and of the small increase in confining pressure due to ballast widening rather than increasing depth.)

Even if the elastic properties of the subgrade remain constant as the granular depth increases, there is nevertheless an improvement in lateral deformations. This is apparent from a comparison of the horizontal displacements for case 4 (see Figure 10) with those for case 2 (Figure 7). How important this reduction in lateral deformations is in reducing deterioration under repeated loading (i.e., that due to the passage of large numbers of wheel loads) is unknown. However, it is not unreasonable to suspect that the larger the deformation, the greater the adverse effect in terms of the fatigue life of the whole support system. In particular, the overlying granular material, which generally has a much higher resilient modulus than clay, can be expected to be adversely affected because of the incompatibility of strains at the ballast-clay interface.

Figure 8. Longitudinal vertical deformation below rail: cases 2, 3, and 4.

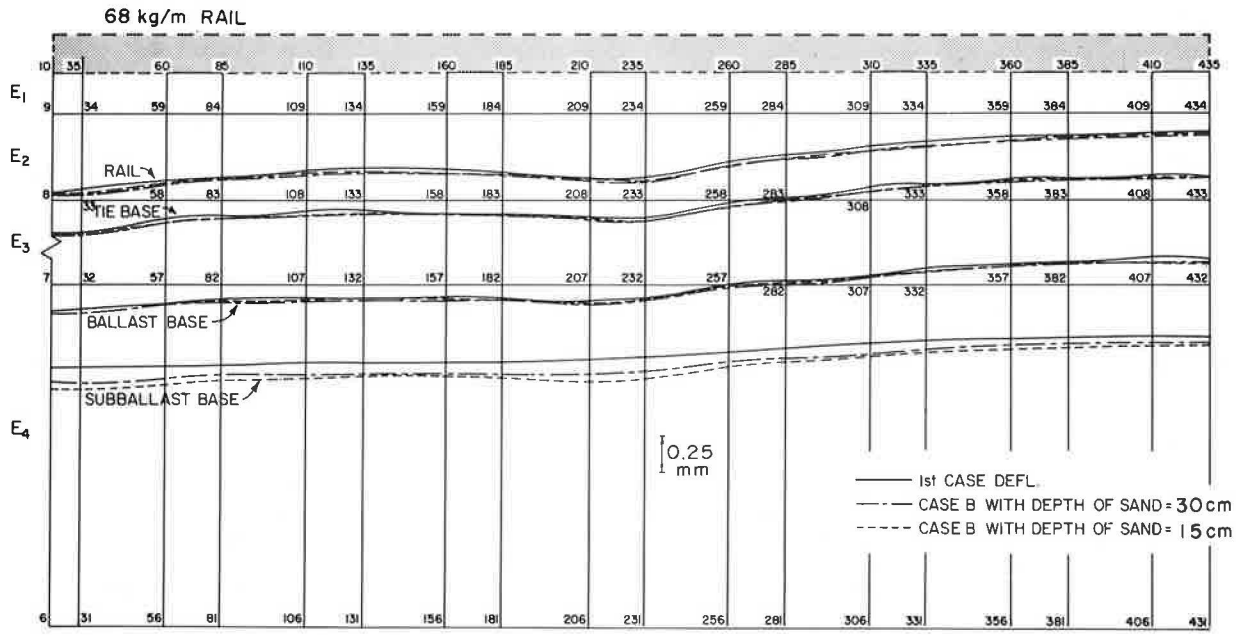

Figure 9. Change in resilient modulus with change in stress difference.

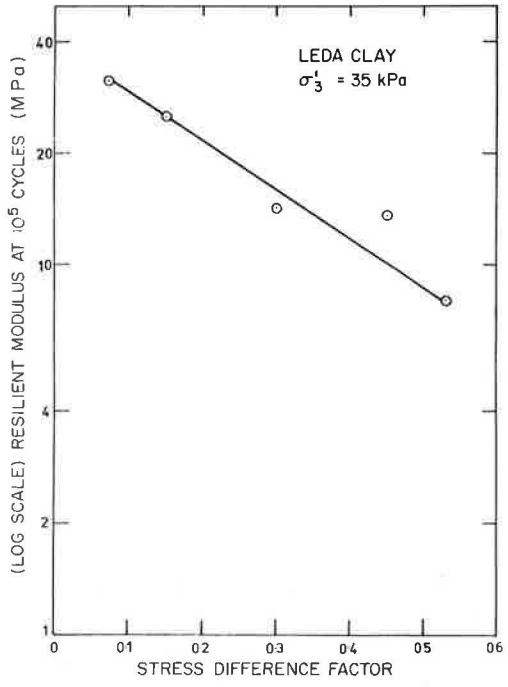

Figure 10. Transverse horizontal deformation below central tie: case 4.

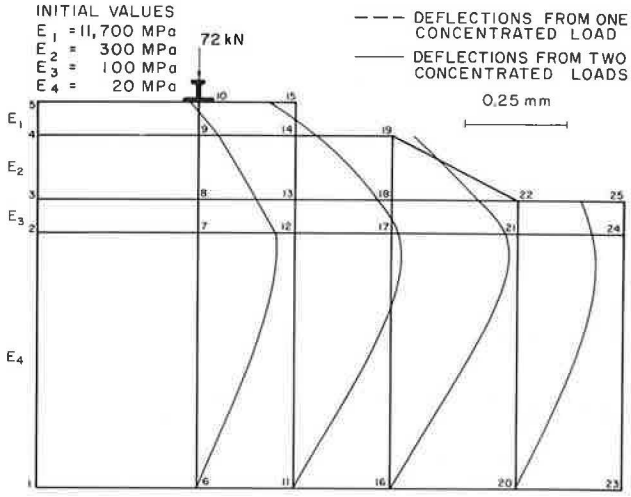

CONCLUSIONS AND PROGRAM SUMMARY

A three-dimensional finite-element model of a rail track structure is presented. It is shown how the complicated stress-path-dependent behavior of the ballast and subgrade materials can be conveniently traced by this numerical technique. Further work will be required to complete the programming of the problem of an incremental piecewise linear numerical process.

Results obtained by using the linear portion of the program indicate that the effect on vertical deformation of the interaction of several wheel loads is increased as the resilient modulus of the subgrade decreases. The percentage increase in the lateral deformation was found to be approximately independent of the modulus; however, the magnitude increased as the resilient modulus decreased.

When the resilient modulus of the subgrade remains constant, there is little decrease in vertical deformation obtained from increased granular depths; however, the lateral deformations are decreased. Test data on clay material show the fallacy of a constant-modulus assumption and thus the importance of a nonlinear analysis.

The program has the following capability: Static linear or nonlinear analysis for moments, deflections, stresses, and strains of a three-dimensional railroad track structure under static loads. It is written around two types of elements—8- and 20-nodal hexahedral and 6- and 15-nodal pentahedral elements. The program

allows the calculation of contact forces between two structures (i.e., the ground and the tie-rail system). Triaxial test data for ballast or granular material can be processed in a cubical spline form to allow for variable Young's moduli and Poisson's ratios. A beam stiffness can be added to the total system if it is desired not to model the rails as three-dimensional elements. The input data are described in terms of a railroad, but the program could be used to describe other structures.

The following method is used: Loads and railroad details are defined for each point of the three-dimensional mesh (nodal system). Analysis is by the finite-element method with displacements as the primary variables. The maximum number of nodes is 999 nodal points. However, the size can be increased by changing the dimension statements in the main program. The programming language used is FORTRAN IV.

The input of the program includes node numbers, element numbers, nodal-point coordinates or element half lengths and side projections, boundary conditions, material properties (Young's modulus, Poisson's ratio, and unit self-weight), material tension identifier, triaxial test results (for nonlinear analysis only), rail-tie system geometry and material properties, contact-structure elements and nodes duplication (for contact-structure analysis only), loads (point and uniformly distributed or both), and nodal point displacements (optional). The output includes nodal-point incremental and total displacements, principal strains, nodal-point stresses and strains, and element total moments, stresses, and strains.

Typical running times are 25 min for 480 nodal points (approximately two days data preparation) and 110 min for 626 nodal points.

ACKNOWLEDGMENT

The work described in this paper is part of a general study of geotechnical problems of railroad structures and fills financed by the Canadian Institute of Guided Ground Transport, Queen's University. We wish to acknowledge the discussions with and the advice and help obtained from the personnel of the Canadian National and Canadian Pacific Railways, particularly L. Peckover, C. Dalton, and N. Caldwell.

REFERENCES

1. C. S. Desai. Nonlinear Analyses Using Spline Functions: Closure. Journal of the Soil Mechanics and Foundations Division, Proc., ASCE, Vol. 98, No. SM9, Sept. 1972, pp. 967-972.
2. O. C. Zienkiewica, S. Valliappan, and I. D. King. Stress Analysis of Rock as a "No Tension" Material. Geotechnique, Vol. 18, 1968, pp. 56-66.
3. O. J. Svec. The Unbonded Contact Problem of a Plate on the Elastic Half Space. Computer Methods in Applied Mechanics and Engineering, Vol. 3, 1974, pp. 105-113.
4. E. D. Wilson, K. J. Bathe, and W. P. Doherty. Direction Solution of Large Systems of Linear Equations. Journal of Computers and Structures, Vol. 4, 1974, pp. 363-373.
5. G. P. Raymond, P. N. Gaskin, and P. Y. Addo Abedi. Repeated Compressive Loading of Leda Clay. Canadian Geotechnical Journal (accepted for publication).

Publication of this paper sponsored by Committee on Earth Masses and Layered Systems.

Field Observations of Ballast and Subgrade Deformations in Track

Tai-Sung Yoo, Daewoo Engineering Company, Seoul, Korea
Ernest T. Selig, Department of Civil Engineering, University of Massachusetts, Amherst

An extensive instrumentation program has been undertaken at the Facility for Accelerated Service Testing track located at the Transportation Test Center in Pueblo, Colorado, to monitor the performance of ballast, subballast, and subgrade layers under repeated traffic loading. Test sections are involved that contain wooden and concrete ties, tangent and curved track, ballast depths of 36-53 cm (14-21 in), and three different types of ballast. Soil strain gauges were installed in the ballast and subballast layers to measure the vertical and horizontal strains caused by train traffic loading and by track maintenance operations. Vertical extensometers were used to determine the settlement of the subgrade surface, and soil stress gauges at the subballast-subgrade interface were used to measure the vertical stress on the subgrade. The monitoring included both long-term measurements of the permanent strain and deformation accumulated with traffic and dynamic measurements of the elastic response under train loading. The study has provided extensive and unique data on the nature of the deformation response of a track system as a function of various track parameters. The system responded elastically, but nonlinearly, under each repeated axle-load cycle. However, permanent deformation did accumulate and continue to develop even after 667 GN [75 million gross tons (MGT)] of train load. Most of the readjustment after tamping disturbances occurred within the first 89-178 GN (10-20 MGT) load, with about half complete within 8.9-17.8 GN (1-2 MGT).

The performance of track structures is significantly affected by the behavior of the ballast and the subgrade under the repeated stresses caused by train loadings. The properties of these materials are a function of their physical state, which is influenced by maintenance and traffic history. Very little data are available from previous experience of actual track structures that can provide direct information on the physical states and deformation responses of ballast and subgrade, a situation that leaves considerable uncertainty about the specific ways in which these materials affect track performance.

A significant advance in the understanding of track performance has resulted, however, from the instrumentation program initiated in 1976 at the Facility for Accelerated Service Testing (FAST) track at the Transportation Test Center (TTC), U.S. Department of Transportation, in Pueblo, Colorado, to monitor the response of the ballast and subgrade layers under traffic. The instrumented sections contain both wooden and concrete

Figure 1. Strain gauge layout beneath railroad tie.

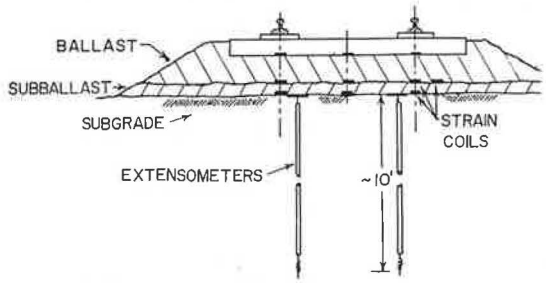

Note: Depth of extensometers = 3.05 m (10 ft).

Figure 2. Location of soil stress gauges beneath railroad tie.

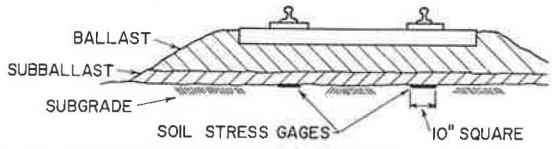

Note: Area of soil stress gages = 25.4 x 25.4 cm (10 x 10 in).

Figure 3. Gradation of materials in instrumented sections at FAST.

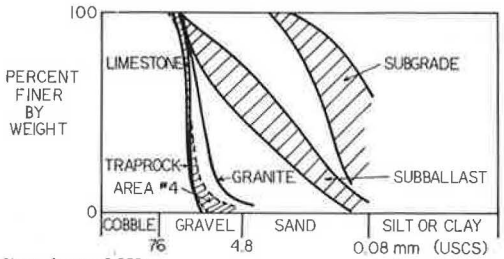

Note: 1 mm = 0.039 in.

Figure 4. Dynamic measurements in wooden tie section.

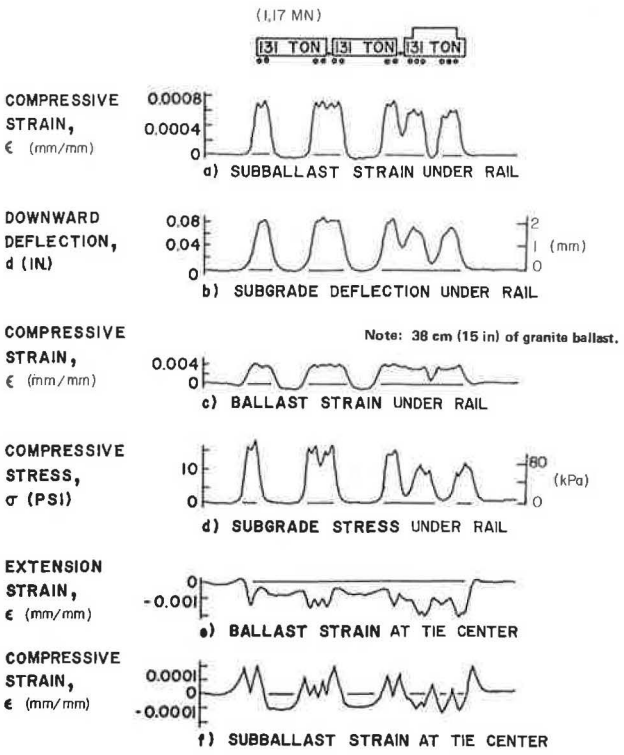

ties, tangent and curved track, ballast nominal depths of 38-53 cm (15-21 in), and three different types of ballast (granite, limestone, and traprock).

In this program, soil-stress gauges at the subballast-subgrade interface are used to measure the vertical stress on the subgrade caused by vehicle loading on the rail. Strain gauges in the ballast and subballast are used to measure the vertical and horizontal strains, both the instantaneous elastic under vehicle loading and the cumulative inelastic caused by vehicle loading and by track maintenance operations. Vertical extensometers in the subgrade are used to measure the instantaneous elastic and the cumulative, inelastic vertical deformations of the subgrade surface under vehicle loading relative to a reference anchor 3.05 m (10 ft) below the subgrade surface.

The trends for residual strains and deformations as a function of cumulative traffic loading are described for the first 1556 GN [175 million gross tons (MGT)] of traffic. The recorded peak values of the parameters measured during vehicle loading were examined after 26.7 GN (3 MGT) of train traffic and again after 667 GN (75 MGT) of traffic. The effects of track parameters on these results are illustrated.

INSTRUMENTATION PLAN

The stress, strain, and extensometer gauges were designed and fabricated based on previous experience (1, 2). In each case, the transducer is a pair of inductance coils connected to a special signal conditioner and readout device (3). [Details of the instrumentation and the installation procedures are given elsewhere (4).]

A typical instrumentation layout for ties involving strain coils in both the ballast and subballast and extensometers in the subgrade is shown in Figure 1. The top coils in the ballast are recessed into the bottoms of the wooden ties but are taped to the bottoms of the concrete ties. Each coil is electromagnetically coupled to a coil directly below it at or near the ballast-subballast interface. No physical connection exists between the coils, so that they are free to move with the track structure and also so that they will not be damaged by normal tamping operations or by tie movements in the horizontal plane. Each coil at the subballast surface is also electromagnetically coupled to the underlying coil on the subgrade surface. Each extensometer is installed in a 3.05-m-deep bore hole with the top anchor plate located at the subgrade surface.

Because the rails were already in position at the time of instrumentation, the bore holes for the extensometers could not be positioned directly under the rail-seat locations. Hence, they are located as close as possible to the inside of the rails at the centerline of the tie.

To obtain replicate measurements of the ballast and subballast strains, additional tie locations are instrumented in each test section by using some of the coils in Figure 1 but omitting the extensometers. Stress gauges are also placed at the subgrade surface under other ties as shown in Figure 2.

At each location to be instrumented, the tie was extracted and the ballast and subballast removed by hand shoveling. Backfilling was done by replacing the materials in about 15-cm (6-in) layers and compacting by using a heavy, pneumatic vibrating-plate tamper having a 15-cm-diameter circular-plate tamping foot. The tie was then carefully placed back into its previous position, and the cribs and shoulder were filled.

SITE CONDITIONS

Six sets of different track conditions are represented by

the instrumented sections. The defining variables are tie type, ballast type, ballast depth, and track geometry. The rail used is 68 kg/m (136 lb/yd), continuously welded on the concrete-tie sections and jointed on the wooden-tie sections. Two types of tie are used: 27.3-cm x 2.59-m (10.75-in x 8.5-ft) concrete on 61.0-cm (24-in) spacing and 17.8x22.9-cm x 2.59-m (7x9-in x 8.5-ft) hardwood on 49.5-cm (19.5-in) spacing. The subballast is a 15-cm layer of well-graded gravelly sand, and the subgrade is a silty, fine-to-medium sand. The six sections are described below (1 cm = 0.4 in).

Section	Tie Type	Ballast Type	Ballast Depth (cm)	Track Geometry
1	Concrete	Granite	41-48	Curved
2	Concrete	Granite	36	Tangent
3	Hardwood	Granite	53	Tangent
4	Hardwood	Granite	38	Tangent
5	Hardwood	Limestone	38	Tangent
6	Hardwood	Traprock	38	Tangent

Three different types of ballast are involved in the instrumented sections of the FAST track. Their index properties, as determined by tests conducted at the University of Illinois (5), are described below (1 mm = 0.04 in).

Property	Granite	Limestone	Traprock
Particle index	14.2	12.2	16.4
Flakiness index	20.8	9.4	22.7
Soundness	0.77	11.9	0.5
Los Angeles abrasion	18.8	25.7	13.2
Bulk specific gravity	2.68	2.68	2.94
Absorption (%)	0.40	1.65	0.20
Crushing value	18.4	19.3	13.1
Particle-size range (mm)	1-40	15-50	15-50

The limestone and traprock ballasts correspond to AREA no. 4 gradation, while the granite ballast is finer (see Figure 3).

The individual particles of all of the ballasts are relatively angular. The granite and traprock ballasts have sharper edges than the limestone, and the hardness of the particles is higher for the granite and traprock than the limestone. At the time of sensor installation, the ballasts were quite clean, without contamination.

The subballast material is a well-graded gravelly sand (Figure 3). It is designated SW in the Unified Soil Classification System (USCS) or A-1 in the American Association of State Highway and Transportation Officials (AASHTO) system. The subballast was compacted by using a vibratory roller before the track was constructed. Inspection records indicate that the compaction exceeds 90 percent of the AASHTO T-99 value at water contents of 6-12 percent. At the time of instrument installation, the moisture content was 3-5 percent.

The subgrade material is generally classified as a silty-to-very-silty, fine-to-medium sand, in some areas becoming a sandy silt (Figure 3). The principal designation is SM in the USCS system and A-1 to A-4 in the AASHTO system. No distinct subgrade layer boundaries are evident from borings; however, observations made during drilling of the extensometer holes suggest a general tendency toward increasing silt content with depth. In general, the moisture content of the subgrade material decreases from 6-12 percent in the top 1.2 m (4 ft) to 1-5 percent in the next 1.8 m (6 ft).

DYNAMIC MEASUREMENTS

The dynamic measurements to monitor instantaneous responses under wheel loading were first obtained after 26.7 GN of accumulated train traffic and have since been taken periodically at 222-GN (25-MGT) intervals. Throughout the dynamic measurements, very consistent patterns of the ballast, subballast, and subgrade responses have been observed. A typical response, that obtained during the 26.7 GN recording, is shown in Figure 4. The loading during the measurements was produced by a work train consisting of a six-axle locomotive and two four-axle hopper cars, each weighing about 1.17 MN [262 000 lbf (262 kips)].

Except for the ballast strain at the tie center, the maximum response for each measurement occurred directly under an axle. However, the reduction between two adjacent axles on a truck was generally minor. When the sensor location is beneath the center of a car, the subgrade deflections and stresses are generally zero, although some extensional strains are registered in the ballast and subballast locations under the rail, possibly due to rail spring-up.

The responses of the coils located under the center of the tie follow a different trend from the responses of those under the rail. For the center ballast strain, the response amplitudes are greater when the tie is located between two adjacent axles than when it is directly under an axle. This is probably because the tie experiences a greater bending moment under this loading condition.

Both the ballast and subballast coils under the center of the tie exhibit marked extensional strains. The subballast center strain is extensional under the middle of a car, but it is compressional directly under a truck. On the other hand, the ballast center strain is consistently extensional regardless of its location relative to the axles, except for the first and last wheel applications, when some relatively small compressive strains are registered. The extensional strains in the ballast could have two causes: (a) tie bending, because the top coil is fastened to the tie, and (b) extensional deformation caused by a horizontal stress that is incrementally greater than the vertical stress. However, the extensional strains in the subballast from traffic loading can have only the latter cause.

One of the most significant features shown by the dynamic records is the almost completely recoverable deformation of the track system under the transient axle loads, as indicated by the fact that none of the recorded base lines shows any noticeable permanent set. However, the static measurements taken periodically between the applications of train traffic show that there is a gradual accumulation of permanent strains with traffic.

What these records show is that, for each application of the transient wheel loads, the deformations of the track support system are mostly elastic and the plastic deformations are negligible. This, therefore, justifies the use of elastic models and resilient soil properties for predicting the response of the track system under vehicle loads.

Figures 5 and 6 summarize the dynamic responses of the ballast, subballast, and subgrade. The lines shown in Figures 5 and 6 represent the average values of peak responses under the rails when the car axle is directly over the sensor. Although significant variability occurred in each measurement, the average, which represents a minimum of eight measurements within each set of track conditions, should provide a reasonably reliable indication of the general trends of track response.

As shown in Figure 5, the ballast strains in the granite and limestone sections were about the same and consistently larger than those in the traprock section throughout the loading range studied. However, the strains in the subballast and subgrade layers under the traprock-ballast section exhibited the largest values,

and those under the limestone- and granite-ballast sections followed in decreasing order.

In the 53- to 147-kN [12 000- to 33 000-lbf (12- to 33-kip)] axle-load range, the measured parameters are approximately linearly related to wheel load. However, the intercept is not zero, which indicates that the stiffness properties of the materials are nonlinear. Thus, superposition of the effects of different wheel loads cannot be done simply by direct proportion.

Figure 5. Effect of ballast type on dynamic measurements under rail ballast during 667 GN recordings.

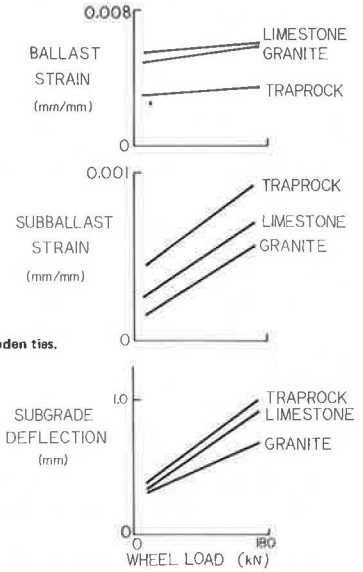

Note: 1 mm = 0.039 in; 1 kN = 225 lbf; 38 cm (15 in) of ballast under wooden ties.

Figure 6. Effect of ballast depth, tie type, and track geometry on dynamic measurements under rail during 667 GN recordings.

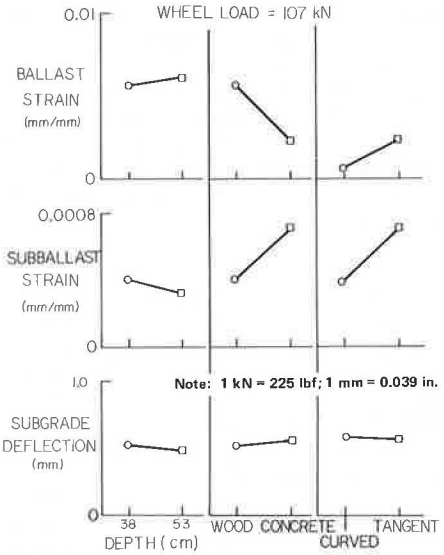

Similar comparisons for the effect of ballast depth are shown in the left column of Figure 6. Both the 38- and the 53-cm-thick sections had granite ballast and wood ties. The ballast strain in the 53-cm-thick ballast layer was slightly larger than that in the 38-cm-thick layer, the difference being greater with increased axle load. As expected, the subballast strain under the 38-cm-thick ballast section was greater than that under the 53-cm-thick section. The subgrade deflections are also slightly larger under the 38-cm-thick ballast section.

The effect of tie type is illustrated in the center column of Figure 6. Larger ballast strain occurred in the wooden-tie section and larger subballast strain occurred in the concrete-tie section [although both had the same (38-cm-thick granite) ballast]. However, the subgrade deformations were almost the same, even though the subgrade stress was considerably higher in the concrete-tie section. The difference in the stresses between the two different tie types increases as the wheel load increases. The reasons for these differences are complicated because (a) the concrete-tie section had a larger tie spacing (61-cm nominal) than the wooden-tie section (49.5-cm nominal), (b) the concrete-tie section had continuously welded rail while the wooden-tie section had jointed rail, and (c) the concrete tie was stiffer and had a larger bearing area than the wooden tie.

The comparisons between the tangent and curved sections are shown in the right column of Figure 6. Both sections had concrete ties with the same tie spacing and granite ballast. However, the average ballast thickness was greater for the curved track because of the required superelevation. The tangent section exhibited considerably higher ballast and subballast strains under the rail than did the curved section, but the subgrade deformations were about the same.

DYNAMIC DATA VARIABILITY

Further work is needed to evaluate the statistical significance of the trends for the static and the dynamic response measurements. The results given in this paper represent the averages of all replicate measurements within a test section. However, there was considerable variation among the values for different locations in a section. These variations were a function of location; there was little variation among the values obtained by repetitive measurements of the effects of the same wheel load at any given location.

To assist in judging the significance of the differences between the average values for each section, the coefficient of variation (CV) (i.e., the ratio of the standard deviation to the mean) for each dynamic measurement was calculated for the 147-kN [33 000-lbf (33-kip)] wheel load (see Table 1). The subgrade deformation had the smallest CV, averaging 0.21 for the five sections.

Table 1. Coefficient of variation of dynamic measurements: 147-kN wheel loads after 667 GN of traffic.

	Test Section											
	1		2		3		4		5		6	
Measurement	CV	N	CV	N	CV	N	CV	N	CV	N	CV	N
Ballast strain	0.32	3			0.35	4	0.29	8	1.10	7	1.08	8
Subballast strain	0.34	3	0.96	4	0.27	3	0.30	4	0.25	4	0.54	4
Subgrade relative deformation	0.12	4	0.16	4	0.15	4	0.47	4	0.13	4	0.23	4
Subgrade stress			0.69	4			0.33	4				

Note: 1 kN = 225 lbf (0.225 kip).

Figure 7. Accumulated ballast strain and subgrade deflection in curved concrete-tie section.

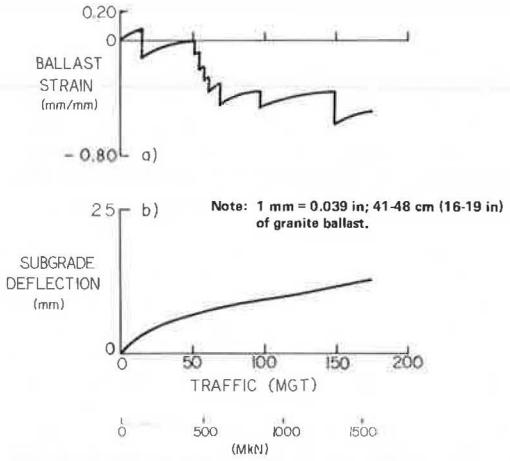

The ballast strain had the largest with an average of 0.63. The subballast strain and subgrade stress were intermediate with average values 0.44 and 0.51, respectively. The relatively large magnitude of the variability represented by these numbers limits the degree of certainty with which conclusions can be drawn when comparing results from the different test sections.

INELASTIC MEASUREMENTS

The static or long-term measurements were periodically obtained to determine the cumulative changes in the ballast strains, subballast strains, and subgrade deformations that resulted from the traffic and various track maintenance procedures. Static stress measurements were also taken, but these have not been evaluated because they represent only the pressure from the track and the ballast mass.

In general, the inelastic ballast strain, subballast strain, and subgrade deformation increased at a decreasing rate with accumulated traffic so long as no external disturbance (such as track maintenance) occurred. The ballast and subballast strains, regardless of location and direction of measurement, accumulated rapidly at the beginning of the traffic application. Accumulation of the subgrade deformation was relatively slower than that of the strains but continued for a longer period of traffic.

The strain-growth pattern was significantly changed by the disturbance caused by maintenance. Most of the track maintenance, particularly tamping, surfacing, lining, and tie and fastener replacement, involved raising the track structure and therefore created extension strain in the ballast layer.

An example of the effect of track maintenance on the ballast strain and the subgrade deflection is illustrated in Figure 7. This ballast strain clearly shows that the track rose with each tamping operation and subsequently settled after maintenance. In fact, in those examples, the amount of track raise was so large that the thickness of the ballast layer increased with each successive maintenance operation because the settlement under traffic was less than the raise. The associated subgrade-permanent-deformation pattern does not appear to be affected by the maintenance operation.

The vertical-strain accumulation in the ballast layer seems to be very rapid after the commencement of traffic. Although there were some variations from one tie location to another, about 50 percent of the probable ultimate strain that would be achieved without additional tamping or maintenance disturbance generally occurred during the first 8.9 or 17.8 GN (1 or 2 MGT) of traffic and about 90 percent by 89-178 GN (10-20 MGT). After that, the strain accumulation seemed to diminish and the growth rate slowed. Immediately after maintenance or tamping, however, the pattern was repeated. In most cases, the frequency of measurements following maintenance was not sufficient to determine the regrowth pattern adequately.

Unlike the dynamic strains, the static ballast strain under the rails shows the same trends as that under the center of the tie. The cumulative permanent strain at the center of the tie was compressive, except for a few ties that exhibited definite evidence of center binding.

Compared with the vertical ballast strain, the longitudinal and transverse ballast strains seem to have a much faster strain-growth pattern. As the track apparently settles to achieve a stable condition at the very early stage of traffic, the horizontal strains seem to reach a constant level at 8-9 GN and remain essentially the same until 356-445 GN (40-50 MGT) when the maintenance-caused irregularities begin to occur.

The magnitude of the transverse and longitudinal ballast strains was much smaller than that of the vertical ballast strain, as would be expected. However, it is interesting to note that these strains were generally extensional under traffic conditions without maintenance or disturbance. This indicates lateral spreading of the ballast or subballast.

The accumulation pattern of the vertical subballast strain is very similar to that of the vertical ballast strain, although the magnitude of the subballast strain was much smaller than that of the ballast strain. However, the subballast strain was obviously less sensitive to maintenance than was the ballast strain, which indicates that most of the maintenance procedures involved only the ballast layer (as would be expected).

In contrast to the ballast and subballast strains, the subgrade deformation accumulated gradually with traffic after the first 44.5-89 GN (5-10 MGT) of traffic. The subgrade deformation in the concrete-tie section increased more rapidly than that in the wooden-tie section. This difference seems to be due to the fact that the dynamic subgrade stress developed during train operation is higher in the concrete-tie section than in the wooden-tie section.

Again, a direct comparison of results for the three different ballast sections throughout the entire period of train operation is very difficult, especially in terms of ballast and subballast strains, because of the different amounts and nature of maintenance work involved in each section. However, the measurements obtained during the initial portion of traffic (when no maintenance was involved) are directly comparable.

The average accumulated ballast strains under the rails were compared for the three different ballast types. During the period without any disturbance from maintenance, the limestone and granite ballasts had about the same strains and the traprock slightly less. However, in the subballast layer, as shown in Figure 8a, the traprock section showed the largest strain, and this was followed by those of the limestone and granite sections in decreasing order. In contrast, the trend is exactly reversed for subgrade deformation (Figure 8b).

It is not known at present why the traprock section deformed less in the ballast layer, more in the subballast layer, and again less in the subgrade than did the other ballast sections. But these trends are generally consistent with those observed in the dynamic records. Also, these strain data do not conclusively show which

ballast performed better in terms of overall track performance.

As for the dynamic responses, the 53-cm granite ballast layer accumulated a larger strain under the rails than did the 38-cm granite layer (see Figure 9a), but the subballast strain showed the reverse trend (Figure 9b).

Figure 8. Comparison of accumulated subballast strain and subgrade deflection under rails in three types of ballast.

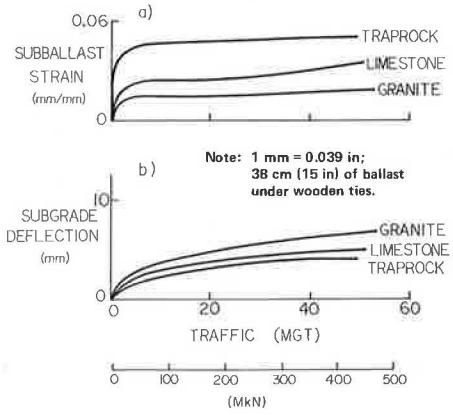

Figure 9. Comparison of accumulated ballast and subballast strains under rails: depth of granite ballast under wooden ties.

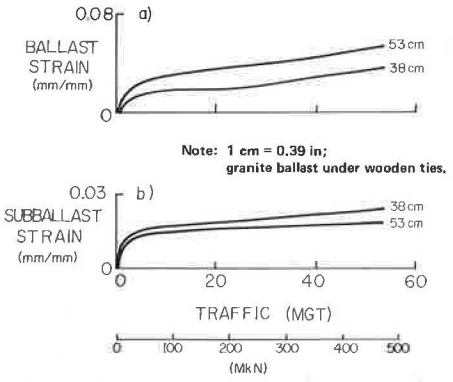

Figure 10. Comparison of accumulated ballast strain, subballast strain, and subgrade deflection under rails for concrete and wooden ties.

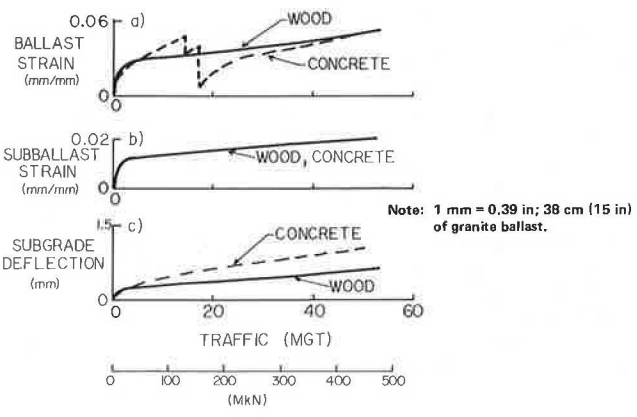

The subgrade deformation was about the same for the two ballast depths.

The concrete-tie section and the wooden-tie section showed about the same accumulated ballast and subballast strains (see Figures 10a and 10b), but the subgrade deformation was considerably larger in the concrete-tie section (Figure 10c). Again, the role of the different types of tie on the results is not clear because of the reasons discussed above. However, the higher dynamic pressure on the subgrade layer in the concrete-tie section might explain its higher subgrade deformation.

The curved concrete-tie section had a higher ballast deformation than did the tangent section. But, again, the trend is reversed in both the subballast and the subgrade layers. These trends are the same as those observed for different ballast thicknesses, which suggests that they might be mainly attributable to the difference in ballast thickness of the two types of sections.

SUMMARY

This paper presents experimental results that illustrate the static and dynamic responses of ballast, subballast, and subgrade to train loading. The absence of previous data of this type has limited the understanding of track behavior and prevented a needed assessment of alternative analytical models for track structure. The difficulty in making such measurements is considerable, and the observed experimental variability was large. Nevertheless, the outcome is believed to be highly successful.

An important observation was that, under repeated train loading, the system response is almost completely recoverable. The permanent deformation from any cycle was negligible. Only after many cycles did permanent strain begin to accumulate to values that could be observed.

Because of the rail stiffness, the two adjacent axles on a truck create a single load pulse that has little ballast unloading between them. Most of the strains and deformations were compressive under the load. However, midway between the rails under the tie center, extension strains were observed in the ballast and in the subballast. Tie spring-up in the center during loading at the rail seats may be a related cause.

In the 53- to 147-kN range, the response was related approximately linearly to the wheel load. However, the response for the first 53 kN of load was proportionally greater than that for the increase from 53 to 147 kN. Thus, the behavior of the track system was highly nonlinear. As a result, superposition of load response must be done with caution.

After tamping disturbance, most ballast readjustment occurred within 89-178 GN additional traffic load, with half of the change developing by 8.9-17.8 GN. This pattern was repeated after each successive raise and tamping in any section. The residual-strain development in the subballast and the subgrade was not affected by tamping. The subgrade continued to settle under the influence of the repeated load more gradually than did the ballast, but continuously throughout the 667-GN period of observation.

The transverse and longitudinal residual strains indicated that some lateral spreading of ballast accompanied the vertical ballast compression.

The smallest dynamic ballast strain and the largest dynamic subballast strain occurred with the traprock-ballast section.

The 38-cm-thick ballast section had the smallest dynamic ballast strain and the largest dynamic subballast strain.

The wooden-tie section had much larger dynamic ballast strains, but lower dynamic subballast strain and

subgrade stress than did the concrete-tie section. The larger ballast strain could have resulted from the development of a gap between the tie and the ballast because the upper part of the ballast strain gauge was fixed to the tie.

The ballast and subballast dynamic strains were greater for the tangent concrete track than for the curved concrete track, possibly because the tangent track had a thinner ballast layer.

ACKNOWLEDGMENT

This study was conducted at the State University of New York at Buffalo (SUNYAB) for the Transportation Systems Center (TSC) of the U.S. Department of Transportation and supported by funds from the Federal Railroad Administration. Technical monitor was Andrew Sluz. The installed gauges were designed by E. T. Selig and Irvine G. Reinig of Buffalo and fabricated under the direction of I. G. Reinig. Clement W. Adegoke and Hwang-Ming Chen of SUNYAB assisted with the gauge installation. Participating staff from TTC were Gerald W. Matthews, Richard Reiff, John Connors, and Mel Levine, and from TSC was Bruce Bosserman. The static data and the dynamic data after 667 kN of traffic were recorded by staff at TTC. The casings for the extensometer were installed by Jerold W. Klug of Denver, Colorado, and Charles W. Lockhart, Jr., of Colorado Springs, who also assisted with the gauge installation. Data processing for the 26.7- and 667-kN dynamic recordings was performed by Clement W. Adegoke and Harry E. Stewart, also of SUNYAB, respectively. The static data were processed by Michael J. Mann.

REFERENCES

1. E. T. Selig. Soil Strain Measurement Using Inductance Coil Method. In Performance Monitoring for Geotechnical Construction, ASTM, Special Tech. Publ. 584, Aug. 1975, pp. 141-158.
2. E. T. Selig. Instrumentation of Large Buried Culverts. In Performance Monitoring for Geotechnical Construction, ASTM, Special Tech. Publ. 584, Aug. 1975, pp. 159-181.
3. Model 4101A Soil Strain Gage. Bison Instruments, Inc., Minneapolis, MN.
4. E. T. Selig, T.-S. Yoo, and C. W. Adegoke. Mechanics of Ballast Compaction: Volume 2—Ballast, Subballast and Subgrade Instrumentation of FAST Track. Transportation Systems Center, U.S. Department of Transportation, Cambridge, MA, May 1978.
5. M. R. Thompson. FAST Ballast and Subgrade Materials Evaluation. Federal Railroad Administration, Rept. FRA/ORD-77/32, Dec. 1977.

Publication of this paper sponsored by Committee on Mechanics of Earth Masses and Layered Systems.

Study of Analytical Models for Track Support Systems

Clement W. Adegoke, Department of Civil Engineering, University of Ife, Nigeria
Ching S. Chang and Ernest T. Selig, Department of Civil Engineering, University of Massachusetts, Amherst

Data on the dynamic responses of ballast, subballast, and subgrade of track sections at the Facility for Accelerated Service Testing track in Pueblo, Colorado, are compared with predictions from three available analytical models for track support systems. The response data include ballast strain, subballast strain, subgrade deflection, and subgrade stress. The analytical solutions are provided by (a) a model that combines Burmister's three-dimensional elasticity solution with a structural analysis model that solves for the tie-ballast reaction (MULTA), (b) a finite-element, three-dimensional model that has prismatic elements combined with a structural analysis model (PSA), and (c) a quasi-three-dimensional, finite-element model, in which a longitudinal two-dimensional analysis is followed by a transverse two-dimensional analysis (ILLI-TRACK). The results show that all three models can reasonably predict the behavior of the track system, provided that values for the material properties and model parameters are correctly specified. Each model has advantages and limitations compared with the others. ILLI-TRACK is the only model that can vary properties in the vertical, longitudinal, and transverse directions and also the only one having a nonlinear stress-strain representation. However, the accuracy of ILLI-TRACK predictions is less certain because it depends on two empirical parameters, the effective tie-bearing length and the angle of distribution. The PSA model permits property variation in the transverse and vertical directions, but its computer costs are an order of magnitude greater than those for the other two models. The MULTA model is restricted to homogeneous layers of ballast and underlying materials, but it combines the features of both three-dimensionality and economy.

To provide a foundation for the prediction of track performance, which is a prerequisite for rational track design and maintenance-life prediction, it is necessary to have an analytical model that realistically represents the actual behavior of a track system subjected to various vehicle-loading conditions. One of the requirements for such a model is that it adequately characterize the three-dimensional aspects of the problem. Another is that it must distinguish the various soil and ballast layers and give them independent properties.

Several models that use the beam-on-elastic-foundation approach (1-3) have been employed to provide a basis for track design procedures in the past (4, 5). Although this approach has been extended to include a nonuniform foundation modulus (6) and a nonuniform finite-beam section (3, 7) to represent more closely the rail-tie system, its significant limitations are that it does not adequately model the ballast and subgrade system and that the interaction between the soil and the track structure is not properly represented.

To interrelate the components of the track structure to properly represent its complex interactions in determining the net effect of traffic loads on the stresses, strains, and deformations developed, several more-

comprehensive models are available. However, some of these models involve a plane-strain assumption, which does not represent the three-dimensionality condition (8), and others use three-dimensional finite elements, which are too expensive and not feasible for practical purposes (9). Considering all alternatives currently available, three models, which do account for the three-dimensionality condition, include soil-structure interaction and proper representation of the soil layers, and are reasonably economical to use, were chosen for study. They are

1. MULTA: a model that combines Burmister's three-dimensional, multilayer elastic solution with a structural analysis model that solves for the tie-ballast reaction;
2. PSA: a three-dimensional finite-element model that uses prismatic elements together with a similar structural analysis model; and
3. ILLI-TRACK: a quasi-three-dimensional finite-element model, in which a longitudinal two-dimensional analysis is followed by a transverse two-dimensional analysis.

In this paper, a brief description is given of the basic assumptions, important features, and limitations of the three models. Then, the general trends of the track behavior predicted by using them are presented and compared with the results of field measurements made at the Facility for Accelerated Service Testing (FAST) track in Pueblo, Colorado. Finally, the models are evaluated in relation to the suitability of their predictions and their cost-effectiveness.

MULTA MODEL

The MULTA model is a combination of two computer codes: BURMISTER and LOADS AND COMBINATIONS (LAC).

The BURMISTER code uses Burmister's multilayer elastic theory to represent the ballast and the soil layers. The tie-bearing area is divided into segments of approximately square dimensions, and then the area of each segment is converted to a circular area of uniform pressure (see Figure 1) that represents the same vertical force. These uniformly loaded circular areas are used to generate influence coefficients for stresses and displacements for the multilayer linear-elastic model.

Figure 1. Schematic representation of BURMISTER code.

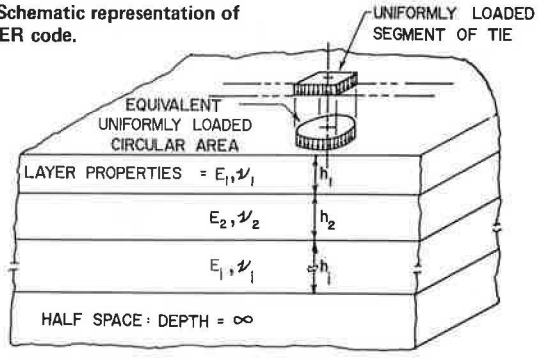

Figure 2. Schematic representation of PSA model.

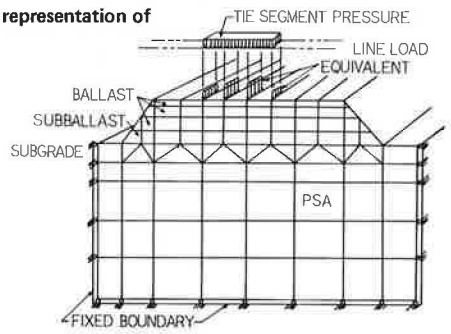

The LOADS-AND-COMBINATIONS code is a matrix structural-analysis model that solves for the tie-ballast reactions by using the method of consistent deformations. Wheel loads are applied on the opposite rails to represent an axle load. Each rail is assumed to be a beam of finite length that is supported by 11 ties, which are also represented as beams having multiple supports (one for each segment of the tie-ballast contact area, as indicated in Figure 1).

In each division, the uniformly distributed pressure that is converted into a resultant tie-support force is assumed to be unknown. The force is represented by the influence coefficients from the BURMISTER program (10). The reaction between rails and ties and the displacement at the intersection of rail and ties are also unknowns. This indeterminate structural problem is then solved by imposing compatibility and equilibrium equations to form a set of simultaneous equations containing the unknowns.

After the magnitude of the tie-ballast pressures is determined for each division of each of the ties, these pressures are superimposed on the roadbed system for all ties, by using BURMISTER, to obtain the displacements and stresses within the multilayer soil system.

Some limitations of this model include the following:

1. There is no relative displacement between tie and ballast. In addition, no separation of tie and ballast is allowed and tension may be developed between tie and ballast (which is not realistic).
2. The reactions between rail and tie and between tie and ballast are in the vertical direction only; shear forces are neglected.
3. The material properties for each roadbed layer are linear elastic, and they are constant throughout the layer. Thus, each layer is assumed to be composed of a homogeneous, isotropic, linear elastic solid.

PSA MODEL

This model is similar to MULTA in that it also considers the foundation representing the ballast and subgrade layers separately from the track structure for developing stress and displacement influence coefficients and then imposes the compatibility of displacements and stresses between the bottom of the structure and the top of the foundation to effect an overall solution to the system.

The PSA code generates foundation stress and displacement influence coefficients based on an analysis of periodically loaded prismatic solids (11-16), as shown in Figure 2. A prismatic solid is defined as a body that (a) is infinite in extent in the longitudinal direction (i.e., z), (b) has a cross-section (which may be arbitrary in shape) that is identical for all values of z, and (c) has material properties that do not vary in the z-direction. The analysis is restricted to those problems in which the spatial dependence of the loading can be approximated as periodic in the z-direction. The period of the loading, however, can be made sufficiently large so that the effects of isolated single loads or groups of loads can be effectively considered.

In the currently used PSA code, materials are con-

sidered to be linear elastic, but different elements in the vertical plane perpendicular to the rails (i.e., the x-y plane) may have different elastic constants. The three-dimensional solution is approximated as a Fourier series in the direction parallel to the rails (z). The coefficients in the series are obtained from two-dimensional finite-element analyses (one for each term in the series) that produce displacement series coefficients of all the nodes as a function of the x and y coordinates. Summation of those series terms gives the final displacements from which the strains and stresses at any point in a prismatic solid can be obtained. The input to the program consists of a finite-element representation of the cross-section of the body and the Fourier coefficients of the body forces, temperature terms, and boundary conditions. The output consists of displacements, strains, and stresses for any desired point in the body.

The main advantage of the prismatic-solid analysis is that it can provide solutions to three-dimensional elasticity problems at a relatively low cost when compared with an equivalent general three-dimensional finite-element analysis (that uses three-dimensional brick elements), which usually requires inordinately high and often impractical costs. The PSA model has the same limitations as MULTA. Its advantage over MULTA is the ability to vary the material parameters across the track section along the length of the tie.

Figure 3. Typical representation of the two ILLI-TRACK two-dimensional finite-element meshes.

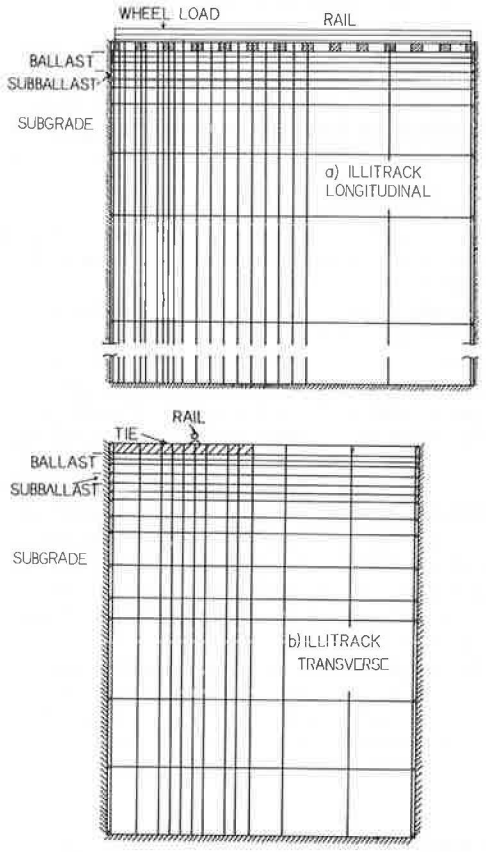

Figure 4. Pseudo-plane-strain approximation for ILLI-TRACK longitudinal analysis.

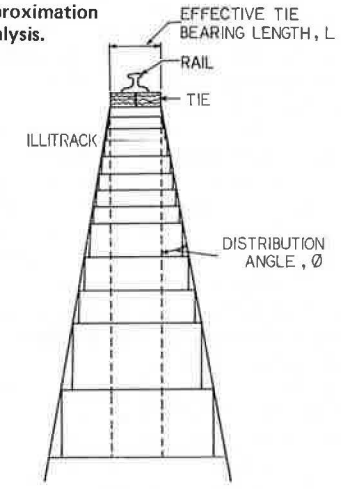

ILLI-TRACK MODEL

The ILLI-TRACK model (17-19) represents an attempt to incorporate a realistic representation of the nonlinear and stress-dependent behavior of roadbed materials.

Recognizing the three-dimensional nature of the geometry and loading conditions of a track system and the complexity and inordinate cost associated with actual three-dimensional finite-element formulation, Robnett and others (17) have attempted to simulate the track system by using two two-dimensional, pseudo-plane-strain finite-element analyses. A longitudinal two-dimensional analysis (see Figure 3a) is performed, and this is followed by a transverse two-dimensional analysis (see Figure 3b) that uses as input the results of the longitudinal analysis. Rectangular plane-strain elements are used to represent the ballast, subballast, and subgrade, and beam-spring elements are used to represent the rail-tie subsystem as a continuous beam supported on tie springs.

In standard two-dimensional, plane-strain finite-element formulations, the thickness of the elements (t) is maintained constant in all the elements. Thus, in the plane-strain state, the load is distributed in two directions only. Three-dimensional load dissipation is simulated by allowing the finite-element thickness to increase with depth. It is assumed that the rate of increase of element thickness with depth is constant. This is denoted by a parameter called the angle of distribution (ϕ) as shown, for example, in Figure 4 for the longitudinal analysis.

Also for the longitudinal analysis, it is assumed that the initial thickness of the element at the surface is equal to an effective tie-bearing length (L). This length is assumed to be the region of effective load transfer between the tie and the ballast.

Material nonlinearity is accounted for in the ILLI-TRACK model through the use of a resilient modulus, which is defined as the repeated deviator stress divided by the elastic or recoverable strain in a triaxial test, as established in pavement research (20, 21). For granular materials, such as ballast and subballast, the resilient modulus (E_r) has been found to increase with increasing bulk stress (Θ), as given by Equation 1.

$$E_r = K_1 \Theta^{K_2} \qquad (1)$$

where

Θ = sum of the principal stress = $\sigma_1 + \sigma_2 + \sigma_3 = \sigma_1 + 2\sigma_3$ in a triaxial test, and

K_1 and K_2 = constants determined from laboratory tests.

Table 1. Rail, tie, and roadbed properties assumed for FAST section 18B.

Material	Cross-Sectional Area (cm^2)	E (MPa)	Moment of Inertia About Major Axis (mm^4)	Layer Thickness (cm)	
Rail[a]	86.13	207 000	39.5×10^6		
Tie[b]	406	10.3	107.2×10^6		
Roadbed					
Ballast[c]		207		38	0.37
Subballast		13.3		15	0.37
Subgrade		3.3			0.33

Notes: 1 cm^2 = 0.155 in^2; 1 MPa = 145 lbf/in^2; 1 mm^4 = 2.40×10^{-6} in^4; 1 cm = 0.39 in.
The properties of Section 18 A are identical to those given above except that the ballast layer thickness is 53 cm (21 in).
[a] 68 kg/m (136 lb/yd) jointed.
[b] 17.8 x 22.9-cm x 2.59-m (7x9-in x 8.5-ft) hardwood on 49.5-cm (19.5-in) center-to-center spacing.
[c] Granite.

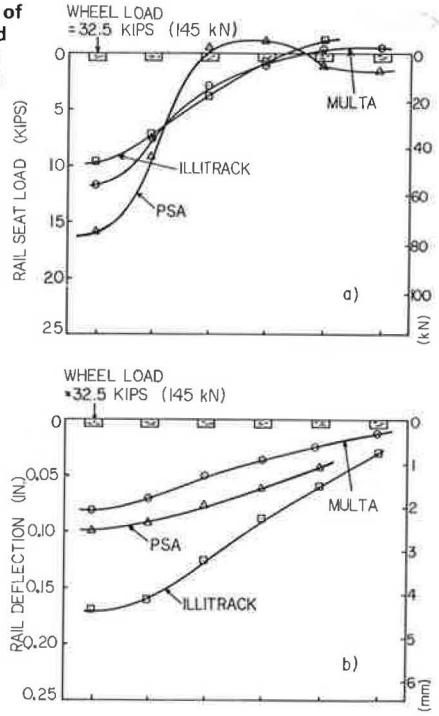

Figure 5. Comparison of calculated rail-seat load and deflection profiles under single-axle load: MULTA, PSA, and ILLI-TRACK.

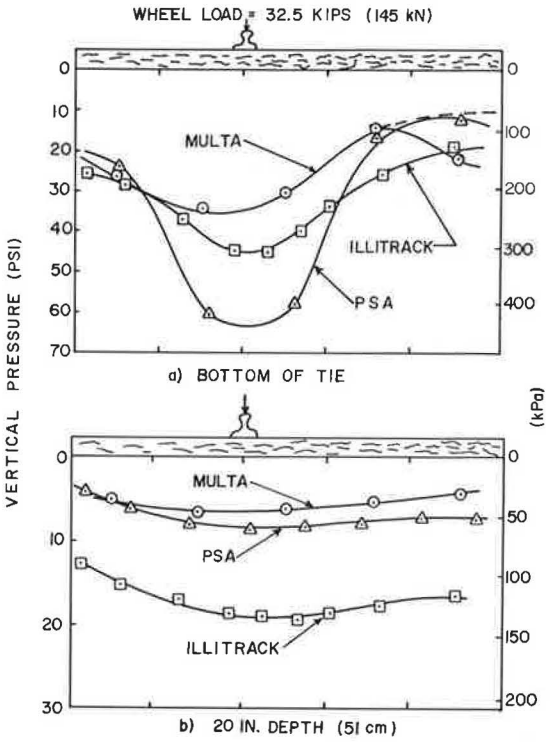

Figure 6. Comparison of vertical pressure distribution across tie under single-axle load: MULTA, PSA, and ILLI-TRACK.

The E_r of fine-grained soils has been found to decrease with increases in the deviatoric stress (17, 20, 22). At higher values of deviatoric stress, the E_r is almost constant, resulting in a bilinear relationship.

The basic limitation of the ILLI-TRACK model is the pseudo-three-dimensional assumption. The accuracy of the model predictions depends critically on assumed model parameters, such as effective tie-bearing length and angle of distribution. However, the criteria for choosing these parameters have not been well defined.

FIELD MEASUREMENTS OF INSTRUMENTED SECTIONS

As described by Yoo and Selig in the preceding paper in this Record, an extensive instrumentation program has been undertaken at the FAST track to monitor the performance of ballast, subballast, and subgrade layers under repeated traffic loading. Sensors were installed in the ballast and subballast layers under the rails to determine the vertical strains in these layers. Vertical extensometers were used to measure the settlement at the subgrade surface relative to that at a depth of 3.05 m (10 ft) below the top of the subgrade. Soil stress gauges were installed at the subballast-subgrade interface to measure the vertical stress on the surface of the subgrade. The measurements of instantaneous response during traffic loading obtained were then compared with the values predicted by using the three analytical models, MULTA, PSA, and ILLI-TRACK.

The single axle load for the test cars was 289 kN [65 000 lbf (65 kips)], assumed to be equally distributed to each of the two wheels. The distance between the axles on a truck was 178 cm (70 in).

COMPARISON OF THE THREE MODELS

The track response was predicted by using each of the three models and the same geometry, soil and track properties, and loading conditions. These predictions were then compared to develop an understanding of the variations and trends of predicted results.

Because the present forms of the MULTA and PSA models are limited to a linear elastic assumption, constant modulus values (Es) and Poisson's ratios (νs) for each layer were selected from the range for track and highway roadbed materials available in the literature (14-18, 22, 23-25). These values and the

Figure 7. Comparison of distribution of vertical pressure with depth under single-axle load: MULTA, PSA, and ILLI-TRACK.

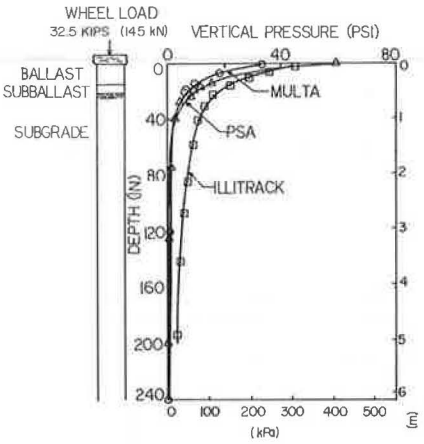

Figure 8. Comparison of distribution of vertical displacement with depth under single-axle load: MULTA, PSA, and ILLI-TRACK.

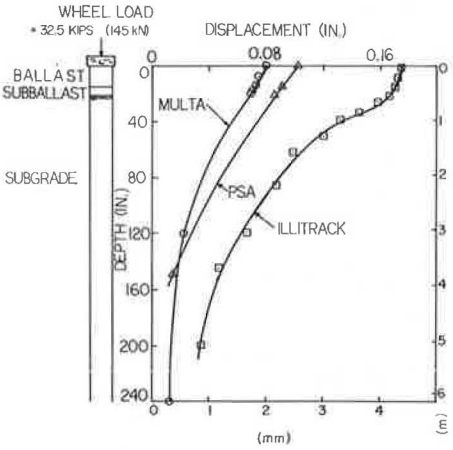

measured values for the FAST materials are summarized in Table 1.

In order to directly compare the models, rather than using the nonlinear version of ILLI-TRACK, the same constant moduli and Poisson's ratios were used in that also.

Figure 5a shows the distribution of the rail-seat load when a single-wheel load is supported over 11 ties. The distribution, in general, agrees with the trend observed by Talbot (1) over 7-9 ties from a single wheel load. The prediction obtained by using the PSA model indicates that a substantial part of the single-wheel load is distributed to only 3 ties, i.e., the loaded tie plus one tie on either side. The distributions obtained by using the MULTA and ILLI-TRACK models indicate that the load is distributed to about 5 ties. MULTA predicts a higher rail-seat load for the tie directly beneath the wheel load than does ILLI-TRACK.

Except for MULTA, the predicted pressures at the tie-ballast interface are highest under the rail and lowest at the center (see Figure 6a), which is considered to be typical of flexible wooden ties. The subgrade surface pressure along the tie under the wheel load is relatively smooth and close to being uniform (Figure 6b). ILLI-TRACK predicts much higher values of subgrade stress than do MULTA and PSA. This discrepancy may be caused by the value of ϕ [10° (19)] used for the pseudo-plane-strain analysis. A larger value of ϕ is required to match the predicted subgrade pressures of ILLI-TRACK with those of MULTA and PSA.

Vertical pressures under the wheel load are shown as a function of depth in Figure 7. The pressures predicted by PSA in ballast and subballast and at the top of the subgrade are higher than those predicted by MULTA, because, in the PSA model, more load is transmitted to the tie under the wheel than to the adjacent ties. ILLI-TRACK predicts much higher vertical pressure with depth than do PSA and MULTA. The low dissipation rate of stress with depth is caused by the small angle of distribution. The high vertical stress predicted by ILLI-TRACK is also reflected in the high vertical displacements, as shown in Figure 8. For the same reason, PSA predicts greater vertical deformation than does MULTA.

The rail-deflection profile is shown in Figure 5b. The deflections of the rail under the wheel load are 2.0, 2.5, and 4.3 mm (0.08, 0.10, and 0.17 in), respectively, for MULTA, PSA, and ILLI-TRACK. It can be seen that rail deflection is still significant up to the fifth tie away from the loaded tie. Superposition is therefore necessary to represent the effect of the adjacent axle load.

ILLI-TRACK predicts higher deflection than do other models, perhaps due to the value [46 cm (18 in) (19)] used for the tie-bearing length under each rail in the longitudinal analysis.

In general, except at the tie-ballast interface, PSA and MULTA predict similar vertical pressures and deflections, while ILLI-TRACK predicts values in the order of 100 percent higher.

The PSA model predicts the highest values of tie-ballast pressure and rail-seat load directly under the load and lowest values away from the load. The reason for this greater stress concentration is not known.

EFFECT OF ILLI-TRACK PARAMETERS

Tie-bearing length is one of the parameters used to simulate the three-dimensional effect of ties in the longitudinal analysis of the ILLI-TRACK model. The wheel load transmitted through this tie-bearing area into the roadbed system, and therefore the stiffness of the rail-tie system, depends very much on the specified value of this parameter. Angle of distribution is another parameter used in the ILLI-TRACK model to further simulate the three-dimensional problem. This parameter allows the thicknesses of the elements to increase with depth for both transverse and longitudinal analysis. The stiffness of the roadbed system is also a function of the angle of distribution.

The currently used values of the tie-bearing length and the angle of distribution are 46 cm and 10°, respectively. The 10° value for the angle of distribution was selected to give the best agreement between the ILLI-TRACK solution and a closed-form elastic solution of stress distribution with depth under a strip footing (25). This value however, does not appear to be suitable for the FAST track structure. Calculations also show that the vertical pressure distribution with depth given by the longitudinal analysis is not the same as that given by the transverse analysis when this angle of distribution is used. Thus, various values of the tie-bearing length and the angle of distribution were used, and the results were compared with solutions given by MULTA.

The tie-ballast and subgrade pressures were shown to be affected significantly by the tie-bearing length.

Table 2. Comparison of MULTA, PSA, and ILLI-TRACK predictions with measured response at FAST sections 18B and 18A.

	Section 18 B					Section 18 A		
		Predicted					Predicted	
				ILLI-TRACK				
Response	Measured[a]	MULTA	PSA	Constant Moduli	Nonlinear[b]	Measured[c]	MULTA	ILLI-TRACK (constant moduli)
Ballast strain (mm/mm)	0.004	0.0007	0.0006	0.0008	0.0005	0.006	0.0006	0.001
Subballast strain (mm/mm)	0.0005	0.0005	0.0008	0.0009	0.0006	0.0004	0.0003	0.001
Subgrade surface deflection (mm)		2.46	3.02	6.17	2.03		1.04	1.88
Subgrade deflection at extensometer bottom-anchor location (mm)		1.07	0.64	1.85			1.22	3.71
Subgrade surface deflection relative to extensometer bottom anchor (mm)	0.79	1.40	2.39	4.32				
Subgrade surface vertical stress (kPa)	45.5	48.3	68.9	186	139		38.6	153

Note: 1 mm/mm = 1 in/in; 1 mm = 0.039 in; 1 kPa = 0.145 lbf/in^2.
[a]Average for ties 18 B - 0375, 18 B - 0383, 18 B - 0391, 18 B - 0399, 18 B - 0417, and 18 B - 0425.
[b]Taken from results of Tayabji and Thompson (26).
[c]Average for ties 18 A - 0319 and 18 A - 0147.

Table 3. Types of roadbed stiffness.

Type of Roadbed		Young's Modulus (MPa)		
Ballast	Foundation	Ballast	Subballast	Subgrade
Stiff	Stiff	2067	138	138
Stiff	Soft	2067	138	34.5
Soft	Stiff	207	138	138
Soft	Soft	207	138	34.5

Note: 1 MPa = 145 lbf/in^2.

Similarly, the magnitude of the vertical pressure distribution with depth is greatly affected by the angle of distribution. Better agreement between the vertical stress distributions given by MULTA and ILLI-TRACK is achieved by using $\phi = 30°$ and a tie-bearing length of 61 cm (24 in).

The values of the angle of distribution and the tie-bearing length are expected to be different for different tie spacings, rail and tie stiffnesses, roadbed moduli, and loading conditions for any roadbed-track-structure-interaction problem. Further studies on the appropriate values to use for these two parameters are necessary to use the ILLI-TRACK model effectively.

COMPARISON BETWEEN PREDICTED AND MEASURED BEHAVIOR

A preliminary analysis showed that the two axles on a truck are close enough so that the peak response measured directly under one axle is affected by the load from the other axle. Thus, to compare the predictions with the field measurements, the computations were done by using superposition of two axles. The results are given in Table 2. For comparison, the results given by the nonlinear version of ILLI-TRACK (26) are also shown in Table 2.

To study the effect of roadbed moduli on the predictions, moduli for four types of roadbed systems were assumed and analyzed by using MULTA. The assigned moduli for ballast and foundations ranged from stiff to soft and are shown in Table 3. The results are given in Table 4 compared with the average and range of measured values.

As can be seen from these results, all three models predict ballast strains that are significantly lower than the values measured at FAST. A possible explanation for this discrepancy is that the measured displacements at the tie-ballast interface actually include the closure of the small gap that may exist between the tie and the ballast before the application of the train loads, i.e., tie-seating effects. This can significantly affect the measured ballast strains, because the upper coils are attached to the tie.

The MULTA predictions for various roadbed moduli give values of subballast strains, subgrade deflections, and subgrade pressures that are in the range of the measured data at FAST Section 18B. It is believed that reasonable predictions can be made by using MULTA if appropriate moduli values for roadbed layers are chosen.

In general, MULTA, which is a three-dimensional elasticity solution, and PSA, which is a three-dimensional finite-element solution, predict values that are nearly the same at the subgrade level. Although the tie-ballast pressures predicted by PSA are significantly higher than those predicted by MULTA (Figure 6), the rate of pressure dissipation with depth is nearly the same.

The ILLI-TRACK model appears to be the most complete model in the sense that it is a nonlinear, stress-dependent model that incorporates failure criteria for roadbed materials. It is, however, suspected that the two-stage pseudo-plane-strain analyses do not truly represent the three-dimensional state of the track system. Thus, it is possible that no advantage will accrue from sacrificing the three-dimensionality of the track system by using these detailed nonlinear formulations. It should be pointed out, however, that it may be possible to obtain realistic predictions from the ILLI-TRACK model by using a systematic variation of the angle of distribution and an effective tie-bearing length. However, because these are empirical parameters whose values may vary from problem to problem, the accuracy of predictions obtained by using this model is uncertain.

In terms of computer cost and input-data preparation effort, the ILLI-TRACK model is the least expensive.

Table 4. Comparison between measured and predicted responses (MULTA) for different types of roadbed stiffness.

Response	Predicted				Measured	
	Stiff Ballast and Stiff Foundation	Stiff Ballast and Soft Foundation	Soft Ballast and Soft Foundation	Soft Ballast and Stiff Foundation	Average	Range
Ballast strain (mm/mm)	0.000 13	0.0007	0.000 25	0.0007	0.004	0.001-0.005
Subballast strain (mm/mm)	0.000 58	0.000 48	0.000 35	0.0005	0.0005	0.0003-0.0007
Subgrade surface deflection relative to extensometer bottom anchor (mm)	0.38	1.06	0.46	1.40	0.79	0.20-0.89
Subgrade surface vertical stress (kPa)	56.5	31.7	71.0	48.2	45.5	30.3-60.6

Note: 1 mm/mm = 1 in/in; 1 mm = 0.039 in; 1 kPa = 0.145 lbf/in^2.

The ILLI-TRACK model also has an attractive automatic mesh-generating feature that reduces the number of cards needed to describe the track system.

The PSA model is an order of magnitude more expensive than the MULTA model. The input data preparation for PSA requires a minimum of one day compared with about five hours for MULTA. In addition, a lot of time is needed to check the connectivity data, nodal-point coordinates, and Fourier coefficients needed by the PSA model. In the present form of the PSA model, the influence coefficients for each of the five tie divisions are generated in separate computer runs. This requires a large turnaround time in order to obtain all the influence coefficients.

The close agreement between the predictions obtained by using the MULTA and PSA models and the measured responses and the fact that these models are three-dimensional and incorporate most of the required components of the track system make them good potential candidates for use in track analysis. Their basic limitation is that, in their present form, they are linear elastic and do not account for the stress-state- and stress-path-dependent behavior of roadbed materials.

The PSA model is more advanced than MULTA in that it permits variation of the properties of the roadbed transverse to the rail. This capability is particularly attractive for the study of center-bound track conditions.

SUMMARY AND CONCLUSIONS

Three analytical models—MULTA, PSA, and ILLI-TRACK—have been studied and evaluated by comparing their predicted results with field measurements.

1. For a set of chosen roadbed properties, the predictions obtained by using MULTA and PSA show similar trends of behavior in comparison with field measurements. On the basis of a materials parametric study of MULTA and the similarity of PSA and MULTA in the mathematical representation of the three-dimensionality of the track system, it is believed that PSA and MULTA can reasonably predict the response of a track system.
2. It is not certain whether the pseudo-plane-strain assumption in ILLI-TRACK is actually representing the three-dimensionality of the track system as desired. The parameters involved in this assumption—angle of distribution and effective tie-bearing length—are both problem dependent and require experience in their specification. The usefulness of this model might be improved by a systematic study of these two parameters to provide a guideline for selecting the proper values.
3. Relative to cost-effectiveness, the PSA model is an order of magnitude more expensive than MULTA and ILLI-TRACK.
4. The linear elastic assumption currently used in MULTA and PSA is not considered adequate for representing the actual stress-dependent behavior of roadbed materials. Further studies of material characterization and the adaptation of these models to properly represent the nonlinear behavior of roadbed materials should be carried out.

ACKNOWLEDGMENT

The studies described in this paper were based on the results of a research project sponsored by the Office of University Research, U. S. Department of Transportation. This support is gratefully acknowledged. The computer programs used were kindly provided by Battelle-Columbus Laboratory, the Association of American Railroads, and the University of Illinois and were adapted to the computer system at the State University of New York at Buffalo by Jorge E. Alva-Hurtado. Appreciation must also be expressed to S. D. Tayabji for his help and comments on using the ILLI-TRACK model.

REFERENCES

1. A. N. Talbot. Stresses in Railroad Track. Repts. of Special Committee on Stress in Railroad Track, Proc., AREA, Vol. 19, 1918, pp. 873-1062; Vol. 21, 1920, pp. 645-814; Vol. 24, 1923, pp. 297-453; Vol. 26, 1925, pp. 1081-1245; Vol. 31, 1930, pp. 69-366; Vol. 35, 1934, pp. 66-308.
2. H. C. Meacham and others. Study of New Track Structure Design. Battelle Memorial Institute, Columbus, OH; U. S. Department of Transportation, Summary Rept., Aug. 20, 1968.
3. M. Hetenyi. Beams on Elastic Foundations. Univ. of Michigan Press, Ann Arbor, 1946.
4. C. W. Clarke. Track Loading Fundamentals: 1. Railway Gazette, Vol. 106, No. 2, Jan. 11, 1957, pp. 45-48.
5. C. W. Clarke. Track Loading Fundamentals: 3. Railway Gazette, Vol. 106, No. 6, Feb. 9, 1957, pp. 157-160.
6. L. Barden. Distribution of Contact Pressure Under Foundations. Geotechnique, Vol. 12, No. 3, Sept. 1962, pp. 181-198.
7. H. B. Harrison. General Computer Analysis of Beams on Elastic Foundations. Proc., Institution

of Civil Engineers, London, Vol. 55, Pt. 2, Sept. 1973, pp. 605-618.
8. J. R. Lundgren, G. C. Martin, and W. W. Hay. A Simulation Model of Ballast Support and the Modulus of Track Elasticity. Civil Engineering Studies, Univ. of Illinois, Urbana-Champaign, Transportation Series, Vol. 4, Sept. 1970.
9. O. J. Svec, G. P. Raymond, K. Van Dalen, P. N. Gaskin, and K. R. Davies. Analytical and Experimental Investigation of a Rail Track Structure. Proc., 2nd Symposium on Applications of Solid Mechanics, McMaster Univ., Hamilton, Ont., June 1974.
10. W. So and others. Mathematical Models for Track Structures. Association of American Railroads, Rept. R-262, April 1977.
11. L. R. Herrman. User's Manual for PSA: Three-Dimensional Elasticity Analysis of Periodically Loaded Prismatic Solids. Univ. of California, Davis, Nov. 1968.
12. K.-H. Chu, G. C. Martin, and D. C. C. Ma. Track Foundation Stresses Under Vertical Loading. Rail International, Dec. 1977, pp. 617-626.
13. I. C. Chang. Track Foundation Stresses Under Horizontal Loads. M. S. thesis, Department of Civil Engineering, Illinois Institute of Technology, Chicago, May, 1975.
14. R. Pichumani. Finite Element Analysis of Pavement Structures Using AFPAV Code (Linear Elastic Analysis). Air Force Weapons Laboratory, Kirtland Air Force Base, NM, Rept. AFWL-TR-72-186, May 1973. NTIS: PB 239/244/7SL.
15. J. E. Crawford. An Analytical Model for Airfield Pavement Analysis. Air Force Weapons Laboratory, Kirtland Air Force Base, NM, Rept. AFWL-TR-71-70, May 1972.
16. C. W. Adegoke and C. S. Chang. Initial Evaluation of the PSA and ILLI-TRACK Models. Department of Civil Engineering, State Univ. of New York at Buffalo, Internal Rept., April 1978.
17. Q. L. Robnett, M. R. Thompson, R. M. Knutson, and S. D. Tayabji. Development of a Structural Model and Materials Evaluation Procedures. Federal Railroad Administration, Rept. FRA/ORD-76-255, July 1976. NTIS: PB 262 987/1SL.
18. S. D. Tayabji and M. R. Thompson. Track Support System Parameter Study. Federal Railroad Administration, Rept. FRA/ORD-76-256, July 1976. NTIS: PB 263-370/9SL.
19. S. D. Tayabji and M. R. Thompson. Program ILLI-TRACK: A Finite-Element Analysis of Railway Track Support System—User's Manual. Federal Railroad Administration, Rept. FRA/ORD-76-257, July 1976.
20. C. L. Monismith and F. N. Finn. Flexible Pavement Design: State-of-the-Art—1975. Transportation Engineering Journal, Proc., ASCE, Vol. 103, No. TE 1, Dec. 1977, pp. 1-53.
21. Test Procedures for Characterizing Dynamic Stress-Strain Properties of Pavement Materials. TRB, Special Rept. 162, 1975.
22. A. Aziz. Analysis and Design Procedure for Highway-Railroad Grade Crossings. Texas A&M Univ., College Station, Ph. D. dissertation, 1976.
23. R. H. Prause and J. C. Kennedy. Parametric Study of Track Response and Performance. Federal Railroad Administration, Rept. FRA/ORD-77/75, Dec. 1977.
24. P. Rebull. Goetechnical Properties of FAST Test Section 17. Metrek Division, Mitre Corporation, McLean, VA, Feb. 1977.
25. M. R. Thompson. FAST Ballast and Subgrade Materials Evaluation. Federal Railroad Administration, Rept. FRA/ORD-77/32, Dec. 1977.
26. S. D. Tayabji and M. R. Thompson. Analysis of Track Support Systems at FAST. Association of American Railroads, Washington, DC, Letter Rept., May 1977.

Discussion

L. Raad and M. R. Thompson, Department of Civil Engineering, University of Illinois at Urbana-Champaign

The development and justification of the ILLI-TRACK model is described elsewhere (17, 19). The emphasis in the development of this model was the proper and realistic simulation of the ballast, subballast, and subgrade materials in the track support system.

The repeated-load behavior [as characterized by the resilient modulus (E_R = repeated deviator stress/recoverable strain)] of granular materials and fine-grained subgrades is stress dependent (17). Because stress states vary throughout the support system (ballast-subballast-subgrade), adequate materials modeling cannot be achieved by assigning a constant modulus.

In the MULTA and PSA models, it is assumed that the materials are linearly elastic and no provision is made for failure. Stress-dependent resilient behavior and failure criteria, however, are considered in the original ILLI-TRACK program; there is no advantage to using this model for the analysis of linear-elastic systems in which stress-dependent resilient behavior and material failure criteria are not stipulated.

In the initial ILLI-TRACK model, material failure criteria were defined in terms of the maximum principal stress ratio (σ_1/σ_3) and the minimum-allowable minor principal stress (σ_3) (generally, $\sigma_3 = 0$; i.e., no tensile stress is permitted) for granular materials. A maximum-allowable shear stress $[(\sigma_1 - \sigma_3)/2]$ was designated for fine-grained soils. If an element failed during the ILLI-TRACK analysis, a failure modulus was assigned. A value of 27.6 MPa (4000 lbf/in^2) was recommended for the failure modulus of granular materials. The assigned failure modulus for a fine-grained soil was the resilient modulus corresponding to a repeated deviator stress equal to the shear strength of the soil. The effects of the assumed failure criteria on ILLI-TRACK-predicted responses are significant (18).

A new failure criterion for granular materials and subgrade soils under repeated states of stress has recently been developed by Raad and Figueroa (27) and incorporated into the original ILLI-TRACK model. In this modified version (ILLI-TRACK 2), the nonlinear properties of the granular material and subgrade layers are included by means of a successive iteration technique. The principal stresses are modified at the end of each iterative step so that they do not exceed the strength of the material as defined by the Mohr-Coulomb envelope. This is achieved by using the vertical stress (σ_v) in each element at the end of the iterative step to calculate limiting values for the major and minor principal stresses $(\sigma_1)_{max}$ and $(\sigma_3)_{min}$, respectively, in terms of cohesion

Table 5. Summary of response data.

Case	Failure Criteria: Ballast	Failure Criteria: Subgrade	Maximum Tie Reaction (kN)	Maximum Tie Deflection (mm)
1[a]	$\sigma_1/\sigma_3 = 10$, $(\sigma_3)_{min} = 0$	$\tau^b_{max} = 173$ kPa	36.1	1.30
2[c]	$\sigma_1/\sigma_3 = 5.8$, $(\sigma_3)_{min} = 0$	$\tau_{max} = 173$ kPa	32.7	3.30
3	$\phi = 45°$, C = 0	$\phi = 0$, C = 173 kPa	37.6	1.45

Notes: 1 kPa = 0.145 lbf/in²; 1 kN = 225 lbf; 1 mm = 0.039 in.
Details of loading and track system data are given by Tayabji and Thompson (18); 133.5-kN (30 000-lbf) wheel loads, wooden ties at 51-cm (20-in) spacing, and 68 kg/m (136 lb/yd) rail were used.
[a] Modulus of ballast at failure is assumed to be 27.6 MPa (4000 lbf/in²).
[b] τ_{max} = maximum-allowable shear stress.
[c] Modulus of subgrade at failure is assumed to be 690 kPa (100 lbf/in²).

Figure 9. Variation of vertical and horizontal stresses in ballast and subgrade.

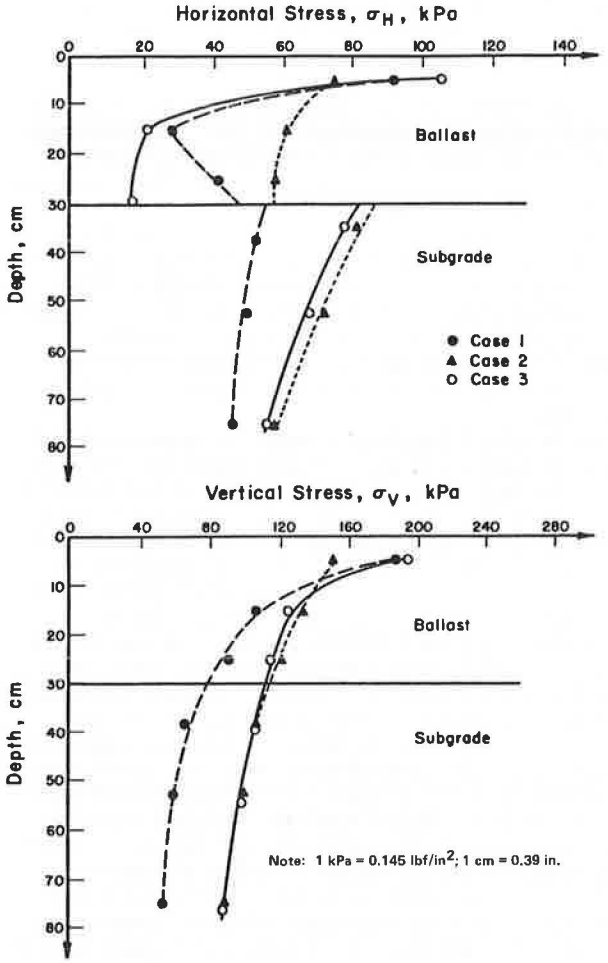

(C) and angle of friction (ϕ), such that

$$(\sigma_1)_{max} = \sigma_v \tan^2 [45 + (\phi/2)] + 2C \tan [45 + (\phi/2)] \quad (1)$$

$$(\sigma_3)_{min} = \sigma_v \tan^2 [45 - (\phi/2)] - 2C \tan [45 - (\phi/2)] \quad (2)$$

If σ_3 and σ_1 are the minor and major principal stresses at the end of the iterative step, respectively, then σ_3 should not be smaller than $(\sigma_3)_{min}$ and σ_3 should not be larger than $(\sigma_1)_{max}$. However, σ_1 should not assume a value greater than σ_1', the major principal stress associated with σ_1 at failure, where

$$\sigma_1' = \sigma_3 \tan^2 [45 + (\phi/2)] + 2C \tan [45 + (\phi/2)] \quad (3)$$

The detailed procedure for the modification of σ_1 and σ_3 is described elsewhere (27). Elements that have modified stress states are in a plastic state and would exhibit large permanent deformation while maintaining a constant resilient response (defined by the specified nonlinear constitutive relationships of the subgrade and granular materials).

An example problem similar to that given by Tayabji and Thompson can be solved for the purpose of comparing the response obtained when the new failure model is used with that obtained when the original model is used. The results are given in Table 5 and Figure 9.

Although there is partial agreement between the responses predicted by the original model (cases 1 and 2) and those predicted by the new model (case 3), there are significant differences when predictions for total response are compared. For example, although vertical stresses for cases 2 and 3 seem to compare quite well (as shown in Figure 9), the resilient deformation for case 2 is twice that for case 3 (Table 5).

Stress state has a tremendous effect on the permanent deformation behavior of granular materials and subgrade soils subjected to repeated loadings (28). Adequate stress-state predictions are thus essential if a rational evaluation of a track support system (ballast-subballast-subgrade) is desired. For example, as shown in Figure 9, there are significant discrepancies in the predicted horizontal and vertical stresses. Linear-elastic theories such as MULTA and PSA frequently indicate the existence of significant tensile stresses at the bottom of the granular layer (even though the granular material has no tensile strength).

Therefore, we believe that ILLI-TRACK 2 (modified to incorporate the improved failure criteria) is the only currently available track-structure model capable of providing a realistic characterization of ballast, subballast, and subgrade response.

REFERENCES

27. L. Raad and J. Figueroa. Response Prediction of Transportation Support Systems. Journal of the Transportation Engineering Division, Proc., ASCE, to be published, 1980.
28. R.M. Knutson, M.R. Thompson, T. Mullin, and S.D. Tayabji. Materials Evaluation Study. Federal Railroad Administration, Rept. FRA/ORD-77-02, Jan. 1977.

Publication of this paper sponsored by Committee on Mechanics of Earth Masses and Layered Systems.

Model Studies of Track Support Systems

Robert J. Mitchell, Department of Civil Engineering, Queen's University, Kingston, Ontario
Keung Pak, EBA Consultants, Ltd., Calgary, Alberta

Geometric, behavioral, and loading complexities create difficulties in analytical approaches to the prediction of track performance characteristics. The use of model testing as an alternative to more-expensive full-scale testing in providing direct results, as well as data for analytical correlation, is discussed in this paper. Equations of similitude are presented, and the choice of model scales and materials is considered. Model track systems at a linear scale-reduction factor of 6 were constructed and tested. The test variables were tie shape and spacing. Vertical and longitudinal repeated loads were applied in phase, and deformations were measured at various points in the structure. The conventional tie shape was found to be marginally superior to others tested, except for resistance to longitudinal loads. Minimizing tie spacing (or maximizing contact area) was found to be important for resisting continued settlements. The main purpose of the tests, however, was to demonstrate that model studies are capable of producing reliable results. Successful correlation with full-scale test results was achieved from the simplified model, and it is suggested that more-sophisticated real models could produce direct design information at significant savings in research resources.

Track-system maintenance is a cause of major expenditure in rail transport operations. Maintenance requirements are increased by the continued permanent deformation of the subgrade and track structure under repeated train loads. The track support system, however, must exhibit some flexibility to dampen the loading harmonics; an elastic support system would be ideal. Because soils (subgrade, embankment, and ballast) are not ideal elastic materials, the problem appears to be one of defining the conditions of placement and loading over which the system deformations will be mainly recoverable. Stiffening of the elastic system components (rail and ties) has been suggested [see, for example, Timoshenko and Langer (1) and Meacham (2)], but the steady increases in axle loads and train speeds make this alternative less and less attractive from both economic and track-stability considerations. The complex nature of the behavior of soil materials excludes analytical evaluation of the second alternative, namely, engineering a more-elastic response in the earth support system. This is particularly true in the rail track system due to the interactions of the various system components and the repeated loadings. The obvious approaches to an engineering solution are

1. Basic research to define the constitutive equations for the soil materials under appropriate test conditions, combined with the development of analytical techniques for predicting system performance, and
2. Model studies.

The first approach has gained research support in recent years, and considerable work is now in progress [see, for example, Raymond and others (3)]. The second approach does not appear to have been used to the same extent, although it would be desirable to develop both approaches in parallel for two reasons:

1. Although testing to provide soil parameters for analytical models appears to be a more fundamental approach, it must be acknowledged that soil mechanics tests are essentially model tests in that they are carried out on assemblages of discrete particles under various boundary conditions. Such tests may not provide self-consistent constitutive relationships, and empirical correlations may be necessary. Thus, although analytical predictions can be correlated with present prototype behavior, the predictions of behavior of new systems (alternative prototypes) are still empirical.
2. Model studies can be carried out on any alternative system (as well as the present prototype) and will provide an early preliminary evaluation of its potential for success. Even the results of imperfect models can be valuable in evaluating the relative importance of various parameters. Track system has a large number of independent variables, a factor that makes the use of model studies cost-effective.

The two approaches can, obviously, be complementary. Certain problems, such as the pumping or intermixing of ballast, subballast, and subgrade materials or the breakdown of ballast under repeated loading, can be evaluated by an imperfect full-scale model test in a large cylindrical oedometer. Such test data have been reported by Gaskin and Raymond (2). Problems that involve system interaction, however, require that the track system be represented. Full-scale testing is both expensive and time consuming. This paper discusses the modeling of track support systems, presents some model test data at the smallest recommended scaling, and makes some recommendations for future model studies.

DIMENSIONAL SIMILITUDE AND MODEL SCALES

The linear scale used for model testing of a conventional track support system will be limited by the prototype ballast-size distribution because the model ballast must exhibit similar characteristics. Figure 1 compares the Canadian National Railway specification A ballast and the model ballast, as well as the grain-size distributions for other layers, used in this study. The linear scale factor is $\lambda_L = 6$, and it is recommended this be considered a minimum model size (i.e., model $\geq \frac{1}{6}$ prototype scale) to produce similarity of the tie-ballast and ballast-subgrade interaction. Figures 1 and 2 show the similarity of test characteristics between the model and the prototype ballasts.

By considering the rail-tie system as a continuous beam on an elastic foundation and using Winkler's hypothesis (subgrade reaction is proportional to deflection at a point), the deflection and reaction are given, under static load, by Hetényi (5) as

$$y = (p\beta/2K)\, e^{-\beta X} (\cos \beta X + \sin \beta X) \quad (1)$$

and

$$\sigma_{max} = (p\beta/2K)(S\,K/A) = p\beta S/2A \quad (2)$$

where

y = rail deflection at a point located distance X

Figure 1. Comparison of grading curves: model materials and prototype ballast.

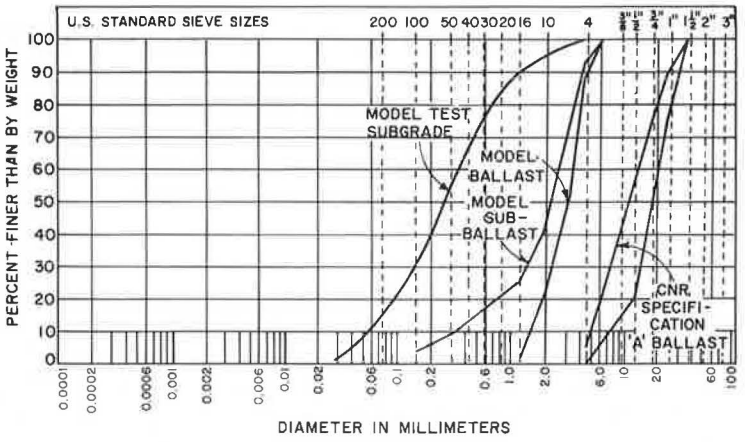

Figure 2. Triaxial test results for ballast.

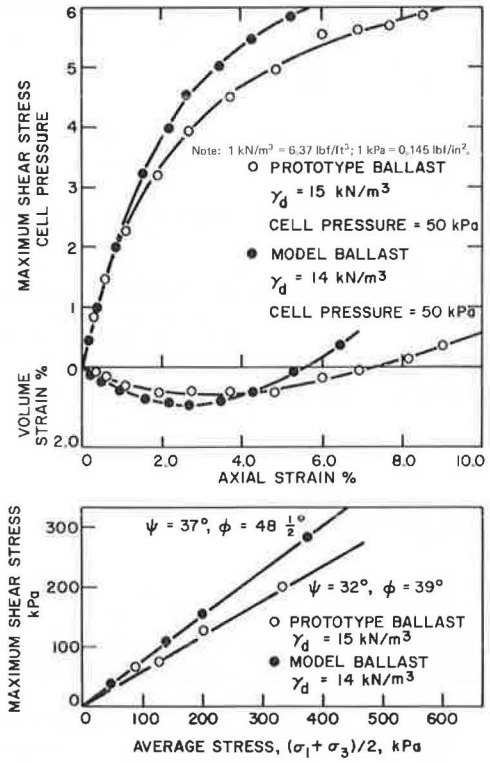

from the point of load application,
p = applied load at X = 0,
K = subgrade modulus (assumed elastic),
$\beta = (K/4EI)^{1/4}$ (where EI = rail-section modulus),
σ_{max} = maximum contact stress between tie and ballast,
S = tie spacing, and
A = area of contact between tie and ballast.

To provide similitude in the forms of the deflection curves and maintain the linear scale for tie spacings, the values of βX must be similar for model and prototype; thus

$$\lambda_\beta = 1/\lambda_L \tag{3a}$$

and

$$\lambda_K/\lambda_{EI} = 1/\lambda_L^4 \tag{3b}$$

where

λ_β = scale factor for the value of β,
λ_L = linear scale factor,
λ_K = scale factor for the subgrade modulus, and
λ_{EI} = scale factor for the rail-section modulus.

The contact stress and the factor of safety against bearing-capacity failure of individual ties must now be considered. To provide the same contact stress in model and prototype, Equations 2 and 3 give

$$\lambda_p = \lambda_L^2 \tag{4}$$

where λ_p = scale factor for the applied load.

The factor of safety of a footing on a purely frictional soil is

$$F = (\gamma/2)\, N_\gamma B/\sigma_{max} \tag{5}$$

where

γ = unit weight of the material (ballast),
N_γ = bearing-capacity factor, and
B = footing (tie) width.

To provide the same value of F in the prototype and in a model using a model ballast of the same density, the stress scale factor (λ_σ) is given by Equation 6.

$$\lambda_\sigma = \lambda_N \lambda_L \tag{6}$$

where λ_N = scale factor for the bearing-capacity factor N_γ. From Equations 4 and 6,

$$\lambda_\sigma = \lambda_p/\lambda_L^2 = \text{unity} \tag{7a}$$

and

$$\lambda_N = 1/\lambda_L \tag{7b}$$

It is theoretically possible to obtain the correct model ballast density that satisfies Equation 7 by using strength data from tests at various densities, together with standard design graphs relating N_γ and ϕ. In practice, this may be quite difficult.

Equation 1 gives model displacements at a scale of

$$\lambda_y = \lambda_p \lambda_\beta/\lambda_K = \lambda_L/\lambda_K \tag{8}$$

The accuracy to which model displacement measurements should be determined can be estimated from Equa-

Table 1. Scaling factors used for model studies.

Item	Prototype	Model	Scaling Factor
Rail-section			
Designation	RE 100	RE 100/6	
Moment of inertia (m^4)	2.04×10^{-5}	1.57×10^{-2}	$\lambda_{EI} = 1296^a$
Rail length (m)	10.97	1.83	$\lambda_L = 6^b$
Tie section (cm wide × cm deep)	23 × 20	3.8 × 3.4	$\lambda_L = 6^b$
Tie spacing (cm)	51-91	8.5-15.0	$\lambda_L = 6^b$
Axle load (kN)	267	7.42	$\lambda_p = 36^c$
Ballast depth (cm)	30	5	$\lambda_L = 6^b$
Subballast depth (cm)	30	5	$\lambda_L = 6^b$
Subgrade depth (cm)	75	13	$\lambda_L = 6^b$
Ballast strength (angle of internal friction) (°)	40	50	$\lambda_N \doteq 1/3^d$
Subgrade modulus (kPa)	15 000	15 000	$\lambda_K = 1^e$

Note: 1 m^4 = 2.41 × 10^6 in^4; 1 m = 3.28 ft; 1 cm = 0.39 in; 1 kN = 225 lbf; 1 kPa = 0.145 lbf/in^2.
[a] From Equation 3.
[b] Selected.
[c] To give $\lambda_\sigma = 1$.
[d] From design graphs of ϕ versus N_γ.
[e] From Figure 2: $K = E/(1 - \nu^2)$.

Figure 3. Track structure.

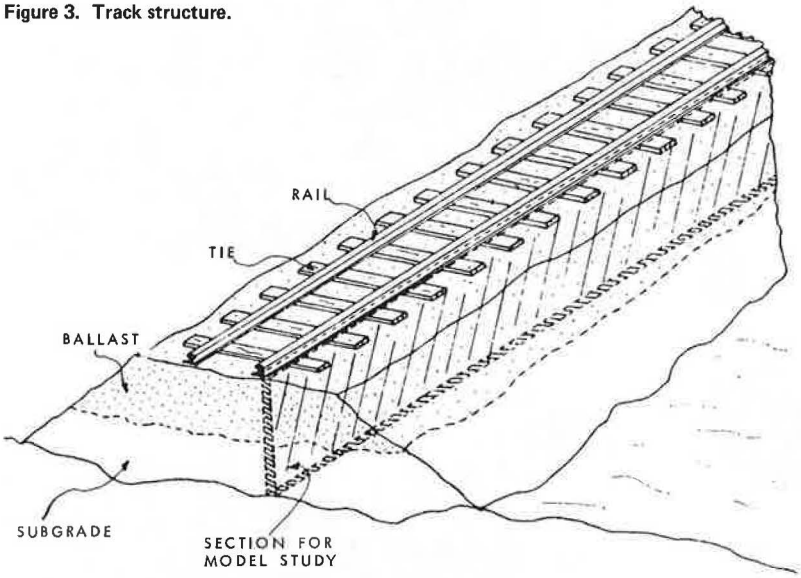

Figure 4. Schematic view of model arrangement.

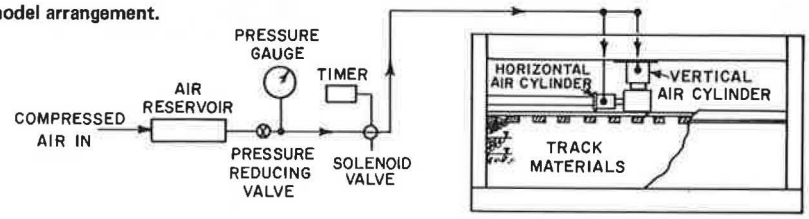

tion 8. The subgrade modulus (K) is known to increase with increased density of the ballast. To satisfy Equation 7, the model subgrade modulus (λ_K) must be <1 and the accuracy of model displacement measurements will have to be increased. If similarity of model and prototype ϕ-values are maintained (hence, $\lambda_N = \lambda_K = 1$), Equation 6 can be satisfied by $\lambda_\sigma = \lambda_L$, $\lambda_p = \lambda_L^3$ and the model displacements would be expected to develop at a scale of $\lambda_y = \lambda_L^2$ (which would require extremely accurate measurement techniques). Reduced contact stress, in this case, might also create modeling problems, particularly because the behavior in the prototype situation is not elastic and the loadings are not static. Maintaining similarity of both density and contact stress is indicated by the general observation that continued permanent deformation in granular soils under repeated loadings is dependent, mainly, on the initial density and applied stress level (4). Because the deformation of soils is nonlinear, the subgrade modulus will decrease as the factor of safety is decreased. By using a safety-factor scale (λ_F) of >1, it would be possible to make $\lambda_K = \lambda_L$, so that Equation 8 will give $\lambda_y = 1$ (model deformations equal to prototype deformations), which reduces the accuracy required in model measurements. It is estimated that the bearing-capacity factor of safety in the prototype case is about 8-10 and that a similar deformation could be obtained by using a model factor of safety of ≅ 4. Thus, the best approach to physical modeling appears to be to maintain similarity in contact stress level and ballast density by using a model-scale large enough so that the safety factor against bearing capacity is ≥3-4. It would then appear to be of little significance that Equation 6 would, in general, not be satisfied. A single bearing-capacity test on a model tie would provide the additional data needed to determine λ_K.

When λ_K is determined, the rail-section modulus can be designed according to Equation 3.

MODEL TESTS

To demonstrate the practical use of model studies of track support systems, model materials (Figures 1 and 2) were prepared and two-dimensional models were tested by using a linear scale, $\lambda_L = 6$, and the scale factors given in Table 1.

Various tie shapes and tie spacings were tested. Figure 3 shows the longitudinal track section modeled, although the model width was arbitrarily chosen as 0.18 m and the contact stress was appropriately adjusted. Rectangular, round, and wedge-shaped tie sections were tested at three different spacings—$1/\lambda_L$, $1.4/\lambda_L$, and $1.8/\lambda_L$ times the normal prototype spacings; between 11 and 20 ties were included in each test; and the model wheel load was applied directly over the central tie. A horizontal load of 4 percent of the vertical load was also applied (to represent wheel traction) and both loadings were cycled, simultaneously, by using the system shown in Figure 4. The physical model and the loading pattern are shown in Figures 5 and 6, respectively. Figure 7 shows a closer view of the test section; dial gauges were used to monitor the rail deformation under static load and after 10^n loading cycles, where m = 0:1:5. Photographic techniques were used to measure tie-soffit settlements and internal deformations at the same intervals of repeated loadings. Two methods for monitoring internal deformations were tested, and the method (Figure 7) of placing 2-mm diameter rods in the profile was adopted. By using stecometer analysis of photographic negatives, an accuracy of ±0.04 mm in the measured rod movements was obtained (95 percent confidence limit). [Details of test preparation and measurement techniques are given by Pak (6).]

Figure 5. Model test: round ties.

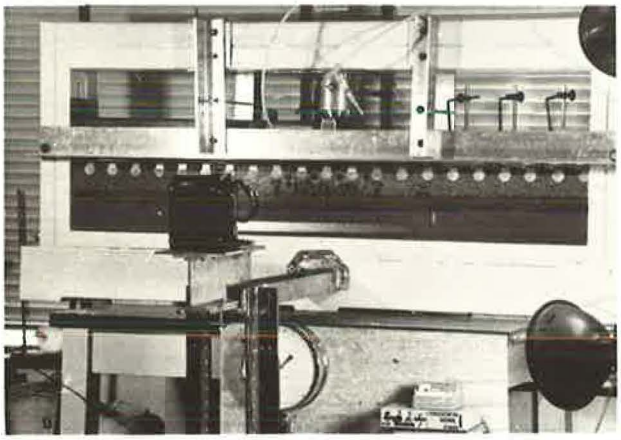

Figure 6. Form of pressure variation in air cylinders (frequency = 1 Hz).

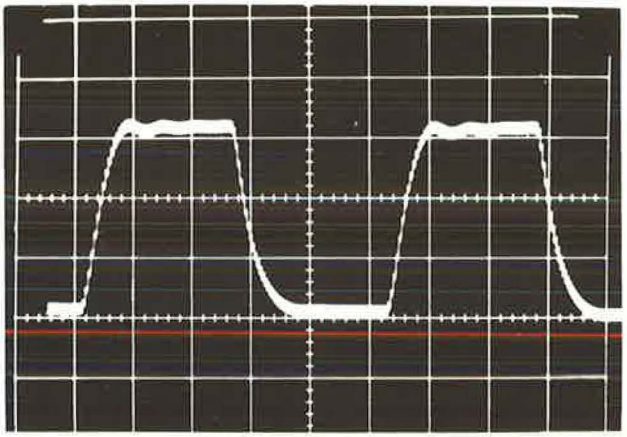

Figure 7. Close-up view of test section that has wedge-shaped ties.

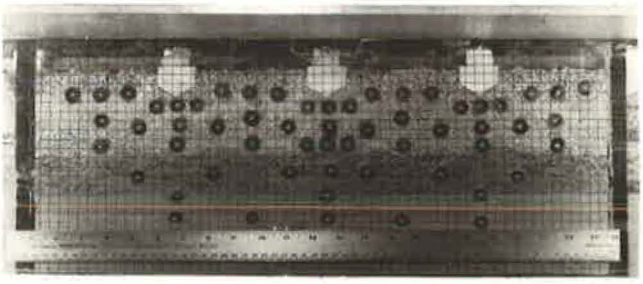

Figure 8. Maximum vertical deformation contours of two identical tests.

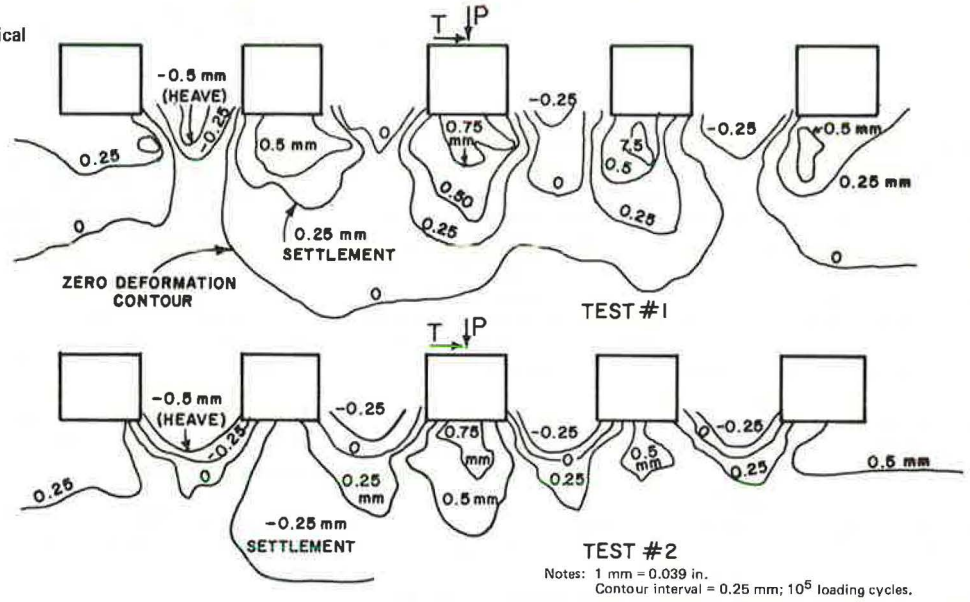

Notes: 1 mm = 0.039 in.
Contour interval = 0.25 mm; 10^5 loading cycles.

MODEL TEST RESULTS

Stecometer readings from the photographic plates were analyzed and plotted by using a computer program. The results of two similar tests are compared in Figure 8 to demonstrate the reproducibility of the test data. Figure 9 shows the rod-displacement vectors for test 2 in Figure 8, and it is noted that small longitudinal displacements developed due to the applied longitudinal load. Figure 10 shows the effect of increasing the tie spacings. By considering the displacements of the rods at the corners of triangular elements, the volume changes in the supporting soils can be calculated (see Figure 11); the dilation (volume increase) of ballast between the ties is quite apparent. The results for the other two tie shapes were quite similar although, as can be seen by comparing Figure 12 with Figure 9, the wedge shape reduced the lateral displacements and the intertie dilation while slightly increasing the vertical displacements. The wedge-shaped and circular tie soffit shapes exhibited marginally superior performance at the larger tie spacings, but the rectangular ties exhibited the least amount of vertical deformation at the conventional spacing. Figure 13 shows, typically, how deformation developed with the number of repeated loadings and that continued inelastic deformation does develop. A direct comparison of the data in Figure 13 indicates that there was little variation among the various tie shapes but that tie spacing is an important consideration. The data indicate that ties should be placed as closely as the practical limitations of economics and compaction methods will allow.

Figure 9. Movement of rods after 10^5 cycles of repeated loading: rectangular ties at 85-mm center-to-center spacing.

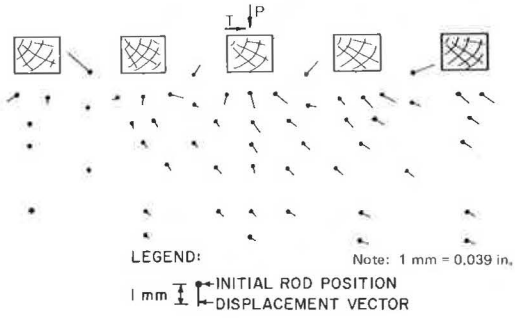

Alternatively, the bearing area of each tie could be increased at the same tie spacing.

Foundation subgrade moduli were calculated by using dial-gauge readings taken from the first loading applied after track preparation and compaction. Two methods were used: the first involved a summation of the deflections at all ties in the form

$$K = P/S\sum_{i=1}^{N} y_i \qquad (9)$$

where y_i = deflection ordinates of the rail, measured at all N tie locations.

The second method used only the deflection at the center tie (y_o) and is given as

$$K = p\beta/2y_o \qquad (10)$$

The results are shown in Figure 14. The first method gave moduli of 1.5-3 times that of the second method, and the rectangular ties consistently gave lower moduli. In theory, this modulus reflects the integrity of the track foundation; in practice, the modulus is largely dependent, for a given tie size and spacing, on the compaction conditions directly beneath the ties. Compaction around and under the ties was carried out, in the model, by using curved steel probing rods to simulate prototype compaction methods. Because the performance of the rectangular ties was essentially similar to that of the other shapes, the lower moduli for the rectangular shape are attributed, mainly, to the greater difficulty in achieving good compaction under this shape. (Other workers have also concluded that compaction under rectangular ties is difficult.) Thus, the rectangular ties might have proved superior if it were not for the negative effect of the compaction problem. The difference between the two methods of moduli determination is considered to be due to the inelastic nature of the geotechnical support media and to the fact that the model rail system was the finite length. It therefore appears that the second method (that using Equation 10) gives the best relative values of moduli for model test analysis. The usefulness of model studies based on the beam-on-elastic-foundation approach is considered to be supported by the fact that Equations 9 and 10 gave moduli values that were of the same order of magnitude.

Figure 10. Vertical deformation contours of tests with rectangular ties.

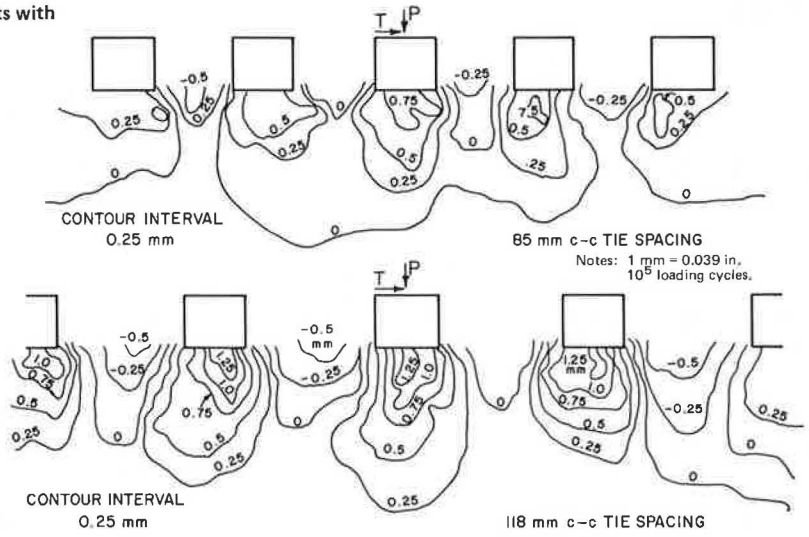

Figure 11. Volumetric strain in various zones after 10^5 loading cycles: rectangular ties at 85-mm center-to-center spacing.

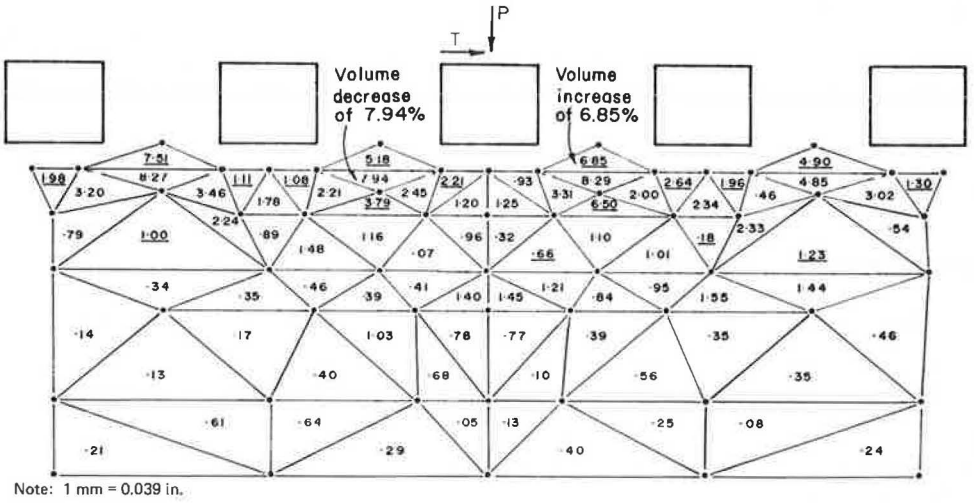

Figure 12. Movement of rods after 10^5 cycles of repeated loading: wedge-shaped ties at 85-mm center-to-center spacing.

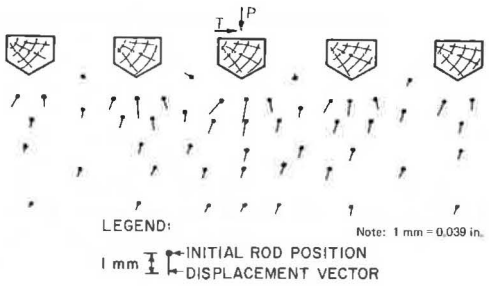

Figure 13. Vertical deformation of ballast: 85- and 118-mm spacing.

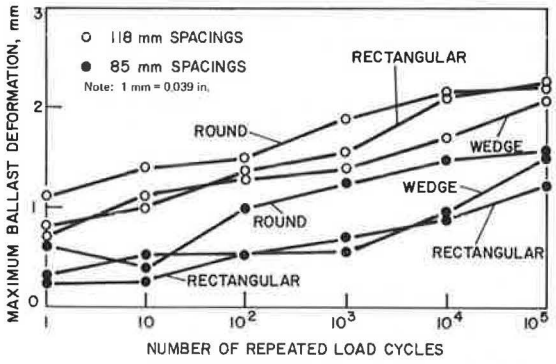

Figure 14. Calculated foundation moduli.

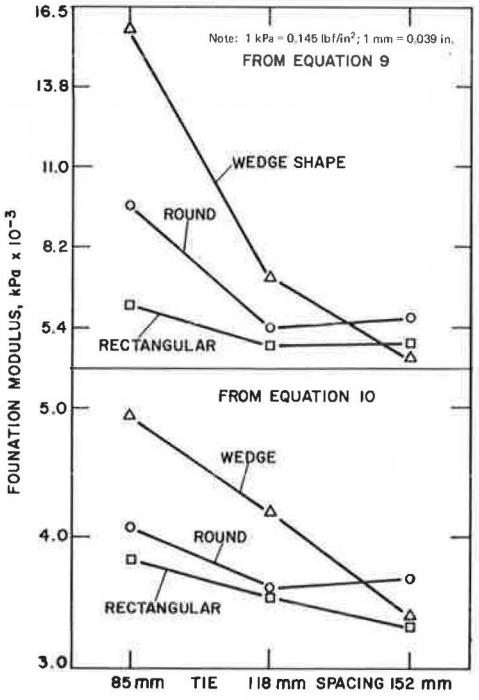

COMPARISON OF MODEL TESTING WITH PROTOTYPE TESTING

To compare the results with prototype behavior, the scaling factors must be compared with the prototype. Raymond and others (3) have published the results of a full-scale test section of limited length (11 ties) loaded at the central tie by a simulated, repeated axle load. The full-scale section used a 66-kg/m (132-lb/yd) RE rail section having a moment of inertia of $3.67 \times 10^{-5} m^4$ ($88 in^4$) and the conventional tie spacing of 0.23 m (9 in). From Equation 10, the prototype subgrade reaction was found to be 14 680 kPa ($2129 lbf/in^2$) compared with the model value of 3860 kPa ($560 lbf/in^2$) (Figure 14). The scaling factors are then $\lambda_{EI} = 2338$ and $\lambda_K = 3.8$. The remaining factors are the same as given in Table 1 and, because the system is relatively flexible [i.e., $(KL^4/4EI)^{1/4} >> \pi$], the differences in subgrade moduli would not alter the contact stresses under the loaded ties significantly. The value of λ_β is then given as $(\lambda_K/\lambda_{EI})^{1/4} = 16.25 \times 10^{-4} = 0.2$, which is close to the ideal value of 0.16 given by Equation 3. The factor of safety scale is calculated by using Equations 5 and 6 as $\lambda_F = \lambda_N \lambda_L / \lambda_\sigma = 2$, and the deflection scale is given by Equation 8 as $\lambda_y = 1.89 \doteq 2$.

Thus, the model displacements should be about 50 percent of the prototype displacements. Figure 15 shows that the model deformations are of the same magnitude as the prototype and that reasonably good correlation is obtained between model and prototype deformations. The deviation between the calculated displacement factor of 2 and the observed deformation factor of 1 is considered to be due to the nonlinearity of the load-deformation characteristics and the differences in bearing-capacity safety factors. Because the safety factor of the model is

Figure 15. Comparison of model and full-scale foundation deformation: 10^5 loading cycles.

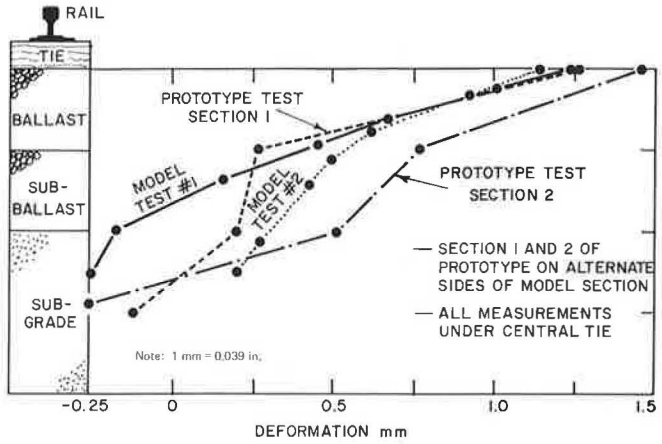

only 50 percent of that existing in the prototype, the deformations in the model are about twice those expected. It may be concluded that the beam-on-elastic-foundation approach, as described above, is quite suitable for designing models of track support systems. Despite the lack of exact similitude, it is concluded that models, down to one-sixth of the prototype size, are suitable for comparison of the effects of varying system components.

Pak (6) has reported 10 model tests that were carried out in a five-month testing period. The full-scale test conducted by Raymond and others required more than six months. A field-test program carried out over a two-year period on eight test sections of a main-line track and reported by the Association of American Railroads Research Center (7) arrived at many conclusions similar to those found in the model studies described here. In addition to the direct cost savings, the size and cost of associated laboratory testing equipment are proportionally reduced when model-scale materials are used.

MODEL SCALES, TEST VARIABLES, AND MODEL FACILITIES

As described above, the linear scale-reduction factor (λ_L) is limited by the ballast-size distribution to about 6. Internal instrumentation must be miniaturized to reduce interference but, because loads and deformations are reduced in the ideal model, the problems of instrumentation should be similar at both model and prototype scales. Because of the large number of potential test variables, a model test facility should be designed to be as versatile as possible, even to the extent of using models of prototype compaction devices for preparing tests. Considering the relationships discussed in this paper and the behavior of soils materials, a model scale factor of $\lambda_L = 5$ would probably be most suitable. A 250-kN (56 250-lbf) prototype axle load would then become a 10-kN (2250-lbf) model axle load. For such reduced loads, it would be feasible to design and construct a real model facility that incorporated mobile, rather than fixed, repeated loads (air or hydraulic loading cylinders mobilized between a fixed overhead-guidance rail and model railway cars). A real model facility would, of course, provide increased testing capabilities, including wear testing on model rails and rolling stock.

Approximate models that use fixed repeated loadings are appropriate for basic study of the track system variables. Optimization of ballast grading and depth, rail stiffness, and tie size and spacing for various track requirements (loads, speeds, traffic density, deceleration sections, and such) is one area for potential studies. The tests reported in this study indicate that the present prototype system is not well suited to resisting longitudinal traction forces (as would occur during deceleration). Intuitively, the lack of lateral confinement in the ballast and subballast layers appears to be a possible reason for continued settlements despite efforts to achieve optimal compaction of these layers. Possible methods of increasing lateral confinement by earth reinforcement techniques could be studied economically at a suitable model scale.

SUMMARY AND CONCLUSIONS

The primary purpose of this paper is to demonstrate the capabilities and usefulness of model studies for evaluating the performance of track support systems. The following general conclusions are noted:

1. The beam-on-elastic-foundation theory can be used to evaluate model similitude providing that the nonlinear behavior of the soil materials and the bearing capacity are adequately considered. Data for correlation with theoretical predictions or for predicting prototype behavior can be obtained from model studies.
2. Model studies are efficient and can be extended to evaluate factors or systems that would involve excessive costs if evaluated at the prototype size. Indeed, a real rolling-stock model is considered practical at a linear scale factor of about 5.

The model studies reported in this paper indicate that, for a given load, reducing the tie spacing will reduce settlements. Of the three tie shapes tested, the rectangular-shaped ties were, at normal spacing, superior in resisting vertical settlements, although a simple wedge shape was superior in resisting longitudinal loads and also performed better at larger tie spacings. The model studies also indicated that, except for the advantage of better resistance to longitudinal loads, no gain is realized by divergence from the normal rectangular shape. Tie-size variations were not investigated. The behavior in the model tests under repeated loading was found to be reproducible and correlated well with the observations made in a prototype scale test.

ACKNOWLEDGMENT

Financial support from the National Research Council of Canada is gratefully acknowledged.

REFERENCES

1. S. Timoshenko and B. F. Langer. Stresses in Railroad Track. Trans., ASME, Vol. 54, 1932, pp. 277-302.
2. H. C. Meacham. Study of a New Track Structure Design: Phase 1. Federal Railroad Administration, Rept. FRA-RT-72-12, 1972.
3. G. P. Raymond, R. W. Lake, and C. J. Boon. Stresses and Deformations in Railway Track. Canadian Institute of Guided Ground Transport, Rept. 76-11, 1976, pp. 1-171.
4. P. N. Gaskin and G. P. Raymond. Contribution to Selection of Railroad Ballast. Journal of the Transportation Engineering Division, Proc., ASCE, Vol. 102, No. TE2, May 1976, pp. 377-394.
5. M. I. Hetényi. Beams on Elastic Foundations, 5th ed. Univ. of Michigan Press, Ann Arbor, 1958.
6. K. Pak. Model Studies of Railway Track Performance. Queen's Univ., Kingston, Ontario, M.Sc.

thesis, 1975, pp. 1-130.
7. Cooperative Research on Wood Ties. Railway Tie Association and Research and Test Department, Association of American Railways, Illinois Institute of Technology, Chicago, 5th and 6th Progress Repts., 1969 and 1971.

Publication of this paper sponsored by Committee on Mechanics of Earth Masses and Layered Systems.

Railroad-Highway Grade-Crossing Analysis and Design

Aziz Ahmad, Robert L. Lytton, and Robert M. Olson, Texas Transportation Institute, Texas A&M University, College Station

This paper presents a computerized design system for a highway-railroad grade-crossing foundation. The design criterion used is the permanent differential deformation between the railroad track and the adjacent highway pavement. This design criterion is related to two performance criteria: dynamic-load profile and roughness index (which is a measure of the ride roughness experienced by a vehicle passing over the grade crossing). The effect of the permanent differential deformation on increasing highway dynamic load is included in the computer program, as is the increase in dynamic railway wheel loads. Characteristic properties of materials, including the effects of environmental factors (such as temperature and suction), on subgrade material properties are considered. The computer program calculates the permanent differential deformation (the design criterion) caused by repetitive wheel loads during a design period for both highway and railway traffic. The number of wheel-load repetitions (to serve a design period) for highway and railway traffic are considered separately in the calculations; therefore, this design system can handle any combination of high and low volumes in railway and highway traffic. Design examples are included.

Highway-railroad grade crossings are a subject of continuing concern because of the maintenance problems caused by load-associated roughness. The magnitude of dynamic highway loads over a grade crossing increases with time as the pavement on each side of the crossing becomes distressed because of the repeated loads. The relative permanent deformation between track and pavement determines, to a large extent, the degree of roughness experienced by passing traffic. Therefore, the material properties (such as resilient modulus and permanent strain) of grade-crossing materials are important in design.

Length of trains, weight of rail cars and locomotives, and speed contribute to failures of track structures and crossings. Railroads are also concerned with ridability and operation of trains at grade crossings.

PRESENT STATUS

There are more than 200 000 public grade crossings in the United States. Surface materials include timber, bituminous pavements, concrete slabs, rubber panels, metal sections, and others. It is clear that, regardless of the type of surface material, the proper design of track structure, base, and subgrade materials (including adequate drainage) determines the performance and life of a grade crossing (1).

Committee 9 (highways) of the American Railway Engineering Association has published reports on the merits and economics of various types of grade-crossing surfaces. However, this literature does not provide information for grade-crossing-foundation design. Important characteristics such as (a) the influence of crossing profile (roughness characteristics) and highway-vehicle speeds on dynamic loads at the crossing and its approaches; (b) the interactions between individual physical and geometrical characteristics of the grade crossing; and (c) the stresses and deformation in ballast, base, and subgrade, due to both highway and railway loadings and their dynamic effects, are not well defined.

The performance of a grade crossing is measured by three performance criteria:

1. Dynamic-load profile,
2. Roughness index, and
3. Permanent differential deformation.

These criteria are related to each other; i.e., an increase in one will increase the other two. The application of loads on a grade crossing causes the track structure and the adjacent pavement to deform differentially. This difference in deformation is due to the differences in material properties, loading, and thickness of the two structures.

Permanent deformation is a function of the level of stresses at varying depths produced by the size of the applied loads, the number of load applications, material properties, and environmental factors such as temperature and moisture balance.

This paper describes a design procedure that includes all of these effects and a computer program that was developed to calculate the necessary parameters.

DEVELOPMENT OF DESIGN PROCEDURE

The design procedure is divided into three phases:

1. Fixing the required dimensions and geometry of the grade crossing,
2. Selecting the materials for foundation layers (emphasizing the effects of environmental factors such as temperature, moisture balance, and drainage on the properties of these materials), and
3. Establishing design criteria and acceptable limits to control the design system.

Design Criteria

Three design criteria are considered: (a) dynamic-load profile, (b) roughness index, and (c) permanent differential deformation between track and adjacent pavement.

Dynamic-Load Profile

The dynamic load experienced by a vehicle depends on the interactions between the roughness characteristics of the riding surface, the vehicle characteristics, and the vehicle speed. In Figure 1, the roughness that develops with time and repeated traffic load is represented as dimensions SM1, SM2, BH1, and BH2. These dimensions, which can be positive, negative, or zero (i.e., up, down, or flat), are the input data used in computer program DYMOL (2). This program is used to predict dynamic loads on grade-crossing profiles as a function of differential deformation caused by highway vehicles and speeds. The dynamic load on the rear axle of a simulated dump truck traveling 88.5 km/h (55 mph) is shown in Figure 2. Finney (3) has shown that, for highway traffic, the dynamic loads are greater than the static weight by factors of 22-35, 35-42, and 42-65 percent in good, average, and poor pavement zones, respectively.

Figure 1. Idealized highway-railroad grade-crossing profile.

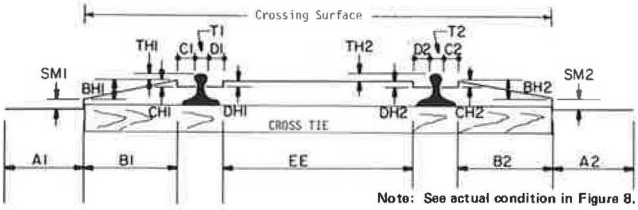

Roughness Index

This is defined as the ratio of the sum of the rear-axle excursions of a vehicle [in centimeters (or inches as recorded by a Mays Ride Meter)] to the distance it travels [in kilometers (miles)] (4). Mays Ride Meter readings are a measure of the serviceability of a pavement surface. A typical Mays Ride Meter chart for a grade crossing is shown in Figure 3, where x is the effective crossing length. The Mays Ride Meter reading is incorporated into the program DYMOL by using a simulated passenger vehicle. Figure 4 shows a correlation between actual and simulated values for pavement surfaces that have various serviceability indices for a 1972 passenger vehicle that was calibrated on the dates shown; the shift of the curve to the right indicates a change in the suspension characteristics of the vehicle. The computed relationship between the railroad track and the adjacent pavements is shown in Figure 5, in which the values of roughness index were generated by inputting parametric values of differential deformations to the DYMOL program.

Permanent Differential Deformation

Repetition of wheel loads causes permanent differential deformation between the railroad track and the adjacent pavement structures. As shown in Figure 6, a vertical deformation occurs at the interface between the track

Figure 2. Variation of dynamic wheel load of dump-truck rear axle: effect of geometry of grade-crossing profile at different amounts of differential deformation.

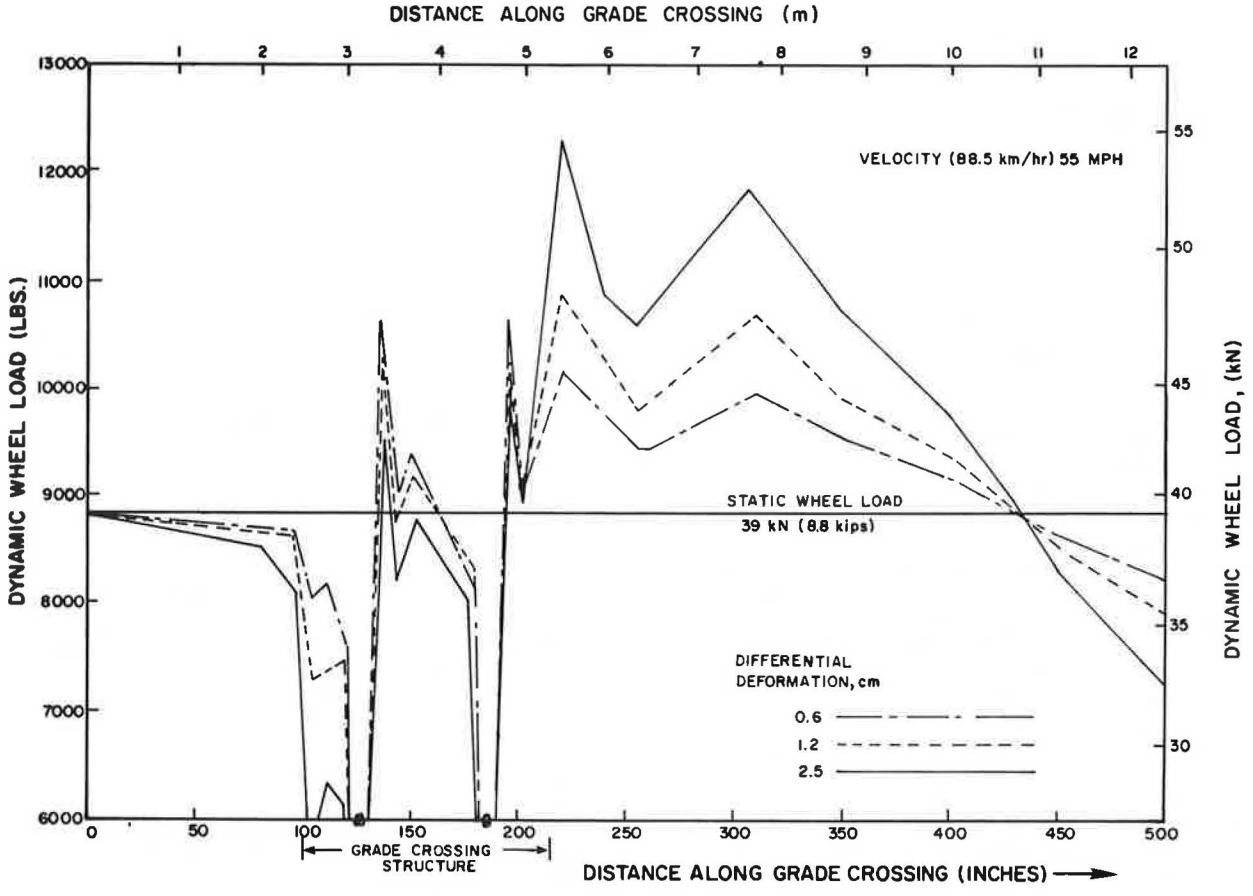

Figure 3. Typical Mays ride meter chart for grade-crossing profile.

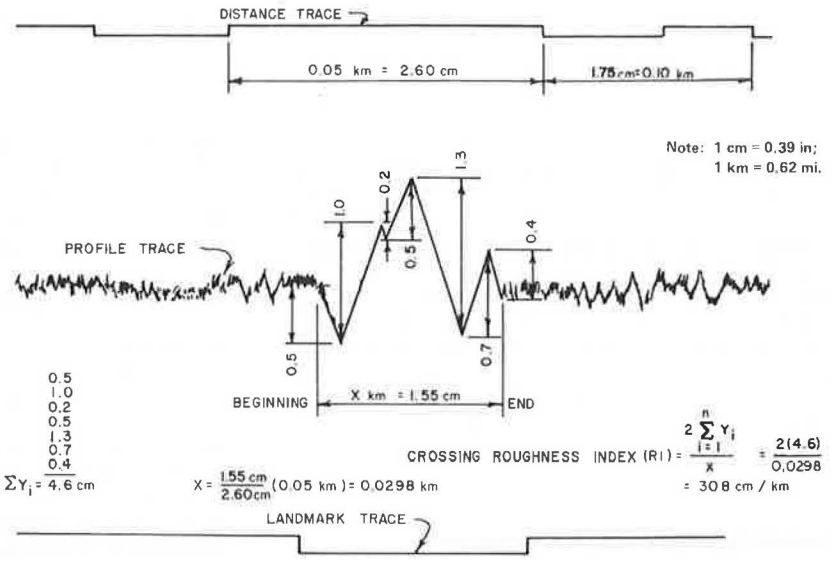

Figure 4. Correlation between actual and predicted Mays ride meter reading.

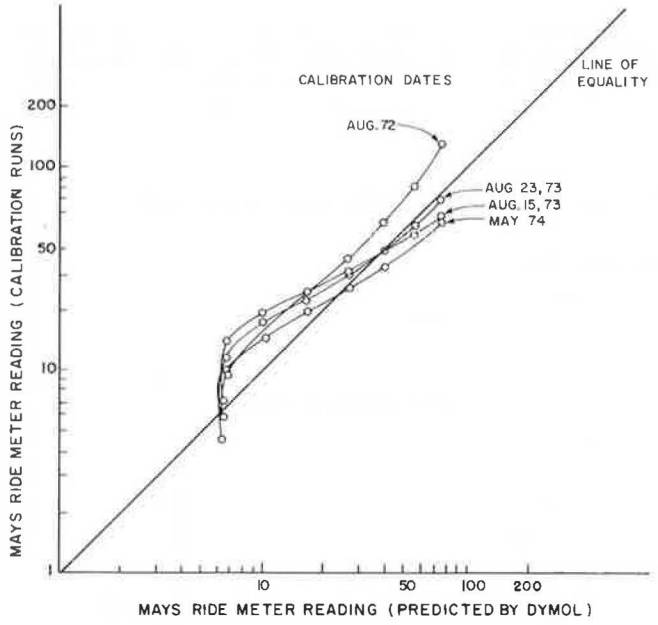

Figure 5. Relationship between roughness index and differential deformation of a grade crossing.

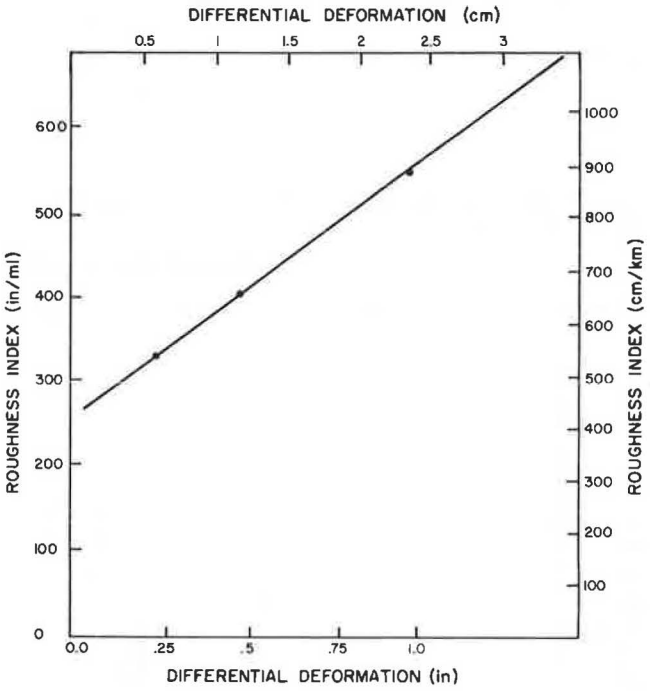

and the approach pavement, but the surface between the two rails deforms uniformly. This differential deformation causes roughness on the surface and, consequently, highway traffic produces a dynamic-load effect that increases as the differential deformation increases (see Figure 7). It should also be noted that a dynamic load decreases with speed; i.e., a given static weight produces a greater dynamic load at a speed of 48.3 km/h (30 mph) than at a speed of 88.5 km/h (55 mph). This is because dynamic load depends on the frequency response of the vehicle, which typically peaks at 1-2 Hz and again at frequencies higher than 10-12 Hz. Lytton and others (5) observed that maximum dynamic loads occur on a pavement surface with expansive clay roughness at vehicle speeds of 32-64 km/h (20-40 mph). The design limit of this criterion depends on the choice of the maximum-allowable dynamic load for highway traffic over a crossing, which will vary with the ridability requirements.

Thus, the following limiting design criteria were adopted:

1. Dynamic load—35-42 percent greater than the static weight,
2. Roughness index—660-760 cm/km (420-480 in/mile) (from Figure 5), and
3. Permanent differential deformation—1.4-1.9 cm (0.55-0.75 in) (from Figure 7).

Development of Polynomial Stress Equations

Because the permanent differential deformation mainly depends on the magnitude and repetition of stresses at different depths, calculation of the stress in the track

structure and the adjacent pavements is important in this design system. Several computer programs are available for calculating stresses in foundation layers, but most of them require long computation times and large memory cores. Thus, to calculate stresses at different depths rapidly, polynomial stress equations that require shorter computation times were developed separately for track and pavement foundations. These equations were developed by calculating stresses by using the BISTRO computer program and a variety of layer thicknesses and material properties, as shown in Table 1. A single 80-kN [18 000-lbf (18-kip)] axle load was used as a typical highway loading, and the axle loads and wheel spacings corresponding to a GE-V-50 locomotive were used as a typical railway loading. A computer program Select Regression (6) was used to obtain equations relating the computed stresses to the original independent variables (moduli and thicknesses).

The polynomial stress equations are given below:

$$\sigma = A0 \pm A1h \pm A2h^2$$
$$= f\,[A_i, (H_i)^{a^n}, (E_i)^{c^n}, (E_i)^{d^n}, (H_i)^{b^n}, (E_i)^{e^n}, h \ldots] \quad (1)$$

where

A_i = coefficients,
a^n, b^n, c^n, d^n, e^n = exponents,
E_i = initial tangent modulus,
H_i = thickness of layer, and
h = depth from surface.

Equations for major and minor principal stresses, deviation stress, and sum of principal stresses have been developed for the pavement and track foundations.

Figure 6. Highway-railroad grade crossing showing typical differential permanent deformation between railroad and adjacent pavement structures.

Figure 7. Effects of differential deformations of grade crossing and of vehicle speeds on dynamic wheel load.

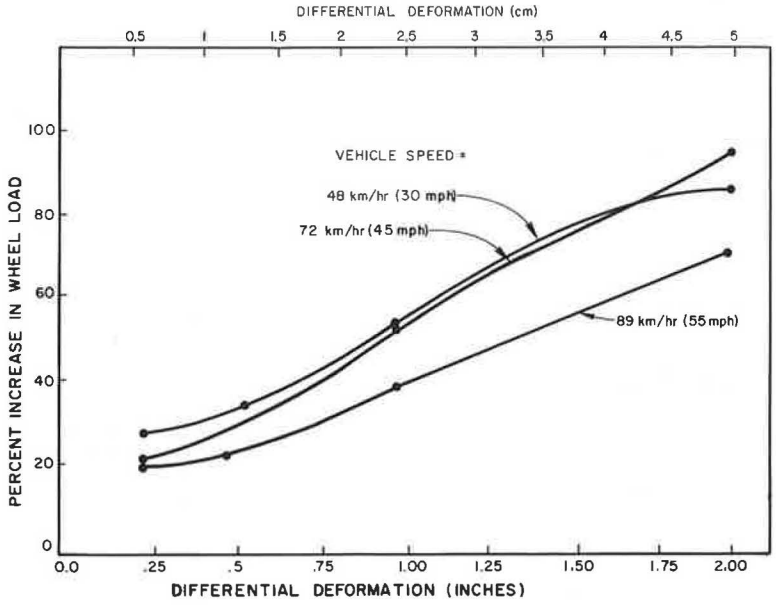

Table 1. Upper and lower limits of variables used in polynomial stress equations.

Item	Pavement Structure		Track Structure	
	Upper Limit	Lower Limit	Upper Limit	Lower Limit
H1 = thickness of surface layer (cm)	22.9	7.6	76.2	25.4
H2 = thickness of base layer (cm)	35.6	15.2	35.6	15.2
E1 = modulus of surface layer (MPa)	3620	517	2070	345
E2 = modulus of base layer (MPa)	793	103	793	103
E3 = modulus of subgrade (MPa)	172	34.5	172	34.5

Notes: 1 cm = 0.39 in; 1 MPa = 145 lbf/in^2.
Ties and ballast are considered to act together as a composite material in the surface layer of track structures. The dominant modulus in this composite material is that of the ballast.

These equations and a code listing are given elsewhere (7).

Effect of Dynamic Effect on Stresses

Irregularities in the riding surface interact with vehicle characteristics and speed to induce dynamic effects in vehicle loadings that may increase or decrease their static weight at a particular location. For highway traffic, a grade crossing is a source of surface irregularities. It has been observed that dynamic loads are produced by train movements at higher speeds (8), even though the rail surface is essentially smooth under train wheel loads. Therefore, it is important to include the dynamic effects of both highway and railway traffic in the stress calculations.

Highway Traffic

A newly constructed grade-crossing surface provides a smooth riding surface and, hence, low dynamic effects. The limiting value of the dynamic load will be reached with time and number of load applications. Therefore, an average increase of 20 percent above the static stresses was used in this design for the dynamic effect on the pavements adjacent to a grade crossing. Also, as illustrated in Figure 2, the increase in the dynamic load over a grade crossing is approximately half of that on the adjacent pavement surface. Therefore, a 10 percent increase in static stresses was incorporated for the dynamic effect of highway loads on the grade-crossing surface.

Figure 8. Rate of increase in rail stress relative to stress at 8 km/h.

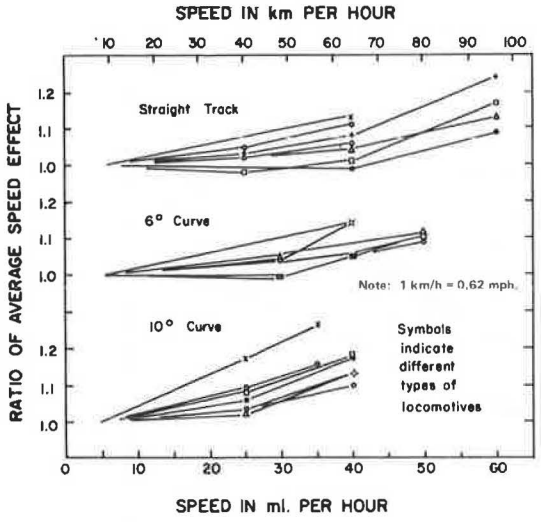

Railroad Traffic

Slight imperfections in the rail surface or in the wheel roundness, the lateral movement of the train, and such create dynamic loads that increase with train speed. Centrifugal forces, superelevation, turning forces, and such increase the dynamic effect on curves. Talbot (8) measured rail stresses for various locomotives and trains at varying speeds. The ratios of stresses at several speeds with respect to stress at 8 km/h (5 mph) are shown in Figure 8; the effect of curvature is obvious. For the design computations, a 15 percent increase in rail stress [straight track at 97 km/h (60 mph)], was selected from the figure to account for dynamic effects.

Design Technique

Because the stress equations and material characterization involve many terms, a computer program was written that calculates the stresses at different depths below the railroad track and adjacent pavement structures. Permanent deformations in each structure are calculated as a function of these stresses, the deformation characteristics of the materials, and the number of repetitions of wheel loads applied in a design period. The difference in these deformations (permanent differential deformation) serves as the design criterion. If this difference in deformations exceeds the permissible maximum limit (established on the basis of ridability need), the layer thicknesses and their material properties are revised and the analysis is repeated to estimate new values of differential deformation. This value is compared with the maximum permissible limit, and the process is continued until a suitable design is obtained. Figure 9 summarizes the design system.

MATERIAL CHARACTERIZATION FOR DESIGN APPLICATION

Analysis and design procedures for pavements and grade crossings are based on the determination of primary-response variables such as stresses, strains, and deflections at different locations in these structures. The variables are determined through the formulation and

Figure 9. Grade-crossing design system.

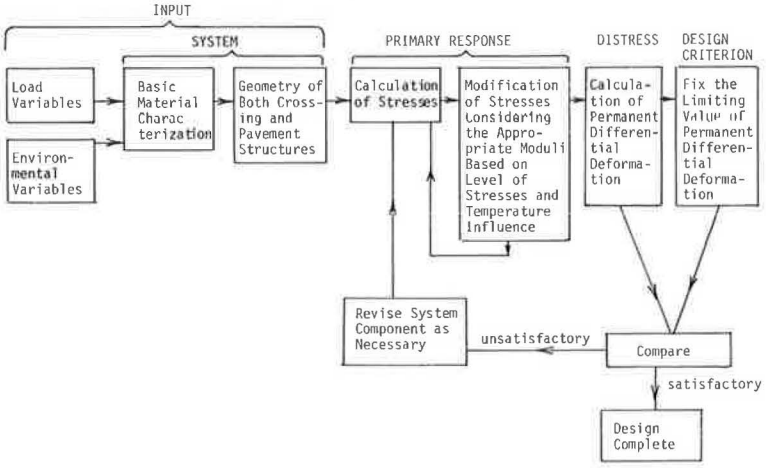

solution of boundary-value problems. In formulating the governing differential equation, the properties of the various materials are considered in the form of constitutive equations that describe the stress-strain relationship of the materials. In a complete design system, however, determination of the primary-response variables is not sufficient in itself; it is also necessary to establish limiting (failure) criteria in terms of these variables for the loading and environmental conditions. Excessive permanent deformation due to repetition of loads is taken as the failure criterion. Material characterization includes selection of the constitutive properties and definition of the failure criteria.

Surface Layer Materials

Ties and ballast combine to form a surface layer on which the rails rest. In a flexible pavement system, asphalt concrete is used as the surface layer.

The maximum downward deflection of a tie under load occurs below the outer edge of the rails. The pressure intensity along the length of the tie decreases as the distance from the rail increases and is a minimum at the midpoint and at both the ends. It is assumed that the total wheel load is transmitted by the tie to the ballast through an area directly under the rail and that the dimension of the area is equal to that of a tie plate.

The modulus of elasticity of timber ties is generally very high [10-14 $\times 10^3$ MPa (1 500 000 to 2 000 000 lbf/in^2)] compared with the moduli of the other layers (such as ballast, base course, and subgrade). Therefore, no material characterization of ties is considered here.

Ballast

Very little adequate research to characterize ballast material has been conducted up to the present time. Recently, however, Gaskin and Raymond (9) have published some work on the selection of railroad ballast in which their conclusions are based on a limited number of repetitive load tests. Hargis (10) has studied the strain characteristics of limestone gravel, typically used as base-course material in Texas. Because this material is similar to ballast material, it was used as a representative sample for ballast and its characteristic properties were used in this study.

The modulus of elasticity varies from 300 to 2000 MPa (50 000 to 300 000 lbf/in^2), depending on the condition and degree of compaction of the ballast layer, and generally increases with the number of load repetitions and the magnitude of load. Hargis has developed a regression model that predicts the permanent deformation in the material caused by variable stress levels and numbers of repetition of such stress.

Asphalt Concrete

The modulus of asphalt concrete is temperature dependent. It is important to use the modulus value that corresponds to the actual temperature, because a variation in modulus will greatly affect the level of stresses in the structure. Although the typical failure in an asphalt concrete layer is caused by fatigue, only permanent deformation due to repetition of load is considered as the design criterion in this procedure.

Base-Course Materials

Granular materials (treated or untreated) are commonly used in the base-course layers of both pavements and railroad tracks. A variety of such materials are in use at present that vary widely in their aggregate type, gradation, and constitutive representation. Comprehensive studies of these materials have been conducted by Smith and Nair (11), Hicks (12), Barksdale (13), and others.

Untreated Granular Base-Course Material

Hicks studied the time dependency of untreated granular materials to determine whether these materials should be characterized by elastic or by viscoelastic theory. He imposed stresses on these materials over a variety of time durations and found no significant influence on their resilient modulus values and Poisson's ratios. Creep-test results on untreated granular base and subbase materials used at the AASHO Road Test reported by Coffman and others (14) also showed no indication of time dependency in their characteristic properties. Thus, it appears that the constitutive representations of granular base course (untreated) materials can be adequately expressed by elastic theory. These studies also indicate that the resilient moduli of these materials are stress (especially confining) dependent. Dunlap (15), Mitry (16), Seed and others (17), and Barksdale (13) have reported significant increases in resilient modulus in granular materials with increase in confining stress.

Stress analyses in typical pavement systems show that small tensile confining stresses can be developed in the base-course layer. Heukelom and Klomp (18) suggest that the action of tensile confining stress causes local decompaction of the granular base, which results in a reduction of modulus. Hicks found that an untreated granular material in an unconfined condition can have a vertical modulus of elasticity of 34 MPa (5000 lbf/in^2) or more. Therefore, 34 MPa was considered as the lowest modulus value for a base-course material when subjected to a small tensile stress.

Deformations of granular base-course materials under a single application of load are completely recoverable. However, a large number of such load applications causes permanent deformation in the material. Permanent deformation increases as degree of saturation increases, which indicates the importance of proper drainage. Barksdale studied the permanent deformation on several untreated granular materials. He found that a hyperbolic stress-strain representation, analogous to that used by Duncan and Chang (19) to describe static triaxial tests, can be used to describe the relationship between cycled stress and permanent strain.

In design, it is necessary to know the magnitude of permanent deformation corresponding to a large number of load applications. An equation was developed from Barksdale's data to predict the growth of such deformation for a large number of load applications from known data corresponding to a lower number of load applications. The permanent deformation accumulates approximately logarithmically with the number of load applications, and the rate of accumulation of such deformation is increased by an increase in magnitude of deviator stress.

Asphalt-Treated Granular Base-Course Material

Asphalt-treated granular base-course (ATB) materials are commonly used as flexible-pavement base. There is only a limited amount of published information available regarding the constitutive properties of ATB materials. Smith and Nair found that the constitutive properties of ATB materials are dependent on both temperature and time (duration of load), which requires the use of viscoelastic theory to represent them. However, elastic constitutive representations for these materials can be used and the temperature and time effects ac-

Table 2. Calculated deformations: example problem 1.

Type of Structure	Type of Loading	No. of Load Applications	Deformation (cm)			Total Deformation (cm)
			Top Layer	Second Layer	Subgrade	
Highway pavement	Highway traffic	1 000 000		0.04	0.45	0.49
Railroad track	Railway traffic	1 000 000	2.49	0.06	0.54	3.09
	Highway traffic	1 000 000	0.69	0.02	0.23	0.94

Note: 1 cm = 0.39 in.

Table 3. Calculated deformations: example problem 2.

Type of Structure	Type of Loading	No. of Load Applications	Deformation (cm)			Total Deformation (cm)
			Top Layer	Second Layer	Subgrade	
Highway pavement	Highway traffic	1 000 000		0.21	0.94	1.15
Railroad track	Railway traffic	1 000 000	3.93	0.300	0.55	4.78
	Highway traffic	1 000 000	1.07	0.11	0.30	1.48

Note: 1 cm = 0.39 in.

counted for through the selection of appropriate constitutive values. The elastic material properties must first be defined over the range of temperatures and load durations of interest, and then the values of such parameters must be selected for applicable temperature and load duration.

A thick layer of ATB material will also accumulate some amount of permanent deformation due to the repetition of loads, but this deformation will be very small compared with that in untreated granular base-course materials (due to their higher modulus values and compressive strength). Asphalt treatment causes granular base-course materials to develop a cohesive force. Goetz and Schaub (20) found that, with an increase in asphalt content, the angle of internal friction decreased sharply and at an almost constant rate and the cohesive value increased to a maximum value at about 4 percent asphalt and then decreased. At present, no mathematical model for predicting the permanent deformation characteristics of asphalt-treated material is available, so it was assumed that the same deformation law used for untreated base-course material can also be used for ATB materials.

Subgrade Materials

The capacity of the subgrade support affects the structural design of pavements and other structures. Usually, subgrade materials are composed of fine-grained sand and silt and clay fractions that have a high plasticity index. The strength and performance of such materials are greatly affected by environmental factors such as temperature, moisture balance, drainage, and such. Edris (21) has conducted a comprehensive study of subgrade materials from different climatic zones in Texas. These materials had clay contents ranging from 20 to 70 percent. He developed regression equations for the resilient modulus and permanent deformation of these materials and also temperature-correction factors. In these equations, two factors—number of load applications and soil suction—were most important. Other factors that enter are degree of saturation, volumetric moisture content, volumetric soil content, deviator stress, confining stress, and mean principal stress. These equations were used for the design calculations.

To determine the effect of temperature on resilient modulus and permanent strain, factors other than temperature (such as number of load cycles, deviator stress, and soil suction) were also considered. A reference state—temperature of 22.2°C (72°F), 10 000 load cycles, a 94.5-kPa (13.7-lbf/in^2) deviator stress, and soil suction corresponding to a moisture content of 2 percent dry of optimum—was used to determine the ratios of the above factors. These ratios were used to determine the temperature-correction factor for resilient modulus and permanent strain. The actual values of resilient modulus and permanent deformation of a subgrade at a particular temperature can be determined by multiplying their predicted values at 22.2°C by their corresponding temperature-correction factor.

Design Examples

The first step of the design procedure is to determine the amount of traffic that is to be served by the grade crossing. The railroad track must carry both the railway and highway wheel loads, whereas the adjacent highway pavement carries only the highway wheel loads. [The standard highway and railway wheel loads used in this design are described by Ahmad (22).] The second step involves fixing the layer thicknesses of each structure (railroad track and adjacent pavement). The third step is the selection of materials for each layer, which requires careful consideration of resilient modulus and permanent deformation characteristics. In the fourth step, temperature, suction, and clay-content information is input into the computer program to calculate the differential deformation between the railroad track and the adjacent pavement structure. Limits are placed on the values of some of the variables to ensure that all calculated results stay within a reasonable range of values.

Example Problem 1

The following input information is assumed: the average temperatures in the top layer, the base course, and the subgrade are 32.2°C, 29.4°C, and 22.2°C (90°F, 85°F, and 72°F), respectively; the number of repetition of wheel loads (required to serve a design period) is considered to be 1 000 000 for both highway and railway traffic; and the base course under both highway and railroad is to be asphalt treated. The layer thicknesses and the material characteristics to be used are given below

(1 cm = 0.39 in and 1 kPa = 0.145 lbf/in^2).

Item	Value
Top layer of track (ballast)	
Thickness (cm)	46
Resilient modulus (MPa)	345
Top layer of pavement (asphalt concrete)	
Thickness (cm)	10
Resilient modulus at 32.2°C (MPa)	2400
Second layer of both	
Thickness (cm)	
Resilient modulus at 19.4°C (MPa)	830
Cohesion (kPa)	172
Angle of internal friction (°)	45
Subgrade of both	
Initial estimate of resilient modulus (MPa)	100
Clay content (%)	30
Suction level for 70 percent clay content (kPa)	190

The calculated deformations in each layer in the track and the highway pavement are shown in Table 2; the calculated differential deformation is 3.54 cm (1.39 in). It should be noted that the railroad track deformed more than the highway pavement and that the major portions of the deformations were, as expected, in ballast and subgrade materials. The differential deformation of 3.54 cm is unacceptable (see Figure 7), according to the criterion established above.

Example Problem 2

The input information for this example problem is identical to that for example problem 1, except that the unstabilized base course described below is used.

Item	Value
Thickness (cm)	30
Resilient modulus	15 000 x (confining pressure)$^{0.5}$
Cohesion (kPa)	0
Angle of internal friction (°)	50

The calculated layer deformations are shown in Table 3; the differential deformation is 5.11 cm (2.01 in). As can be seen, the ballast and the subgrade under the railroad deformed more than in example problem 1 and, due to higher stresses in the subgrade, the pavement also deformed more. Thus, the differential deformation is again greater than the acceptable limit.

Because neither solution meets the established criterion, the next experiment would involve placing a stabilized base beneath the track structure and an unstabilized base in the highway pavement structure. Then, trial depths would be selected for each layer until the permanent deformation of the two structures approached each other within the acceptable limit.

Lighter traffic than that used in these problems will require lighter crossing designs, but the same attention must be given to the subgrade soil.

In a location that has good drainage conditions and a low water table, the suction level in the subgrade will be controlled by the climate (7). However, this value can be varied according to the expected drainage or water-table condition in the particular area of interest.

CONCLUSIONS

A unique design criterion of the differential deformation between the railroad pavement and the adjacent pavement structures is proposed for the design of a highway-railroad grade crossing. Actually, the differential deformation produces a dynamic load in highway traffic that gradually causes loss of ridability and total grade-crossing failure. Differing structural dimensions in railroad track and the adjacent highway pavements and selection of different construction materials can increase or decrease the differential deformation. However, the individual deformations in each layer are also important design parameters. A design may look promising from the point of view of the differential deformation criterion, but it should be rejected if deformation in any individual layer is large.

The effects of environmental factors on subgrade materials are included in the design program. Because of this, this design system can be used effectively to find the most-effective ballast depth for different climatic and soil conditions. By using this design system, the performances of currently available commercial crossing materials can be predicted.

REFERENCES

1. W. J. Hedley. State of the Art on Rail-Highway Grade Crossing Surfaces. Federal Highway Administration, 1973.
2. A. Ahmad and R. L. Lytton. Computation of Dynamic Loads at Grade Crossings: A User's Manual of the Computer Program. Texas Transportation Institute, Texas A&M Univ., College Station, Res. Rept. 164-2, Jan. 1976.
3. E. A. Finney. Better Concrete Pavement Serviceability, 1st Ed. American Concrete Institute, Monograph 7, 1973.
4. T. M. Newton, R. L. Lytton, and R. M. Olson. Structural and Geometrical Characteristics of Highway-Railroad Grade Crossings. Texas Transportation Institute, Texas A&M Univ., College Station, Res. Rept. 164-1, Aug. 1975.
5. R. L. Lytton, R. L. Boggess, and J. W. Spotts. Characteristics of Expansive Clay Roughness of Pavements. TRB, Transportation Research Record 568, 1976, pp. 9-23.
6. D. A. Dubose. Variable Selection Procedure: Implementing the Hocking-LaMotte-Leslie Method. Institute of Statistics, Texas A&M Univ., College Station, Nov. 1970.
7. A. Ahmad, R. L. Lytton, and R. M. Olson. An Analysis and Design Procedure for Highway-Railroad Grade Crossing Foundations. Texas Transportation Institute, Texas A&M Univ., College Station, Res. Rept. 164-4F, Nov. 1976.
8. A. N. Talbot. Stresses in Railroad Track: Fourth Progress Report of the Special Committee on Stresses in Railroad Track. Proc., AREA, Vol. 26, 1925, pp. 1081-1245; Trans., ASCE, Vol. 88, 1925.
9. P. N. Gaskin and G. P. Raymond. Contribution to Selection of Railroad Ballast. Transportation Engineering Journal, Proc., ASCE, Vol. 102, No. TE2, May 1976, pp. 377-394.
10. L. L. Hargis. A Study of Strain Characteristics in a Limestone Gravel Subjected to Repetitive Loading. Texas A&M Univ., College Station, M.S. thesis, 1963.
11. W. S. Smith and K. Nair. Development of Procedures for Characterization of Untreated Granular Base Course and Asphalt-Treated Base Course Materials. Federal Highway Administration, Rept. FHWA-RD-74-61, Oct. 1976. NTIS: PB 239 839/4SL.
12. R. G. Hicks. Factors Influencing the Resilient Properties of Granular Materials. Univ. of California, Berkeley, Ph.D. thesis, 1970.

13. R. D. Barksdale. Laboratory Evaluation of Rutting of Base Course Materials. Georgia Highway Department, Atlanta, 1972.
14. B. S. Coffman, D. G. Kraft, and J. Tamayo. A Comparison of Calculated and Measured Deflections for the AASHO Road Test. Proc., AAPT, 1964, pp. 54-91.
15. W. A. Dunlap. A Report on a Mathematical Model Describing the Deformation Characteristics of Granular Materials. Texas Transportation Institute, Texas A&M Univ., College Station, Res. Rept. 27-1, 1963.
16. F. G. Mitry. Determination of Modulus of Resilient Deformation of Untreated Base Course Materials. Univ. of California, Berkeley, Ph.D. thesis, 1964.
17. H. B. Seed, F. G. Mitry, C. L. Monismith, and C. K. Chan. Prediction of Flexible Pavement Deflections from Laboratory Repeated Load Tests. NCHRP, Rept. 35, 1967, 117 pp.
18. W. Heukelom and A. J. G. Klomp. Dynamic Testing as a Means of Controlling Pavements During and After Construction. Proc., 1st International Conference on Structural Design of Asphalt Pavements, Ann Arbor, MI, 1962, pp. 667-679.
19. J. M. Duncan and C. Y. Chang. Nonlinear Analysis of Stress and Strain in Soils. Journal of the Soil Mechanics and Foundations Division, Proc., ASCE, Vol. 96, No. SM5, Sept. 1970, pp. 1629-1654.
20. W. H. Goetz and J. H. Schaub. Triaxial Testing of Bituminous Mixtures. ASTM, Special Tech. Publ. 252, 1959.
21. E. V. Edris. Dynamic Properties of Subgrade Soils, Including Environmental Effects. Texas A&M Univ., College Station, M.S. thesis, 1976.
22. A. Ahmad. Analysis and Design Procedure for Highway-Railroad Grade Crossings. Texas A&M Univ., College Station, Ph.D. dissertation, Dec. 1976.

Publication of this paper sponsored by Committee on Mechanics of Earth Masses and Layered Systems.

Assessment of Hybrid Model for Pile Groups

Michael W. O'Neill and Osman I. Ghazzaly, Department of Civil Engineering, University of Houston, Texas
Ho-Boo Ha, Lawrence Allison Associates, Houston, Texas

The effects of mathematical modeling of pile groups by representing the soil response against the piles through unit-soil-resistance relationships for isolated piles and using elasticity methods to account for group effects were studied by modeling three pile-group tests in clay reported in the literature. Emphasis is placed on the effect of varying the Young's modulus of the soil surrounding the piles and the effects of imperfect pile alignment. The errors in computed cap translation were small; and the errors in load distribution to piles and the axial load distribution along the piles were insignificantly affected by the value of the modulus and could not be eliminated by this modeling method.

Mathematical modeling of pile groups is usually conducted with one or more of the following objectives:

1. Determination of the load-settlement behavior of the group as a whole for use in a superstructure analysis,
2. Calculation of the stresses within the piles to assess their structural integrity, and
3. Determination of the ultimate capacity of the group.

This paper is concerned with deterministic mathematical models that are addressed mainly to the first two objectives.

The objectives of this paper are

1. To demonstrate a concept that permits modeling of group effects in groups that have arbitrary geometries and six degrees of freedom at the pile cap,
2. To investigate the effects of the choice of assumed elastic parameters to represent the soil between and around the piles on the response of pile groups in clay, and
3. To investigate the effects of pile alignment on computed response.

The latter effects have been studied by modeling three well-documented load tests.

MATHEMATICAL MODELS

An ideal model is one that incorporates the nonlinear behavior of piles and soil, large deformations, the three-dimensional geometry and structural flexibility of the piles, and the effects of pile installation on the properties of the soil. Such a model is beyond the current state of the art, although reasonable attempts at modeling pile groups by using finite-element representations have been made (1, 2). More practically, static equilibrium models that represent piles as linear or nonlinear springs attached to a rigid or flexible cap have been used to model groups having more than one degree of freedom (3, 4). Groups having one or more uncoupled degrees of freedom have been modeled by techniques that envision piles as discrete-element elastic bodies embedded in an elastic-solid soil mass (5-7). The principal consideration in any of these models is the means of defining pile-soil interaction (e.g., the form of the spring relationships at the cap in the cap-spring model). In the cap-spring model, the effect of pile-soil interaction can be approximated in the working-load range by representing the piles as equivalent columns and cantilevers (4). More-precise analysis requires that pile-soil interaction be modeled more fundamentally. This can be done by modeling each individual pile as a discrete-element elastic body (8, 9) that is supported by independent, non-

linear axial, lateral, and torsional unit soil-reaction springs, whose properties can be obtained from published criteria developed for single piles in various soils. Unit soil-reaction relationship criteria include axial criteria (8, 10, 11), lateral criteria (12, 13), and torsional criteria (14).

In the elastic-solid model, pile-soil interaction in axial, lateral, and torsional loading is considered by means of elasticity theory (which has obvious limitations). This approach has the advantage that it considers the effect of load transferred from one discrete pile element to the soil on the load-deformation behavior at other elements directly. This effect is considered only indirectly (through use of criteria based on load tests where the effect occurred) in models that use unit soil-reaction curves. However, it is possible to track the complete nonlinear behavior of soil reaction by using unit-soil-reaction curves, whereas the use of elasticity theory to represent pile-soil interaction (even where modified to account for slippage at the pile-soil interface) gives a less-precise response.

The cap-spring model is incapable of considering pile-soil-pile interaction (group action) except by difficult, and often empirical, manual adjustment of the pile-head-spring relationships to account for assumed softening or stiffening effects in the various modes of loading.

Focht and Koch (15) have proposed a rational, approximate model for consideration of group action in groups of laterally loaded vertical piles that allows the use of unit-soil-resistance relationships in geometrically simple groups. This model can be classified as a hybrid model, because it combines salient features of elastic-solid and of cap-spring models. In essence, the hybrid model first uses unit-soil-reaction curves to represent the behavior of individual piles and then uses elastic methods to modify those curves for group action, based on the soil reactions against the piles computed in a noninteractive analysis (without consideration of group action). This concept has been extended to three-dimensional pile groups by O'Neill and others (16) by using several important algorithmic modifications. The hybrid model is a rational and reproducible way to model significant pile-soil interaction effects (including gap zones behind laterally loaded piles, soil degradation due to the cyclic loading, and nonlinear soil response) that are difficult to model by elasticity methods alone.

Figure 1. Modification of unit-soil-resistance curve at element on generic pile.

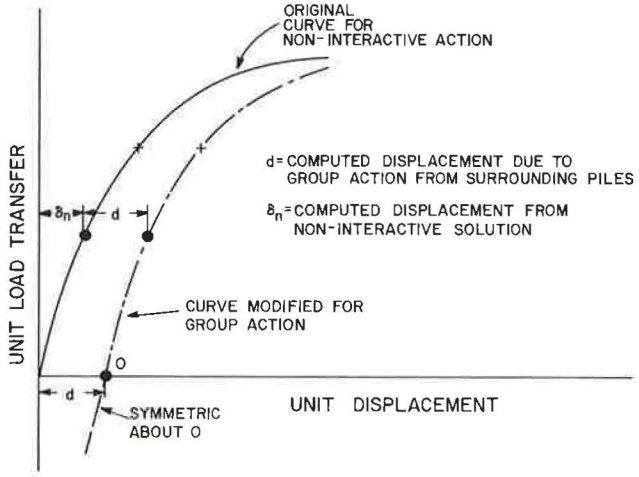

Figure 2. General flow diagram for hybrid algorithm.

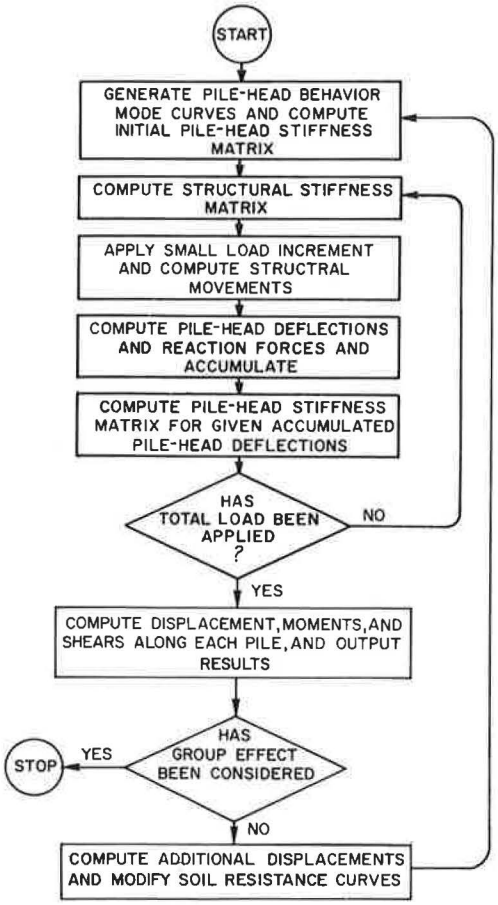

MECHANICS OF HYBRID MODEL

The basic mechanics of the hybrid model are described in detail elsewhere (16) and are reviewed only briefly here. First, a noninteractive solution is made by using a nonlinear cap-spring model (3) that includes nonlinear cap-support spring relationships for the component piles obtained by modeling them as independent discrete-element bodies supported by nonlinear unit-soil-reaction springs. The soil reactions along all piles in the system are obtained from this solution. Then, pile-soil-pile interaction is considered by applying corrections to the unit-soil-reaction curves used in the noninteractive analysis (see Figure 1). This is accomplished for a generic pile by computing added displacements in three dimensions due to soil loads imposed from all other piles in the soil at the centers of the discrete elements along the generic pile. The added displacements are obtained from Mindlin's equations for displacement (7). The displacements so obtained are then transformed into displacements parallel and perpendicular (in two orthogonal directions) to the pile axis, and these are applied as offsets to the unit-soil-reaction curves. That is, group effects are accounted for by displacing the unit-soil-resistance curves for individual piles at various nodes along a pile an amount equal to the displacement that would have occurred in the soil mass at the node had the pile not been present but had the surrounding piles produced soil reactions identical to those obtained in the noninteractive analysis. It is assumed that the piles are spaced at a distance such that the added displacements are essentially elastic in nature.

The modified soil-reaction relationships are input back into the model used in the noninteractive analysis,

and the entire solution is repeated, yielding a new set of displacements and loads at the pile heads and stresses and soil reactions along the piles that more nearly equal those in the real system. Progressively better solutions can be obtained through iteration. The analyses described below are those obtained after only one sequence of corrections. A general flow diagram of the computational scheme is shown in Figure 2.

The chief limitations of the current version of the hybrid model (although not limitations to the concept of hybrid analysis) are that (a) the interference of piles between an active pile (one whose soil loads are used to compute added displacements at a generic pile) and the generic pile is not directly considered; (b) if the elastic modulus of the soil mass varies with depth, pile-soil-pile interaction can be approximated only; (c) the pile cap is rigid and receives insignificant support from the subgrade; and (d) true ultimate capacity (plunging load) is constrained to be the sum of the ultimate capacities of the individual piles. The use of the model to predict pile-group response is most successful when pile installation does not produce significant changes in the in situ stress-strain properties of the soil mass, as would occur, for example, for a displacement pile group in initially loose sand.

The hybrid model is therefore nonrigorous because of the superposition of elastic displacements on nonlinear displacements obtained from unit soil-resistance relationships, but it is an efficient and practical systematic way to consider group action in three-dimensional pile groups.

EFFECT OF VARIABLES

The user selects the modulus of the soil for representation of group action independent of the soil properties implied for individual pile behavior. This permits mitigation (to some degree) of the well-known limitation of pile reinforcement of the elastic halfspace that represents the soil. The input modulus of the soil thus becomes a modulus for reinforced soil, which can best be evaluated by correlating computed results with field measurements. Such a process is not possible with the elastic-solid model.

It remains to evaluate the elastic modulus for use with the hybrid model. The effect of the modulus has been studied by using the following methodology.

1. Three well-documented load tests on two full-scale test groups in clay were modeled. The soils at the two test sites were similar: CL clays having a thin layer of desiccated soil overlying a softer, slightly preconsolidated soil. The pile tips floated at one site and were driven to rock at the other. The tests included a vertical load test on one group and a lateral and a combined lateral-vertical load test on the other.
2. For both test groups, single piles were tested separate from the group tests in the axial or lateral modes or both. The individual piles were modeled independently before the hybrid analysis was conducted by using unit-soil-reaction curves from published criteria and then adjusting the curves to produce computed load-deformation responses compatible with the measured responses in the single piles. The adjusted unit-soil-reaction curves were then used for each pile in the group analysis. Differences in calculated and measured group responses therefore should be strongly dependent on the choice of elastic modulus, which is the primary variable being investigated. All piles were divided into 50 discrete elements.
3. The groups were modeled by varying the Young's modulus of the soil mass while holding Poisson's ratio at a constant value representative of undrained conditions. Modeling was also conducted without considering group action. The results from the model were compared with measured values, where measured values were available, to assess the effects of varying the modulus and of neglecting pile-soil-pile interaction.
4. In each analysis, the modulus was related to the reported undrained cohesion of the soil as obtained by conducting Q-type compressive-strength tests on samples obtained by using routine sampling techniques, which result in partial disturbance of the samples.

One of the test groups was asymmetric due to pile drift that had occurred during driving. By modeling this group in its ideal geometric configuration and in its as-driven configuration, it was possible to investigate the effects of deviation from ideal geometry on the behavior of the group.

Test Group 1

Schlitt (17) has reported a vertical load test on a square group of nine friction piles in clay. Although the piles were nominally plumb and the load was applied only vertically, the test was modeled in three dimensions because one corner pile was driven to a depth considerably greater than the remaining piles, causing the pile-head surface to tilt during loading and produce lateral reactions against the piles. The group geometry and site conditions are shown in Figure 3.

The piles were of the Monotube type, with butt diameters of 30.5 cm (12 in) and tip diameters of 20.3 cm (8 in). Load was applied to the group by jacks resting on an I-beam cap placed across the pile heads.

The profile of undrained cohesion of the clay is suggestive of slightly overconsolidated soils at a depth greater than 6 m (20 ft) below the ground surface and having more highly overconsolidated clay nearer the surface. Because in situ stress-strain data were not available for the test site, correlative methods were used to obtain the modulus (E) of the in situ soil. Ladd (18) implies that the secant modulus of undisturbed, normally consolidated clay at a stress level of 20 percent of failure in undrained triaxial shear is approximately 550-1000 times the undrained cohesion. It was assumed for purposes of modeling that the soil mass would be disturbed but would reconsolidate during the installation process to a condition near, but degraded from, the in situ condition and that the reinforcement effect of the piles would return the effective modulus to near its in situ value. Soil samples had been obtained by using tube samplers with an 18 percent area ratio and tested in Q-type triaxial compression. Because most of the soil was only slightly overconsolidated, the modulus of the soil mass was chosen within the range suggested by Ladd. One analysis was conducted at E = 23 100 kPa (3350 lbf/in^2) (570 times the average undrained cohesion of the soil from the surface to the pile tips), and one was conducted at E = 34 500 kPa (5000 lbf/in^2) (850 times the average measured undrained cohesion). A Poisson's ratio of 0.48 was used in both analyses.

The unit axial soil-resistance curves for modeling isolated pile behavior were developed by using the criteria of Vijayvergiya (11) (with lambda correlation), and the unit lateral and torsional curves were developed by using the criteria described by Reese and others (13) and by Dutt (14). Tip resistance was neglected.

The precise form of the unit axial soil-resistance curves was varied until the computed load-settlement behavior of the isolated test pile (pile 1) reasonably matched the measured behavior under initial test loading. The unit-resistance (f versus s) curves obtained from the

Figure 3. Physical arrangement: test group 1.

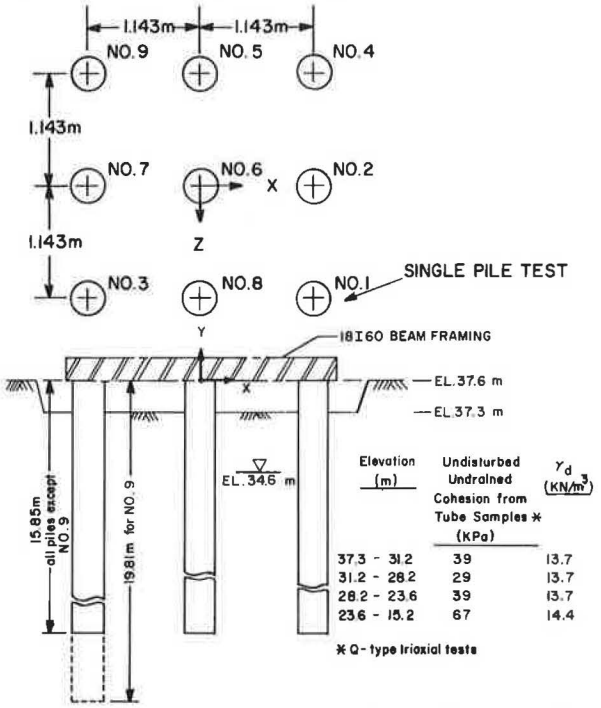

NOTE : 1 m = 3.28 ft, 1 kPa = 0.145 lbf/in^2 , 1 kN/m^3 = 6.37 lbf/ft^3

Figure 4. Axial unit-soil-resistance curves: test group 1.

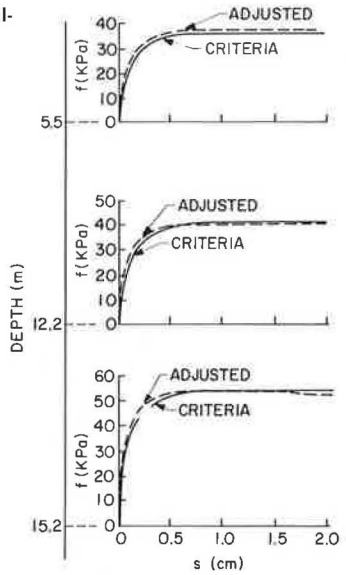

NOTE : 1 m = 3.28 ft, 1 cm = 0.394 in, 1 kPa = 0.145 lbf/in^2

criteria and those that were needed to replicate measured behavior are shown in Figure 4. The measured and computed load-settlement curves are shown in Figure 5, in which comparison to an immediate-reload test is also shown. Adjusted relationships were used. Computed settlements were somewhat too large for the immediate reload, possibly due to rebound effects in the test pile.

After pile 1 was tested, the remaining piles were driven and the group loaded to about one-half of the predicted failure load and unloaded. The group was then loaded a second time in increments to a load exceeding

Figure 5. Load-settlement curves for single pile: test group 1.

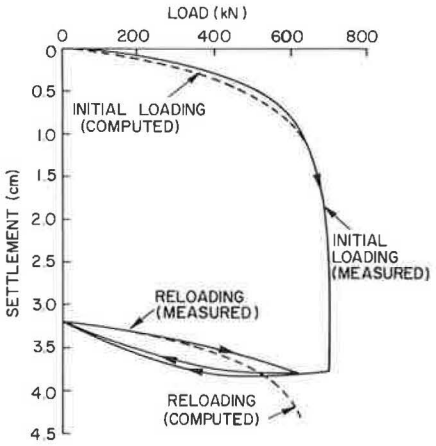

Note: 1 cm = 0.394 in; 1 kN = 225 lbf.

the required failure load. The second loading was modeled for applied loads of approximately one-third and two-thirds of predicted failure by using the adjusted unit-soil-reaction curves for initial loading, which are more appropriate than those for reloading of the single pile because the group was not failed during the first loading. Measured and computed pile-head loads and settlements are tabulated in Table 1. Measured and computed load-transfer relationships are compared for the center pile (6) and for an edge pile (7) in Figure 6 for E = 850 times undrained cohesion.

The effects of the choice of E on the computed distribution of loads to pile heads, group settlement, and validity of pattern of load transfer are described in Table 2. For distribution of load, the ratio of the SDs of the differences in computed and measured loads to mean pile-head load was selected as a measure of the accuracy of the model. For settlement, the effect of E is expressed by the percentage error of the difference between the computed and the measured mean pile-head deflections. For load-transfer pattern, the effect of E is expressed as the percentage error of the mean load transferred from pile to soil in the upper 9.2 m (30 ft) of embedment.

The variations in the measured load on the pile heads may be caused by (a) slight asymmetric positioning of load jacks coupled with the use of a flexible cap, (b) unknown variations in soil properties over the site, or (c) slight variations from the intended pile alignment that were not reported and hence are not modeled.

Pile 6, the middle pile, was the pile most affected by the flexibility of the cap, which led to a measured load greater than the modeled load. As shown in Figure 6, the greatest differences in computed and measured load transfer occurred near the top of the pile, where additional pile-head settlement due to dishing of the cap would have forced transfer of the excess load in a flexible pile.

The effects of E for this test can be summarized as follows: (a) the prediction of group settlement was significantly better when pile-soil-pile interaction was considered, particularly where E = 850 times the undrained cohesion, (b) the inclusion of pile-soil-pile interaction improved the prediction of distribution of load to pile heads only slightly, and (c) the inclusion of pile-soil-pile interaction did not improve predictions of load-transfer relationships within the group. There were

Table 1. Individual pile-head loads (settlements): test group 1.

	Group Load = 2427 kN								Group Load = 4199 kN							
	Measured		Model Results						Measured		Model Results					
			E = 34 500 kPa		E = 23 100 kPa		E = ∞[a]				E = 34 500 kPa		E = 23 100 kPa		E = ∞[a]	
Pile No.	Load (kN)	Settlement (cm)	Load (kN)	Settlement (cm)	Load (kN)	Settlement (cm)	Load (kN)	Settlement (cm)	Load (kN)	Settlement (cm)	Load (kN)	Settlement (cm)	Load (kN)	Settlement (cm)	Load (kN)	Settlement (cm)
1	267.0	0.48	290.90	0.46	295.88	0.58	269.94	0.20	529.6	0.99	513.98	1.04	532.40	1.42	467.70	0.41
2	345.3	0.48	261.66	0.46	260.55	0.56	269.71	0.20	562.5	1.04	452.65	1.02	439.30	1.37	466.81	0.41
3	262.5	0.36	279.26	0.43	279.53	0.56	269.54	0.20	405.0	0.81	492.66	1.02	494.95	1.32	465.96	0.38
4	290.1	0.51	279.26	0.43	279.53	0.56	269.54	0.20	502.0	1.07	492.66	1.02	494.95	1.32	465.96	0.38
5	186.9	0.51	250.80	0.43	245.64	0.53	269.31	0.18	364.0	1.02	413.81	1.02	406.18	1.27	465.11	0.38
6	331.1	0.56	248.09	0.43	243.94	0.56	269.54	0.20	491.3	1.17	406.86	1.02	404.06	1.32	465.11	0.38
7	224.3	0.43	250.80	0.43	245.64	0.53	269.31	0.18	365.8	0.89	413.81	1.02	406.18	1.27	465.11	0.38
8	192.2	0.48	261.66	0.46	260.55	0.56	269.71	0.20	401.4	0.91	452.65	1.02	439.30	1.37	466.81	0.41
9	327.5	0.36	304.60	0.43	315.77	0.51	270.43	0.18	577.6	0.71	559.94	1.02	581.70	1.22	469.60	0.38
Total	2427		2427		2427		2427		4199		4199		4199		4199	
Avg		0.46		0.44		0.56		0.20		0.97		1.02		1.32		0.39

Note: 1 kN = 225 lbf; 1 kPa = 0.145 lbf/in^2; 1 cm = 0.39 in.
[a] I.e., pile-soil-pile interaction is neglected.

Figure 6. Measured and predicted axial load distribution: test group 1.

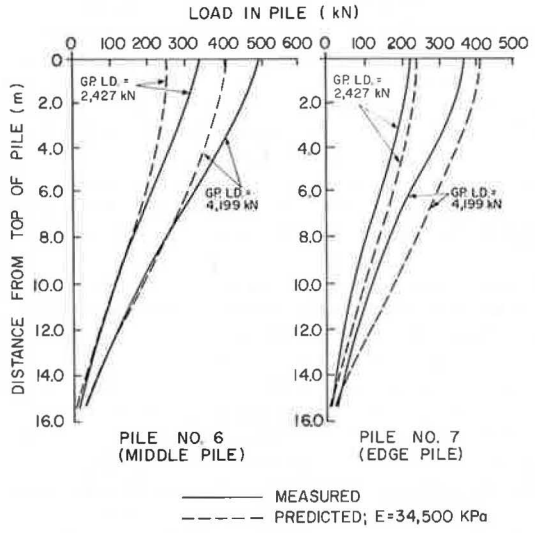

Note: 1 m = 3.28 ft; 1 kN = 225 lbf.

minor differences in these effects when the load level was varied.

Test Group 2

A group of H-piles has been tested by Kim and others (19) by a procedure in which lateral load was first applied and then lateral and vertical loads were applied simultaneously. The group is illustrated in Figure 7, which shows the planned configuration of the piles and the actual configuration as driven. The loads L (lateral) and A (vertical) were representative of working-load values. Soil conditions at the site consisted of overconsolidated clay to clay loam to a depth of 4 m (13 ft) and slightly overconsolidated clay and clay loam with gravel layers from 4.0 to 10.7 m (13 to 35 ft) underlain by limestone. The undrained cohesion values were determined as described above for test group 1.

Unit f-versus-s curves for isolated piles were developed as described above for test group 1 by assuming fixity of the tip in the limestone. Unit lateral resistance curves (p versus y) and torsional curves were obtained from Reese and others (13) and from Dutt (14). The axial and lateral curves are shown in Figure 8, from which axial and free-head lateral load-deformation curves were developed. The curves were then adjusted to produce pile-head load-deformation curves in the axial and lateral modes identical to the curves measured from the initial loading of isolated piles in these modes. Based on the reported cohesion values and the fact that most of the soil was not heavily overconsolidated, the following ratios of E to undrained cohesion were selected for modeling purposes: 250 and 750 with respect to cohesion of the surface layer (c_{s_L}), which may be more appropriate for a lateral load, and 250 and 750 with respect to the average cohesion (c_{A_V}) of the entire clay profile, which may be more appropriate for combined axial and lateral loading. Poisson's ratio was taken as 0.48, and the underlying limestone was treated as a continuation of the overburden for purposes of calculating additional displacements, an assumption that is justified in light of the fact that imposed loads produced little axial or lateral soil reaction near the pile tips.

Table 2. Statistical parameters: test group 1.

	Effect of E		
E (kPa)	On Distribution of Load[a]	On Settlement[b]	On Load-Transfer Pattern[c]
34 500			
Group load = 2427 kN	20.7	5.6[d]	19.2[d]
Group load = 4199 kN	14.2	5.3	16.0[d]
23 100			
Group load = 2427 kN	20.6	22.2	24.4[d]
Group load = 4199 kN	14.3	36.8	22.7[d]
∞[e]			
Group load = 2427 kN	21.8	55.6[d]	15.2
Group load = 4199 kN	17.8	60.5[d]	4.8[d]

Note: 1 kPa = 0.145 lbf/in^2; 1 kN = 225 lbf.
[a] Expressed as the ratio of the SDs of the differences in computed and measured loads to the mean pile-head load as percentage.
[b] Expressed as the percentage error of the difference between the computed and the measured mean pile-head deflections.
[c] Expressed as the percentage error of the mean load transferred from pile to soil in the upper 9.2 m (30 ft) of embedment.
[d] Computed value is less than measured value.
[e] I.e., pile-soil-pile interaction is neglected.

The hybrid model was used to compare the cap translations and the load distributions to piles for cases of both ideal and as-driven geometry. The results of the analyses, in which E was varied as indicated, are summarized in Tables 3, 4, and 5. Table 4 describes the effects of both E and pile geometry on the solution for three of the piles. While ideal geometry results are reported, the value of E giving the best overall results for cap translation was used in order to separate the

geometric effects from the effect of modulus.

The percentage errors in the computed cap translations are summarized below (1 kN = 225 lbf).

E	Lateral Load Test		Combined Load Test (L = 890 kN and A = 1922 kN)	
	L = 890 kN	L = 445 kN	Lateral Component	Vertical Component
250 c_{SL} (as-driven)	56			
750 c_{SL} (as-driven)	0	3		
250 c_{AV} (as-driven)	91		73	64
750 c_{AV} (as-driven)	16	21	1	2
Neglected (ideal)	38		58	67
Neglected (as-driven)	31		51	67

(It should be noted that, for all cases in which the effect of E was neglected, the computed value was less than the measured value.)

1. For the lateral-load test, the best value of E in terms of correlation with cap translation for as-driven conditions was 750 c_{SL}. For the combined-load test, the best correlation was for E = 750 c_{AV}, although the errors associated with both values of E were small in the lateral-load test at 890 kN [200 000 lbf (200 kips)].
2. When the lateral load was 445 kN [100 000 lbf (100 kips)], the error in computed cap translation under as-driven conditions was approximately equal to that at 890 kN, which indicates that the choice of E is not significantly affected by the level of load within the working-load range.

Figure 7. Physical arrangement: test group 2.

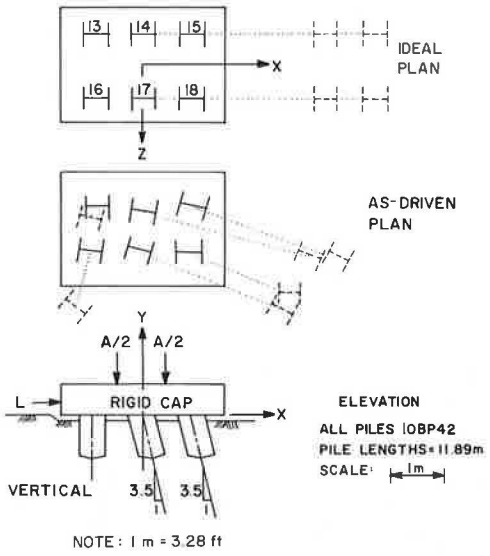

Figure 8. Axial (f versus s) and lateral (p versus y) unit-soil-resistance curves: test group 2.

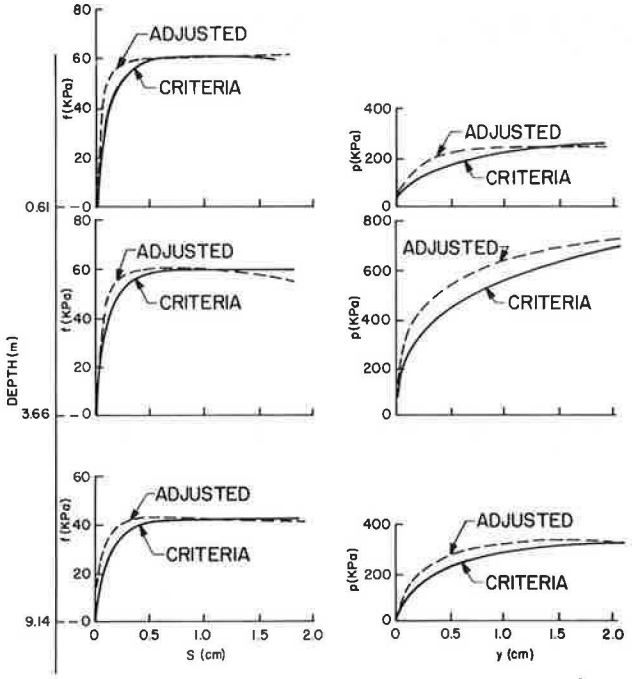

Table 3. Comparison of predicted and measured cap motion: test group 2.

Loading	E		Translation (cm)			Rotation (radians × 10^{-4})		
	Value (kPa)	With Respect to Cohesion	X	Y	Z	X-axis	Y-axis	Z-axis
Lateral (L = 890 kN)								
Ideal geometry	1.55×10^6	250 c_{SL}	1.17	0.20	0.0	0.0	0.0	6.21
	4.65×10^6	750 c_{SL}	0.74	0.13	0.0	0.0	0.0	2.87
	1.03×10^6	250 c_{AV}	1.40	0.25	0.0	0.0	0.0	8.07
	3.10×10^6	750 c_{AV}	0.86	0.15	0.0	0.0	0.0	3.80
	∞[a]		0.51	0.10	0.0	0.0	0.0	1.62
As-driven geometry		250 c_{SL}	1.27	0.18	0.005	1.88	0.76	3.18
		750 c_{SL}	0.81	0.10	0.005	0.02	0.28	0.72
		250 c_{AV}	1.55	0.20	0.003	1.65	0.83	4.63
		750 c_{AV}	0.94	0.13	0.005	1.91	0.43	1.35
	∞[a]		0.56	0.08	0.008	2.10	0.10	-0.25
Measured			0.81					
Combined (L = 890 kN and A = 1922 kN)								
Ideal geometry		250 c_{AV}	0.79	-0.23	0.0	0.0	0.0	-4.31
		750 c_{AV}	0.57	-0.13	0.0	0.0	0.0	-2.79
	∞[a]		0.28	-0.05	0.0	0.0	0.0	0.24
As-driven geometry		250 c_{AV}	1.17	-0.25	-0.13	-0.93	4.78	-12.85
		750 c_{AV}	0.69	-0.16	-0.10	-1.53	2.68	-6.29
	∞		0.33	-0.05	-0.08	-0.78	1.32	-1.05
Measured			0.68	-0.15				

Note: 1 kPa = 0.145 lbf/in²; 1 cm = 0.39 in; 1 kN = 225 lbf.
[a] I.e., pile-soil-pile interaction is neglected.

Table 4. Comparison of modeled pile-head loads for three piles: test group 2 (L = 890 kN and A = 0).

Pile No.	E (with respect to cohesion)	Force (kN)			Moment (kN·cm)		
		U	V	W	U-Axis[a]	V-Axis[b]	W-Axis[c]
16	250 c_{SL}	-352.00	-1.78	115.26	-0.3	-13 179	54.3
	750 c_{SL}	-295.93	-0.89	121.04	-0.2	-11 563	28.3
	250 c_{AV}	-377.36	-2.23	112.59	-0.3	-13 948	-79.1
	750 c_{AV}	-313.28	-0.89	119.71	-0.2	-12 038	0.0
	750 c_{AV}[d]	-306.61	0.0	116.59	0.0	-11 789	0.0
17	250 c_{SL}	351.55	2.67	107.25	-0.1	-12 603	265.6
	750 c_{SL}	270.12	2.23	115.70	0.1	-11 201	226.1
	250 c_{AV}	388.04	3.12	105.02	-0.1	-13 360	276.9
	750 c_{AV}	296.82	2.67	112.14	0.1	-11 529	235.1
	750 c_{AV}[d]	265.67	0.0	109.92	0.0	-11 405	0.0
18	250 c_{SL}	24.92	2.67	115.26	-0.2	-13 179	262.2
	750 c_{SL}	55.18	2.23	121.04	0.0	-11 586	210.2
	250 c_{AV}	13.36	3.12	112.59	-0.2	-13 959	272.4
	750 c_{AV}	44.95	2.23	119.71	0.0	-12 049	240.8
	750 c_{AV}[d]	119.71	0.0	121.93	0.0	-12 286	0.0

Note: 1 kN = 225 lbf; 1 cm·kN = 88.5 lbf·in.
[a] Coincides with pile axis, positive downwards.
[b] Normal to U-axis, parallel to strong axis of bending, positive in general negative Z-direction.
[c] Normal to U-axis and to strong axis of bending, positive in general positive X-direction.
[d] Ideal geometry.

Table 5. Comparison of modeled pile-head loads: test group 2 (L = 890 kN and A = 1922 kN).

Pile No.	E (with respect to cohesion)	Force (kN)			Moment (kN·cm)		
		U	V	W	U-Axis[a]	V-Axis[b]	W-Axis[c]
16	250 c_{AV}	117.48	8.46	79.21	-3.8	-8506.6	612.6
	750 c_{AV}	119.26	10.68	83.66	-2.0	-7701.9	669.1
	750 c_{AV}[d]	198.92	0.0	68.53	0.0	-6308.2	0.0
17	250 c_{AV}	380.48	15.58	90.78	-3.8	-9210.8	1199.2
	750 c_{AV}	389.82	16.02	90.34	-2.3	-7957.3	1085.1
	750 c_{AV}[d]	386.26	0.0	73.87	0.0	-6411.1	0.0
18	250 c_{AV}	404.51	23.59	89.89	-3.6	-9052.6	1703.4
	750 c_{AV}	400.95	21.36	91.23	-2.1	-8000.3	1382.4
	750 c_{AV}[d]	449.90	0.0	78.77	0.0	-6688.0	0.0

Note: 1 kN = 225 lbf; 1 cm·kN = 88.5 lbf·in.
[a] Coincides with pile axis, positive downwards.
[b] Normal to U-axis, parallel to strong axis of bending, positive in general negative Z-direction.
[c] Normal to U-axis and to strong axis of bending, positive in general positive X-direction.
[d] Ideal geometry.

Figure 9. Computed bending moments for pile 14: combined-loading case—test group 2.

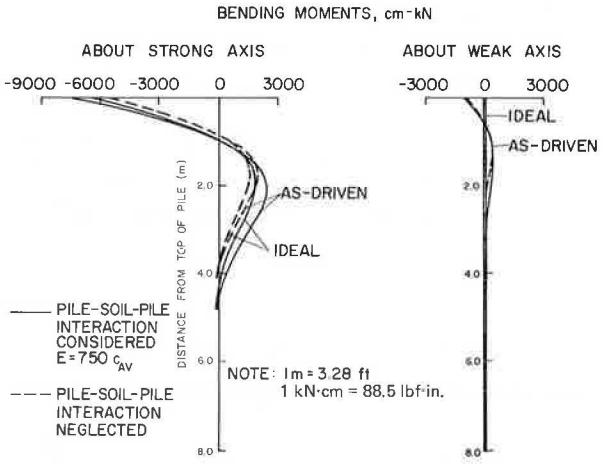

The effect of failure to include as-driven geometry was measured as the ratio of the standard deviation of the difference between the pile-head loads computed from the ideal case (E = 750 c_{AV}) and the loads computed from the as-driven case to the mean absolute value of the loads computed for the as-driven case (expressed as a percentage).

Item	Lateral Load Test (L = 890 kN)	Combined Load Test (L = 890 kN and A = 1922 kN)
Axial load	16.2	17.6
Strong-axis shear	3.8	18.2
Strong-axis moment	4.0	18.3

[It should be noted that these values were computed for the following conditions: (a) the as-driven (best computed) value of E that gave the best agreement with the cap deflections (i.e., E = 750 c_{SL} for lateral and E = 750 c_{AV} for combined loads) and (b) the ideal value based on ideal geometry and E = 750 c_{AV}.] This effect is seen to be the strongest for axial pile-head loads in the lateral load tests and to be equally strong for axial loads, moments, and shears at the pile head for the combined load test. The probable error in computing these pile-head loads for any pile, using ideal geometry and combined loading, is about 12 percent.

The effects of pile-soil-pile interaction and of group geometry on the computed bending in a typical pile (pile 14) for the combined-load test is shown in Figure 9. Maximum moments about the weak axis were computed to be about 17 percent of those about the strong axis when as-driven geometry was considered. Furthermore, the inclusion of group action produced a computed maximum moment whose value was 14 percent higher and whose location was 33 percent farther down the pile than that calculated when group action was neglected in the as-driven case. Torsional moments were insignificant for all cases considered.

CONCLUSIONS

1. The hybrid model appears to be a useful tool for predicting load-deformation response of complex pile groups in normally to slightly overconsolidated clay that are loaded vertically, laterally, or by a combination of vertical and lateral loading.
2. The hybrid model can be employed by using published criteria for unit-soil-resistance curves, but the results are improved when the unit-soil-resistance curves for individual piles are adjusted by using the results of

load tests conducted on isolated piles near the group to be modeled that are loaded in a manner representative of group loading.

3. For both vertical and lateral loading in the cases studied, the best correlation between measured cap movement and equivalent soil modulus (E) occurred for E = 750 to 850 times the undrained cohesion of the soil (as indicated by Q-type laboratory tests on samples recovered by methods that do not attempt to minimize soil disturbance during sampling). This value represents, to some extent, the effect of pile reinforcement of the soil and may therefore be affected by pile spacing and total number of piles in the group. Use of E-values one-third too low in the axial tests increased the error in computed settlement by 17-32 percent, and use of E-values two-thirds too low in the lateral test increased the error in computed translation by 56 percent. The error in computed cap movement when the best value of E was used was relatively independent of the load direction and magnitude within the working-load range, even though the load-movement response of the cap was nonlinear for the axial, lateral, and combined load tests.

4. Use of the hybrid model did not significantly improve the computed axial load transfer along the piles or the distribution of loads to pile heads in comparison with the results obtained when group effects were neglected.

5. For test group 2, a probable error of 12 percent was inferred in computed pile-head thrusts and strong axis shears and moments when ideal group geometry, rather than as-driven geometry, was included under conditions of combined loading. Conclusions 4 and 5 have important implications with respect to the need for probabilistic modeling of pile groups.

REFERENCES

1. C. S. Desai, L. D. Johnson, and C. M. Hargett. Finite Element Analysis of the Columbia Lock Pile System. U.S. Army Engineer Waterways Experiment Station, Vicksburg, MS, Rept. TR-5-74-6, 1974, 31 pp.
2. M. Ottaviani. Three-Dimensional Finite Element Analysis of Vertically Loaded Pile Groups. Geotechnique, Vol. 25, No. 2, June 1975, pp. 159-174.
3. L. C. Reese, M. W. O'Neill, and R. E. Smith. Generalized Analysis of Pile Foundations. Journal of the Soil Mechanics and Foundations Division, Proc., ASCE, Vol. 96, No. SM1, Jan. 1970, pp. 235-250.
4. W. E. Saul. Static and Dynamic Analysis of Pile Foundations. Journal of the Structural Division, Proc., ASCE, Vol. 94, No. ST5, May 1968, pp. 1077-1100.
5. H. G. Poulos. Analysis of the Settlement of Pile Groups. Geotechnique, Vol. 18, No. 3, Sept. 1968, pp. 351-371.
6. H. G. Poulos. Lateral Load-Deflection Prediction for Pile Groups. Journal of the Geotechnical Engineering Division, Proc., ASCE, Vol. 101, No. GT1, Jan. 1975, pp. 19-34.
7. H. G. Poulos and E. H. Davis. Elastic Solutions for Soil and Rock Mechanics. Wiley, New York, 1974.
8. H. M. Coyle and L. C. Reese. Load Transfer for Axially Loaded Piles in Clay. Journal of the Soil Mechanics and Foundations Division, Proc., ASCE, Vol. 92, No. SM2, March 1966, pp. 1-26.
9. H. Matlock. Application of Numerical Methods to Some Problems in Offshore Operations. Journal of Petroleum Technology, Vol. 15, No. 9, Sept. 1963.
10. H. M. Coyle and I. H. Sulaiman. Skin Friction for Steel Piles in Sands. Journal of the Soil Mechanics and Foundations Division, Proc., ASCE, Vol. 93, No. SM6, Nov. 1967, pp. 261-296.
11. V. N. Vijayvergiya. Load-Movement Characteristics of Piles. Proc., Ports '77 Conference, Long Beach, CA, March 1977, 16 pp.
12. H. Matlock. Correlations for Design of Laterally Loaded Piles in Soft Clay. Proc., 2nd Offshore Technology Conference, Houston, TX, May 1970, pp. 577-594 (paper OTC 1204).
13. L. C. Reese, W. R. Cox, and F. D. Koop. Field Testing and Analysis of Laterally Loaded Piles in Stiff Clay. Proc., 7th Offshore Technology Conference, Houston, TX, Vol. 2, May 1975, pp. 671-690 (paper OTC 2312).
14. R. N. Dutt. Torsional Response of Piles in Sand. Univ. of Houston, Houston, TX, Ph.D. thesis, Dec. 1976.
15. J. A. Focht, Jr., and K. J. Koch. Rational Analysis of the Lateral Performance of Offshore Pile Groups. Proc., 5th Offshore Technology Conference, Houston, TX, Vol. 2, May 1973, pp. 701-708 (paper OTC 1896).
16. M. W. O'Neill, O. I. Ghazzaly, and H.-B. Ha. Analysis of Three-Dimensional Pile Groups with Nonlinear Soil Response and Pile-Soil-Pile Interaction. Proc., 9th Offshore Technology Conference, Houston, TX, Vol. 2, May 1977, pp. 245-256 (paper OTC 2838).
17. H. G. Schlitt. A Report on Steel Pile Tests, Q Street Viaduct, Omaha, Nebraska. Nebraska Department of Roads and Irrigation, Lincoln, 1950.
18. C. C. Ladd. Stress-Strain Modulus of Clay in Undrained Shear. Journal of the Soil Mechanics and Foundations Division, Proc., ASCE, Vol. 90, No. SM5, Sept. 1964, pp. 103-132.
19. J. B. Kim, R. J. Brungraber, C. H. Kindig, J. L. Goodman, and L. P. Singh. Pile Group Foundations, Analysis and Full-Scale Load Tests. Civil Engineering Department, Bucknell Univ., Lewisburg, PA, July 1973.

Publication of this paper sponsored by Committee on Foundations of Bridges and Other Structures.

Lateral Load Test of a Drilled Shaft in Clay

Harry M. Coyle and Richard E. Bartoskewitz, Department of Civil Engineering,
Texas Transportation Institute, Texas A&M University, College Station
Vernon R. Kasch*, McClelland Engineers, Inc., Houston, Texas

The behavior of a laterally loaded drilled shaft in clay was investigated by conducting a lateral load test on an instrumented shaft. Lateral deflections, shaft rotation, and soil resistance were measured for each applied load. Dial gages were used to measure lateral deflection, and the shaft rotation was determined by means of an inclinometer. Pneumatic pressure cells were installed in the shaft at various depths to measure the soil resistance. The applied lateral load was measured by using a strain-gage load cell. Structural failure of the shaft occurred before the soil failed and prevented determination of the ultimate lateral soil resistance. However, the ultimate soil reactions predicted by several analytical procedures were compared with the soil reaction calculated from the maximum recorded soil resistance. Also, an ultimate lateral load for the test shaft was predicted by various analytical methods, and a comparison was made between the maximum recorded load and the various predicted ultimate loads. Finally, a comparison was made between two ultimate test loads reported in the technical literature and the ultimate loads predicted by the analytical methods.

The Texas State Department of Highways and Public Transportation has in recent years developed a new concept in retaining-wall design and construction. The new type of retaining structure is the precast-panel retaining wall. As shown in Figure 1, this structure makes use of precast panels that are placed between T-shaped pilasters. The pilasters are spaced at even intervals and supported by drilled shafts (in other locales, these may be referred to as drilled piers, bored piles, or drilled caissons). The precast panel derives its restraining ability from the pilasters, which are located at the edges of the panel. The forces acting on the panel are transmitted to the pilasters and must be resisted by the soil in contact with the drilled shafts.

The drilled shaft must be designed to withstand both axial and lateral loads. However, because the axial load on a shaft supporting a precast-panel retaining wall is minimal, it is the lateral load that is of primary interest. Passive and active pressures are developed in the soil as a result of being in contact with the foundation. The magnitude and distribution of these pressures is dependent on many factors, including the size of the lateral load, the type of soil and its physical properties, and the diameter and flexibility of the foundation. Because the forces that resist lateral loads are the resultants of earth pressures, field pressure measurements should be beneficial in the development of improved design criteria.

Several investigators have made pressure measurements on cylindrical foundations. Stobie (1), in 1930, used mechanical pressure gages to measure soil pressures on laterally loaded utility poles. The pressures were calculated from the deformation of calibrated lead wires in the gages. Direct measurement of pressures on laterally loaded piles has been reported by Mason and Bishop (2) and by Heijnen and Lubking (3). Mason and Bishop used friction-steel, ribbon-type pressure gages, and Heijnen and Lubking used pressure cells, but did not specify the kind. Adams and Radhakrishna (4) report the use of hydraulic-displacement pressure cells on lateral-capacity tests of drilled shafts. In addition to these direct measurements of soil pressure, several other investigators have reported soil reactions that were determined indirectly from instrumented piles or drilled shafts (5-9). The soil reactions were determined by double differentiation of the bending moments that were obtained from strain-gage measurements.

Improvements in design procedures may result in significant savings in construction costs. The objective of this research study was to obtain field data by the measurement of loads, lateral earth pressures, deflections, and rotations on a laterally loaded drilled shaft. The results of the analysis of the field data will be used to develop rational criteria for the design of drilled shafts that support precast-panel retaining walls.

TEST SITE AND LOADING SYSTEM

A lateral load test was conducted on an instrumented drilled shaft to collect field data for use in the development of rational design criteria. To minimize potential installation problems with the shaft, a site consisting entirely of clay was selected. This site was found at the Texas A&M research annex at the southwest end of the northeast-southwest runway.

Soil conditions at the test site were investigated by using three soil borings and one Texas cone penetrometer (TCP) test. The boring locations, designated B-S1, B-S2, and B-S3, are shown in Figure 2. Undisturbed soil samples were taken with a 3.81-cm (1.50-in) thin-wall tube sampler. The location of the TCP test, designated TCP-1, is also shown in Figure 2.

Laboratory tests on the undisturbed samples included Atterberg limits, moisture contents, and unit weights. The undrained cohesive shear strength (C_u) of the samples was determined by unconfined compression tests and miniature vane tests. Typical results of the tests for boring B-S2 are shown in Figure 3. The test results indicated that the soil conditions were fairly uniform. The site consisted of stiff to very stiff clay having an average undrained cohesive shear strength of about 124 kPa (17.8 lbf/in^2). The clay to a depth of approximately 1.5 m (5 ft) had Unified Soil Classification of CL. The clay at a depth lower than approximately 1.5 m was classified as CH. A slickensided structure was noted in the clay at depths lower than about 3.0 m (10 ft).

The N-values (blow counts) obtained from the TCP test were also used to develop a shear-strength profile. The correlation developed by Duderstadt and others (10) was used to determine the undrained cohesive shear strength from the N-values. An average undrained cohesive shear strength of about 110 kPa (16 lbf/in^2) was obtained by using this method. This value compares quite well with the shear strength of 124 kPa obtained from the unconfined compression and miniature vane tests.

On completion of boring B-S3, an open standpipe was installed for groundwater observations. A perforated polyvinyl chloride pipe covered with screen wire was placed in the bore hole and surrounded with clean gravel. Water-level readings indicated that the water level was steady at a depth of 4.6 m (15 ft).

The loading and reaction system used in testing the instrumented drilled shaft is shown in Figure 4. The

reaction system consisted of two reinforced-concrete drilled shafts connected by a reinforced-concrete tie beam. Each shaft was drilled to a depth of 6.1 m (20 ft) and was 0.9 m (3 ft) in diameter. The shaft spacing was 6.1 m, center to center. The steel reinforcing cages for each shaft consisted of twelve no. 11 bars (grade 60) having a no. 3 spiral at a 15-cm (6-in) pitch. The beam connecting the shafts was approximately 1.2 m (4 ft) wide and 1.07 m (3.5 ft) deep. It was reinforced with 14 no. 6 steel bars having no. 3 stirrups at a 61-cm (24-in) spacing. A 5-cm (2-in) diameter steel reaction bar was embedded about 1.2 m deep on both reaction shafts. A steel plate was welded to each reaction bar to increase the bearing area. The winch was anchored to the rear reaction shaft by six 3.18-cm (1.25-in) anchor bolts embedded to a depth of approximately 1.2 m.

The test shaft was located on line with the centers of the reaction shafts at a center-to-center distance of approximately 9.1 m (30 ft) from the front reaction shaft. The shaft was nominally 0.9 m in diameter by 6.1 m deep. Wobble in the auger produced a diameter that varied from about 99 cm (39 in) at the ground surface to about 91 cm (36 in) at a depth of about 4.9 m (16 ft). The actual depth of the shaft was 6.16 m (20.2 ft). The reinforcing cage for the test shaft was the same as for the reaction shafts. As shown in Figure 4, the lateral load was applied to a steel column that was bolted to the test shaft. The column was a 12 WF 120, which was welded to a 2.5-cm (1-in) steel base plate. Twelve 3.18-cm anchor bolts were used to connect the column to the shaft. The bolts were embedded to a depth of 2.4 m (8 ft).

The lateral load was applied to the test shaft by a winch and pulley system. The winch was a single-drum, 178-kN [40 000-lbf (40-kip)] capacity Garwood cable winch driven through a four-to-one gear-reduction unit by a gasoline-powered hydraulic unit. A 12:1 mechanical advantage was provided by two, six-sheave, 890-kN [200 000-lbf (200-kip)] capacity pulley blocks. The cable was a 1.91-cm (0.75-in), 6x19 standard hoisting wire rope. As shown in Figure 4, one block was connected to the anchor bar and the other was connected to the test shaft. The load cell was placed between the block

Figure 1. Precast-panel retaining wall.

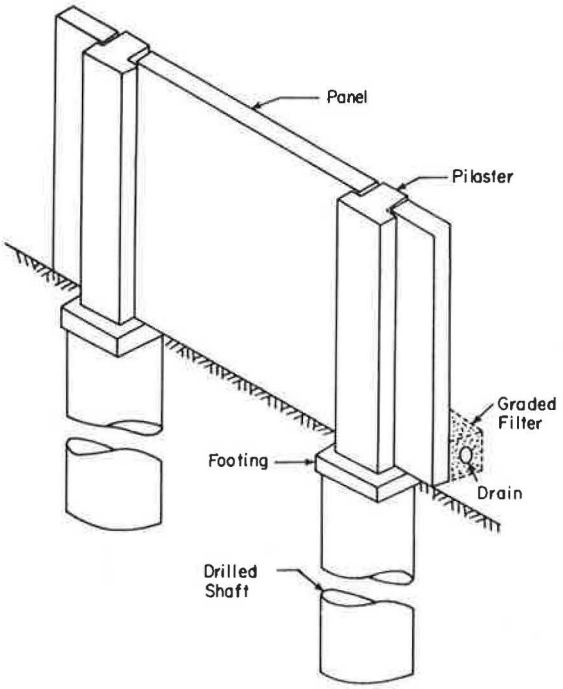

Figure 2. Location of borings.

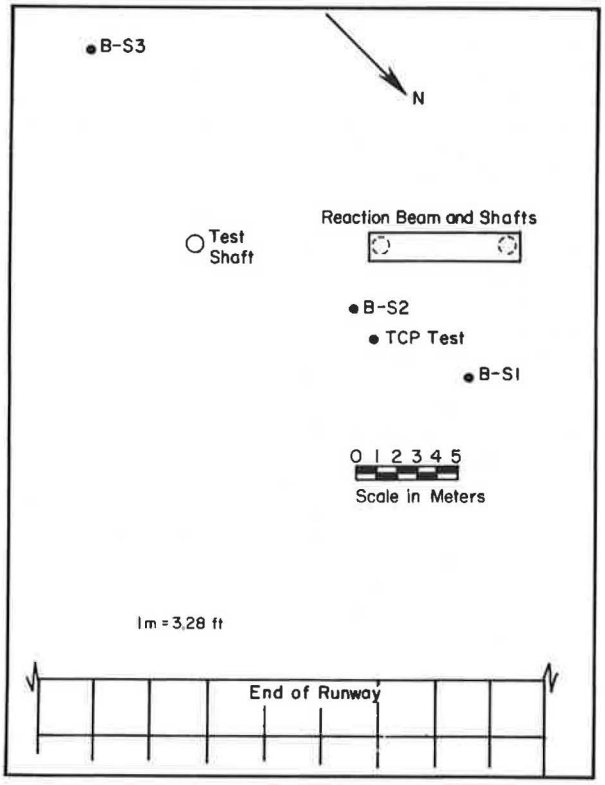

Figure 3. Boring log: B-S2.

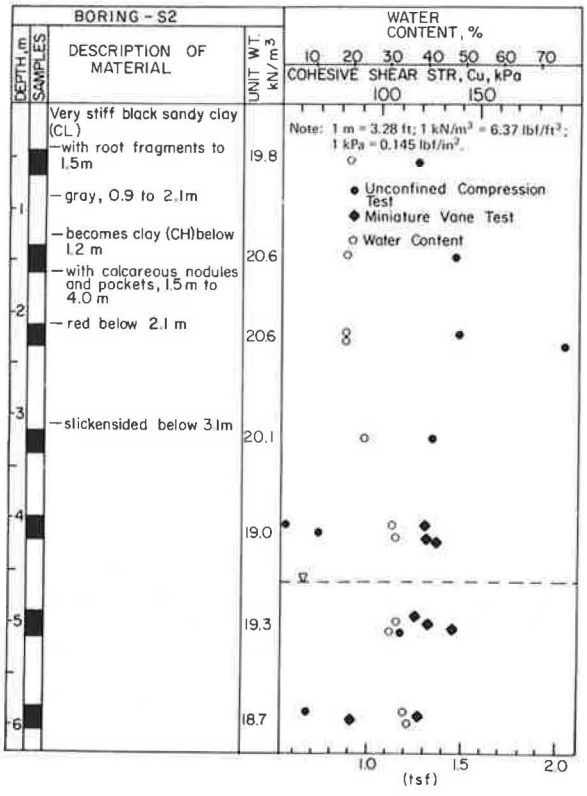

Figure 4. Lateral loading system.

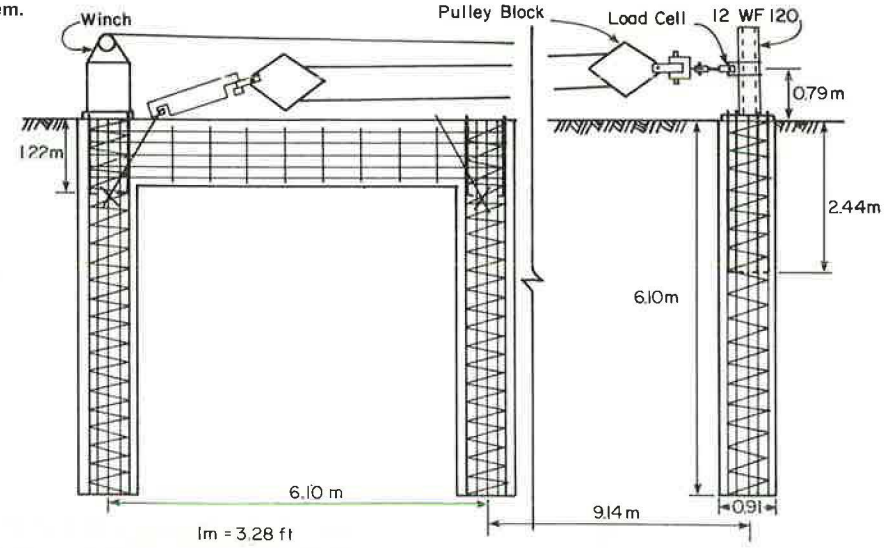

Figure 5. Location of pressure cells.

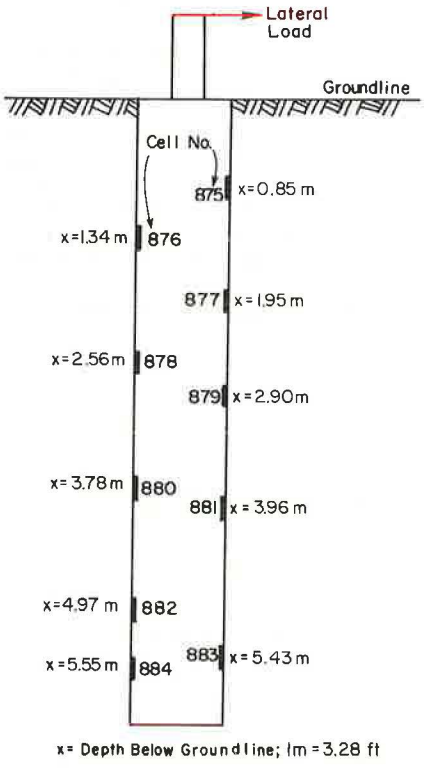

and the test shaft at a height of 0.79 m (2.6 ft) above the groundline.

INSTRUMENTATION AND LOADING PROCEDURE

The test shaft was instrumented with Terra Tec pneumatic pressure cells. These cells have been used successfully by Wright and others (11) in a study of active pressures on precast-panel retaining walls. Before the cells were installed in the test shaft, they were individually checked in a pressure chamber. The zero reading of each cell was determined; no malfunctions were observed in any of the cells.

The spacing and location of the pressure cells on the test shaft is shown in Figure 5. The cells were installed directly in line with the direction of the applied load. Five cells were located on the front of the shaft facing the reaction system, and five cells were located directly opposite on the back side. The cells were placed in the soil along the side of the excavation and held in place by steel pins.

The load applied to the test shaft was measured by a 890-kN-capacity strain-gage load cell. The load was indicated on a Budd P350 indicator in units of microstrain and converted from microstrain to kips by a predetermined calibration constant. The accuracy of the load cell and Budd indicator unit is approximately ±178 N (40 lbf).

The rotation of the shaft was determined by a Hilger and Watts TB108-1 inclinometer. The rotation could be read in degrees to an accuracy of approximately ±1 min. Rotational readings were taken by placing the inclinometer at five predetermined locations on the steel column. A back-up system was also devised for the determination of the shaft rotation. Horizontal measurements from a vertical reference line to five points on the steel column allowed the determination of the relative movements of the points. The reference line was established by using a plumb bob suspended from a frame welded to the top of the column. Initial measurements were made before the lateral load was applied and then subtracted from the subsequent measurements to obtain the movement relative to the initial position of the plumb line.

The deflection of the shaft at the groundline was measured by two 0.025-mm (0.001-in) dial gages. The gages were mounted on a steel beam behind the shaft, which was bolted to footings placed approximately 3.0 m (10 ft) on each side of the shaft. A bench mark was set about 15.2 m (50 ft) behind the shaft as a safety measure in case the dial gages were disturbed.

The decision to load test a drilled shaft having dimensions of 6.1-m depth and 0.9-m diameter was based on the study reported by Wright and others (11). The precast-panel retaining wall instrumented in that study was founded on drilled shafts having those dimensions. Because the lateral load acting on a drilled shaft supporting a precast-panel retaining wall is the resultant of the backfill acting on the panel, the initial loads applied to the test shaft were selected to simulate those loads.

Wright and others have presented a method for calculating the maximum resultant force of the backfill

Table 1. Initial pressure-cell readings.

Cell	Laboratory Zero Reading: April 1977 (kPa)	Shaft Initial Reading: May 24, 1977 (kPa)	Shaft Reading After Concrete Placement: May 24, 1977 (kPa)	Shaft Reading Before Application of First Load: June 23, 1977 (kPa)
875	63.5	51.1	60.1	51.1
876	114.5	113.7	128.3	113.2
877	53.1	49.7	67.6	59.3
878	48.3	44.9	57.3	44.9
879	69.0	62.1	78.7	71.8
880	69.0	52.4	62.1	55.2
881	72.5	69.0	85.6	79.4
882	104.9	97.3	116.6	119.4
883	53.1	45.5	71.1	72.5
884	79.4	74.5	103.5	106.3

Note: 1 kPa = 0.145 lbf/in^2.

Figure 6. Relationship between lateral pressure and depth.

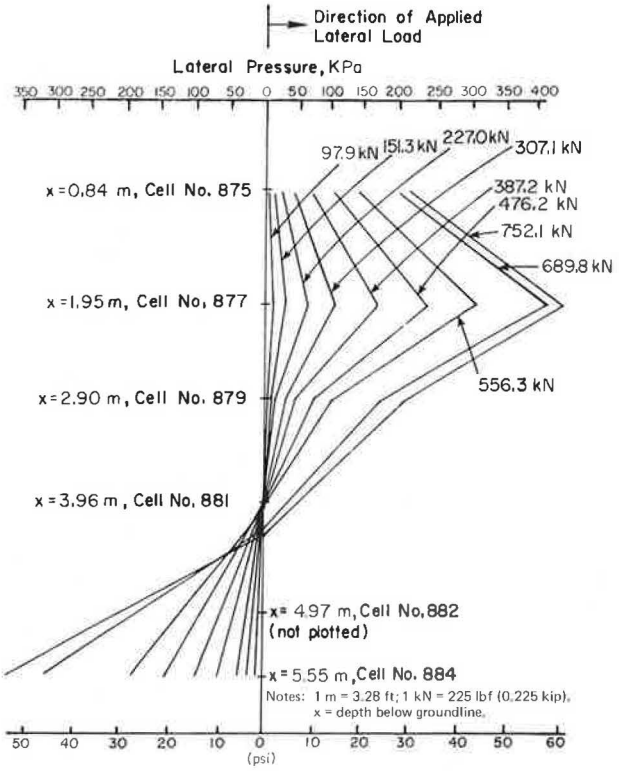

acting on a retaining wall. For the retaining wall reported in their study, the maximum resultant force was calculated to be 155 kN/shaft (34 900 lbf/shaft). The backfill producing the resultant force in that study was deposited over an eight-day period. To simulate the backfilling of that particular retaining wall as closely as possible, the initial loads on the test shaft in this study were applied over a six-day period. The applied force on the test shaft at the end of the six-day period was 153.5 kN [34 500 lbf (34.5 kips)]. Minor inaccuracies in the loading system prevented the exact simulation of the retaining-wall backfill.

After the load of 153.5 kN was applied, no additional loads were added for a period of 13 days in an attempt to determine whether any creep was occurring in the soil in front of the shaft. However, it was not possible to hold a constant load on the shaft, because daily temperature changes caused the cables in the loading system to expand and contract, creating a cyclic effect of as much as 31 kN/day (7000 lbf/day) in the applied load.

At the conclusion of the 13-day constant-load period, the load was increased daily in increments of approximately 40 kN [9000 lbf (9 kips)] until the lateral load reached 641 kN [144 000 lbf (144 kips)]. At that point, two steel pins connecting the load cell to the loading assembly and the shaft fractured. Consequently, the load had to be taken off the shaft and a two-week delay occurred while the connections were redesigned and rebuilt. When repairs were completed, the shaft was reloaded and the load test continued until structural failure of the shaft occurred at 752 kN [169 000 lbf (169 kips)]. Excavation of the shaft indicated that the reinforcing bars on the back of the shaft, along with the concrete, had fractured at a depth of 2.4 m (8 ft). The fracture occurred directly below the level of the anchor bolts.

TEST RESULTS AND ANALYSIS

Table 1 shows four sets of pressure cell readings: (a) the laboratory-calibration zero readings; (b) the initial readings taken after the cells were installed in the shaft, but before the concrete was placed; (c) readings taken after the concrete was placed; and (d) readings taken 30 days after concrete placement, but before the application of the first load.

As shown in Table 1, the initial zero readings taken in the shaft differed from the zero readings obtained in the laboratory calibration. In most cases, the readings taken in the shaft were 3.4-10.3 kPa (0.5-1.5 lbf/in^2) lower than the laboratory calibration; the reason for this is not known. As expected, the readings taken after the placement of the concrete were higher than the initial readings and the largest increases were recorded by the cells on the bottom of the shaft. Thirty days later, before the first lateral load was applied, cell readings indicated that most of the pressures had decreased by 7 kPa (1 lbf/in^2) or more, an effect that may be accounted for by concrete shrinkage during the 30-day curing period.

The lateral soil pressures resulting from the lateral loads on the shaft were determined by subtracting the initial cell readings from the cell readings obtained for a particular lateral load. The initial cell readings used were those obtained on June 23, just before application of the first lateral load. [Detailed pressure-cell data are described elsewhere (12).]

When the lateral pressures were calculated, the pressures recorded for cells 880 and 883 (see Figure 5) were consistently negative. It is probable that these two cells experienced a loss of contact with the soil as a result of rotation of the shaft, an effect that could have resulted in a pressure decrease. However, it should be noted that cells 876 and 878, which should also have experienced a loss of soil contact, did not record a significant number of negative pressures. This probably indicates that the initial pressures being used for cells

880 and 883 were too high by 7-14 kPa (1-2 lbf/in^2).

When the pressure cells were installed, it was assumed that the lateral loading would cause the shaft to rotate about a point 3.0-4.6 m (10-15 ft) deep. Consequently, the top three cells (see Figure 5) on the front side of the shaft (cells 875, 877, and 879) and the bottom two cells on the back side (cells 882 and 884) would be recording passive pressures and would have the highest pressure readings. These assumptions were essentially verified by the load test.

The pressure-cell data indicate that, of the five cells on the front side of the shaft, the top three (cells 875, 877, and 879) showed significant pressure increases and the fourth (cell 881) showed a slight increase. The pressure of the bottom cell (cell 883) was essentially constant. Of the five cells on the back side of the shaft, only the bottom one (cell 884) showed a significant increase in pressure. The pressures in the top three cells (cells 876, 878, and 880) remained constant, indicating essentially no active pressure, while the fourth cell (cell 882) showed a slight increase in pressure.

The lateral pressures indicated by cells 875, 877, 879, 881, and 884 are plotted with respect to depth for various lateral loads in Figure 6. The second cell from the top on the front side of the shaft (cell 877) consistently recorded the highest pressures. The next-highest pressures were recorded by the lowest cell on the back side (cell 884). The pressure recorded by cell 881 remained essentially constant; little or no lateral pressure was shown until the latter stages of the load test. This would seem to indicate that the rotation point of the shaft was in the general area of this pressure cell. The pressures recorded by cell 882 did not correlate well with those recorded by cell 884; cell 882 was located less than 0.6 m (2 ft) above cell 884 and yet did not record a lateral pressure in excess of 7 kPa until the load was more than 445 kN [100 000 lbf (100 kips)]. Because this cell was located in the slickensided clay, it is possible that some clay fell out from behind the cell during installation, thus creating an insufficient bearing area. Thus, the pressures recorded by cell 882 may be erroneous and, consequently, they are not included in Figure 6.

Considering the results shown in Figure 6, it is possible to draw some general conclusions about the shape of the lateral-soil-pressure distribution curve for cylindrical foundations in relatively homogeneous cohesive soil. (The lateral-soil-pressure distribution will be referred to as the soil resistance.) For loads that do not exceed the ultimate lateral resistance of the soil, the soil resistance appears to increase from some value in excess of zero at the ground surface to a maximum value that occurs at some depth between the ground surface and half of the foundation embedment and then decrease to zero at the rotation point (which occurs roughly between half and three-quarters of the foundation-embedment depth). Below the rotation point, the resistance again increases to a maximum value at the bottom of the foundation. It has been stated by Davisson and Prakash (13) that the upper point of maximum soil resistance shifts downward along the foundation, although the shape of the soil-resistance curve remains the same. The fixed location of the pressure cells on this test shaft prevented the observation of this phenomenon in this study.

As discussed above, the initial loads applied to the drilled shaft were a simulation of the loads produced during the backfilling of the retaining wall studied by Wright and others (11). The daily loads applied to the retaining wall, calculated from the data given by Wright and others, the loads applied to the test shaft, and the resulting deflections are shown below [1 kN = 225 lbf (0.225 kip) and 1 mm = 0.039 in].

Day	Calculated Load (kN)	Actual Load (kN)	Deflection (mm)
1	0.3		
2	2.4		
3	8.1	10.9	0.05
4	19.4	20.5	0.18
5	37.7	33.8	0.30
6	65.0	59.2	0.56
7	103.7	101.5	1.37
8	155.3	153.5	3.05
21	155.3	153.5	4.11

The table above also shows the deflection that occurred during the 13 days when no load was added to the shaft; the shaft movement during this period was only 1.07 mm (0.042 in). This movement was probably due to a combination of creep and a slight amount of structural breakdown of the soil due to the cyclic loading effect of the expanding and contracting cables caused by temperature variation.

The load-deflection curve for the load test is shown in Figure 7. The shaft had deflected 8.18 cm (3.22 in) when it failed structurally at 752 kN [169 000 lbf (169 kips)]. Figure 7 also shows the unloading and reloading curves that resulted from the two-week delay for repairs. It appears that the delay had little effect on the shape of the curve.

The load-rotation curve for the load test is shown in Figure 8. The structural failure of the shaft occurred at a rotation of about 2°. Laboratory tests conducted by Ivey and Dunlap (14) on model rigid piles indicate that the ultimate load for most of the tests occurred at a shaft rotation of about 5°. Figure 8 also indicates that there is a decrease in slope between the final portion of the initial loading curve and the initial portion of the reloading curve.

The location of the rotation point of the test shaft as indicated by the results of the inclinometer did not agree with the location indicated by the pressure cells. As the lateral load exceeded 445 kN, the inclinometer results (obtained by dividing the measured deflection of the shaft at the ground surface by the tangent of the rotation angle) indicated that the shaft was rotating about a point approximately 2.4 m (8 ft) deep. The pressure-cell readings seemed to indicate that the rotation point was in the area of cell 881, i.e., about 4.0 m (13 ft) deep. After the structural failure of the shaft, it became apparent that flexural bending had been occurring below the bottom of the anchor bolts at a 2.4-m (8-ft) depth. Consequently, the shaft was probably rotating as a unit about a point approximately 4.0 m deep and, at the same time, experiencing a flexural rotation at a depth of 2.4 m (8 ft).

Analytical studies by Hays and others (15) indicate that the rotation point is not constant but shifts downward from some point below the middle of the foundation for light loads to a point beyond three-quarters of the embedment depth for failure loads. Because the test shaft in this study experienced flexural bending and an ultimate load was not attained, it was not possible to verify Hays' results.

ULTIMATE SOIL RESISTANCE

Because structural failure occurred in the test shaft before soil failure was attained, it was not possible to determine the ultimate lateral soil resistance. However, it is possible to compare the soil resistance recorded by the pressure cells for the highest applied lateral load with the calculated ultimate soil reactions predicted by others. The soil reaction (p) is defined as the force per unit length of shaft. It can be calculated by multiplying the soil resistance by the shaft diameter (B). Figure 9 presents a comparison of the soil reactions to a depth of 3.0 m (10 ft) recorded on the test

Figure 7. Relationship between lateral load and deflection at groundline.

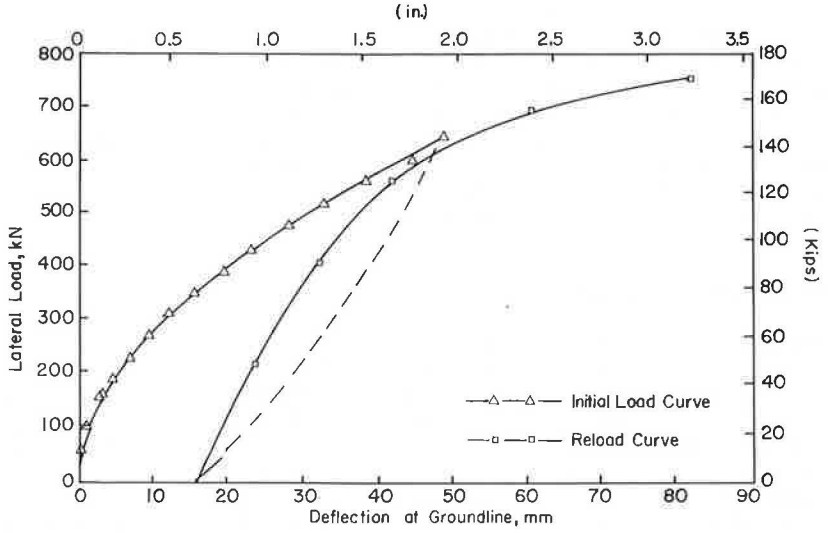

Figure 8. Relationship between lateral load and rotation.

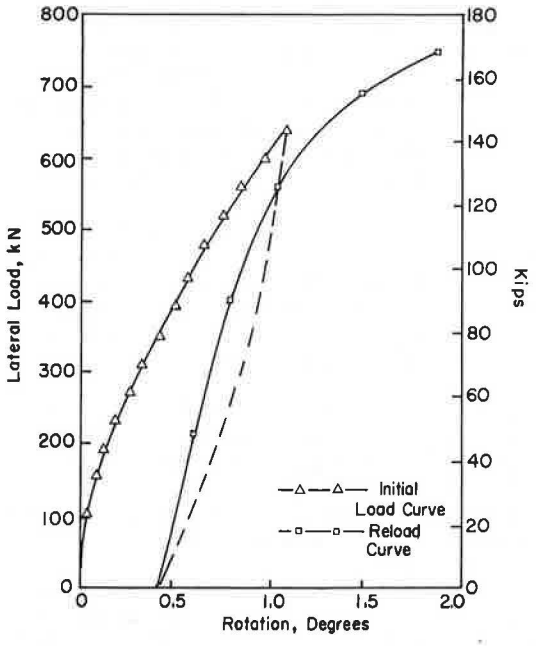

Figure 9. Relationship between ultimate soil reaction and depth below groundline.

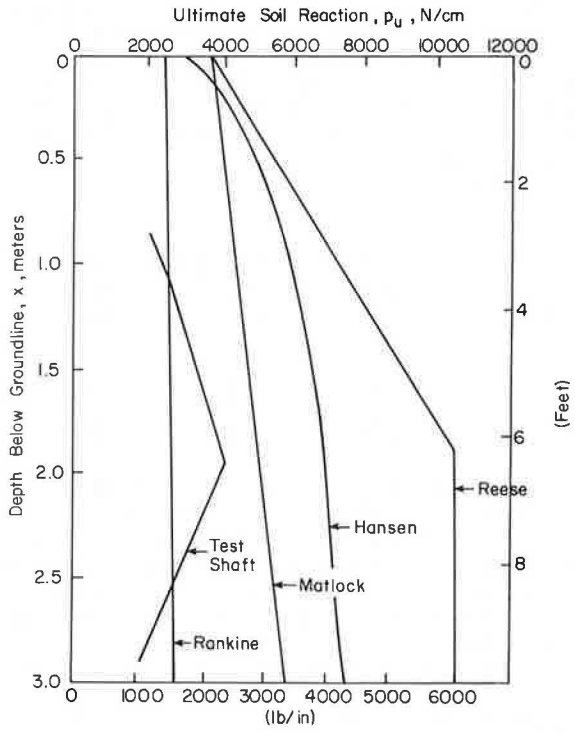

shaft at the maximum load of 752 kN [169 000 lbf (169 kips)] with the ultimate soil reactions (p_u) calculated by the methods proposed by Rankine (16), Hansen (17), Matlock (6), and Reese (18). The soil reaction for the test shaft was calculated from the pressures recorded on cells 875, 877, and 879. The following equations were used to predict the ultimate soil reactions:

Rankine

$$p_u = (\gamma x + 2C_u) B \quad (1)$$

Hansen

$$p_u = K_c C_u B \quad (2)$$

Matlock

$$p_u = [3 + (\gamma x/C_u) + (0.5x/B)] C_u B \quad (3)$$

and

Reese

$$p_u = [3 + (\gamma x/C_u) + (2.83x/B)] C_u B \quad (4)$$

where

γ = unit weight of the overburden material,
C_u = undrained shear strength of the soil,
x = depth below the ground surface, and
K_o = calculated earth-pressure coefficient.

Figure 9 indicates that, even though the load test did not produce ultimate soil reactions, the Rankine predictions were exceeded, thus verifying the conservative nature of this method. The equation used by Matlock, which is based on Reese's general equation, has been

empirically adjusted by using the results of lateral load test on piles in soft clays. However, in lateral load tests in stiff clays, Matlock's equation has in some instances predicted satisfactory results, while Reese's equation has given values in excess of those determined experimentally (8, 9). Additional testing will be needed before it can be determined which of the above equations can best predict ultimate soil reactions. This is especially true because an ultimate value was not attained on this test.

ULTIMATE LATERAL LOADS

The phrase "ultimate lateral load" as used in this paper means the maximum lateral load that the soil in contact with the foundation can withstand. Continued foundation deflection and rotation may occur with no increase in load when the ultimate load is reached. Many methods for calculating the ultimate load of a foundation can be found in the literature. Among these are the methods of Ivey and various coworkers (14, 18-21), Seiler (22), Hays and others (15), Broms (23), and Hansen (17). In addition, Ivey and Dunlap (20) have presented data from full-scale field tests of rigid shafts conducted at Bryan, Texas, and Galveston, Texas. Although an ultimate load was not attained for the load test described in this paper, it is informative to compare the predicted ultimate loads calculated by the aforementioned methods with the highest load applied to the test shaft. The table below presents a comparison of calculated ultimate loads and the measured loads for the load test described in this paper and for the two field tests reported by Ivey and Dunlap [1 kN = 225 lbf (0.225 kip)].

	Load (kN)		
Method	Current Study	Galveston Test	Bryan Test
Measured	752.1	24.5	55.2
Ivey and Dunlap	1272.7	12.8	67.4
Ivey and Dunlap with $\phi = 0$	578.5	6.0	38.8
Ivey and Hawkins	396.1	4.3	26.4
Broms	1157.0	6.9	42.5
Hays and others	983.5	7.8	39.8
Hansen	1206.0	9.0	55.2

Of the three load tests, the Bryan test probably offers the best comparison. The Galveston test was conducted without any problems but, as shown above, the measured load greatly exceeded any of the predicted ultimate loads. This was probably due to a stiff surface layer of clay that had a cohesive shear strength six times greater than the shear strength of the soil on the lower half of the shaft. It should also be noted that two variations of the method given by Ivey and Dunlap were used to calculate ultimate loads. This method is a semiempirical one in which a modifying factor is applied to the Rankine coefficients of passive and active earth pressure. Laboratory tests on cohesive samples to determine the modifying factor for these types of soils were conducted in such a way that both the angle of shearing resistance (ϕ) and the undrained cohesive shear strength (C_u) were determined. Consequently, the determined modifying factor assumes the use of both the cohesive shear strength and the angle of shearing resistance when determining the ultimate load of a foundation.

As expected, the Ivey and Hawkins method, which is based on Rankine passive earth pressures, consistently gives the most conservative results. The Ivey and Dunlap method with $\phi = 0$ also gives consistently conservative results, although not nearly as conservative as those of the Ivey and Hawkins method. The Ivey and Hawkins method underpredicted the measured load for the Galveston test by 473 percent, while the Ivey and Dunlap method was conservative by 307 percent. For the Bryan test, the Ivey and Hawkins method was 108 percent on the conservative side, while the Ivey and Dunlap method was conservative by 42 percent. The Ivey and Dunlap method, using both the cohesive shear strength and the angle of shearing resistance, consistently predicted the highest ultimate load. The method was conservative by 91 percent for the Galveston test, but 18 percent unconservative for the Bryan test. The other three methods—Broms, Hays and others, and Hansen—all predicted ultimate loads between those predicted by the two variations of the Ivey and Dunlap method.

CONCLUSIONS

Even though the test shaft failed structurally during lateral loading and an ultimate load was not attained, several useful observations were made during the test.

1. The serviceability and aesthetic appeal of a retaining wall depend on the amount of lateral deflection experienced by the wall. However, the magnitude of deflection that may be allowed is arbitrary. When the resultant force corresponding to that measured on the wall reported by Wright and others (11) was applied to the test shaft, the magnitudes of the resulting deflection, rotation, and soil reaction were small. Based on these observations, it is concluded that the drilled shafts supporting the precast retaining wall studied by Wright and others were probably overdesigned. Probably, the dimensions of those shafts could have been reduced by some amount without resulting in an objectionable deflection.
2. Before the structural failure of the test shaft occurred, its lateral deflection was of such magnitude as to probably be aesthetically objectionable. It is concluded that allowable deflection, rather than ultimate lateral load, may be the controlling criterion for the design of drilled shafts supporting precast-panel retaining walls.
3. The Ivey and Hawkins design method, which is based on Rankine's passive-earth-pressure formula, is not recommended for the design of laterally loaded drilled shafts because of its conservative nature. As shown by Figure 9, even though the lateral load test did not produce ultimate soil reactions, the Rankine predictions were still exceeded.
4. Based on the comparison of the load tests shown above, it is concluded that the Ivey and Dunlap method with $\phi = 0$ will produce conservative designs for drilled shafts. However, its use is recommended until additional lateral load tests can be conducted.

ACKNOWLEDGMENT

We gratefully acknowledge the support and assistance of the Texas Department of Highways and Public Transportation and the Federal Highway Administration, U.S. Department of Transportation, for their cooperative sponsorship in making this study possible.

The contents of this paper reflect our views; we are responsible for the facts and accuracy of the data presented herein. The contents do not necessarily reflect the views or policies of the Federal Highway Administration. This paper does not constitute a standard, specification, or regulation.

REFERENCES

1. J. C. Stobie. Pole Footings. Journal of the Institute of Engineers, Australia, Vol. 2, 1930, pp. 58-63.

2. H. G. Mason and J. A. Bishop. Measurement of Earth Pressure and Deflection Along the Embedded Portion of a 40-ft Steel Pile. ASTM, Special Tech. Publ. 154-A, 1954, pp. 1-21.
3. W. J. Heijnen and P. Lubking. Lateral Soil Pressure and Negative Friction on Piles. Proc., 8th International Conference on Soil Mechanics and Foundation Engineering, Moscow, USSR, Vol. 2.1, 1973, pp. 143-147.
4. J. I. Adams and H. S. Radhakrishna. The Lateral Capacity of Deep Augered Footings. Proc., 8th International Conference on Soil Mechanics and Foundation Engineering, Moscow, USSR, Vol. 2.1, 1973, pp. 1-8.
5. B. McClelland and J. A. Focht, Jr. Soil Modulus for Laterally Loaded Piles. Journal of the Soil Mechanics and Foundations Division, Proc., ASCE, Vol. 82, No. SM4, Oct. 1956, pp. 1081-1 to 1081-22.
6. H. Matlock. Correlations for Design of Laterally Loaded Piles in Soft Clay. Proc., 2nd Annual Offshore Technology Conference, Houston, TX, May 1970, pp. 577-594 (paper OTC 1204).
7. L. C. Reese, W. R. Cox, and F. D. Koop. Analysis of Laterally Loaded Piles in Sand. Proc., 6th Annual Offshore Technology Conference, Houston, TX, May 1974, pp. 473-483 (paper OTC 2080).
8. L. C. Reese, W. R. Cox, and F. D. Koop. Field Testing and Analysis of Laterally Loaded Piles in Stiff Clay. Proc., 7th Annual Offshore Technology Conference, Houston, TX, May 1975, Vol. 2, pp. 671-690 (paper OTC 2312).
9. R. C. Welch and L. C. Reese. Lateral Load Behavior of Drilled Shafts. Center for Highway Research, Univ. of Texas at Austin, Res. Rept. 89-10, May 1972.
10. F. J. Duderstadt, H. M. Coyle, and R. E. Bartoskewitz. Correlation of the Texas Cone Penetrometer Test N-Value with Soil Shear Strength. Texas Transportation Institute, Texas A&M Univ., College Station, Res. Rept. 10-3F, Aug. 1977.
11. W. V. Wright, H. M. Coyle, R. E. Bartoskewitz, and L. J. Milberger. New Retaining Wall Design Criteria Based on Lateral Earth Pressure Measurements. Texas Transportation Institute, Texas A&M Univ., College Station, Res. Rept. 169-4F, Aug. 1975.
12. V. E. Kasch, H. M. Coyle, R. E. Bartoskewitz, and W. G. Sarver. Lateral Load Test of a Drilled Shaft in Clay. Texas Transportation Institute, Texas A&M Univ., College Station, Res. Rept. 211-1, Nov. 1977.
13. M. T. Davisson and S. Prakash. Review of Soil-Pole Behavior. HRB, Highway Research Record 39, 1963, pp. 25-48.
14. D. L. Ivey, K. J. Koch, and C. F. Raba, Jr. Resistance of a Drilled Shaft Footing to Overturning Loads: Model Tests and Correlation with Theory. Texas Transportation Institute, Texas A&M Univ., College Station, Res. Rept. 105-2, July 1968.
15. C. O. Hays, J. L. Davidson, E. M. Hagan, and R. R. Risitano. Drilled Shaft Foundation for Highway Sign Structures. Engineering and Industrial Experiment Station, Univ. of Florida, Gainesville, Res. Rept. D647F, Dec. 1974.
16. K. Terzaghi and R. B. Peck. Soil Mechanics in Engineering Practice, 2nd ed. Wiley, New York, 1967, pp. 198-200.
17. J. B. Hansen. The Ultimate Resistance of Rigid Piles Against Transversal Forces. Danish Geotechnical Institute, Copenhagen, Bull. 12, 1961.
18. L. C. Reese. Discussion of paper, Soil Modulus for Laterally Loaded Piles, by B. McClelland and J. A. Focht, Jr. Trans., ASCE, Vol. 124, 1958, pp. 1071-1074.
19. D. L. Ivey. Theory, Resistance of a Drilled Shaft Footing to Overturning Loads. Texas Transportation Institute, Texas A&M Univ., College Station, Res. Rept. 105-1, Feb. 1968.
20. D. L. Ivey and W. A. Dunlap. Design Procedure Compared to Full-Scale Tests of Drilled Shaft Footings. Texas Transportation Institute, Texas A&M Univ., College Station, Res. Rept. 105-3, Feb. 1970.
21. D. L. Ivey and L. Hawkins. Signboard Footings to Resist Wind Loads. Civil Engineering, Vol. 36, No. 12, Dec. 1966, pp. 34-35.
22. J. F. Seiler. Effect of Depth of Embedment on Pole Stability. Wood Preserving News, Vol. 10, No. 11, Nov. 1932, pp. 152-168.
23. B. B. Broms. Lateral Resistance of Piles in Cohesive Soils. Journal of the Soil Mechanics and Foundation Division, Proc., ASCE, Vol. 90, No. SM2, March 1964, pp. 27-63.

Publication of this paper sponsored by Committee on Foundations of Bridges and Other Structures.

**V. R. Kasch was at the Texas Transportation Institute when this research was performed.*

Geology and Tunneling Economics in Montreal

Hugh Grice, Department of Geological Sciences, McGill University, Montreal
Marc Durand, Department of Earth Sciences, Université du Québec à Montréal

The economic construction of transportation projects depends in part on the availability of all relevant geological and geotechnical data. In Montreal, Canada, all of the 120 km (75 miles) of subways, major sewers, and aqueducts constructed during the last 18 years have been affected by local geological factors. Contracted costs for subway tunnels in shale were about 20 percent higher than for those in limestone. Locally, the presence of weathered zones in limestones and shales, where they have been faulted or intruded, increased actual costs to six times the normal unit price in good limestone. The contracted cost was 12.5 times the normal for a transition from an open cut into a tunnel in soil or rock. Variations of costs for contractors were estimated from rates of advance, amounts of concrete required to backfill overbreaks, and numbers of

steel arch ribs used for roof supports. Tunnel-boring machines were more sensitive to geological surprises than were normal construction methods. Comparisons were made between data from preconstruction investigations and both construction records and site mapping. It was confirmed that, although preconstruction data usually give general warning of problems, precise notice is often lacking. Even the use of techniques such as the measurement of rock-core lengths gives only a partial indication of actual tunneling conditions, which emphasizes the need for continuous detailed mapping during construction.

The costs of constructing facilities for road, rail, sea, and air transportation systems include the factors of availability of contractors for an acceptable construction schedule, costs of rights-of-way or land, the surface topography and geometry of geological units, and the geological conditions.

This paper reviews some of the major geological features of Montreal that have been significant in transportation tunneling engineering. Examples are given from the subsurface Montreal Metro system, now about 40 km (25 miles) long, as well as from the deep tunnels of the sewer and aqueduct systems, which have similar problems within their 75-km (46-mile) length. Attempts are made to relate costs to geological features, even though it is very difficult to separate the effects of geological and nongeological factors.

TYPES OF DATA

Three different classes of geological and geotechnical data are available:

1. Original field and laboratory notes and records in which data are related precisely to their source locations on past and current projects,
2. Detailed compilations and analyses of the original records (these usually have limited circulation), and
3. Generalized compilations and interpretations with some detailed examples such as are often published by government agencies.

Newly acquired data for a current project are usually by far the most valuable; however, their cost is very high compared with that of retrieving existing data. The latter should always be examined, even though they usually provide only useful generalizations and so must be supplemented by new detailed investigations.

The major problem in the assessment of the value of existing and new geological and geotechnical data is the scarcity of precise accounting that is available and can be released by designers and contractors (particularly under the present system of tendering and contract administration). Nevertheless, there are specific unit costs for the construction of structures in standard conditions, and it should be possible to relate extra payments for work caused by abnormal, and usually unforeseen, conditions to the cost of detailed exploration that would reduce those extras.

The specific unit costs in tenders are estimated by contractors from various factors and past experience in the same area. The completion and cost of each component of past contracts in Montreal has been dependent on the proportion of bad and good geological conditions, as well as on other factors discussed below. Thus, even if they are not specifically identified and located for each new project, the ground conditions are taken into account statistically in the average unit cost per item of a contract. The profit or loss for a bidder usually comes from the lack or excess of adverse conditions. Unfortunately, these profits and losses are seldom released publicly.

In this paper, three costing parameters are used to discuss the Metro, sewer, and aqueduct systems. First, abnormally high volumes of concrete used in lining tunnels can indicate local zones of excessive overbreak (1) (although this effect can be caused by poor technique as well as by poor rock conditions). Second, relative rates of advance by a given excavation method are possible indicators of costs and soil and rock quality when the effects of a number of nongeological factors (such as local experience of crew, size of crew, efficiency of equipment, and strikes and holidays) are taken into account. Third, details of the types and extent of supports generally indicate the stability of a cut or tunnel (although local occurrences of poor technique must be remedied by otherwise unnecessary support and some methods of support may be used as a minimum throughout some contracts as a practical compromise).

LOCAL DATA

There are several reports and maps of the physical characteristics of the Montreal region (2) and of the geology of the area (3-8) that summarize the observations from outcrops, temporary excavations, and drill holes. The locations of some data are more or less closely described, but most information has been correlated and generalized on maps having scales of 1 cm to 180 m (1 in to 1500 ft) (1:18 000) to 1 cm to 633.6 m (1 in to 1 mile) (1:63 360). Some sections are also available. Most of the early geotechnical records are qualitative and describe troublesome problems such as marine clays and quicksands (3). Clark (5) has deduced and plotted an extensive fault pattern chiefly from stratigraphic studies, as there are few positive indications of faults on the surface except in quarries.

A major construction period started in about 1960, and there was a great increase in the amount of exploratory drilling. Much has been summarized in the latest reports and maps and, in 1972, data from some 25 000 holes were coded in computer format. Unfortunately, there was insufficient funding for the implementation of a computer system having ready availability of selective printouts. An earlier pilot system did produce tabular and graphic output (9), but that too could not be kept operational.

Thus, at present, although there are the above-cited published reports and others on particular areas (1, 10-15), searches of the files of individual organizations must be made for specific projects. For government projects, consulting engineers may be given authorization for full access to previous government data held by other consultants. The cost of such searches is often relatively small and there is the possibility of obtaining personal comments not in reports, yet there are definite chances that knowledge of isolated but significant geologic anomalies may remain hidden in the files of some small organization.

GEOLOGY

The geological succession to today can be summarized briefly by the sequence of geological happenings shown in Figure 1. The generalized succession of geological units is fill; peat; sands and gravels; lake clays and silts; marine clays and silts; tills; and limestones, dolomites, and shales or sandstones, all having weakened zones associated with local faulting and igneous intrusions.

The so-called normal geological factors significant in engineering are those that can usually be extrapolated from preexisting data and can be handled on a routine basis during construction; the special factors are frequently both difficult to locate and expensive to treat (15).

Figure 1. Geological history of Montreal: sections showing principal events and features.

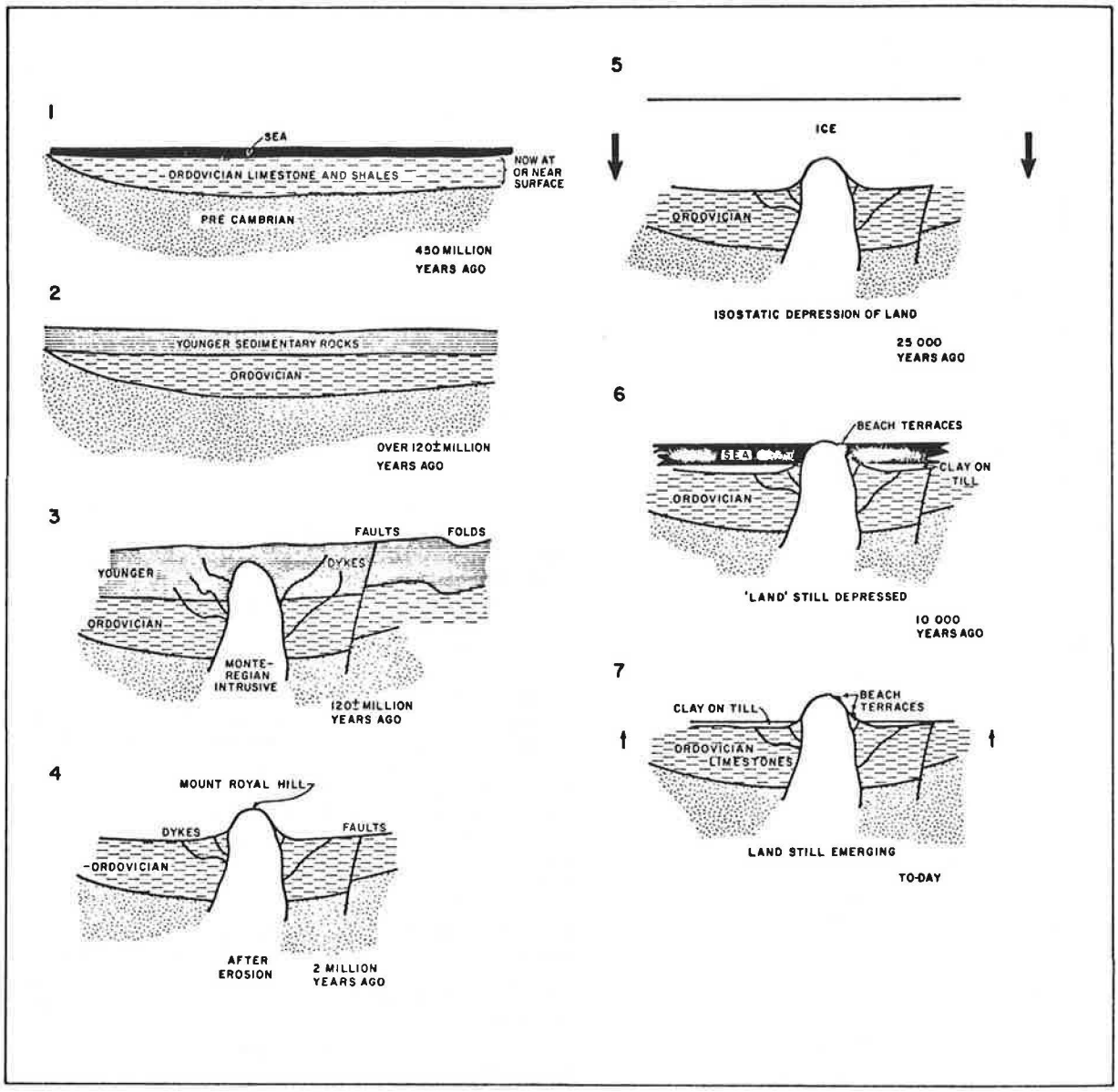

Figure 2. Montreal Metro: Intersection of subway tunnels and the White Horse Rapids Fault.

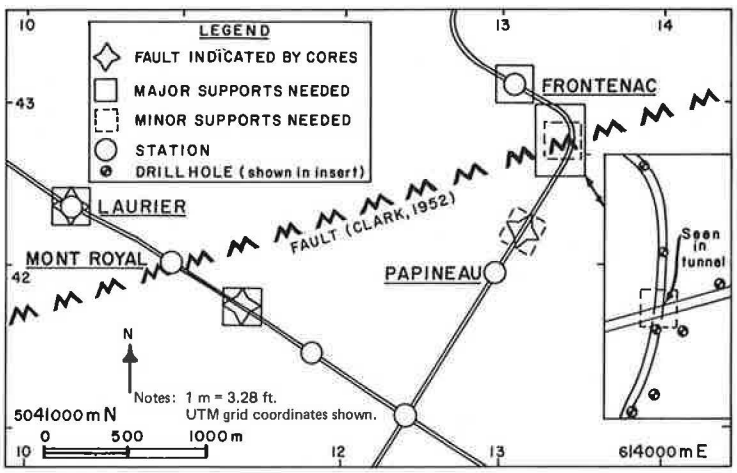

Figure 3. Montreal Metro: effect on construction of a disturbed zone in Utica shale—(a) profile showing locations of exploration drill holes, core recoveries, and tunnel supports; (b) average core recoveries; (c) relative monthly advances; and (d) estimated relative costs.

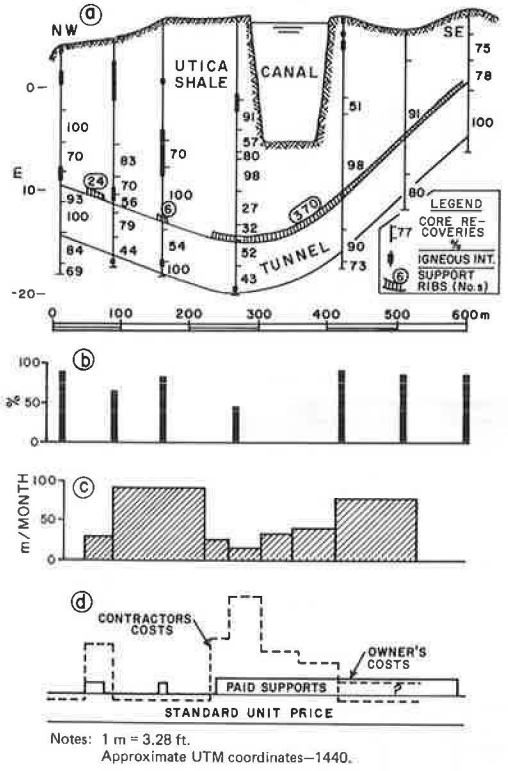

Notes: 1 m = 3.28 ft.
Approximate UTM coordinates—1440.

Figure 4. Montreal Metro: effect on the construction of a small fault zone in shaley Trenton limestone—(a) profile showing locations of fault and exploration drill holes, (b) RQD values, (c) average daily advances, and (d) actual and theoretical volumes of concrete lining.

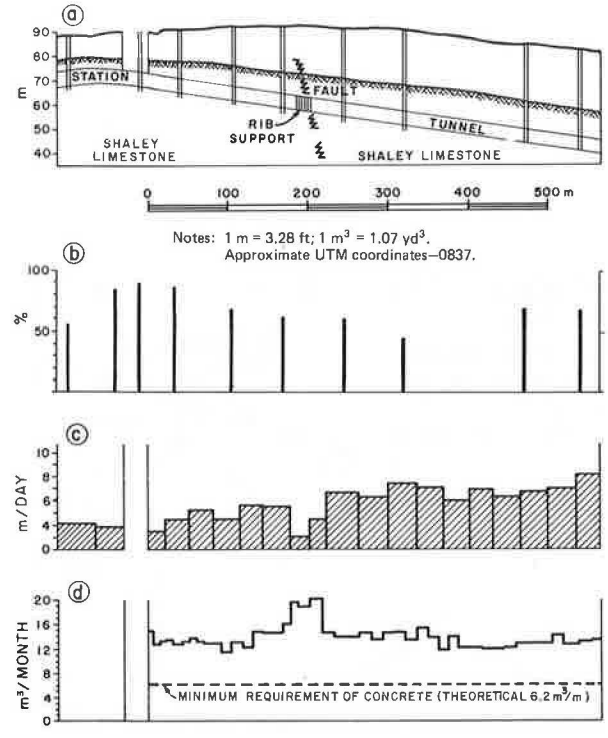

Notes: 1 m = 3.28 ft; 1 m^3 = 1.07 yd^3.
Approximate UTM coordinates—0837.

Table 1. Relative unit costs for excavation and construction of Metro lines.

Cost Item	Relative Cost
Contracted	
Open cut in normal soil and rock and tunnels in rock	1[a]
Tunnel in rock at times of high economic activity	2[b]
Open cut in unstable soil	3
22-m-long open cut in soil and close to buildings	10
400-m-long open cut that has a slurry trench in 25-m deep soil and transition to rock	12.5
Extra accepted by client in addition to those above 560-m-long open cut in Bentonite near river	0.03
Tunnel in shale	
3000 m long, few intrusions	0.12
2200 m long, adjacent to moderate-sized intrusion	0.17
1200 m long, few intrusions, thin rock roof	0.20
640 m long, adjacent to moderate-sized intrusion	0.25
Total actual to contractor	
18-m wide tunnel in limestone with altered intrusive zone	6
Cost of standard exploration drilling at 90-m centers	0.005

Note: 1 m = 3.28 ft.
[a]Standard unit price. [b]Twice standard unit price.

Nevertheless, if the occurrence of special factors in an area has been well documented, even if they are not encountered by chance, close drilling, or geophysical methods, during exploration, continuous careful observation can be made to minimize their effects.

METRO SYSTEM

Preliminary work on the Montreal Metro subway system began about 1960 at a time when Clark's report (5) was about eight years old and Prest and Hode-Keyser's report (7) was about to be published. Thus, the planners were fortunate in having two recent government interpretations on hand. Nevertheless, a standard pattern of holes at 90-m (300-ft) spacing was drilled that proved to be necessary. Examination of the cores confirmed the existence of Clark's faults but, more important, many of the features were located precisely by direct intersections with follow-up drill holes. In addition, data on the order of irregularities of the bedrock surface were obtained. This information was essential as many of the tunnels were planned to be at minimum depths compatible with safe rock cover.

The major White Horse Rapids Fault (see Figure 2) had been indicated by Clark on his map. The fault intersections appeared to be close to the proposed Mount Royal Station and between the Papineau and Frontenac Stations. Preconstruction drilling indicated that the fault is a disturbed zone about 180 m (600 ft) wide and located across the next station, Laurier, nearly 700 m (2300 ft) from the Mount Royal Station.

When the tunnel was excavated, the situation was found to be even more complex. The Laurier fault zone was confirmed and required 101 steel ribs for support, although a fault interpreted from cores to be north of Papineau Station caused no problems. A fault in an unexpected location was found in Frontenac Station and required 77 ribs, although the rock cores from the drill holes in the area were of good quality.

As another example, a 240-m (670-ft) long section of the tunnel through the Sainte-Helene Island breccia was excavated in a month. This was very stable, as might have been expected from the excellence of the breccia as a building stone. However, soon after, a 200-m (650-ft) long stretch (see Figure 3) of Utica shale was encountered. Here, the drill holes had intersected intrusions and there were some low core recoveries near tunnel elevations. Forward progress decreased to an average of less than 40 m/month (130 ft/month) for five

Table 2. Tunnel excavation rates.

Excavation Method	Type of Rock	Type of Support Installed	Rate in Normal Rock (m/day)[a]	Faulted Zone		
				Rate (m/day)[a]	Length (m)	Decrease Factor
Conventional	Shale	Ribs-shotcrete	9.5	4.3	75	2.2
	Shale-limestone	Shotcrete	10.4	5.5	45	1.9
	Limestone	Ribs	6.1	2.4	185	2.5
	Limestone	Rock bolts	6.7	4.6	150	1.5
	Limestone	Ribs-shotcrete	6.7	2.0	165	3.3
	Limestone	Shotcrete-bolts	15.2	7.3	250	2.1
TBM	Limestone	Some ribs	27.8	13.7	180	2.0
	Limestone	Steel plates	31.4	1.4	30	22.4
	Limestone	Steel plates	30.5	7.5	230	4.1

Note: 1 m = 3.28 ft.

[a]Rates computed as mean values for normal operating days only.

months, and continuous support, including complete backfilling of the tunnel with concrete after the ribs were squeezed, was necessary. The possible order of contractor's losses is shown in Figure 3d.

This case history demonstrated that rates of monthly advance can be cut to a quarter of the normal in disturbed zones within a kilometer (half mile) of a breccia plug and suggested that more core drilling during the construction period would have been desirable. This in fact was done a few months later when the first signs of instability were encountered at another heading in the Utica shale and resulted in a decrease to about 30 percent of normal production for only one month.

A third example is at an intersection of the Metro with a fault trace in shaley limestone (see Figure 4). The relative importance of one of the features is shown by the need for 13 ribs and the reduction in the rate of advance from about 6 m/day (20 ft/day) to about 2 m/day (7 ft/day) for 7 days, followed by a period of zero advance for 11 days.

The excavation began at the station and progressed to the right, at an increasing daily average rate unrelated to the rock-quality designation (RQD) of the core (16). The above-average overbreak and a decrease in excavation performance that occurred in the small fault zone where the ribs had to be installed had not been predicted by the RQD data because no bore hole was in the fault itself. After excavation, mapping of the tunnel showed that the overbreak was associated mainly with the fracture pattern and the presence of small intrusives related to the fault.

Contract and extra costs are summarized in Table 1. The 7 km (4.5 miles) of tunnels in shale appear to be the least stable and cost, on the average, an additional 20 percent. Costs for open cuts are also included. Nevertheless, the unit cost for the more weathered locations (usually with faults and more intrusions) must have been appreciably greater for the contractors (Figure 3). The delays were chiefly at the contractors' expense, as far as salaries and equipment were concerned, although the owner paid directly for additional supports and, in a few cases, some redesign. Other owner costs have been for loss of revenue when openings of new sections of the system have had to be delayed.

SEWER AND AQUEDUCT DEEP-TUNNEL SYSTEMS

Although sewers and aqueducts cannot be considered as true transportation systems, the data from a major network of deep-tunnel aqueducts built in the last 10 years are relevant. About 75 km of tunnels of varying diameters [from 2 to 6 m (7 to 20 ft)] were built in rock, mainly at depths of 10-70 m (30-200 ft) by using construction methods quite similar to those used for the Metro [with the exception of the use of tunnel boring machines (TBMs) for a fifth of the total length].

The recent introduction of TBMs in Montreal has demonstrated their excellent performance in normal conditions in sedimentary rocks. Excavation rates of up to 30 m/day, with a peak of 65 m/day, have been achieved; comparable lengths of tunnels excavated by conventional method required four or six headings with two or three working shafts to be completed in the same time. However, the encountering of fault zones affects the rate of advancement when TBMs are used more seriously than when conventional methods are used (see Table 2). There is usually only one heading for the less-adaptable TBM rather than the two or more for the conventional method, so that the occurrence of a fault zone has a more pronounced impact on contractors' costs. In three of the nine fault zones that were crossed by TBMs, the rate of advancement was slowed by factors of 2-22, although comparable situations in conventional excavations resulted in decrease factors of only 1.5-3.3. Thus, rock quality should be predicted more precisely for tunnels to be excavated by boring machines. The weekly reports on 6.2 km (10 miles) of one tunnel job summarized below show that progress in bad rock is about 25 percent of that in normal limestone.

Type of Excavation Problem	Tunnel Length (% of total)	Working Time (% of total)
None		
In shale	6.5	7.8
In limestone	64.9	43.0
Equipment (in limestone)	16.4	17.9
Bad rock conditions (in limestone)	11.3	29.6
Personnel (in limestone)	0.8	1.7

DISCUSSION OF COSTS

Costs are minimized if the most economical design is used along the most satisfactory route where, among other factors, all areas of geologically caused difficulties have been located before design is finished. If the costs of overcoming these difficulties can be assessed, then more economical alternatives can be investigated. Intensive surveys are required, because there are enough anomalous geological conditions in Montreal to make it likely that some problems will be encountered along the extended paths of most transportation projects.

Most of the likely geologically related problems (except a large earthquake) have been experienced in Montreal within the last 20 or so years. The most frequently encountered problems include the following.

1. Thin limestones can alternate with shale or other weak interbeds: Assessment of the core is difficult because RQD values are affected not only by fracture

density, but also by bedding thickness; thus, many abnormally low RQD values were observed in relation to the actual rock conditions encountered in Montreal tunnels.

2. Roof instability requiring heavy support can be caused by a thin [approximately 1-cm (0.39-in)] layer in altered sills or dykes, usually in the chilled zones. Core samples of these layers are frequently described as thin clay seams or disintegrate in the core boxes. They do not significantly affect the RQD value computed on a 3-m (10-ft) length but are very important if they are located near or intersect the crown elevation at a low angle.

3. Fault zones sometimes have thicknesses of a tenth or less of the standard spacing of boreholes: This does not mean that the spacing should be decreased to the dimension of the expected fault, but rather that RQD values are only rough indicators of support requirements. Detailed geologic analysis of the cores is more effective. Bore holes located near a fault, but in good rock that has a high RQD, showed other indications of a probable fault: core joints with slickensides, lack of stratigraphic correlation with adjacent holes, abnormally high values of the apparent dip, or even the occurrence of a high proportion of minor intrusions. When such an analysis points out the approximate location of a fault, additional drilling, preferably inclined, should be done to precisely evaluate the location and extension of the bad-condition zone.

This should lead to lower bid prices because contractors will be less likely to encounter the costly problems that require the self-insurance of higher bid prices. Certainly, this study provides qualitative justification of the need for more-detailed geological observations, including probing during the construction period. This activity carried out daily, and more intensively during the weekend shut-down periods, should alert contractors to the precise locations of localized difficulties that may have been missed by the predesign drilling.

ACKNOWLEDGMENT

We wish to acknowledge the invaluable assistance of many Montreal engineers and geologists, especially P. P. Arbic, M. Quesnel, and M. Chayer of the Office for Metropolitan Transportation of Montreal; R. Perrault, J. Richard, and A. Campeau of the Laboratory for Control and Research, city of Montreal; P. Catafard and F. Couture of the Public Works Service, city of Montreal; and J. Marcotte, G. Legault, and R. Deslauriers, of the Montreal Urban Community Water Purification Department. Access was permitted to many unpublished reports and drawings from which data have been incorporated in this paper. The work was supported by grants from McGill University and from the National Research Council of Canada.

REFERENCES

1. R. H. Grice. Engineering Geology of the Montreal Subway. Engineering Geology, Vol. 3, No. 2, 1966, pp. 59-74.
2. J. M. Wolfe. Caractéristiques Physiques de la Région. Service d'Urbanisme, Ville de Montréal, Bull. Tech., No. 4, 1966, 51 pp.
3. J. Stansfield. The Pleistocene and Recent Deposits of the Island of Montreal. Geological Survey of Canada, Ottawa, Memoir 73, Geological Series 58, 1915, 80 pp.
4. C. L. Cumming. The Artesian Wells of Montreal. Geological Survey of Canada, Ottawa, Memoir 72, Geological Series 60, 1915, 153 pp.
5. T. H. Clark. Montreal Area, Laval and Lachine Map-Areas. Department of Mines, Province of Quebec, 1952, 159 pp.
6. T. H. Clark. Montreal-Area Geological Report: 152. Geological Exploration Service, Ministère des Richesses Naturelles, Québec, 1972, 244 pp. with map.
7. V. K. Prest and J. Hode-Keyser. Géologie des Dépots Meubles et Sols de la Région de Montréal, Québec. Service des Traveau Publics, Cité de Montréal, 1962, 35 pp.
8. V. K. Prest and J. Hode-Keyser. Geology and Engineering Characteristics of Surficial Deposits: Montreal Island and Vicinity, Quebec. Geological Survey of Canada, Ottawa, 1977, Paper 75-77, 29 pp.
9. R. H. Grice. Geological Data Handling in Urban Areas. Canadian Geotechnical Journal, Vol. 8, No. 1, 1971, pp. 134-138.
10. M. Durand and G. Ballivy. Particularities Rencontrées dans la Région de Montréal Résultant de l'Arrachement d'Ecailles de Roc par la Glaciation. Revue Canadienne de Geotechniques, Vol. 11, No. 2, 1974, pp. 302-306.
11. M. Durand. Géologie Urbaine à Montréal: Application aux Travaux d'Excavation de Construction et l'Aménagement. Ecole Polytechnique de Montréal, Québec, Rapport EP 74 R 36, 1974, 150 pp.
12. M. Durand. La Géologie et la Construction du Métro. L'Ingénieur, No. 319, 1977, pp. 3-7.
13. M. Durand. Classification des Phénomênes et Cartographie Géotechnique des Roches Rencontrées dans les Grands Travaux Urbaines à Montréal, Canada. Proc., 3rd International Congress, International Association of Engineering Geology, Madrid, Section 1, Vol. 1, 1978, pp. 45-55.
14. R. H. Grice. Engineering Geology of Montreal. International Geological Congress, Montreal, Field Trip Guidebook B-18, 1972, 15 pp.
15. R. H. Grice. An Approach to Engineering Investigations on the Island of Montreal. Canadian Geotechnical Journal, Vol. 13, No. 4, 1976, pp. 397-417.
16. A. D. Merritt. Geologic Predictions for Underground Excavations. Proc., 1st North American Rapid Excavation and Tunneling Conference, Chicago, American Institute of Mining, Metallurgical, and Petroleum Engineers, Vol. 1, 1972, pp. 115-132.

Publication of this paper sponsored by Committee on Soil and Rock Properties.

Soil Surveys: Review of Data-Collection Methodologies, Confidence Limits, and Uses

Fred P. Miller, Department of Agronomy, University of Maryland, College Park
Donald E. McCormack, Soil Survey Interpretations Division, Soil Conservation Service, U.S. Department of Agriculture
James R. Talbot, Engineering Division, Soil Conservation Service, U.S. Department of Agriculture

The scientific basis of the soil survey is that the locations of soils on the landscape have a degree of predictability. Soil surveys are reasonably accurate and affordably feasible because this soil-landscape association possesses a degree of correlation that is high enough to allow inferences and predictions of soil behavior. The soil surveyor uses a working model of soil genesis on the landscape and tests it through observations. Inferences derived from these observations are extrapolated to the boundaries beyond which the inferences have been judged by the soil scientist to be invalid by virtue of changes in one or more of the factors (e.g., slope, vegetation, parent material) responsible for controlling soil genesis. In most areas, the natural scatter or range of soil properties and the variability of the soil-landscape precludes the delineation of taxonomically pure soil units. This results in inclusions of both similar and dissimilar soils within the soil-unit delineations. Soil scientists recognize these inclusions and describe them as part of the map unit. The composition and variability of soil map units are discussed with examples of how these map attributes can be quantified to provide confidence limits for predictions of soil behavior. It is emphasized that the primary objective of most soil surveys is not to map delineations having taxonomic purity but to provide the user with information as a basis for judgments about soil potentials and behavior for various land uses. Studies and experience have shown that the uniformity of such map units for interpretive purposes is much higher than is their taxonomic purity.

Soil surveys are one of the most widely available forms of geotechnical information. Since 1955, modern soil surveys have been prepared for more than 570 million hm^2 (1.4 billion acres), or nearly 65 percent of the land area of the United States. In addition, there are many soil surveys that were prepared before 1955. Data from these soil surveys can be obtained in the local offices of the Soil Conservation Service, U.S. Department of Agriculture.

It is essential that the definition of soil used by pedologists be distinguished from that in common use in engineering and geology. In the latter fields, soil refers simply to the unconsolidated earthy materials above bedrock. The pedologist, however, defines soil as a three-dimensional natural body at the earth's surface that supports or is capable of supporting the growth of plants, i.e., that part of the earth's crust that is subject to the influence of soil-formation factors.

In soil surveys, the soil horizons within the upper 2 m are observed and described. The characteristics of materials below the soil are sometimes described, but only where sufficient observations have been made to provide reliable information.

USING SOIL SURVEYS IN PLANNING TRANSPORTATION SYSTEMS

Soil surveys can provide data of value in planning the location and construction of highways and are among the most useful sources of information for planning the land uses that will be served by a highway (1).

The design of highways requires that many soil properties be measured by laboratory or field tests or by observations. Many of the measurements that must be made are expensive, e.g., moisture-density relationships and shear-strength, permeability, and consolidation tests.

Because of the time and expense required, intensive investigation, sampling, and testing are done only for design purposes after a site has been selected. It is not practical to make detailed studies of each alternative site for planning.

In planning, however, it is important to have some indication of soil properties over a wide area. This makes it possible to consider other land uses and alternative locations for highways. Data from soil surveys can be obtained by the transportation engineer without extensive work and expense.

Soil surveys provide a general indication of compressibility, density, strength, and bearing capacity. They also provide more specific information about other soil properties and attributes, such as drainage and moisture regime; ease of excavating and hauling; and slope, erosion hazard, and depth. In addition, the following soil properties important to highway planning are indicated by the soil horizon: (a) textural class; (b) mineralogy; (c) soil chemistry, including pH and salt content; and (d) presence of coarse fragments that might affect excavating, spreading, and compacting.

From these properties, general interpretations can be made, including (a) plasticity characteristics and classification according to various engineering and textural classification systems, (b) potential for frost action, (c) potential for shrink-swell, and (d) hazard of flooding.

Several of these properties, such as depth to bedrock and soil slope, are measured directly at sampling points within each map unit. Other items are interpreted or inferred from the data collected and the observations made.

Ratings of soil limitation and potential are prepared on the basis of these soil properties. The ratings provide a quick means of comparing soil map units for numerous land uses.

Although many of the soil engineering data provided in soil surveys are not measured directly and may not provide the precise numbers needed for design analyses, these data do provide valuable information for planning design activities. When supplemented with geologic maps, soil profiles can provide a basis for planning the detailed investigations necessary to obtain design data. Examples include the type of investigation and the sampling tools needed, the approximate location of contact zones between differing conditions, and construction season length as related to temperature and weather conditions.

The methodologies of collecting soil-survey data and information, analyzing the composition of soil map units, and evaluating the variation or range of soil properties

are described below. Understanding these methodologies should help highway engineers and other interpreters of soil-survey information to use soil surveys more effectively, considering the limits of their intended use and the confidence limits of the information.

DATA COLLECTION

The key to making use of the data in soil surveys is to understand exactly what procedures were used to obtain them, the kinds of data collected, and the amount of data collected per unit area. Soil surveys differ widely in the kinds and amount of data collected. The intensity of data collection depends on the objective of the survey.

Scientific Basis of Soil Surveys

The soil survey is basically a data-collecting activity. Soils rarely occur randomly on the landscape, and they can be stratified and mapped with some degree of reliability. Thus, the soil survey is unlike many surveys of either fixed or infinite populations. Because of cost and time constraints, a random data-collection technique that allows every member of the population of soils on the landscape an equal chance of being sampled is neither practical nor necessary in most soil surveys. Therefore, the soil scientist purposely practices a form of sampling bias or stratification of landscapes in selecting the sample sites from which inferences will be extrapolated to derive the soil boundaries. In essence, soil scientists stratify the universe (population of soils) before them in an effort to segregate the landscape into classes that have definable ranges of properties. The geologist also practices this technique out of necessity, producing maps that have a degree of reliability that is based on the association of geologic formations with landscapes or geomorphic units.

The purpose for sampling the soil, therefore, is not simply to obtain a number of random samples from which conclusions will be drawn to make a map when subjected to statistical techniques but rather to either confirm or reject the soil scientists' hypothesis of what soil is expected on a given landscape unit. Soil mapping then is basically the ability of the soil scientist to develop a working model of soil genesis on the landscape and test it by observations.

The soil surveyor observes soil by excavation (borings, for example) only at certain points on the landscape. But, because soils form a continuum on the landscape, it is necessary to infer through judgment where one soil ends and another begins. Therefore, the delineation of soil map units and the interpretations about their behavior are derived from inferences extrapolated from very small samples. More than 99 percent of the soil delineated by the soil surveyor in making a soil map is not observed below the surface. Yet the association of different kinds of soils with certain landscapes possesses a degree of correlation that is high enough to allow inferences and predictions of soil behavior to be made.

Although the soil scientist cannot record what the soil is like at every point on the landscape, those who commission and use soil surveys often want such information (2). They want to be able to infer or predict the nature of the soil at all places (even though relatively few observations were made). And, although the essential objective of soil surveys is the collection of information, many users of this information do not understand the way in which it is obtained and the way in which the interpretations of soil behavior are inferred. Information and inferences made from single observations are extrapolated to the boundaries between the map unit and other units (in which similar observations were made). Therefore, the information is not site specific for each point within a map-unit delineation. Efforts to use this information as site specific for small areas cause substantial problems. The misunderstanding of the soil survey and the arguments that follow are due largely to these problems. Understanding that on-site studies are needed for many site-specific applications would do much to prevent these problems.

The scientific basis of the soil survey, therefore, is that soils and their location on the landscape are predictable (to be sure, some more than others) to an experienced soil scientist who has knowledge of the geology, climate, and landform patterns of the area. In essence, the soil scientist must be able to read and predict the relationship between the landscape and the soils that have formed on it. The sampling technique, therefore, is used to confirm the prediction based on the soil scientist's model. If the observed soil profile fails to confirm predictions, the soil scientist must develop a new working model through further study.

Making Soil Surveys

Preliminary Planning

Preliminary planning of soil surveys centers on discussing and reaching agreement on the kind and amount of data that must be collected. This question is decided on the basis of the land use for which the soil survey is to be prepared.

Soil surveys are prepared for a wide variety of land uses. Categorizing all soil surveys as agricultural has never been appropriate. In some areas, soil surveys are designed to provide data to guide rapid urban development, in other places, they are used to plan irrigated agriculture, woodland, or other land uses. Obviously, a given soil survey can provide useful data for many land uses. However, more data are required for some land uses than for others. For example, in an area of intensive agriculture in California, a soil survey having a scale of 1:24 000 may be adequate for planning crop sequences, fertilizer needs, drainage requirements, and other management practices within fields, but a scale of 1:20 000 or 1:15 840 may be needed to plan the encroaching urban development.

As this implies, the mapping scale is a key early choice in planning soil surveys. It is usually based on the minimum area for which specific soil data are needed for decisions about the use and management of land.

Preliminary Field Investigations

Before operational mapping is done, existing geologic surveys, old soil surveys, and other sources of soil information, along with aerial photographs and topographic maps, are studied to learn as much as possible about the soils and landscapes. Also, the local relationship between soils and plants is studied to ensure that the useful indicators of soil differences are identified.

In preliminary field investigations, some soil profiles and certain small tracts can be given more intensive study than is done in the normal mapping process that is used in the operational stage of the survey. These intensive studies will cover only a portion of the survey area. Their main purpose is to determine the pattern of soil variation in each of the physiographic areas of the survey area (3). Some of these physiographic areas have a complex pattern, whereas others possess a more uniform soil pattern. In the more-uniform areas, it usually is not necessary to collect as many data during operational mapping as in the more-complex areas.

Based on these careful early investigations, the soil map units are described in as much detail as possible before operational mapping. In these descriptions, the pattern of soil occurrence and the relationship of soils to landscapes are emphasized and the proportion of each soil is estimated. During this stage, tentative soil surveys are prepared for the areas studied.

Operational Mapping

Operational mapping requires data collection by three main approaches: (a) inferences drawn from landforms and vegetation, (b) on-site borings, and (c) laboratory characterization.

Soil surveys are made by traversing the land, largely by walking. The surveyor knows the geologic formations in the area. The kinds of vegetation are identified. The surveyor has the benefit of the preliminary field investigations and soil descriptions. In addition, the surveyor draws on his or her own understanding of the relationships between soils, landscapes, and vegetation.

The first step is to use preexisting relationships to infer which soils occur in a given area. The value of inference as a form of data collection has not previously been given proper emphasis in descriptions of mapping procedures. Because it is never practical, regardless of the scale of sampling, to sample all the soil, the assumption is that the areas between samples were properly characterized by the samples taken. This point will be addressed in greater detail below.

As the surveyor traverses the landscape, he or she studies the landforms and other features and infers the soil most likely to exist on each landscape segment. Borings are made to identify the important soil properties and classify the soil. The borings test the inference made. At these boring sites, the type, thickness, structure, and color of each soil horizon are determined. Textural classes are estimated by field procedures. Quick field tests of soil pH and salinity are made as appropriate. Based on these borings and the information derived from them, the kind and sequence of horizons are identified and the soil is classified into the appropriate class or taxa. From this information, the proper soil map unit is decided. The edges of the soil map unit are located by judging the location of transition in one or more of the factors (e.g., slope, vegetation, or parent material) that control soil genesis.

The surveyor sketches the soil boundaries as far ahead as possible along the transect being followed. Then, as he or she proceeds, the accuracy of the projected location of soil boundaries can be determined. This process is essential because it is the only rational method of deciding how far apart the transects should be. The accuracy in projecting ahead is the same as the accuracy in projecting to the side of the transect.

During mapping, the soil observed in a very high proportion of the borings should conform to the surveyor's inferences. Where it does not conform, additional borings are made to determine the reasons for the departure.

The number of borings made is highly variable in a given soil-survey area. It is based on the judgment and experience in the area of the soil surveyor and on the complexity and predictability of the soil-landscape relationship. For example, on a 10-hm^2 (25-acre) moraine front slope where the soil pattern is variable, 10-15 borings may be needed to determine the pattern of soil variation. On a 2000-hectare (5000-acre) lacustrine area, where there is little soil variation, 10 borings may be sufficient.

Laboratory characterization data are obtained from a limited number of soil profiles in a soil survey area. The main purposes for obtaining these data are to provide a basis for improvement of the ability to make accurate field estimates of soil properties and to provide benchmarks for use in classifying and interpreting the soils. Some properties, such as cation exchange capacity, are correlated or associated with observable properties, e.g., pH or texture, and it is necessary to check this correlation occasionally. Laboratory testing is done for similar reasons to determine the engineering index properties of major horizons of selected soil series.

Selection of Sample Sites for Laboratory Characterization and Field Classification

Sample sites are selected—whether for laboratory characterization or for borings for field soil classification—to represent a unique landform position in which a specific kind of soil is expected. For efficiency in mapping, those landform positions most representative of the delineation are chosen. However, positions that differ from the norm must also be examined to determine whether or not the soils expected in these positions actually occur there.

Presentation and Display

Some of the data collected during soil mapping are summarized in soil map unit descriptions. Laboratory data—and, in a few cases, transect data—are presented in tables. By far the greatest volume of data is collected from regular borings and by inference from the landforms and vegetation. These data are presented in the map-unit descriptions, which are thus the most useful reference.

In a map-unit description, the user will find a discussion of the proportion of the delineated area in which the dominant soils occur along with a description of the nature and occurrence of other component soils known to occur within the delineation and their position in the landscape. The user is thus alerted to expect small areas of soils in certain portions of the map unit that are different from the dominant soil from which the delineated map unit is named.

Basis for the Predictive Value of Soil Map Units

Once a soil classification scheme has been developed, data obtained from soil landscape studies can be correlated with classification units. Thus, once soils are classified, their behavior can be predicted or their characteristics can be interpreted with some degree of confidence. This requires that data be collected on the observed behavior of the soils in each of the land uses for which predictions of behavior are made. In other words, to the fullest extent possible, those correlations between soil properties and soil behavior that are assumed to be true are checked against actual soil performance.

The behavior of the soil map units can thus be predicted for a variety of uses with a degree of confidence. But before we can know the confidence limits of our predictions about these map units, we must understand their composition and variability.

COMPOSITION OF SOIL MAP UNITS

Soil Map Units Versus Soil Taxa

Even though soils form a continuum on the landscape, the objective of a soil survey is to break this continuum into a reasonable number of segments or units. Each

unit delineated on the landscape has limited and defined ranges in properties so that one can make quantitative interpretations and predictions of soil behavior (4).

Problems and confusion often arise, however, when the distinction between the concepts used to differentiate or define the soil taxa and the map units themselves is not clear. The taxa are conceptual, but the map units are real and may possess characteristics and properties outside those used as differentiating criteria in the taxonomic scheme. This distinction is especially critical when the taxon and the delineated map unit on the landscape are identified by the same name. Furthermore, because the natural scatter or range of soil properties within a particular landscape usually results in some soils falling outside the dominant taxonomic class for which the map unit is named, soil map units usually contain inclusions of more than one taxon.

Of the six categories in Soil Taxonomy (5), the soil series represents the lowest, i.e., the category having the largest number of differentiae and classes (taxa). There are more than 12 000 soil series recognized in the United States.

Each series is a conceptual image of a specific soil that has a common suite and range of differentiating properties as well as a fixed arrangement of diagnostic horizons. The series concept does not imply any geographic or spatial attributes or any specific aspect on the landscape. The series taxon, therefore, is a mental image or concept of a soil body that is known to occur in certain geographic areas associated with specific parent materials or geomorphic features or both. The soil scientist, in observing the landscape, tries to delineate those areas where the concept of a particular soil series applies. For practical purposes, soil series are further subdivided into phases of slope, erosion, stoniness, substratum, and other properties not diagnostic at the series level, so that differences significant to the uses of the soils within the series can be identified. In mapping the soil, a boundary of the conceptual soil body is located in those places where there is a difference in one or more of the factors that control soil genesis. The experienced mapper has learned to look for these places and use knowledge of soil genesis to improve the accuracy and efficiency of the mapping (4).

The resulting map unit carries the same name as a taxon. However, it is important to differentiate the map unit and taxon. Although identified by the same name, they are not, in fact, the same. The geographic attributes of spatial distribution (including size and shape), slope, and slope orientation are not taxonomic criteria but are primary attributes of map units.

The taxon concept is also used in making soil interpretations in the soil survey report. The interpretive tables are designed as if the map units were pure or uniform bodies of soil representative of the taxon concept for which the unit is named. Although the soil surveyor attempts to delineate a map unit composed predominantly of the soil taxon indicated, the map unit contains attributes beyond the differentiae required for the taxon as well as inclusions of other soils not qualifying for the taxon named. Perhaps soil scientists have not done a good enough job of informing soil-survey users that some of these interpretive tables are based on the taxonomic concept and not on the actual map unit. This distinction remains a troublesome point for many soil-survey users. It is imperative, then, that the composition of map units be understood if one is to use soil-survey information effectively. Recently, some interpretations have been presented for both the soil mapping unit and the soil taxon.

Components of Map Units

Since the beginning of soil surveys, soil scientists have recognized the heterogeneity of their map units. Soil map units do contain inclusions of soils (both similar and dissimilar) other than the kind that provides the map-unit name. The extent and diversity of the inclusions vary and are related to the scale of mapping, the complexity of the soil pattern, and the skill and diligence of the soil surveyor (6). The soil scientist must recognize this fact and describe the nature and extent of the inclusions in the map-unit descriptions to the best available knowledge.

Recent studies (3, 6-9) have indicated to soil scientists that their map-unit delineations contain more inclusions of both similar and dissimilar soils than previously suspected (although many of these inclusions do not alter the delineation interpretation). This should not limit the usefulness of the soil survey as long as the character of the soil inclusions and their composition are identified and described. Too often, however, the users of soil surveys believe that the map units are taxonomically pure or that, to be useful, they should be taxonomically pure. Taxonomic purity of map units is not the primary objective of the soil surveyor in making soil surveys and should not be construed as the sole test of their usefulness (6). In most areas, taxonomically pure map units would be possible only on maps of very large scale, which would then have such complex patterns that they would not be useful.

During the last two decades, the definitions of soil series have changed from a basis of a taxon defined loosely around a central concept to that of narrower units defined in terms of class limits or ranges in properties. As a result, the concept of similar soils was introduced. Thus, the allowable map-unit heterogeneity for map units named for a single taxon has increased from the 15 percent inclusion tolerance permitted in the 1951 Soil Survey Manual (4) to the more than 50 percent inclusions of similar soils allowed in the 1967 soils memorandum 66. The 1975 Soil Taxonomy (5) permits a map unit to include other strongly contrasting soil series to a maximum of 10 percent for a single series and, if the soil pattern is too complex to be represented at the scale of the map, combinations of strongly contrasting series to a maximum of 15 percent. These changes signify not a reduction in quality control of soil surveys but an acknowledgment of the variability that has been there all along. Some of this heterogeneity has resulted from the introduction of narrower definitions of soil taxa.

One result of the use of narrower definitions of soil taxa has been a fragmentation of soil areas delineated by using the same standards and scale as those delineated earlier. These fragmented soil bodies on the landscape now become taxonomic inclusions in the map units delineated before the taxonomic refinement. These narrower limits of taxonomic criteria do not usually detract significantly from the interpretive value of the map unit although, as Cline (6) points out, such inclusions illustrate once again the difference between units of classification as concepts and units of mapping as real soils.

When contrasting inclusions occur with such frequency that the mapper has difficulty separating them on the landscape, the resulting map unit is identified as a complex of more than one series. Where such complexes contain contrasting series, interpretations for the behavior of the map unit become difficult. Regardless of the amount and type of inclusions, the soil surveyor has the responsibility to describe the map unit as accurately as possible to reflect its divergence from a taxonomically pure unit.

Aside from the inclusions that are recognized to be

a result of compromises to scale, correlation, cost, and complexity of the soil pattern, there are also unknown inclusions that result from mapping techniques and unavoidable inclusions of other taxa in the map unit. These unavoidable inclusions are the price we pay for the technique employed in making soil surveys, namely, reading the landscape with its characteristic soil association. Cline has noted that, although such a technique makes soil mapping reasonably accurate and "affordably feasible", some error is unavoidable because (a) the predictive value of landscapes is not perfect, (b) the sampling intensity is inadequate to verify the presence of all soil bodies that may exist, and (c) the sampling tends to be biased toward the most prominent soils and landscape features.

Quantification of Mapping Inclusions

Because soil scientists are aware of inclusions and the limitations of mapping techniques to accommodate all components of map units, studies have been designed to determine quantitatively the composition of map units. These studies have shown that the amounts of inclusions in map units differ enormously among surveys. They also show, however, that many inclusions do not alter the interpretations of the map unit even when taxonomic criteria place those inclusions outside the range of the series identified in the map-unit name.

By using transects, grid-sampling procedures, and other techniques, soil scientists today are quantifying the composition of map units. The objective of these analyses is to obtain estimates of the composition of soil units so that it will be possible to say, for example, that with 90 percent assurance, soil A makes up 60-80 percent of a given delineation of a map unit (10). Or one may prefer to express the variability of this map unit in this way: At the 90 percent probability level, soil A makes up 70 ± 10 percent of the given map-unit delineation. As Arnold points out, this is a simple way to inform soil-survey users that, if we continued to sample areas of the map unit again and again, we believe we would obtain a range in the composition of the map unit that includes the true percentage of soil A. Studies of map-unit composition have increased tremendously in the past 10-15 years (3, 6-9).

Typical of such studies is that of Wilding and others (9), who evaluated the variation of soil morphological properties within 24 delineations of six map units in three counties in west-central Ohio. Ten observations within each delineation were made randomly over a 25-hm^2 (10-acre) tract to determine the character and magnitude of map-unit inclusions. Inclusions occurred within all areas studied and were due primarily to ranges of the properties of solum thickness and drainage that were beyond the class limits of the dominant soil taxon. When all forms of inclusions were taken together (eight measured properties), none of the map units (average of 3 delineations) contained less than 57 percent and none of the 24 individual delineations had less than 30 percent inclusions. At all 240 locations, the soils had been classified in the correct subgroup 83 percent of the time; soil series, 42 percent; and soil type, 39 percent. Parent material had been mapped accurately 88 percent of the time; erosion, 94 percent; pH, 70 percent; solum thickness, 63 percent; and drainage class, 65 percent. Once again, despite the high percentage of inclusions caused by ranges of certain soil properties beyond the class limits of the dominant soil taxon, all but 3 of the 24 mapping delineations were well delineated for interpretations of soil behavior or use.

In contrast to the study of Wilding and others, a similar assessment of map-unit composition on the loess-mantled plains of Nebraska showed that 72 percent of the profiles sampled were members of the series identified in the map-unit name (6).

In summarizing a number of studies to quantify the composition of map-unit delineations, Cline (6) concluded that the delineations had been mapped about as well as could have been expected, considering the technique used, and were adequate for interpretations. Many of the inclusions did not contrast enough to detract significantly from the interpretive value of the map units. It is this situation that led to the recognition of "similar" and "dissimilar" soils in the 1967 soils memorandum 66. Even for highly contrasting or dissimilar soils, as Cline points out, it is important to distinguish between those soils that impose more and those that impose fewer restrictions on soil performance under various uses. Thus, there are both "limiting" and "nonlimiting" dissimilar soils that occur as inclusions. Limiting dissimilar soils are the ones that soil mappers are justified in spending much time and effort to exclude from map units (6).

It is again important to emphasize that taxonomic purity of map units is not a proper measure of the quality or precision of a soil survey. As Cline has stated, the quality of a soil survey should be measured in terms of the amount and accuracy of the information it provides as a basis for judgments about soil potentials and behavior for land use. A map unit may have only 40 percent taxonomic purity or classification accuracy but have 90 percent interpretive accuracy. If one uses the soil survey with the understanding that the interpretive tables are based on the predominant taxon present in the map unit, the objective of the soil survey will have been realized. The interpretive value of soil maps has always been considered as a regional or area evaluation tool. Their use was never intended to be a substitute for on-site evaluations or as a tool precise enough for site-specific interpretations.

SOIL VARIABILITY AND IMPLICATIONS ON USE

Variability: Nature's Ubiquitous Attribute

The soil scientist is by necessity a practitioner of an observational science. Very early in the soil scientist's attempts to characterize the soil and delineate its spatial distribution, he or she is faced with one of nature's most ubiquitous attributes—variability or the natural scatter and range of the population of soils and soil properties. The 1951 Soil Survey Manual (4) reminded the soil scientist that "the variation in nature is fixed; failure to recognize it in no way reduces its magnitude".

The objective of the soil survey is to delineate the landscape into soil units that contain less-variable soil conditions than does the total population of soils. The utility of both the taxonomic system used to classify soils and the resulting soil map depends on the precision of the statements that can be made about the behavior of the delineated units versus that of the area as a whole (11). However, if the magnitude of the variability within these delineated units is not known, the precision of the statements that can be made about them is compromised.

Thus, soil scientists, geologists, soil engineers, and other earth scientists are constantly faced with the problem of determining the confidence limits of their data. How many samples are required to obtain a specified confidence interval in estimating the mean of the entire population? And what are the variability indexes and confidence limits of different properties measured from the same number of samples? The soil scientist cannot speak with equal degrees of confidence about soil

pH and clay content, even though both were measured from the same set of samples. Likewise, the soil engineer must recognize that moisture-density relationships and shear-strength measurements do not have equal degrees of variability and, therefore, do not have similar confidence limits when measured from the same sample.

Measuring Soil Variability and Confidence Limits

There are numerous studies (3, 9, 11-13) of the variation of soil properties over distance, but most of them have relied on analysis of variance, according to Campbell (13). It is Campbell's contention that, despite the variety of sampling plans used in these studies, these methods do not permit concise and complete description of changes over distance, and he has therefore suggested and tested another approach to the analysis of soil variability. This approach uses a portion of regionalized variable theory, which encompasses a body of statistical theory tailored for the analysis of the spatial variation of continuous geographic distributions, and centers on the premise that, although the precise nature of the variation of a regionalized soil property (variable) is too complex for complete description, the average rate of change over distance can be estimated by the statistical parameter of semivariance.

The intensive sampling strategy required for this technique is not practical for routine use by soil surveyors. Campbell, however, maintains that it may be possible to obtain rough estimates of the relative degrees of spatial variability without sampling each and every soil body we wish to study.

The study of Wilding and Drees (11) is typical of those using the coefficient of variability ($\overline{CV}$) to measure the magnitude of soil map-unit variability. These workers used their own data plus data from the literature to determine CVs for selected morphological, physical, and chemical properties within map units. The CVs for most properties ranged from 25 to 35 percent.

Wilding and Drees also addressed the question of variability and the number of observations necessary to estimate the mean within specific limits at a 95 percent confidence interval. In other words, how many samples are necessary to achieve an accuracy of estimating the mean within ±10 percent compared with those necessary for an accuracy of ±20 percent (at the same degree of variability and confidence interval)? For the evaluated data, the number of observations required to achieve an accuracy of ±10 percent is four times that for ±20 percent at the same CV. These data indicate that, to increase the accuracy of estimating the true mean of the soil population, we must increase our sampling or number of observations exponentially. Figure 1 illustrates the relationship between the number of observations necessary to estimate the population mean within specified limits and the CV.

Figures 2-4 illustrate the variability, as measured by the CV, for soil morphological, physical, and chemical properties as determined from the data analyzed by Wilding and Drees. These evaluations of characterization data indicate that we, as interpreters of the data, cannot speak with the same degree of certainty about the confidence limits of soil pH or of Atterberg limits as about depth to mottling and solum thickness. The first two properties are less variable than the latter two (11). Therefore, the degree of confidence and accuracy of our statements about the pH of a soil map unit is much higher than the accuracy we can express about the mean solum thickness. For the property of solum thickness, we may need to observe three to four times as many profiles as would be necessary to establish the same degree of confidence or accuracy for the properties of mean total silt content or of pH. Table 1 presents a ranking of the variability of the soil properties analyzed by Wilding and Drees that shows the number of soil profiles necessary to estimate the mean of the population within similar confidence limits.

Properties that exhibit CVs of more than 30 percent require so many observations or measurements to obtain an accuracy of ±10 percent that sampling may be impractical. But this situation does not relieve the investigator from the obligations of knowing and describing the basic variability and components of the map unit.

Most sampling procedures used in making soil surveys, engineering soil maps, and other soil measurements are never subjected to statistical evaluation to determine the soil-property variation and its central tendency. Samples are often obtained, properties measured, the data cranked through various equations, and interpretations made as if all measured properties possessed the same degree of variation and confidence limits. As shown in Table 1, this assumption is not valid.

TRANSMITTING SOIL INFORMATION THROUGH MAPS

Basis for Predicting Soil Behavior from Soil Surveys

The objective of the soil scientist, geologist, or other earth scientist in making a map is to provide a spatial classification that transmits information about features at or near the earth's surface for a defined purpose. As Varnes (14) points out, this transmission is effective only if the mapmaker, the map, and the map user are so coordinated that the maker's concept is transferred to the user's mind without significant alteration. The success of transmitting information contained in soil or geologic maps to fit the needs of civil engineers (or any other type of user) depends on the accuracy and reliability that are required, how closely the properties of interest covary with the mapped boundaries, and how heterogeneous the soil or geologic units are with respect to these properties.

Predictability of Soil Behavior

Soil maps are used largely as a basis for predicting the behavior of soils. The confidence of the prediction from the map is a function of the variance of the soil property or properties concerned.

The method used by soil scientists to derive predictability of soil behavior for soil maps prepared from sample data is to correlate the data with a soil classification of the area. Prediction for any point, therefore, is based on data from the map unit to which the point belongs (2). The basic premise of this technique is that the variance in the map unit is less than the variance in the population of soils in the area as a whole; hence, the confidence interval for prediction should be narrower.

The map user, however, wants to know about individual soil properties or the suitability of the soil map unit or both for a specified use. A soil map provides a definitive partitioning of the landscape into map units, within which the desired information and interpretations of soil behavior are indexed by virtue of their location (2). As is described above, however, the confidence limits of the information contained within the partitioned classes or map units vary with the parameter of interest and the heterogeneity of the soil.

Figure 1. Relationship between number of observations necessary to estimate the mean within specific limits at a 95 percent confidence level and the CV.

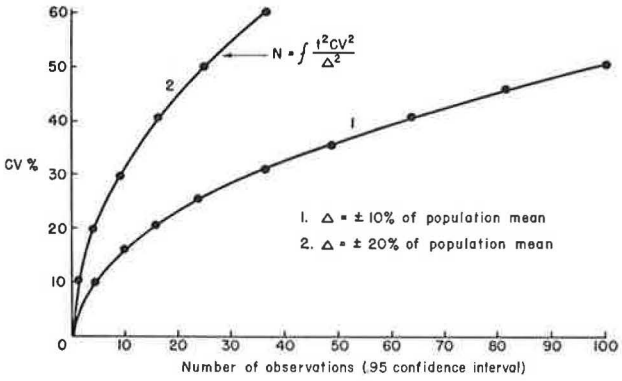

Proper Use of Soil Maps

To use a soil map properly, the user should be aware of how soil landscapes are sampled by the soil scientist and how inferences derived from such observations are extrapolated to produce the delineations that result in the map. The user should also be aware of the composition of the map units with respect to inclusions, the relationship of taxonomic heterogeneity to interpretive accuracy, the different degrees of variability of soil properties, and the confidence limits of interpretations of soil behavior. The credibility of a map is no better than the confidence limits of the statements that can be made about the behavior of the soil map units it delineates.

But maps too often convey greater confidence than is warranted. Varnes (14) points out that a map has great power to persuade, a power that has been termed "carto-

Figure 2. Magnitude of variability of selected morphological properties within map units of a series and a series concept.

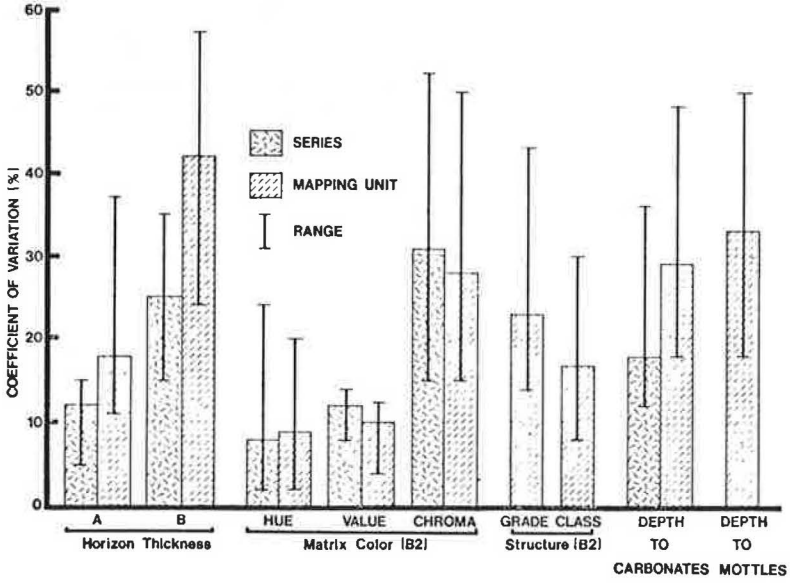

Figure 3. Magnitude of variability for selected physical and chemical properties within map units of a series, a series concept, and a pedon.

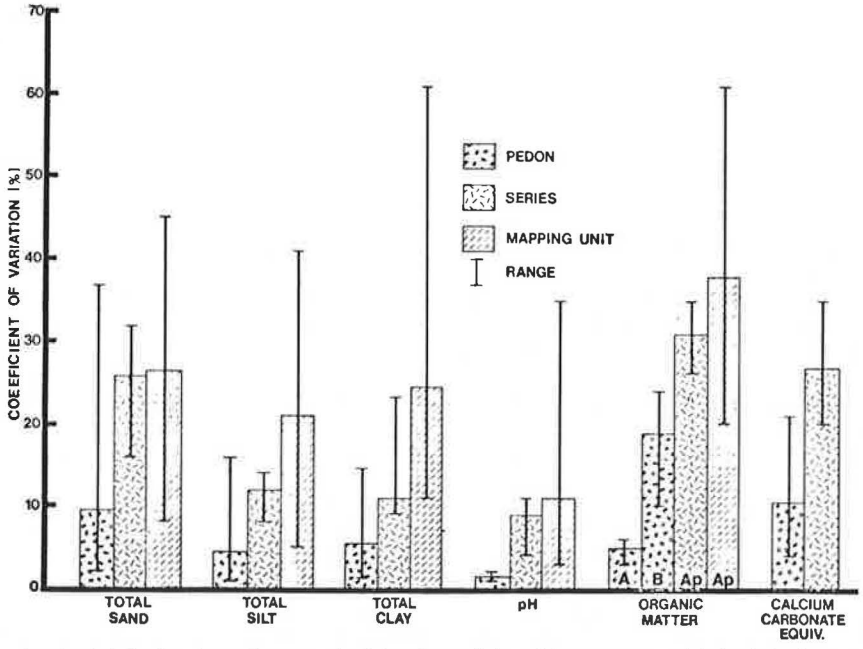

A pedon is defined as the smallest area of soil that shows all the soil layers present and their relationships to one another.

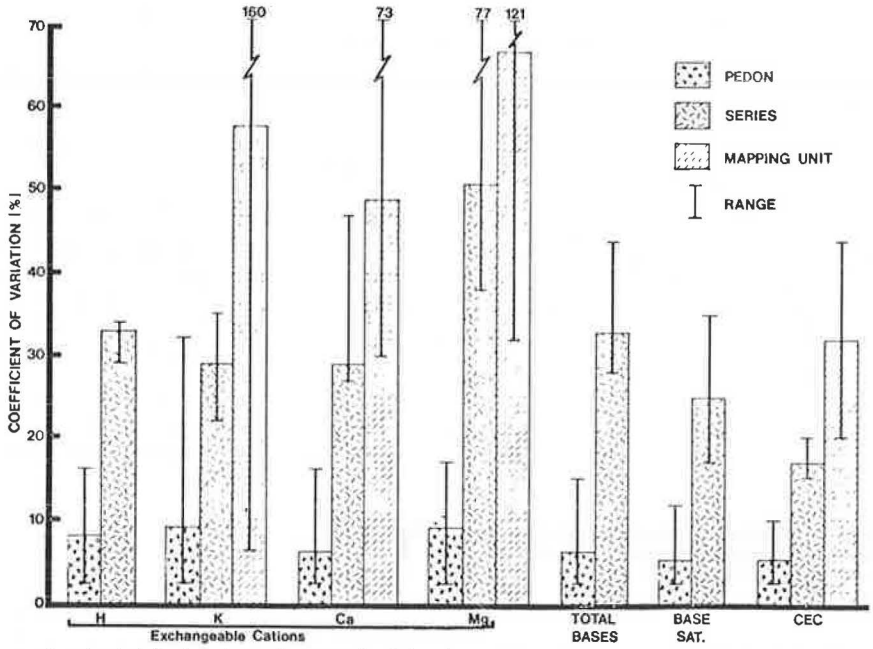

Figure 4. Magnitude of variability of selected chemical properties, including exchangeable cations, within map units of a series, a series concept, and a pedon.

A pedon is defined as the smallest area of soil that shows all the soil layers present and their relationships to one another.

Table 1. Relative ranking of variability of soil properties.

Variability of Property	Number of Profiles Needed	Property
Least	>10	Soil color (hue and value)
		Soil pH
		Thickness of A-horizon
		Total silt content
		Plasticity limit
Moderate	>10 to 35	Total sand content
		Total clay content
		Cation exchange capacity
		Base saturation
		Soil structure (grade and class)
		Liquid limit
		Depth to minimum pH
		Calcium carbonate equivalent
Most	>35	B2 horizon and solum thickness
		Soil color (chroma)
		Depth to mottling
		Depth of leaching (carbonates)
		Exchangeable hydrogen, calcium, magnesium, and potassium
		Fine clay content
		Organic matter content
		Plasticity index

hypnosis". Because most users of a map cannot question its content deeply without direct knowledge of the area and because they naturally tend to believe that some information is better than none, the mapmaker should provide a clear and concise statement of how the map was derived.

The credibility of both the soil map and the interpreter are often at stake. Facts cannot be generated from inferences alone. As map producers, soil scientists, geologists, and other earth scientists must not only evaluate the confidence limits of their products but also clearly relay those confidence limits to the potential user. This is especially critical if the user is unaware of the technique used to generate the map and the degree of variability and heterogeneity within the map units. Too often, the engineer who uses soil maps has not understood their intent, potential uses, and confidence limits because the soil scientist has not done an adequate job in conveying these concepts.

ACKNOWLEDGMENT

We wish to thank L. P. Wilding of Texas A&M University, College Station, for the use of Figure 1.

REFERENCES

1. D. E. McCormack and D. G. Fohs. Planning for Transportation Systems and Utility Corridors. In Planning the Uses and Management of Land (M. T. Beatty and others, eds.), American Society of Agronomy, Madison, WI, Monograph 21, 1979, pp. 531-553.
2. R. Webster. The Soil Survey: Its Quality and Effectiveness. In Soil Resource Inventories, Proc., Workshop, Cornell Univ., Ithaca, NY, Agronomy Mimeo 77-23, 1977, pp. 59-70.
3. D. E. McCormack and L. P. Wilding. Variation of Soil Properties Within Mapping Units of Soil with Contrasting Substrata in Northwestern Ohio. Proc., Soil Science Society of America, Vol. 33, 1969, pp. 587-593.
4. Soil Survey Manual. U.S. Department of Agriculture, Handbook 18, U.S. Government Printing Office, 1951.
5. Soil Taxonomy: A Basic System of Soil Classification for Making and Interpreting Soil Surveys. U.S. Department of Agriculture, Handbook 436, U.S. Government Printing Office, 1975.
6. M. G. Cline. The Soils We Classify and the Soils We Map. Proc., New York Conference on Soil Mapping Quality Procedures, Cornell Univ., Ithaca, NY, 1977, pp. 5-20.
7. D. F. Amos and E. P. Whiteside. Mapping Accuracy of a Contemporary Soil Survey in an Urbanizing Area. Proc., Soil Science Society of America, Vol. 39, 1975, pp. 937-942.
8. J. C. Powell and M. E. Springer. Composition and Precision of Classification of Several Mapping Units of the Appling, Cecil, and Lloyd Series in Walton County, Georgia. Proc., Soil Science

Society of America, Vol. 29, 1965, pp. 454-458.
9. L. P. Wilding, R. B. Jones, and G. M. Schafer. Variation of Soil Morphological Properties Within Miami, Celina, and Crosby Mapping Units in West-Central Ohio. Proc., Soil Science Society of America, Vol. 29, 1965, pp. 711-716.
10. R. W. Arnold. CBA-ABC: Clean Brush Approach Achieves Better Concepts. Proc., New York Conference on Soil Mapping Quality Procedures, Cornell Univ., Ithaca, NY, 1977, pp. 61-92.
11. L. P. Wilding and R. Drees. Spatial Variability: A Pedologist's Viewpoint. In Diversity of Soils in the Tropics, American Society of Agronomy, Madison, WI, Special Publ., 1977, pp. 1-12.
12. F. G. Baker. Variability of Hydraulic Conductivity Within and Between Nine Wisconsin Soil Series. Water Resources Res., Vol. 14, No. 1, 1978, pp. 103-108.
13. J. B. Campbell. Spatial Variation of Sand Content and pH Within Single Contiguous Delineations of Two Soil Mapping Units. Journal of the Soil Science Society of America, Vol. 42, 1978, pp. 460-464.
14. D. J. Varnes. The Logic of Geological Maps, with Reference to Their Interpretation and Use for Engineering Purposes. U.S. Geological Survey, Department of the Interior, Professional Paper 837, U.S. Government Printing Office, 1974.

Publication of this paper sponsored by Committee on Exploration and Classification of Earth Materials.

Physical Environment Report: A Geotechnical Aid for Planners

Edward A. Fernau, Soil Mechanics Bureau, New York State Department of Transportation, Albany

Since 1976, the Soil Mechanics Bureau of the New York State Department of Transportation has produced reports that delineate information on the physical base of a potential transportation corridor or project. These reports have their origin in the traditional engineering soil map. The transportation planner must identify potential changes in the physical base of an area that could result from a transportation improvement and determine how these changes may affect the environment. The reports present physical-base data on geology, soils, groundwater, and surface water in map form and include an explanation of the mapped units in an explanatory legend. Information contained in the reports includes topography, slopes, terrain units, bedrock, aquifers, erodibility, runoff, floodplain and watershed delineation, and stream-classification data. A brief description of the use of the mapped information is included, along with a listing of references and data sources. This paper briefly describes the data-collection and presentation procedures and the cautionary statements and uses made of the reports.

The Soil Mechanics Bureau of the New York State Department of Transportation (NYSDOT) has for many years provided department planners and designers with reports delineating soil and surficial geologic conditions on a reconnaissance level (1, 2). In the mid-1970s, departmental regional planning engineers began requesting additional information on water-soil interactions such as runoff and erosion potential. At this time, bureau personnel were studying a physical inventory—termed a physical environment report—prepared for the Saskatoon, Canada, area (3) that contained many concepts that could be included in an expanded reconnaissance-level report.

A study showed that an inventory limited to factors within the basic terrain-reconnaissance expertise of the bureau could give planners information on topography, geology, soil type, internal drainage, and soil erodibility. Other easily acquired information such as precipitation data, floodplain delineations, stream classification, and widlife food-and-cover criteria based on soil wetness could also be included. This type of inventory information could alleviate the problems of regional planning personnel attempting to provide physical-base data from often inadequate sources or without the necessary interpretations of source data.

INVENTORY DATA BASE

Because more physical-base information would be collected and interpreted for the physical environment reports than for the previous terrain-reconnaissance reports, a review of accessible source material was made. Terrain reconnaissance as practiced in New York relies heavily on the soil surveys produced by the Soil Conservation Service (SCS), U.S. Department of Agriculture. SCS soil mapping units were converted to NYSDOT terrain units (which are based on landform, mode of deposition, and parent material). Because of the ready availability of soil survey data and the bureau's experience in its use, this information was retained as the basis for interpretation into surficial geologic (terrain) units. In addition, information contained in the soil survey on slope, erodibility, runoff, wetness and ponding, and habitat elements for wetlands wildlife was extracted, evaluated, and interpreted. Supplementary references or information sources to which the report user may go for more detailed information on uses and interpretation of the soil survey information were found; these range from the Soil Survey Manual (4) to papers from various technical journals.

Bedrock information was obtained from the New York State Geological Map (5); groundwater bulletins, the Geological Survey, U.S. Department of the Interior (USGS); and New York State Museum and Science Service publications. Information on aquifers, both surficial and bedrock, was obtained from the same sources.

Climatic data were obtained from the monthly and annual summaries for New York reporting stations prepared by the National Weather Service, U.S. Department of Commerce. Floodplain, wetland, and stream data were acquired from the New York State Department

of Environmental Conservation and the U.S. Army Corps of Engineers.

LIMITATIONS OF INFORMATION

The limitations-of-information section of the reports contains the cautionary statements that must be made concerning reconnaissance-level studies, facts, and inferences; for example, the following is a typical general statement that precedes the body of a physical environment report:

> The information contained on the included maps is preliminary and general and as such the maps must be considered as generalizations. The boundaries of the units depicted on the maps represent general indications of where a change occurs. In most instances the changes are transitional and not abrupt as shown on the maps. Some small inclusions of a differing unit may occur within areas mapped as a single unit.
>
> The source data used for statements and interpretations often were specifically intended for purposes other than engineering evaluation. The evaluation of these data together with previous experience and field reconnaissance contribute significantly to the final interpretations. Where information was obtained directly from source material without interpretation on the part of the Soil Mechanics Bureau, the source material will be cited. Inferred or interpreted information will be indicated as such along with the data base source.

It is important to identify information that is passed on from a source or sources virtually unchanged from that which has been subjected to an interpretive process during assimilation and presentation. In addition, some information that is passed on may have been inferred at its source. The reasoning process for the basis of interpretation must be made clear to the user by the inclusion of references to which he or she may turn for further study.

Greer and Moorhouse (6) in their discussion of engineering-geological studies for sewer projects stated that "any generalized data presentation or interpretation contained in an engineering soil or geologic report... should be used only with an understanding of the degree to which such generalizations must be regarded with skepticism." The general statement on limitations of information should put the reconnaissance level of the study firmly in the mind of the report user.

DATA PRESENTATION

There are no new or exciting methodologies used in reporting the data. A brief narrative section precedes the graphical portion of the report. This section contains an introduction that includes the scope of the report, the method of investigation, and an area description. The area description briefly summarizes the location, culture, and climate of the study area, along with the generalized geologic setting (including physiography and topography, unconsolidated deposits, and bedrock). Drainage is described and any USGS surface-water recording stations are tabulated as to type, number, and location.

The next section presents a short discussion of the interactions of soil, water, and transportation facilities. The erosion and sediment production caused by devegetation or increased runoff, along with the resultant potential problems on floodplains, are described, and the transportation facilities impacts on surface waters and on groundwater in shallow surficial aquifers are briefly discussed.

With the exception of three tabular forms of data presentation, all the information is presented on maps. Many decisions about map scale were made. In some instances, especially in urban-suburban areas, regional planning engineers will recommend a map scale, usually 1:9600. It is preferable to use the standard 7.5′ USGS topographic quadrangles. NYSDOT has prepared updated planimetric maps at the same scale (1:24000) as the USGS sheets, and some information is more clearly presented on these sheets. Many mechanical problems present themselves because most pedologic and geologic maps are not prepared on this scale, and one must always remember that enlarging or reducing a data source does not change its accuracy. If the data source is greatly reduced in scale, an interpretation that combines data will be done so as not to clutter the map. If the source data are modified, the modifications should be described in the legend that accompanies the map presentation.

Each parameter is presented as a map that graphically depicts the areal extent of each mapping unit, along with the usual map-related legend, scale, contour interval, north arrow, and such, and is accompanied by an explanation of the map units and an explanation of the rationale for each map-unit division. The purpose of each map and the use of the factor depicted are briefly described. Finally, the references used to produce the map-unit information and any corroborating data sources or references are included. The information presented is divided into three broad categories: physical aspects, soil aspects, and water aspects (although some information may logically appear in more than one category).

Physical Aspects

An elevation map that uses the layer method of representing elevations is produced from the 7.5′ USGS topographic sheet and the total relief of the project area. A series of elevation bands based on the elevation difference that best shows the landscape configuration is used.

A topographic slope map of the project area is used to delineate areas of common slope from level to steep. Because these maps depict average slope ranges (which assumes a uniform slope for the map unit), a cautionary note explaining that slopes may be complex rather than uniform is included. Data are taken directly from SCS map-unit slope-phase information or interpreted from topographic maps if slope data are unavailable.

The generalized terrain-unit map (Figure 1) is the basic terrain-reconnaissance map produced by the landform-depositional-process parent-material interpretations developed in the past (1, 2). This is the type of engineering soil map that many transportation agencies routinely produce. The determination of terrain units is based on a review of the existing literature on the subject area and includes a geotechnical engineering interpretation of the pedologic and geologic maps of the area, as well as a geotechnical engineering interpretation of aerial photographs, a field reconnaissance of the area, and an evaluation of the existing subsurface data. Complementing the terrain-unit map are two tables. The first (Table 1) presents the general characteristics of each terrain-map unit, including the mode of origin, typical landform, common topographic position, soil fractions found in the terrain unit and in the internal structure, relative permeability, and others. The second (Table 2) presents the anticipated earth engineering behavior of the terrain units with respect to vertical gradeline location, subgrade and cut-slope conditions, and utility as a source of construction material. All data sources used for both the map-unit and table information are reported.

A bedrock geology map is used to show the contacts between formations and the areas of outcrop or shallow overburden [which is defined as having less than 1.2 m

(4 ft) of soil cover over bedrock]. Water wells and NYSDOT borings that reach the bedrock surface are shown and depth to rock is given. The bedrock lithology and structure is explained in descriptive paragraphs that accompany the map. References are cited to enable the reader to obtain more-detailed bedrock information.

A map that shows the unconsolidated aquifers is usually taken without change from the appropriate groundwater publications, where they exist. Where no groundwater data are available, the map is based on interpretations of the terrain-unit map. The basis for delineation is the probable yield of a well in volume per minute. In general, glacial till and layered silt and clay deposits yield less than 19 L/min (5 gal/min), layered silts and sands are expected to yield 19-76 L/min (5-20 gal/min), and layered sands and gravels usually yield 76-379 L/min (20-100 gal/min). Where known, the chemical quality of the groundwater is briefly described. This map is accompanied by a table of climatological data, usually limited to monthly and annual average precipitation values, for the nearest weather station.

Figure 1. Generalized terrain-unit map.

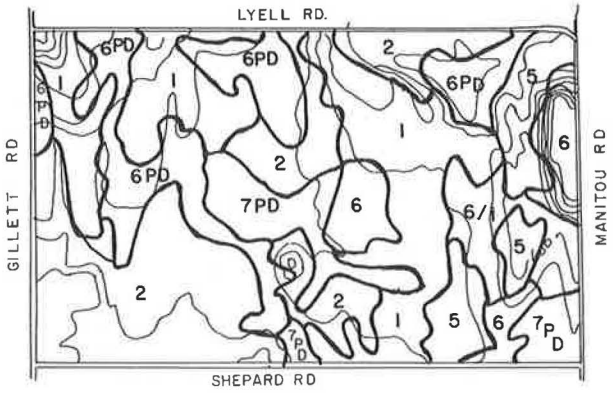

Soil Aspects

The soil engineering classification map (Figure 2) is intended to indicate the geotechnical effort that would be involved at various locations so that lead times can be established for an adequate soils program for proper design. Also, in the early planning stages, information about subsurface conditions can be obtained where necessary to determine whether or not these would become a constraint in design and construction.

The classifications presented are based on an interpretation of the engineering characteristics of the terrain units encountered in the project area. Those terrain units that have similar engineering features are grouped into the following types of map units.

Class 1: Those soil deposits that require minimal exploration, testing, and analysis for proper soils design. These generally have good bearing capacity, negligible settlements, and good cut-slope and subgrade characteristics.

Class 2: Those soil deposits where exploration is necessary to establish the soil profile and detailed exploration, testing, and analysis may be necessary for proper soils design. Included in this class are veneer deposits such as lake-laid sands and floodplain soils,

Table 1. General terrain-unit characteristics.

Terrain Unit	Mode of Origin	Landforms	Common Topographic Position	Particle Size and Distribution	Relative Permeability	Other
Outwash deposits	Sediments transported by meltwaters away from ice mass	Flat to gently undulating terraces	Lower valley walls and floors	Silt to cobbles, mostly sand and gravel; well-sorted, massive, horizontal stratification with some bedding	Moderate to rapid	May have high water table; nonplastic
Lacustrine bottom sediments	Sediments deposited in deep, quiet waters of proglacial lakes	Flat to gently undulating plains	Valley floors; lowlands	Clay to fine sand; mostly silt and clay in well-sorted beds; nearly horizontal, distinct stratification	Very slow vertically; slow horizontally	Laminations of the type commonly called varves, plastic

Table 2. General earth engineering considerations.

Terrain Unit	Highway Location	Cut-Slope Conditions	Subgrade Conditions	Utility as Source of Materials
Outwash deposits	Generally not critical; embankments more than 7.6 m high may have unstable foundations	Generally good; positive drainage may be required to prevent erosion	Generally good; may be nonuniform	Common borrow and granular materials
Lacustrine bottom sediments	Embankments more than 7.6 m high may have unstable foundations; cuts will be troublesome	Generally poor; problems of fine-grained flowing materials; may require slope protection and flattening for stability	Generally soft, wet, fine-grained materials; trafficability difficulties; consider undercut or underdrains	Common borrow; may have moisture content greater than optimum

Note: 1 m = 3.28 ft.

Figure 2. Soil engineering classification map.

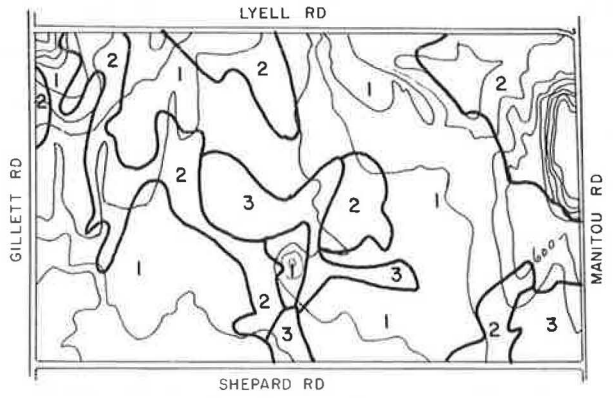

man-modified areas of fill, and urban areas where general soils information is unavailable.

Class 3: Those soil deposits where extensive exploration, detailed testing, and intensive analysis are usually required for proper soils design. These are usually deposits of fine-grained wet soils and organic deposits.

A soil-erodibility rating map is used to delineate areas having similar erodibility characteristics. The ratings are the average of a range determined by the soil erodibility or K-factor of Wischmeier (7, 8). The basic data are obtained from published SCS reports or by using Wischmeier's nomograph. Two maps can be made, one that depicts the relative erodibility of the surface or pedologic A-horizon and one that depicts the parent material or pedologic C-horizon. It is preferable to use the relative erodibility of the parent material, as in most instances surface horizons are removed during construction operations. The narrative that accompanies this map briefly describes the soil parameters used in determining the erodibility factor. Much of the narrative is aimed at defining the difference between soil erodibility (which is based solely on soil characteristics) and soil erosion (which is determined by topographic, vegetative, and climatic considerations, as well).

The soil-runoff factor first proposed by Musgrave (9) is the basis for the map units of the soil-runoff-factor map. Where this information is not available from SCS, the method of Chiang (9) is used to determine the runoff factor. The map units are the same as SCS ratings, i.e., low, moderate, high, and very high runoff. This map is accompanied by a narrative that explains how the factors are derived, what they mean, and how to use the map information.

A soil-wetness-and-ponding map is used to delineate areas of similar soil drainage, based on SCS soil series descriptions [interpretations of the SCS soil-drainage classes based on the depth to soil mottles in the soil pedon (4)]. Those soils not wet for significant times are those whose natural drainage classes are excessively, somewhat excessively, or well drained. Those wet for significant periods include the moderately well and the somewhat poorly drained soils, and those continuously wet or ponded fall into the poorly to very poorly drained range. A 1.2-m depth to seasonal water is used as a break point by assuming a 1.2-m-deep highway ditch from original ground surface. Work by Latshaw and Thompson (11) confirms these categories to be valid. The narrative that accompanies this map explains soil drainage and how the map units were derived.

Water Aspects

Floodplain delineations are based on the 1:24000 scale flood-prone area maps produced by the USGS in their Albany, New York, office for the U.S. Army Corps of Engineers. These are estimated from available flood information and indicate areas that may be occasionally flooded but provide no information on the frequency, depth, duration, and other details of flooding. This information is passed along unchanged. However, where available, a listing of flood maps produced by the Federal Insurance Administration, U.S. Department of Housing and Urban Development, is included to allow the user access to more-detailed floodplain delineations.

Stream classifications and watershed boundaries are delineated, based on information obtained from the New York State Department of Environmental Conservation in regard to the surface-water classification of waterbodies in the project area. Standards in New York are based on best use of the waters and range from drinking-water source to suitability for secondary contact recreation. Watershed delineations are those defined by the U.S. Watershed Protection and Flood Prevention Act of 1954. Standards are briefly described, along with source information.

The wetland food-and-cover map depicts those areas that combine suitable soil and water conditions for the natural production of food and cover plants favorable to wetland wildlife. These ratings are obtained directly from SCS data based on the soil series and the slope phase of the map unit. The description that accompanies this map notes that it may not be substituted for an official freshwater wetlands map because New York law defines wetlands based on vegetation. As official freshwater wetland maps become available, this presentation will be deleted.

SUMMARY

Any or all of these maps may be included for a given project, depending on the regional project manager's desires. Possible future inclusions (when the information becomes available) would be sole-source aquifers, official freshwater wetland maps, and prime or unique farmlands maps.

These reports can help planners free themselves from the task of defining aspects of the physical or abiotic environment in early planning phases. Although these are reconnaissance-stage reports made for a study area or corridor, the references that are included will save much valuable time when more detailed information is required.

REFERENCES

1. E. F. Bennett and G. W. McAlpin. An Engineering Grouping of New York State Soils. HRB, Bull. 13, 1948, pp. 55-65.
2. W. P. Hofmann and J. B. Fleckenstein. Terrain Reconnaissance and Mapping Methods in New York

State. HRB, Bull. 299, 1961, pp. 56-63.
3. E. A. Christiansen, ed. Physical Environment of Saskatoon, Canada. National Research Council of Canada, Ottawa, 1970.
4. Soil Survey Manual. U.S. Department of Agriculture, Handbook 18, U.S. Government Printing Office, 1951, pp. 169-172.
5. D. W. Fisher, ed. Geologic Map of New York. New York State Museum and Science Service, Albany, 1970.
6. D. M. Greer and D. C. Moorhouse. Engineering-Geological Studies for Sewer Projects. Journal of the Sanitary Engineering Division, Proc., ASCE, Vol. 94, No. SA1, Feb. 1968, pp. 20-24.
7. W. H. Wischmeier, C. B. Johnson, and B. V. Cross. A Soil Erodibility Nomograph for Farmland and Construction Sites. Journal of Soil and Water Conservation, Vol. 26, No. 5, 1971, pp. 189-193.
8. W. H. Wischmeier and L. D. Meyer. Soil Erodibility on Construction Areas. HRB, Special Rept. 135, 1973, pp. 20-29.
9. G. W. Musgrave. How Much Rain Enters the Soil? In Water: The Yearbook of Agriculture, U.S. Department of Agriculture, 1955, pp. 151-159.
10. S. L. Chaiang. A Runoff Potential Rating for Soils. Journal of Hydrology, Vol. 13, 1971, pp. 54-62.
11. G. J. Latshaw and R. F. Thompson. Water Table Study Verifies Soil Interpretations. Journal of Soil and Water Conservation, Vol. 26, No. 2, 1968, pp. 65-67.

Publication of this paper sponsored by Committee on Engineering Geology.

Method for Determining Relative Suitability of Existing Geotechnical Data for Regional Planning

David Hoffman and J. Hadley Williams, Missouri Geological Survey Rolla
A. Keith Turner, Geology Department, Colorado School of Mines, Golden
Harry W. Smedes, U.S. Geological Survey

During regional planning studies, the engineering geologists must choose among diverse, competing data sources, each having distinct cost and accuracy characteristics. Recognizing a need for guidelines in this area, the Missouri Division of Geology and Land Survey, Rolla, Missouri, evaluated a sequence of alternative sources of data on the Cape Girardeau quadrangle in southeastern Missouri. Several map sources were compared at three scales: statewide (1:500 000), countywide (1:62 000), and quadrangle (1:24 000). Engineering and geologic considerations were used to establish criteria for 10 land uses associated with residential development. These criteria were used with the appropriate source data to develop a sequence of limitations maps at each scale. Extensive field and laboratory programs were carried out to prepare the best-possible data-reference source with which other map products could be compared. A usefulness index was formulated to measure the degree of agreement between the competing interpreted products and the reference standards. Manual computation of this index proved impractical [a 10-km^2 (4-mile^2) area required 1 person day/comparison]. Thus, computer methods were used that permitted the rapid comparison of approximately 32 000 cells covering the quadrangle and the computation of the resulting usefulness index for about $50.00 (including all salaries and data-processing costs).

The growing interest in and demand for environmental assessment has caused a reappraisal of land-use planning activities and accelerated demands for suitable engineering geology maps. The majority of these demands emphasize the need to display the natural constraints to development of various land uses. These new types of map displays, which range from rather generalized, small-scale displays covering large regions, or even entire states, to more-specific larger-scale ones covering local areas or counties, must be understandable by a variety of people.

Many traditional map forms, however, poorly satisfy these new demands, and considerable experimentation on new mapping formats has been undertaken [some of the new techniques are reviewed elsewhere (1)]. The pressure for the development of new mapping techniques has been felt most intensely by the state geological surveys, and several states have expanded, or even created, agencies to undertake such projects.

In Missouri, a number of environmental geology maps have been developed (2, 3), but a single map, accompanied by tables describing natural conditions and constraints to development, does not always suffice. Planners frequently desire a series of interpretive maps, each showing the degree of constraint for some specified class of use. These maps, reflecting both geologic conditions and estimates of probable hazards to life and property, are used in combination with other planning factors in guiding future development.

In this paper, these interpretative land-use-limitations maps will be called limitations maps. Each such map analyzes for a single land use or for a group of closely associated uses. The development of these maps requires the setting of standards or procedures for their construction in order to maintain quality and consistency.

In the first stages of a program to develop such standards, four steps were undertaken.

1. Limitation categories were defined: Four limitations categories were selected—severe, moderate, slight, and none—to indicate the probable degree of limitation to development.
2. Standard land uses were defined: Ten land uses were chosen—sanitary landfills, road construction, foundations for light structures (i.e., houses), agricultural suitability, septic tank systems, ease of excavation, impoundments, sewage lagoons, soil erosion, and landslide potential—to represent the range of con-

Table 1. Example rating system: sanitary landfill activity.

Rating	Constraint
No limitations	The bottom and sides of the landfill must be of a material such that leachates (a) travel less than 30.5 m horizontally in 1000 days and (b) never reach the groundwater table (unless the leachate will cause no decrease in quality of the highest-quality groundwater body that has historically existed within a 16-km radius) There must be sufficient soil at the site for a 15.2-cm daily cover There must be sufficient soil at the site for a final cover 0.9 m deep The final cover should be equal to or less permeable than the bottom and sides of the landfill The landfill site must never be subject to flooding The site must not be susceptible to collapse, for example, collapse induced by saturation, inundation, or high transmission rates of leachates The landfill must be located at least 1.5 km from the nearest water well or spring that produces 378 L/min and at least 0.75 km from all other water wells or springs There must be a minimum of 3 m of material between the bottom of the landfill and the normal wet-season piezometric surface
Slight limitations	The bottom and sides of the landfill must be of a material such that leachates (a) travel less than 30.5 m horizontally in 1000 days and (b) never reach the groundwater table (unless the leachate will cause no decrease in quality of the highest-quality groundwater body that has historically existed within a 16-km radius) There must be sufficient soil at the side for a 15.2-cm daily cover There must be a sufficient supply of soil located less than 1.6 road-km from the landfill to provide a final cover 0.9 m deep The final cover should be equal to or less permeable than the bottom and sides of the landfill The landfill site may be subject to flooding by a 100-year flood (U.S. Water Resources Council, 1967) The site must not be susceptible to collapse, for example, collapse induced by saturation, inundation, or high transmission rates of leachates The landfill must be located at least 1.5 km from the nearest water well or spring that produces 378 L/min and at least 0.75 km from all other water wells or springs There must be a minimum of 3 m of material between the bottom of the landfill and the normal wet-season piezometric surface
Moderate limitations	The bottom and sides of the landfill must be of a material such that leachates (a) travel less than 61 m horizontally in 1000 days and (b) will not reach the groundwater table in less than 1000 days (unless the leachate will cause no decrease in the quality of the highest-quality groundwater body that has historically existed within a 16-km radius[a] There must be sufficient soil at the site for a 15.2-cm daily cover There must be a sufficient supply of soil located less than 4.8 road-km from the landfill to provide a final cover 0.9 m deep The final cover should be equal to or less permeable than the bottom and sides of the landfill[a] The landfill site may be subject to flooding by a 25-year flood (U.S. Water Resources Council, 1967) The site must not be susceptible to collapse, for example, collapse induced by saturation, inundation, or high transmission rates of leachates The landfill must be located at least 1.5 km from the nearest water well or spring producing 378 L/min and at least 0.75 km from all other water wells or springs There must be a minimum of 0.9 m of material between the bottom of the landfill and the normal wet-season piezometric surface[a]
Severe limitations	All other areas

Notes: 1 m = 3.28 ft; 1 km = 0.62 mile; 1 L = 0.264 gal.
Landfills are rated primarily on surface material and susceptibility to surface and/or groundwater pollution unless corrective measures are taken.
[a]If a site in this area is to be used, this condition must be upgraded by appropriate engineering, to the value(s) given for "no limitations".

cerns related to residential developments.

3. An objective rating system was developed: A standard, objective rating system was developed for each land use to allow the translation of geologic conditions into constraints; an example rating system is shown in Table 1.

4. Data sources and scales were identified: A variety of data sources—federal, state, local, and private—and scales were identified for many types of data, and three distinct mapping scales were identified—statewide at a 1:500 000 scale, countywide at a scale of about 1:62 500, and local and quadrangle at scales of 1:24 000 or larger.

The engineering geologists were thus faced with the problem of reconciling and recompiling existing information available at a variety of scales and accuracies. Each data source had some distinctive, but generally unknown, cost and accuracy characteristics. Obviously the more-expensive data sources are generally more detailed and hence more precise and therefore should yield more-accurate interpretive limitations maps. On the other hand, in the face of budgetary constraints, use of the most expensive data is not always the best solution. For example, if two competing data sources are such that the cost of one is only 25 percent of the cost of the other, but the interpretive results of the first are at least 80 percent as accurate as those of the second, should the cheaper source be used?

In an attempt to answer such questions, a few interpretive limitations maps were produced by using competing data sources. These maps showed similar, but not identical, patterns of limitations. A more-precise method of evaluating the quality of competing data sources was needed and, accordingly, a research task was defined to establish such a method. This paper describes the results of that task.

THEORETICAL BASIS AND METHODOLOGY

The comparison of two or more maps is a common geological and geographical problem. Although quantitative comparisons seem potentially useful to geologists, only a few attempts have been made to produce such values. Fortunately, geographers have studied this problem for several years and have developed a number of techniques (4, 5). None of the existing methods could precisely solve the needs of this study, however, and a modified procedure was developed based on cross-correlation concepts (4).

Limitations Categories and Limitations Units

As shown in Figure 1, by combining any two of the four standard limitations categories, a new distinctive limitations unit can be produced. By using all possible combinations, 10 distinctive limitations units can be shown on each map. The range of each limitation unit is defined by an upper (or ceiling) limitation that reflects the most-restrictive category and a lower (or floor) limitation that reflects the least-restrictive category.

In cases of perfect agreement between the limitations units on two maps, it is easy to see that the two maps are in perfect agreement. Similarly, in those cases where two map units totally disagree (a severe limitations unit on map A corresponding to a moderate limitations unit on map B, for example), it is easy to recognize perfect disagreement. Such situations are rare,

Figure 1. Derivation of 10 distinctive limitations units from four main limitations categories.

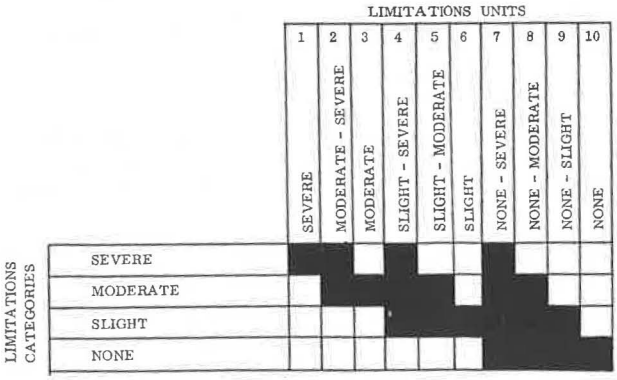

Figure 2. Two maps that have overlapping limitation units: example.

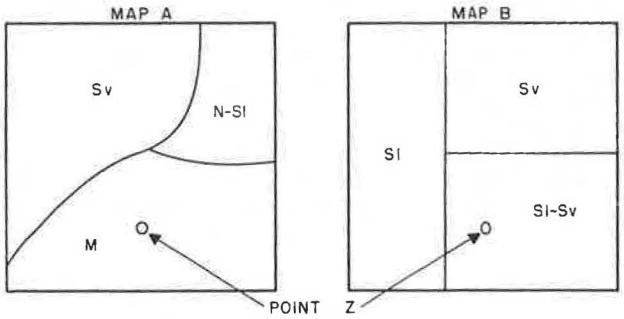

however; most commonly, the limitations units on one map (map A) will partially, but not completely, correspond with the limitations units on the second map (map B). Because the limitations units are defined in terms of the four original limitations categories, the possibility of partial overlaps in their ranges is high. The number of possible partial overlaps ranges from one to four.

Figure 2 shows two theoretical limitations maps. At point Z, map B has the limitation unit "slight-to-severe" and map A has the limitation unit "moderate". Because moderate is not identical to slight-to-severe, it can be argued that the two maps do not correlate. On the other hand, one could argue that, because moderate is included within the range slight-to-severe, the correlation is perfect! Neither of these arguments gives a true representation of the relative similarity of the two maps.

What is required is a method of computing a quantitative degree of correlation between the two maps that takes into account the degree of similarity (or overlay) and the ranges of the two map units. This can be done by the following procedure:

1. Define the concept of an agreement number (a),
2. Compute a usefulness number (U_a) based on the agreement number, and
3. Compute a usefulness index (UI) by summing the usefulness numbers, weighted according to subareas, over the entire area of interest (which may be the entire map).

Thus, the usefulness index is a single value for the entire area of interest, while the other values are essentially point values associated with unit areas.

Agreement Number

The agreement number measures the degree of commonality between two limitations units. It is defined as one more than the number of nonoverlapping limitations categories (n) occurring in the two limitations units being compared (i.e., $a = n + 1$).

Thus, if two limitations units match perfectly, there are no nonoverlapping limitations categories; therefore, $n = 0$ and $a = 1$. Where no commonality exists, the agreement number is defined as zero ($a = 0$). By referring to Figure 1, it can be seen that, provided some commonality exists, n is between 1 and 3 and, thus, the agreement number is between 0 and 4.

Usefulness Number

The usefulness number converts the agreement number to a measure of usefulness of the two data sources. Where there is perfect agreement between the limitations units on the two maps ($a = 1$), both maps are totally useful predictors of the limitations. Where there is total disagreement between the two maps ($a = 0$), the maps are useless as predictors.

The usefulness number should range from 0 (useless) to 1 (totally useful); the distribution between these limits may be linear, geometric, or logarithmic. A geometric distribution was chosen, and usefulness number was calculated by using Equation 1.

$$U_a = 0 \quad (a = 0)$$
$$U_a = [1/2^{(a-1)}] \quad (a > 1) \qquad (1)$$

The relationships among the degree of overlap (commonality), number of nonagreeing limitations (n), agreement number (a), and usefulness number (U_a) are summarized below.

Degree of Overlap	n	a	U_a
None	Not applicable	0	0.0
Perfect	0	1	1.000
Some	1	2	0.500
Some	2	3	0.250
Some	3	4	0.125

Usefulness Index

The usefulness number can be used to compute a single usefulness index that expresses the degree of commonality of one area, region, or map with another. The usefulness index (UI) is the weighted sum of the areas belonging to each level of agreement and can be calculated by using Equation 2.

$$UI = 10 \sum_{a=0}^{l} A_a U_a / A_t \qquad (2)$$

where

A_a = map area(s) belonging to agreement number a,
A_t = total mapped area, and
l = maximum agreement number = number of limitation categories.

The usefulness index will be between 0 and 10; the higher the index number, the better the agreement between the two maps.

As defined, the usefulness index can be used to compare two maps only. Where it is necessary to compare three or more maps, one map should be chosen as a

Figure 3. Landfill limitations map: Section 23 (T 31 N, R 13 E), Cape Girardeau quadrangle—(a) reference standard map (compiled from all 1:24 000 scale data) and (b) compiled from 1:62 500 scale geologic map and enlarged to 1:24 000.

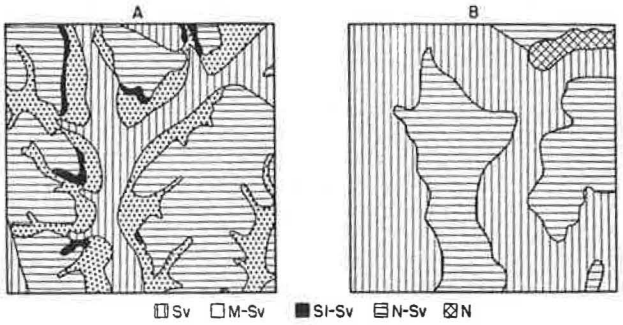

Figure 4. Landfill-limitations comparison map: Section 23 (T 31 N, R 13 E), Cape Girardeau quadrangle.

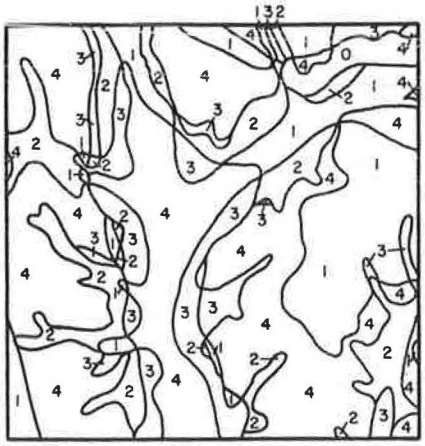

Numbers represent agreement number for area.

base, and all the other maps should be compared with it.

TEST OF THE CONCEPT IN THE CAPE GIRARDEAU AREA

The concept was tested in the Cape Girardeau quadrangle of southeastern Missouri, located on the west bank of the Mississippi River about 50 km north of Cairo, Illinois, and 140 km south of St. Louis. This quadrangle includes some of the Mississippi River floodplain and the adjacent uplands, which are typical of the nonglaciated, midcontinent sedimentary terrains. The following procedure was used.

1. Data sources were identified: Data were collected from maps at three scales—statewide (1:500 000), countywide (1:62 500 approximately), and quadrangle (1:24 000).
2. Field and laboratory investigations were made: Extensive field and laboratory programs were undertaken to confirm the accuracy of the data and to determine the most-accurate source. Costs of all data-collection efforts were carefully monitored.
3. Source maps were converted to limitations maps: By using the existing standardized objective-rating system, a sequence of maps showing the limitations for each of the 10 standard land uses was developed. Limitations maps were constructed for land use that reflected the data available at 1:500 000, 1:62 500, and 1:24 000 scales.
4. Reference standard maps were defined: The limitations maps for each land use at the 1:24 000 scale were based on the best, most-detailed data, and were therefore designated the reference standard maps for each land use.
5. The various limitations maps were compared with the reference standard maps: Comparison of the limitations maps at the 1:500 000 and 1:62 500 scales with the appropriate standard reference map at the 1:24 000 scale indicated the relative usefulness of more-detailed data versus more-generalized data.

The final step was critical to the successful conclusion of the task. The comparison between the derived usefulness indices for each land use and the data-collection costs provided a rational basis for the selection of the best source of data for each land use.

The following example illustrates the steps used in computing the usefulness index. A 10-km^2 (4-mile^2) area [Sections 23, 24, 25, and 26, township (T) 31 north (N), range (R) 13 east (E)] was selected as a typical test site. A landfill constraints map produced from bedrock geologic data at a scale of 1:62 500 (see Figure 3a) was compared with a landfill limitations map (the landfill reference standard map) produced from all available data at a 1:24 000 scale (see Figure 3b). The two maps were then overlaid, and the boundaries of the areas having each agreement number were outlined and the agreement numbers labeled (see Figure 4). Finally, all these areas were planimetered and recorded, and the usefulness index was calculated as shown below.

a	A_as (arbitrary units)	A_t
0	102, 48, 1	151
1	15, 19, 712, 5, 16, 85, 8, 6, 167, 11	1044
2	4, 9, 6, 21, 23, 54, 71, 19	207
3	102, 4, 16, 89, 75, 11, 23	320
4	1068	1068

Therefore,

$\Sigma A_t = 2790$

	a				
Quantity	0	1	2	3	4
A_a/A_t	0.054	0.374	0.074	0.115	0.383
U_a	0.0	1.000	0.500	0.250	0.125
$(A_a/A_t)U_a$	0.0	0.374	0.037	0.029	0.048

and

$UI = 10(0.0 + 0.374 + 0.037 + 0.029 + 0.048) = 4.88 \cong 5$

COMPUTER-ASSISTED CALCULATIONS

The manual calculation method described above required considerable effort to draft each map, develop the overlaid map comparison, determine the degrees of overlap for each area, planimeter each area to determine its extent, and perform the calculations. By the time that the usefulness indices for three small areas (each about 10 km^2) had been calculated manually for two different land uses, it was apparent that the method was not cost effective. On the average, it appeared to take about one person day to compute the usefulness index for one land use for 10 km^2.

The evaluation of the procedure really needed a much larger number of comparisons completed. Also, the usefulness indices should be calculated over the entire map, not just for three small test areas. Although the test sites had been selected to be representative of the dominant conditions within the map area, some uncer-

Table 2. Computer-calculated usefulness indices: comparison of reference standard maps and data source maps.

Data Source Map	Map Scale	Usefulness Index									
		Landfills	Roads	Foundations	Agriculture	Septic Tanks	Excavations	Impoundments	Lagoons	Erosion	Landslides
Rock	1:500 000	5	1	1	6	4	3	4	6	0	2
	1:62 500	4	1	2	5	6	2	4	5	0	1
Soils	1:750 000	4	3	5	1	5	3	2	3	1	1
	1:63 300	5	3	5	2	5	3	3	3	1	1
Engineering bedrock	1:24 000	2				1		5	2		
Surficial geology	1:24 000	2	10	10	7	9	7	8	2	10	10
Groundwater	1:24 000	4					6		4		
Flooding potential	1:24 000	1							2		
Surficial unit permeability	1:24 000	2			5	9		8	2		
Time of travel	1:24 000	7				3			9		
Strength	1:24 000		5	10							
Slope	1:24 000				3						

Table 3. Comparison of usefulness indices for landfills and roads computed manually and by computer.

Data Source Map	Map Scale	Manually Computed Value				Computer Value (entire map)
		Area 1	Area 2	Area 3	Average (areas 1-3)	
Landfills						
Bedrock	1:500 000	3	6	2	3.7	5
Bedrock	1:62 500	5	4	4	4.3	4
Soils	1:750 000	4	5	3	4.0	4
Soils	1:63 360	5	5	5	5.0	4
Roads						
Bedrock	1:500 000	1	1	1	1	1
Bedrock	1:62 500	1	1	1	1	1
Soils	1:750 000	2	3	5	3.3	3
Soils	1:63 360	2	2	3	2.3	3

Figure 5. Landfill limitations map for entire Cape Girardeau quadrangle: computer generated from all 1:24 000 data.

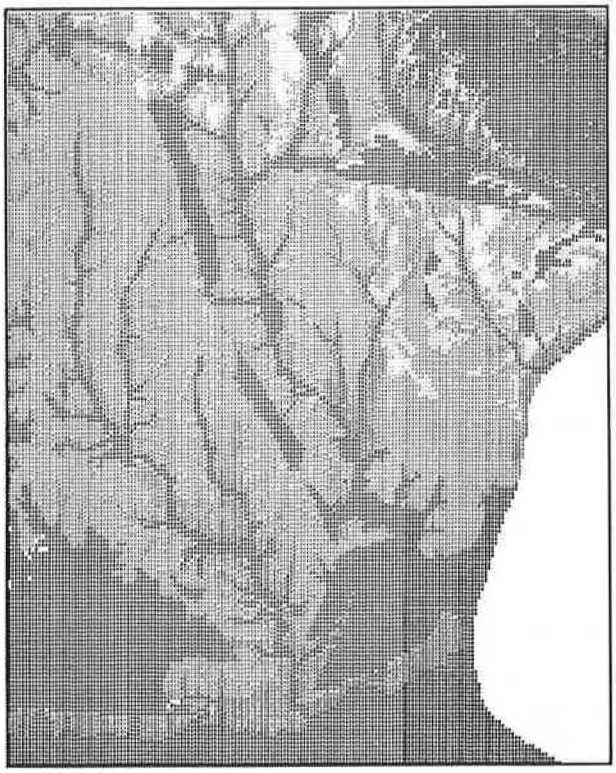

tainty remained with such small areal samples.

Computer techniques were used to solve this problem. A computer-assisted component-cellular mapping system called GMAPS (6, 7) was used to provide for the arithmetic and logical overlaying of maps to form new maps. In the program, all maps are stored in a computer in a matrix format of small cells. These can be repeatedly modified so that a single source map can produce a very large number of permutations. In this step, the source map documents for the Cape Girardeau quadrangle were converted to about 32 000 cells, each covering 2.5 hm^2 (1.1 acres) and having ground dimensions of 61x76 m (200x250 ft).

By using the GMAPS program, it was possible to compute usefulness indices for 70 map pairs (see Table 2). It was also possible to produce limitations maps for each use; Figure 5 shows the landfill limitations map generated by the computer.

The computer calculations produced usefulness indices for the entire quadrangle. The earlier manual calculations had been for only three small areas. Comparison of the manual and computer-derived indices (see Table 3) shows that local variations do change the rankings of some data sources. The computer calculations do agree fairly closely with the average of the usefulness indices for the three areas; perfect agreement could not occur unless there were only three landform types, represented by the three areas, and each covered one-third of the quadrangle.

CONCLUSIONS

A new method for quantitatively comparing two maps has been developed and tested. The method produces a single value, the usefulness index, that defines the degree of commonality between the two map units in a range of 0 to 10. Limitations for a specified land use that are predicted by using a single data source can be compared with those predicted by using a more-complete standard reference map. Such comparison permits ranking of data sources. The use of the method for the Cape Girardeau area showed that surficial materials are, by far, the most critical factor for the majority of land uses in that area. However, for two land uses (landfills and lagoons), the percolation rates data are the most

important. Such information should prove useful in planning future field studies.

Except for very limited test areas, manual calculation of the usefulness index is impractical. Computer-based techniques are feasible, however. These can compute a single usefulness index for a quadrangle for about $50.00 (including data entry, processing, and display costs, for both salaries and computer time). Most of the data entry and checking can be carried out by technicians. Although, in this study, the computation of the indices was performed by senior staff, this is not necessary because the process can be documented and followed in a routine manner by technicians.

ACKNOWLEDGMENT

The program to establish the mapping standards was undertaken jointly by the Missouri Department of Natural Resources, Rolla, the Resource and Land Information program of the U.S. Department of the Interior, and the Colorado School of Mines, Golden.

REFERENCES

1. D. J. Varnes. The Logic of Geologic Maps, with Reference to Their Interpretation and Use for Engineering Purposes. U.S. Geological Survey, Department of the Interior, Professional Paper 837, 1974, 48 pp.
2. E. E. Lutzen and J. D. Rockaway. Engineering Geology of St. Louis County, Missouri. Missouri Geological Survey, Engineering Geology Series 3, 1971.
3. J. D. Rockaway and E. E. Lutzen. Engineering Geology of the Creve Coeur Quadrangle, St. Louis County, Missouri. Missouri Geological Survey, Engineering Geology Series 2, 1970.
4. J. C. Davis. Statistics and Data Analysis in Geology. Wiley, New York, 1973, 550 pp.
5. J. C. Davis and M. J. McCullagh. Display and Analysis of Spatial Data. Wiley, New York, 1975, 378 pp.
6. A. K. Turner. Computer-Aided Environmental Impact Analysis: Part 1—Procedures. Mineral Industries Bull. (Colorado School of Mines, Golden), March 1976, Vol. 19, No. 2, 23 pp.
7. A. K. Turner. Computer-Aided Environmental Impact Analysis: Part 2—Applications. Minerals Industries Bull. (Colorado School of Mines, Golden), May 1976, Vol. 19, No. 3, 16 pp.

Publication of this paper sponsored by Committee on Engineering Geology.

Computerized Information System for Indiana Soils

G. D. Goldberg, Woodward-Clyde Consultants, Clifton, New Jersey
C. W. Lovell and Robert D. Miles, School of Civil Engineering, Purdue University, West Lafayette, Indiana

A comprehensive information storage system for Indiana soils is being operated on a computer at Purdue University, West Lafayette, Indiana, and at the Division of Materials and Tests of the Indiana State Highway Commission. Information is being collected that includes geotechnical, pedological, and geological data from records of subsurface investigations obtained during the period 1950-1978. Test data from more than 2500 soil samples have been stored and, within the year (1978), it is anticipated that data for an additional 6000 soil samples will be recorded. The data have been evaluated by various statistical methods. Results indicate that the range in values to be expected for a given soil parameter depends on the particular physical property and on the population from which the soil has been sampled. Some soil properties appear to be inherently more variable than others. To illustrate applicability, correlations have been made by using the information relative to physiographic unit and parent material. The grouping of soils by physiographic regions or origin of parent material (or both) suggests that the predictability of some parameters can be improved for certain combinations of parameters and soil groups. Specifically, prediction equations were generated for compression index, compression ratio, and unconfined compressive strength for certain soil populations. It is also possible to predict compaction test values, standard American Association of State Highway and Transportation Officials maximum dry and wet densities, and optimum moisture contents for selected physiographic and parent-material groupings.

The accumulation of laboratory and field-test data for characterizing the engineering properties of Indiana soils is extensive. An enormous amount of data, collected and stored from highway projects during the period 1950-1978, have been retained in the form of subsurface investigation reports. These reports were prepared by private consulting firms and governmental agencies from routine soil investigations. In their bulky, voluminous form, the majority of these data are not particularly useful for planning and engineering studies.

The need exists to make this information more accessible to both the engineer interested in detailed information about a site and the engineer interested in general soil characteristics over a large area. A computerized geotechnical data bank was judged to be the most efficient, expedient, and economical way to reduce the accumulated data to a form that could readily be made available to interested individuals.

This paper describes the development of a comprehensive information-storage system for soils data. Geological, pedological, and geotechnical engineering information are being collected and stored in a computerized system. Test data from 2508 soil samples have been stored in conjunction with developing and testing the computer system and, in addition, approximately 5500 other data sets have been stored (for a total of more than 8000 soil test samples).

Various statistical methods have been applied to some of the data. Results indicate that the range in values to be expected for a given soil parameter depends on the particular physical property and on the population from which the soil was sampled. The grouping of

Figure 1. Data input form (DIF).

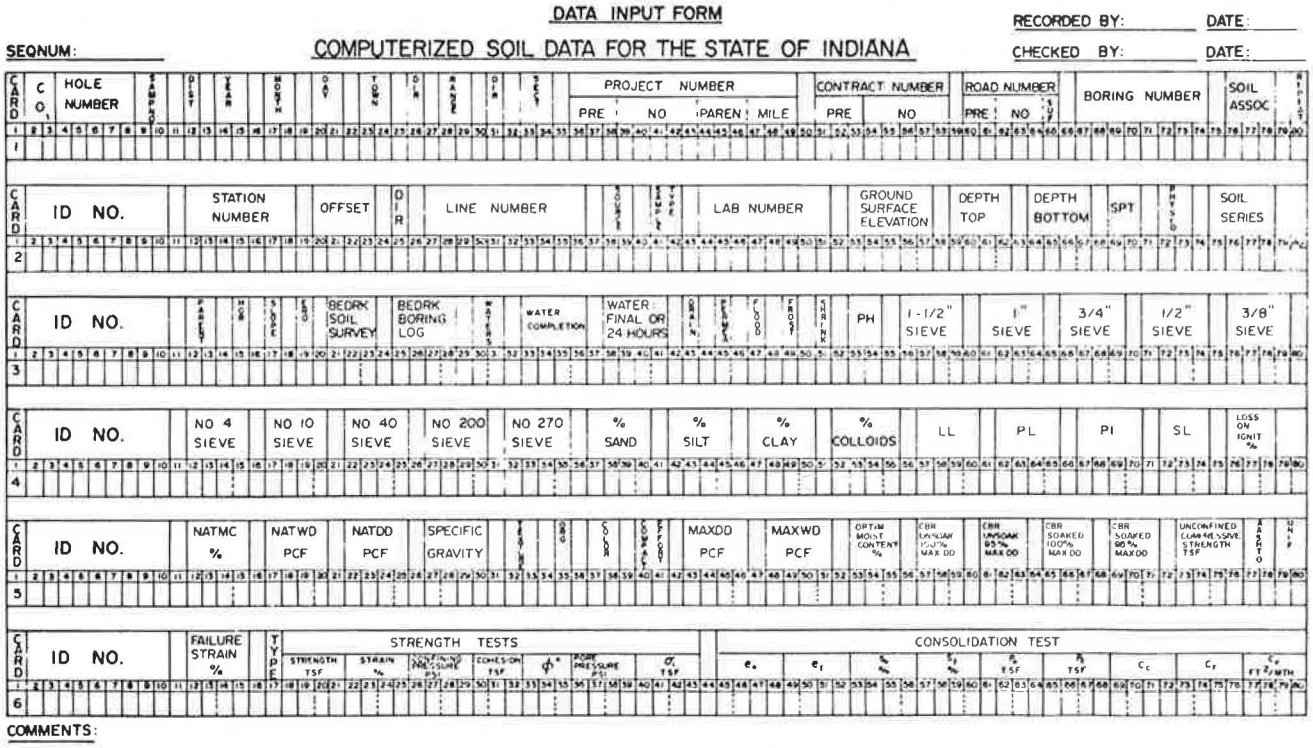

soils by physiographic regions or the origin of their parent material (or both) suggests that the predictability of certain parameters can be improved for such data populations.

DATA COLLECTION

The information gathered during a roadway soil investigation is generally limited. Usually, only simple laboratory testing for classification purposes is performed on a few soil samples; more-specialized testing is reserved for samples taken from sites where structures are to be constructed or where nontypical or unstable soil conditions are encountered. Information gathered is used in selecting the proper locations for the facility and in making design decisions (1, 2).

The information typically available from roadway soil investigation reports includes

1. Project and sample identification,
2. Sample location,
3. Ground surface elevation,
4. Depth from which the sample has been removed,
5. Depths to groundwater and bedrock,
6. Standard penetration resistance,
7. In situ moisture content,
8. Dry density,
9. Visual textural classification,
10. Gradation characteristics, and
11. Atterberg limits.

In addition, the results from special tests are included for selected soils. These data include the results from

1. Compaction tests,
2. California bearing ratio (CBR) tests,
3. Unconfined compression testing,
4. Triaxial and direct shear tests, and
5. Consolidation tests.

The geotechnical data currently being transferred to the data input form (DIF) are shown in Figure 1 [all figures in this paper are taken from Goldberg (3)]. This form serves as a guideline for card punching and subsequent transferral to magnetic tape for computer storage. A computer program has been developed that uses the information to classify each sample according to the American Association of State Highway and Transportation Officials (AASHTO) and the Unified Soil Classification systems.

The position of each sample hole is located on an agricultural soil-survey map (4). The pedological soil association, the soil series, and the soil horizon represented by each sample are recorded on the DIF. Because such descriptive data (5) cannot be directly recorded, this information has been codified to make the system compatible with computerized storage and retrieval. [Details of the coding are given by Goldberg (3).] Additional pedological information required includes the slope (topographic) class of the soil series, the erosion phase, and the natural soil-drainage class, permeability, flooding potential, frost-heave susceptibility, shrink-swell potential, and pH. These data are determined from published soil-series data sheets and coded onto the DIF. The physiographic unit (see Figure 2) and the parent material (see Figure 3) from which the soil has been derived are also entered on the DIF.

DATA MANAGEMENT

The data are punched onto a series of six cards for each sample. The order of the data cards is fixed, and a number, from one to six, is sequentially assigned to each card for identification. Each sample is also assigned a number, as is each hole. These numbers are assigned sequentially within each county. Each county name is coded. The card number, the county code, the hole number, and the sample number

have the purpose of assigning a unique identification number that can be used for internal bookkeeping to each data card.

Because large amounts of data are collected, errors in recording and punching the data are inevitable. Thus, an audit program has been written to identify those errors that can be detected by using the computer and, thereby, allow mistakes to be corrected. For example, if the liquid limit is mistakenly recorded, the liquid limit minus the plastic limit will not equal the plasticity index and the computer will automatically report an error.

A complete instructional User's Manual explaining the operation of the computerized storage and retrieval

Figure 2. Physiographic units based on present topography.

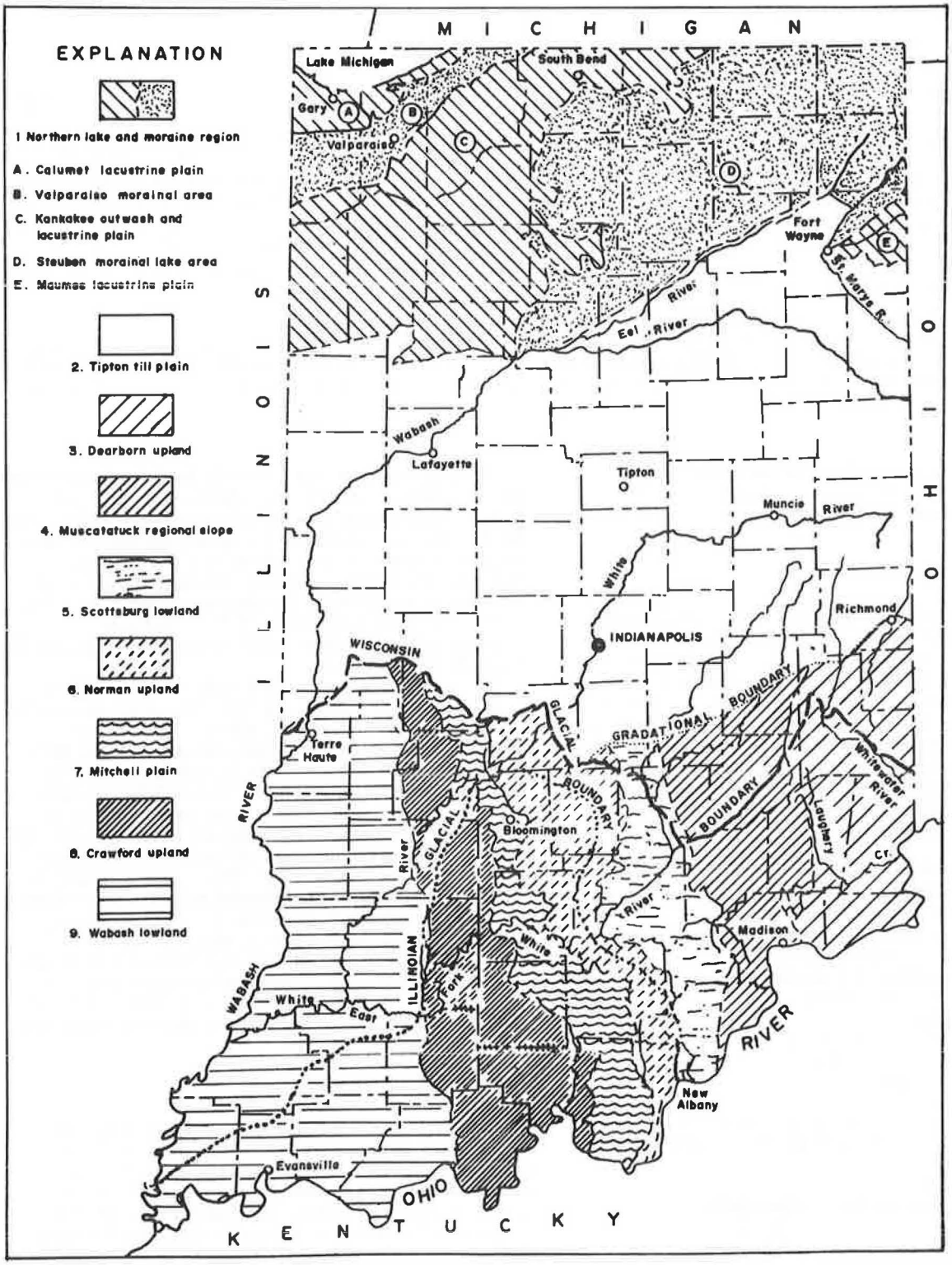

system is described by Goldberg (3). Included in the User's Manual are descriptions of the data items, codification system, formats, card locations, and column locations for each data item, as well as the listing of the programs used to add additional data to the data bank; to check data-input errors, where possible; to use the computer programs for data management and manipulations; and example problems on the use of the data bank.

STATISTICAL ANALYSIS

The collection of large amounts of soil test data and the fact that most natural soil deposits are highly variable in both horizontal and vertical directions require the use of a statistical approach (6-8). By using a computerized geotechnical data bank, an extensive listing of available soil and rock information can be retrieved both quickly and economically. For example, typical ranges of values for different soil parameters in the data system and the distribution of these parameters can be determined as shown in Figures 4-6. Such data are helpful in the selection of suitable sample sites for detailed laboratory testing (9). In addition, the development of correlations among selected soil properties can be helpful to the engineer in reducing the need for extensive laboratory testing (10, 11). This is particularly important to the small engineering unit that needs reliable data but can afford only a small amount of testing.

Regression Analysis

Prediction models usually involve soil parameters that are difficult to determine as dependent variables and more-easily-determined characteristics as independent variables. In the Indiana study (3), the dependent variables of major interest were

1. Compression index (C_c) and compression ratio

Figure 3. Soil regions of Indiana.

Soil Regions, Their Parent Materials and Representative Soil Series

1. Sandy and loamy lacustrine deposits and eolian sand (Maumee, Rensselaer, Plainfield)
2. Silty and clayey lacustrine deposits (McGary, Patton, Hoytville, Dubois)
3. Alluvial and outwash deposits (Fox, Genessee, Warsaw, Wheeling)
4. Eolian sand deposits (Plainfield, Oshtemo, Bloomfield)
5. Thick loess deposits (Alford, Hosmer, Iva)
6. Loamy glacial till (Riddles, Miami, Crosier, Brookston)
7. Clayey glacial till (Blount, Pewamo, Morley)
8. Thin loess over loamy glacial till (Brookston, Crosby, Miami, Parr)
9. Moderately thick loess over loamy glacial till (Fincastle, Russell, Miami, Brookston)
10. Moderately thick loess over weathered loamy glacial till (Cincinnati, Avonburg, Vigo, Ava)
11. Discontinuous loess over weathered sandstone and shale (Zanesville, Berks, Wellston, Muskingrum)
12. Discontinuous loess over weathered limestone (Crider, Frederick, Corydon)
13. Discontinuous loess over weathered limestone and shale (Eden, Switzerland, Pate)

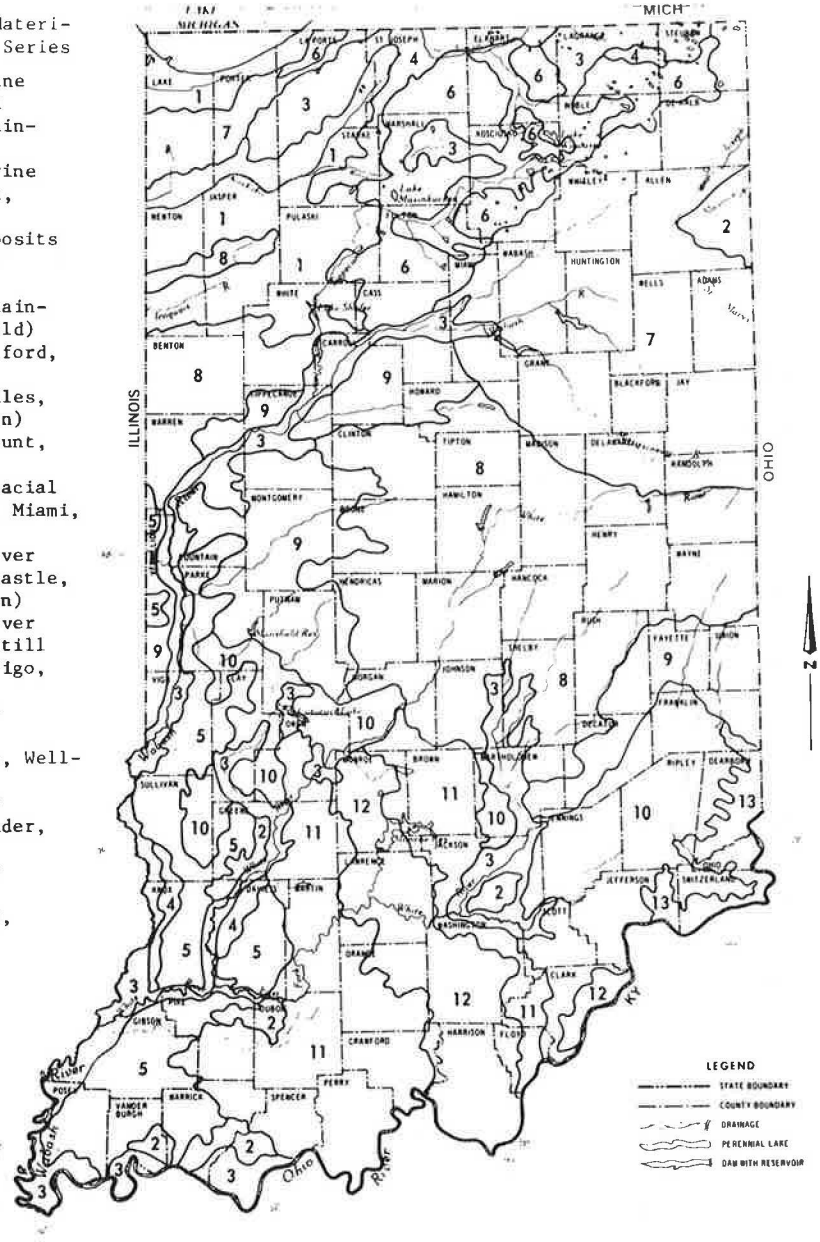

Figure 4. Distributional characterization of percentage passing 2-mm sieve.

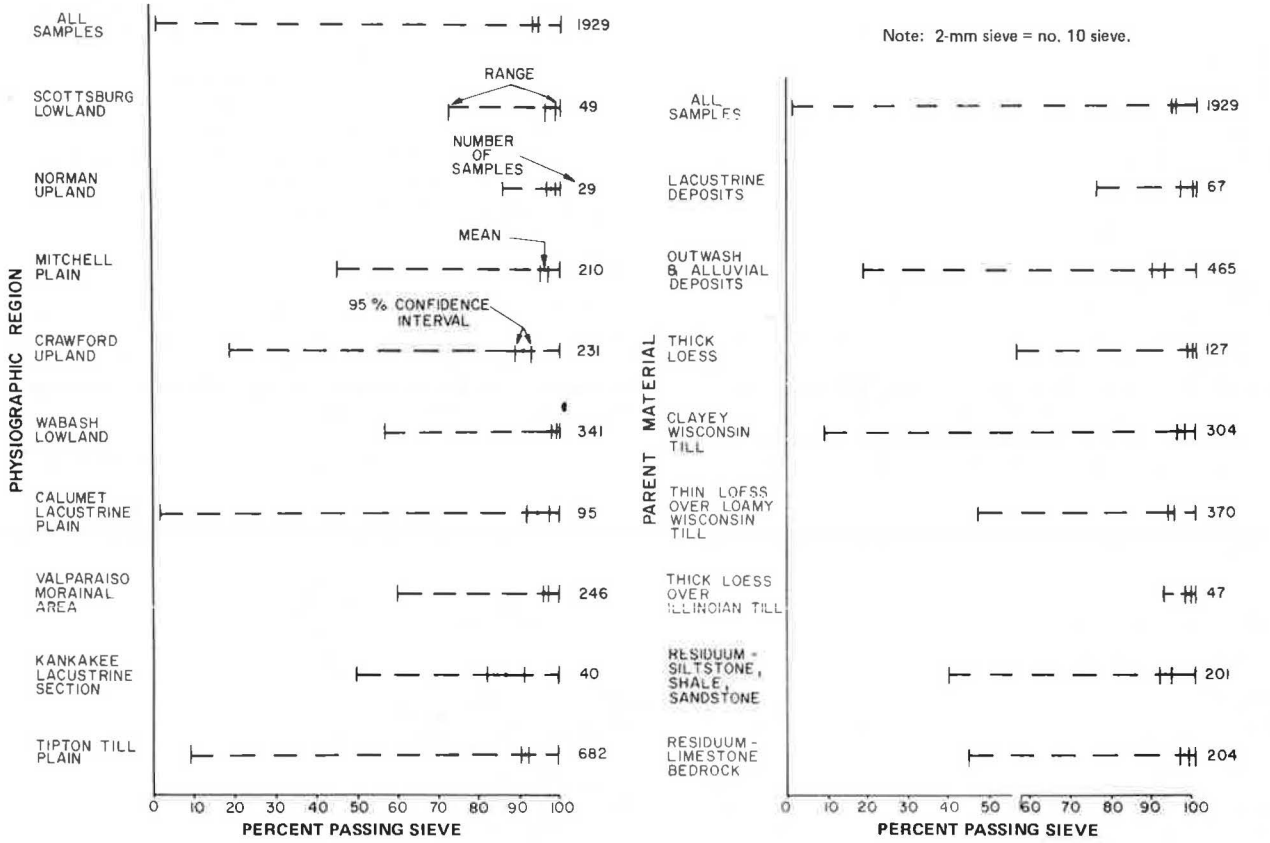

Figure 5. Distributional characterization of liquid limit.

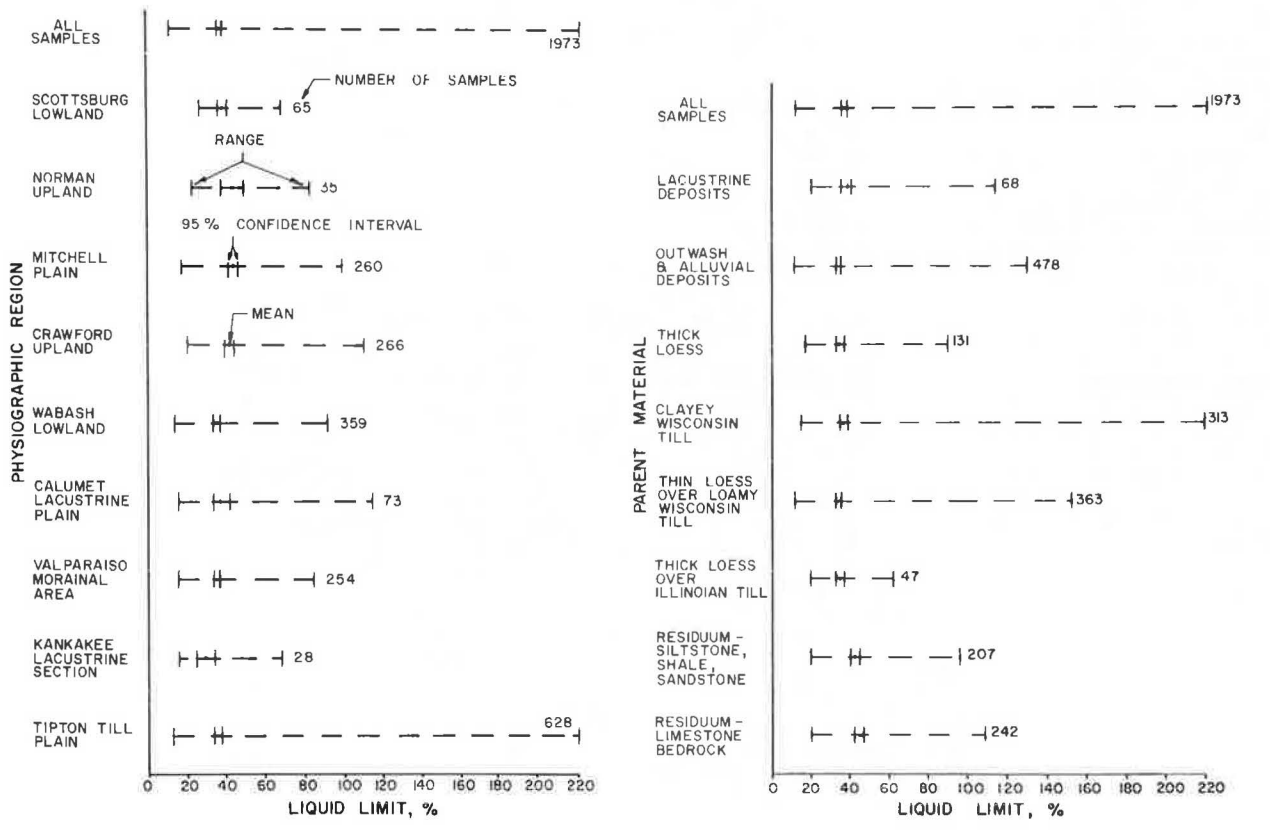

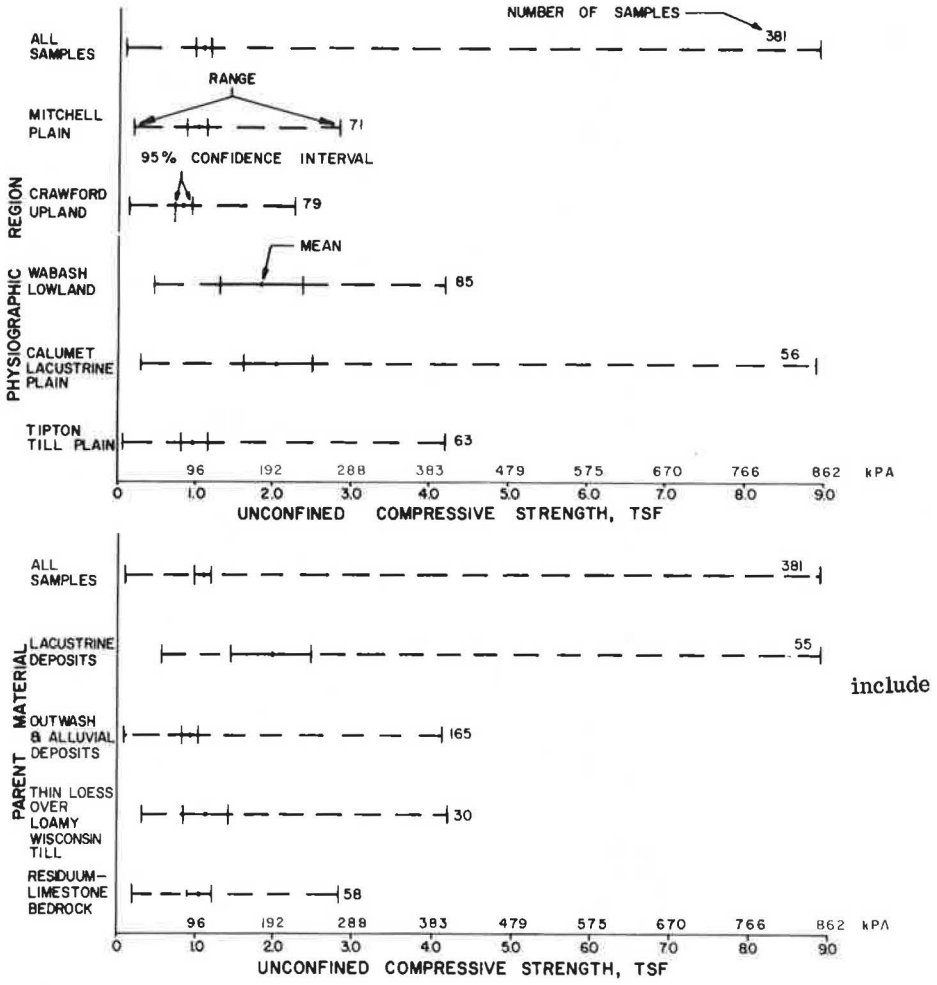

Figure 6. Distributional characterization of unconfined compressive strength.

(C_r), which equals $C_c/1 + e_o$, where e_o is the initial void ratio;

2. Unconfined compressive strength (q_u);
3. Standard AASHTO maximum dry ($\gamma_{d_{max}}$) and wet ($\gamma_{m_{max}}$) densities and optimum moisture content (w_{opt}); and
4. Soaked CBRs at 100 and 95 percent of $\gamma_{d_{max}}$.

The set of easier-to-measure independent variables includes

1. e_o, natural moisture content (w_n), natural dry density (γ_d), liquid limit (w_L), plastic limit (w_p), plasticity index (I_p), and percent clay for the consolidation test data;
2. w_L, w_p, w_n, γ_d, and liquidity index (L_I) for the unconfined compressive-strength data; and
3. w_L, w_p, I_p, and shrinkage limit (w_s) for the compaction and CBR test data.

If a particular dependent variable resisted statewide regression modeling, or if the data were available in amounts large enough to justify modeling on smaller units (that is, physiographic regions, parent-material areas and, in some cases, soil types), the data were grouped accordingly to determine whether the prediction models could be significantly improved.

The soil test data have been collected throughout the entire state as shown in Figure 7, but no attempt was made to collect equal numbers of samples from all parts of the state. Therefore, the correlation and prediction equations presented are applicable for only those areas from which data have been collected.

Each dependent variable was first plotted against each independent variable to investigate the nature of the dependence. These plots indicate whether linear terms, quadratic terms, or transformations of the variables are appropriate. In addition, the coefficient of determination (r^2) was examined to determine the degree of relationship between the dependent and independent variables in each case. Those sets of independent and dependent variables that appeared to exhibit some dependence were then examined by multiple regression analysis methods.

The potential terms in each model were linear independent variables, squared independent variables, reciprocal transformations of independent variables, and linear interactions of independent variables. Logarithmic transformations of dependent and independent variables were attempted when it appeared that the model was intrinsically linear by suitable transformation.

The regression equations that had adjusted coefficients of multiple determination (R_a^2) (12) greater than 0.65 were examined to determine whether the relationships were statistically useful. The criteria included (a) small confidence intervals (at the 95 percent confidence level) and (b) confidence intervals that did not cross zero.

Evaluation of Models

After obtaining good prediction models, it is important to evaluate them to determine whether they are ap-

Figure 7. County data sources.

propriate for the particular data being examined. Certain assumptions are inherent in the formulation of regression models; an examination of the residuals (differences between the observed and corresponding predicted values) will suggest whether any of the usual assumptions are invalid. The usual assumptions are that the errors are independent, have zero mean, a constant variance, and follow a normal distribution.

The residuals of each model were plotted against each independent variable in it, in addition to the dependent variable and its predicted value. The residuals were tested for normality by the Purdue University computer program called NORP. The models that had residual plots that did not display systematic tendencies to be positive or negative, but tended to fall within horizontal bands centered around 0, and also satisfied the normality criterion at the 90 percent confidence level were selected as the final models (see Tables 1-3) (3).

SUMMARY

The computerized data bank described in this paper should facilitate efficient and economical handling of geotechnical information in Indiana. Soils information that was essentially lost after a project was completed can now be used for future highway projects and improvements. The data bank will be maintained by the Indiana State Highway Commission for all potential users.

The application of statistical methods to the geotechnical data stored to January 1978 is promising. However, no soil group studied can be said to produce better correlation equations than any other, overall. The grouping of soils by physiographic regions and parent-material areas certainly appears to be justified for

Table 1. Regression equations for prediction of compression index and compression ratio.

Unit	Dependent Variable	R_a^2	Regression Equation	N
All samples	C_c	0.800	$C_c = 0.5363(e_o - 0.4110)$	96
		0.792	$C_c = 0.0002(w_n^2 - 106.2727)$	
		0.783	$C_c = 0.0129(w_n + 0.1015w_L - 16.1875)$	
	C_r	0.691	$C_r = 0.2037(e_o - 0.2465)$	
Wabash lowland	C_c	0.838	$C_c = 0.5673(e_o - 0.4422)$	29
	$\log C_c$	0.831	$\log C_c = 2.7904(e_o - 0.3346e_o^2 - 0.8449)$	
	C_r	0.750	$C_r = 0.221(e_o - 0.3074)$	
		0.748	$C_r = 0.0065(w_n - 11.6361)$	
		0.735	$C_r = 0.0034[(e_o \times w_n) + 8.3647]$	
Crawford upland	C_c	0.859	$C_c = 0.0101[(e_o \times w_L) - 0.5765w_L + 12.665]$	28
		0.833	$C_c = 0.0114(w_n + 0.2491w_L - 18.8134)$	
		0.788	$C_c = 0.4941(e_o - 0.3507)$	
		0.777	$C_c = 0.0133(w_n - 12.1886)$	
	C_r	0.740	$C_r = 0.0001(w_n^2 + 455.8889)$	
		0.736	$C_r = 0.0033[(e_o \times w_n) + 12.5168]$	
		0.721	$C_r = 0.1164(e_o^2 + 0.3594)$	
Outwash and alluvial deposits	C_c	0.842	$C_c = 0.5621(e_o - 0.4215)$	63
		0.822	$C_c = 0.0153(w_n + 0.1022w_L - 0.3104w_p - 11.6123)$	
	$\log C_c$	0.772	$\log C_c = 2.1389(e_o - 0.2967e_o^2 - 0.9374)$	

Table 2. Regression equations for prediction of unconfined compressive strength.

Unit	Dependent Variable	R_a^2	Regression Equation	N
Calumet lacustrine plain	q_u	0.756	$q_u = 0.0003644(\gamma_d^2 - 2518883.9)$	40
	$\log q_u$	0.750	$\log q_u = 0.3804 \times 10^{-6}(\gamma_d^2 + 2.401 \times 10^6)$	
Lacustrine deposits	$\log q_u$	0.699	$\log q_u = 0.3804 \times 10^{-6}(\gamma_d^2 + 2.570 \times 10^6)$	48

Note: These coefficients were derived for q_u expressed in kilonewtons per square meter and γ_d expressed in kilograms per cubic meter.

Table 3. Regression equations for prediction of standard Proctor maximum dry and wet densities and optimum moisture content.

Unit	Dependent Variable	R_a^2	Regression Equation	N
All samples	w_{opt}	0.894	$w_{opt} = -0.03062(\gamma_{d_{max}} - 2340.3644)$	138
Valparaiso morainal area	$\log \gamma_{d_{max}}$	0.816	$\log \gamma_{d_{max}} = -3.683[(1/w_L) + 0.127\log w_L - 1.109]$	
		0.785	$\log \gamma_{d_{max}} = 0.2239(\log w_L - 16.097)$	
	$\gamma_{m_{max}}$	0.790	$\gamma_{m_{max}} = -1849.7498[\log w_L + 9.9623(1/w_L) - 2.9758]$	26
	$\log \gamma_{m_{max}}$	0.694	$\log \gamma_{m_{max}} = -0.1348(\log w_L - 26.2080)$	
	w_{opt}	0.972	$w_{opt} = 0.04482(\gamma_{m_{max}} - 1.2985\gamma_{d_{max}} + 604.899)$	
		0.870	$w_{opt} = -0.0260(\gamma_{d_{max}} - 2432.7188)$	
		0.810	$w_{opt} = 23.0357 + 0.002(w_L \times w_p) - 285.9386(1/w_L)$	
Residuum of limestone bedrock	$\gamma_{d_{max}}$	0.772	$\gamma_{d_{max}} = -1841.0591[\log w_L + 14.0953(1/w_L) - 2.9063]$	22
	$\log w_{opt}$	0.781	$\log w_{opt} = 0.0042(w_L + 259.0381)$	

Note: These coefficients were derived for γ expressed in kilograms per cubic meter.

some dependent variables and for certain groups of soils.

From the statistical analysis to date, the following preliminary conclusions are drawn.

1. The prediction of C_c values by using simpler soil measures is reasonable on a statewide basis. Soils investigated in the Wabash lowland and the Crawford upland physiographic regions also produce regression equations for C_c that have relatively high correlation coefficients. Furthermore, equations generated for soils derived from outwash and alluvial deposits also are statistically significant for the prediction of C_c.
2. The prediction of q_u by the method of regression analysis is possible for soils found in the Calumet lacustrine plain and soils derived from lacustrine deposits.
3. The prediction of $\gamma_{d_{max}}$, $\gamma_{m_{max}}$, and w_{opt} is possible from simpler-to-determine independent variables for the soils from the Valparaiso morainal area. Soils derived from residuum of limestone bedrock also produced satisfactory regression equations.

As the size of the data base is increased, more complete analyses will be undertaken with the expectation that more meaningful and valid correlations can be achieved. Other data groupings, including the pedologic hierarchy, will also be examined.

ACKNOWLEDGMENT

We are grateful to the Joint Highway Research Project of Purdue University, the Indiana State Highway Commission, and the Federal Highway Administration for their financial support of the research reported herein. Special thanks are due Robert Ringholz for his assistance in the collection of the project data.

The contents of this paper reflect our views; we are responsible for the facts and the accuracy of the data presented herein. The contents do not necessarily reflect the official veiws or policies of the Federal Highway Administration or the Indiana State Highway Commission. This paper does not constitute a standard, specification, or regulation.

REFERENCES

1. D. J. Hagerty, N. G. Schmitt, and W. J. Pfalzer. Retrieval and Use of Geotechnical Information. In Geotechnics in Transportation Engineering, Ohio River Valley Soil Seminar, Lexington, KY, Oct. 1973 (ASCE, Kentucky section), pp. 1-9.

2. Acquisition and Use of Geotechnical Information. NCHRP, Synthesis of Highway Practice 33, 1976, 40 pp.
3. G. D. Goldberg. Development of the Computerized Geotechnical Data Bank for the State of Indiana. Purdue Univ., West Lafayette, IN, M.S.C.E. thesis; Joint Highway Research Project, Rept. 78-6, May 1978, 163 pp.
4. Soil Survey Manuals. Soil Conservation Service, U.S. Department of Agriculture, 1958-present.
5. D. Spradling. A Soils Data System for Kentucky. Bureau of Highways, Kentucky Department of Transportation, Frankfort, Res. Rept. 441, 1976, 58 pp.
6. T. K. Liu and T. H. Thornburn. Engineering Index Properties of Some Surficial Soils in Illinois. College of Engineering, Univ. of Illinois at Urbana, Bull. 477, 1965.
7. P. Lumb. The Variability of Natural Soils. Canadian Geotechnical Journal, Vol. 3, No. 2, May 1966, pp. 74-97.
8. P. Lumb. Application of Statistics in Soil Mechanics. In Soil Mechanics--New Horizons (I. K. Lee, ed.), Elsevier, New York, 1974, pp. 44-111.
9. D. J. A. van Zyl. Storage, Retrieval, and Statistical Analysis of Indiana Shale Data. Joint Highway Research Project, Purdue Univ., West Lafayette, IN, 140 pp.
10. V. Rizkallah and E. El Nimr. Applicability of Regression Analysis in Soil Mechanics with the Help of Data Banks. Proc., 2nd International Conference on the Application of Statistics and Probability in Soil and Structural Engineering, Aachen, Federal Republic of Germany, Vol. 2, 1975, pp. 423-438.
11. M. Van Rooyen. Intercorrelation of Engineering Properties of Soil. Proc., 4th Regional Conference for Africa on Soil Mechanics and Foundation Engineering, Cape Town, South Africa, 1967, pp. 203-208.
12. J. Neter and W. Wasserman. Applied Linear Statistical Models. Irwin, Homewood, IL, 1974, 842 pp.

Publication of this paper sponsored by Committee on Engineering Geology.

Design of Subsurface Drainage Systems for Control of Groundwater

Lyle K. Moulton, Department of Civil Engineering, West Virginia University, Morgantown

In recent years, awareness has grown of the need for subsurface drainage systems that can drain water from the pavement structural system. Much of the emphasis associated with studies of this subject has been on the removal of the moisture that infiltrates through the surface of the pavement, but it has also been recognized that the control of groundwater is an essential part of any effective highway subsurface drainage system. In this paper, rational analytical methods for the design of subsurface drainage systems for the control of groundwater are developed and presented. Although these methods are, in general, approximate in nature, they are soundly based on fundamental seepage theory. The resulting solutions have been used to prepare graphical design aids that can be readily applied by the highway designer. The use of these design aids is illustrated by a series of examples, and the results are compared with more-exact flow-net solutions obtained by the use of electric analogs. On the basis of this comparison, it concluded that the proposed design procedures, although approximate, do permit the development of good practical designs for subsurface drainage systems for the removal and/or control of groundwater in highway applications.

In recent years, there has been a growing awareness of the need for subsurface drainage systems that can drain water from a pavement structural system and thus minimize detrimental effects. Workshops dealing with water in pavements (1) have been conducted, and guidelines for the design of subsurface drainage systems for pavement structural sections have been published (2, 3). Although much of the emphasis of these activities has been on the removal of the moisture that infiltrates through the surface of the pavement, it has also been recognized (3) that the control of groundwater is an essential part of any effective highway subsurface drainage system.

Commonly, the design of groundwater drainage systems is based on empirical rules of thumb that have been developed by trial and error over a period of years or on rather tedious graphical techniques involving the use of flow nets (4). The purpose of this paper is to present some rational, approximate analytical methods for the design of groundwater control systems such as the interceptor drains shown in Figures 1 and 2 and the symmetrical drawdown drains shown in Figure 3. Although, at present, it is not possible to eliminate all elements of empiricism, the methods presented are based on fundamental seepage theory.

LONGITUDINAL INTERCEPTOR DRAINS

Calculation Method

Let us consider the case of the unconfined flow of groundwater over a sloping impervious boundary toward a single interceptor drain, as illustrated in Figure 4. A solution for the shape of the drawdown curve for this situation, which was developed by R. E. Glover of the U.S. Bureau of Reclamation, is given by Donnan (5). This solution, which is based on an adaptation (6) of Dupuit theory, has the form

$$x = \{H\ell n[(H - H_0)/(H - y)] - (y - H_0)\}/S \quad (1)$$

where

x and y = coordinates of a point on the drawdown

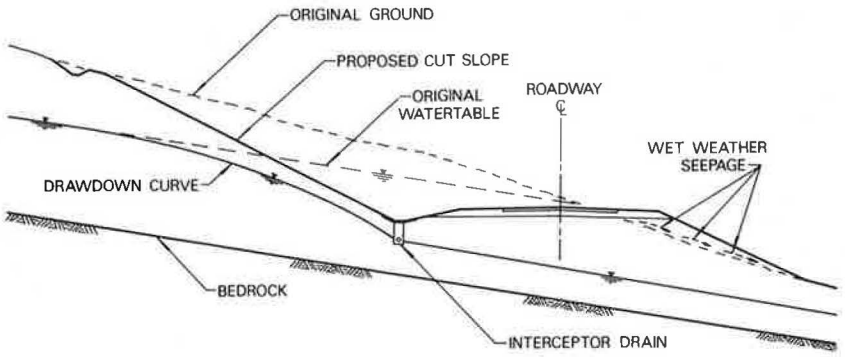

Figure 1. Longitudinal interceptor drain used to cut off seepage and lower the groundwater table.

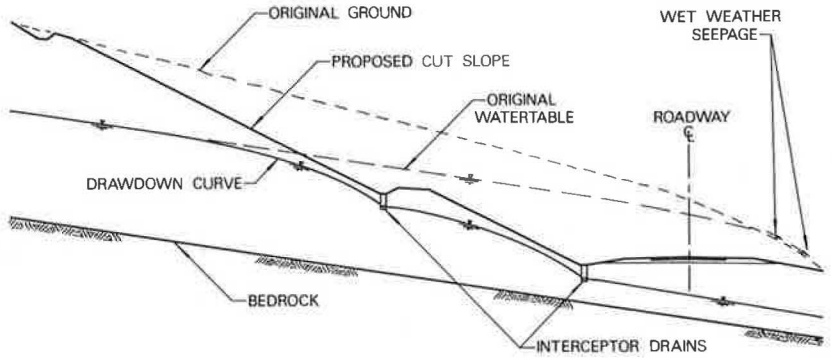

Figure 2. Multiple interceptor drain.

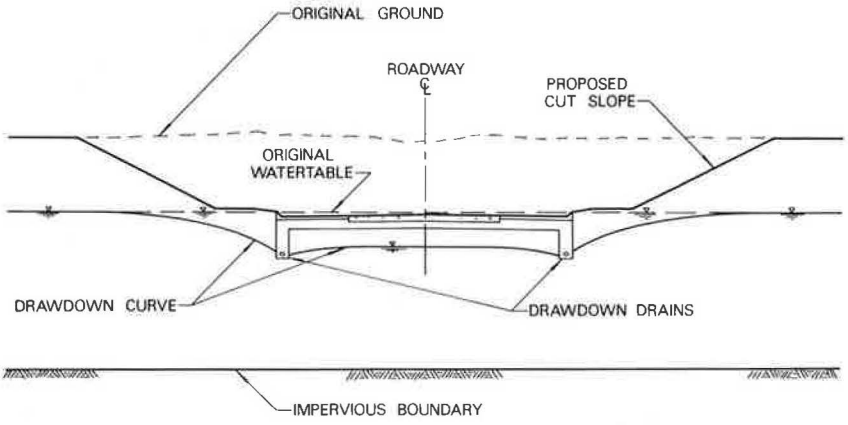

Figure 3. Symmetrical longitudinal drains used to lower the water table.

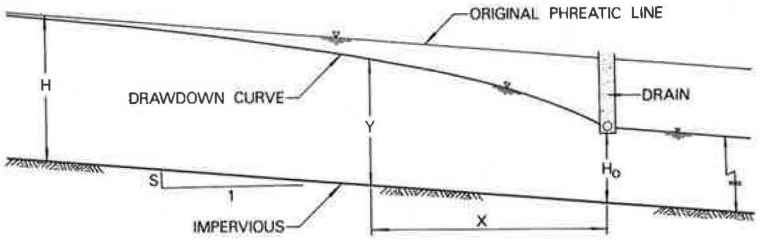

Figure 4. Flow toward a single interceptor drain.

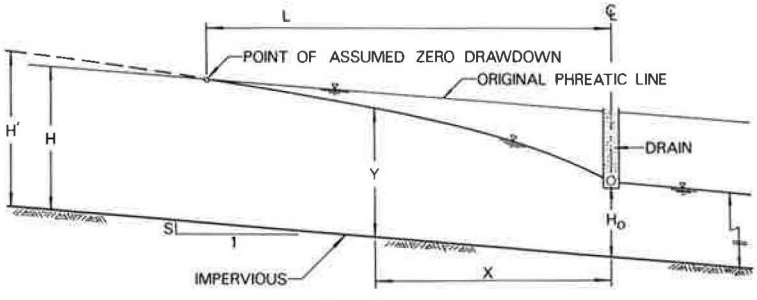

Figure 5. Flow toward a single interceptor drain when the drawdown can be considered to be insignificant at distance L from the drain.

curve, as shown in Figure 4;
H = height of the original groundwater table above an impervious boundary of slope S; and
H_0 = height of the drain above the impervious boundary.

Examination of Figure 4 and Equation 1 shows that the drawdown curve becomes asymtotic to the original free-water surface (phreatic line) at infinity. Dealing with this boundary condition in practical problems is awkward and, consequently, most solutions to gravity-flow problems of this type have assumed that there is a finite distance (L) from the drain at which the drawdown can be considered to be insignificant and at which, for practical purposes, y = H, as shown in Figure 5. In well theory, L is generally referred to as the radius of influence.

In an investigation of interceptor drains of this type, Keller and Robinson (7) conducted a laboratory study in which, for practical purposes, the conditions shown in Figure 5 were duplicated by the use of a finite source of seepage located at distance L from the drain. They found that Glover's equation, i.e., Equation 1, checked the experimental data when modified into the form

$$Sx = H' \ln[(H' - H_0)/(H' - y)] - (y - H_0) \quad (2)$$

where H′ = a point on a fictitious extension of the drawdown curve, as shown in Figure 5. Then, because y = H when x = L,

$$SL = H' \ln[(H'-H_0)/(H'- H)] - (H - H_0) \quad (3)$$

and H′ can be determined for known values of S, L, H, and H_0.

Keller and Robinson also found that the quantity of flow into the drain (q_d) could be determined from the relationship

$$q_d = q_0(H' - H_0)/H \quad (4)$$

where q_0 = magnitude of the approach flow and is given by

$$q_0 = kHS \quad (5)$$

where k = coefficient of permeability of the porous medium. A complete solution to the problem can thus be obtained by using Equations 2, 3, 4, and 5. For convenience, Equations 3 and 4 have been combined in dimensionless form and solved by computer to prepare Figure 6, from which q_d/kHS and H′/H can be determined in terms of known values of SL/H and H_0/H. The same computations also provided the data by which, through a change of variables, Figure 7 was prepared. Figure 7 permits determination of the location of the drawdown curve by giving values of Sx/y for known values of H_0/y and $(H' - H_0)/y$. In practice, a series of values of y (between H_0 and H) are assumed, and Figure 7 is used to assist in the determination of the corresponding values of x.

In order to use Figures 6 and 7 for any highway drainage problem, it is necessary to have an estimate of the value of L. One method for estimating this value might be through the use of the Sichardt (8) equation,

$$L = C(H - H_0)\sqrt{k} \quad (6)$$

which has been widely accepted and used in connection with pumped wells and dewatering systems (9). The value of the coefficient C in Equation 6 is dependent in part on the units of H, H_0, and k. For example, the value proposed by Sichardt (8) would be approximately 6 if H and H_0 were in feet and k were in feet per day. However, a series of experimental flow nets for typical interceptor drain problems constructed by use of an electric analog, suggests that the value of L is independent of k and dependent only on the geometry of the problem. Although this study is at present incomplete, it suggests that, for the range of drawdowns and slopes commonly encountered in interceptor and drawdown-drain problems, the value of L can be estimated, for practical purposes, from the relationship

$$L = 3.8(H - H_0) \quad (7)$$

For the purposes of this paper, Equation 7 has been adopted as the method for estimating the value of L. However, it is anticipated that, on completion of the experimental flow-net analyses, some refinement to this relationship might be forthcoming.

Example 1

Let us consider the proposed construction shown in Figure 1 and, for this problem, (a) compute the reduced flow rate (q_d/k) into the drain and (b) plot the location of the drawdown curve (free-water surface). The detailed dimensions of the problem are given in Figure 8. To keep the left branch of the free-water surface from breaking out through the cut slope and to lower the right branch of the free-water surface well below the pavement structural system, the underdrain was set below the ditch line at a depth of 1.5 m (5 ft). It is proposed to pave the ditch over the drain to avoid infiltration and clogging.

From Equation 7, $L = 3.8(H - H_0) = 3.8(4.27) = 16.2$ m (53.2 ft).
From Figure 6, if $SL/H = 0.15(16.2)/6.1 = 0.398$ and $H_0/H = 1.83/6.1 = 0.3$, $q_d/kHS = 1.57$ and $H'/H = 1.84$ [therefore, $H' = 1.84(6.1) = 11.22$ m (36.8 ft)].

Reduced Flow Rate

Thus, $q_d/k = 1.57HS = 1.57(6.1 \times 0.15) = 1.44$ m (4.71 ft). The reduced flow rate could also be computed from the flow net (see Figure 8), i.e., $q_d/k = \Delta H N_f/N_d = 6.4(6)/28 = 1.37$ m (4.50 ft).

Drawdown Curve

From Figure 7, if $H' = 11.22$ m and the following values are assumed for the y coordinates, the x coordinates of the drawdown curve can be determined as follows (1 m = 3.28 ft):

y (m)	H_0/y	$(H' - H_0)/y$	Sx/y	x (m)
2.26	0.811	4.16	0.041	0.60
2.68	0.682	3.48	0.080	1.43
3.11	0.588	3.02	0.117	2.43
3.54	0.517	2.66	0.149	3.52
3.96	0.462	2.37	0.190	5.02
4.39	0.417	2.14	0.226	6.61
4.82	0.380	1.95	0.265	8.52
5.24	0.349	1.79	0.310	10.83
5.67	0.323	1.66	0.350	13.23

This drawdown curve is shown as the dashed curve in Figure 8; it is only approximate, but can be used as a starting point for constructing the flow net that ultimately yields a more accurate location of the free-water surface.

MULTIPLE INTERCEPTOR DRAINS

Calculation Method

A subsurface drainage system consisting of multiple interceptor drains (such as that shown in Figure 2) can be designed by using the principles outlined above and considering each drain separately. However, to properly define the boundary conditions for each of the upper drains correctly, it is necessary to establish the location of the limiting streamline above which the flow pattern is essentially that of a single drain installed in the flow domain above a sloping impervious boundary. In essence, this establishes an impervious boundary for each upper drain roughly parallel to the lower sloping impervious boundary. Flow-net studies conducted by using an electric analog have shown that boundaries of this type can be established by drawing a line parallel to the sloping impervious boundary and located at a depth below the drain equal to $1/10$ to $1/12$ of the drain spacing. This is an adaptation of the generalized method of fragments, which, according to Aravin and Numerov (10), was first proposed by Pavlovsky in Russia in 1935 and was introduced into the United States, for fragments in series, by Harr (6) in 1962. In this instance, the flow fragments are considered to be in parallel.

Figure 6. Chart for determining flow rate in interceptor drains.

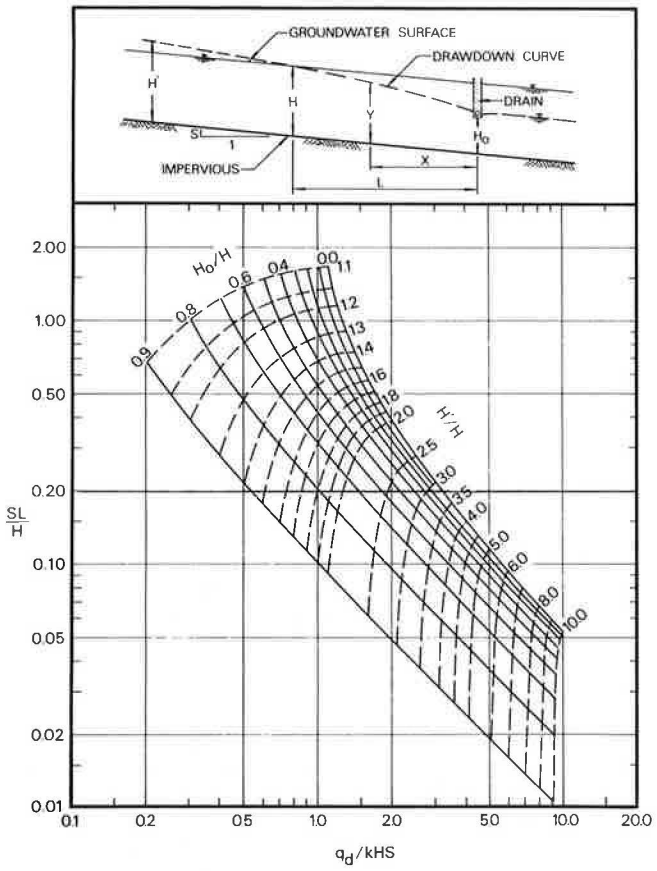

Figure 7. Chart for determining drawdown curves for interceptor drains.

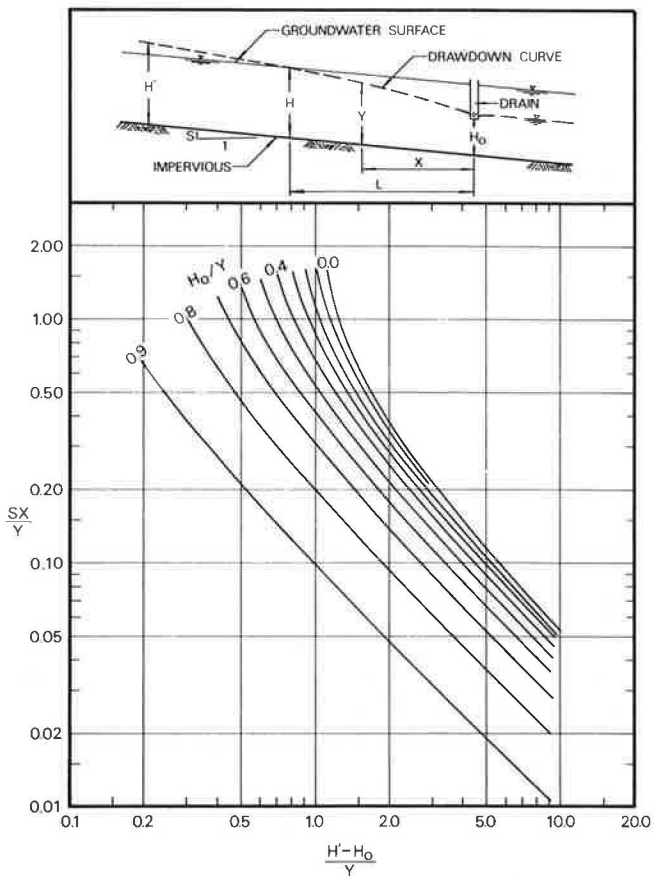

Figure 8. Example 1: flow net, dimensions, and details.

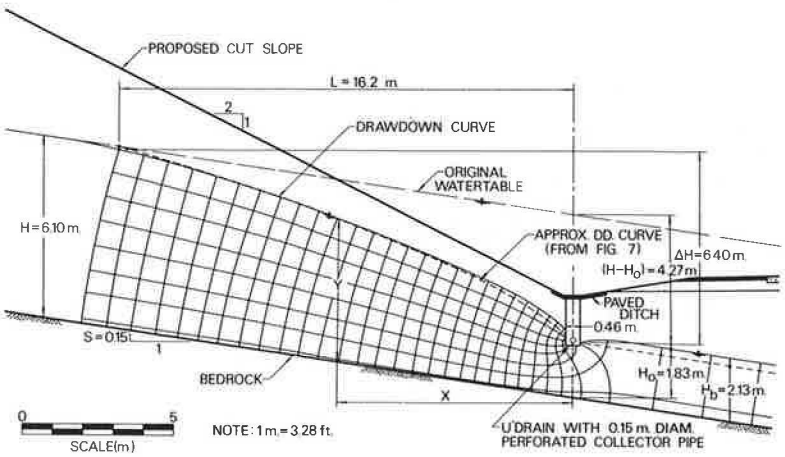

Figure 9. Example 2: dimensions and details required for the use of Figures 6 and 7.

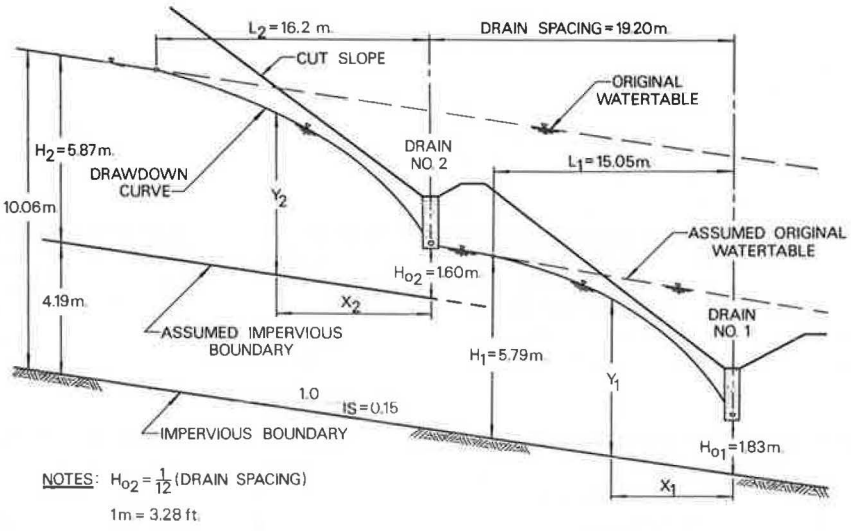

Figure 10. Example 2: flow net, dimensions, and details.

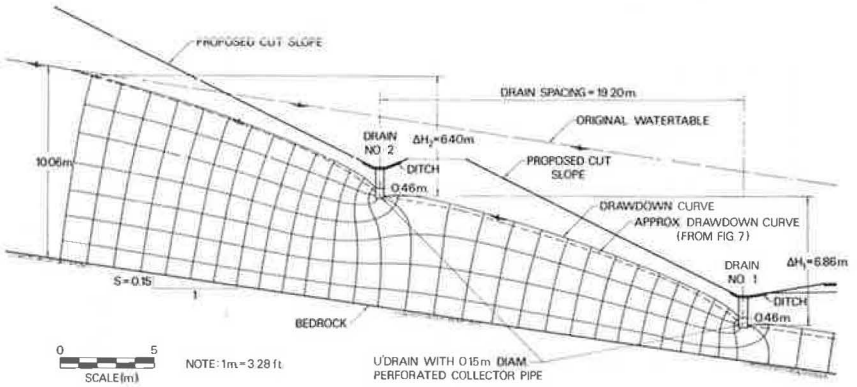

Example 2

Let us consider the proposed construction situation shown in Figure 2, which represents a deeper portion of the cut shown in Figure 1. This situation requires two drains to cut off and drawdown the water table to prevent it from breaking out through the slope and to keep water from this source out of the pavement structure. The detailed dimensions of the problem are shown in Figures 9 and 10. The locations and depths of the drains were established by trial, taking into consideration the desirability of maintaining the free-water surface below the cut slope. The dimensions given in Figure 9 are those required to solve the problem by using the method of fragments and Figures 6 and 7.

From Equation 7, $L_1 = 3.8(H_1 - H_{01}) = 3.8(5.79 - 1.83) = 15.05$ m (49.4 ft) and $L_2 = 3.8(H_2 - H_{02}) = 3.8(5.87 - 1.60) = 16.2$ m (53.2 ft).

For drain 1, Figure 6 shows that, for $SL_1/H_1 = 0.15(15.05/5.79) = 0.389$ and $H_{01}/H_1 = 1.83/5.79 = 0.316$, $q_{d1}/kH_1S = 1.58$ and $H_1'/H_1 = 1.90$ [therefore $H_1' = 1.90(5.79) = 11.0$ m (36.1 ft)].

Similarly, for drain 2, $q_{d2} = kH_2S = 1.57$ and $H_2' = 10.85$ m (35.6 ft).

Reduced Flow Rate

Thus, $q_{d1}/k = 1.57H_1S = 1.57(5.87 \times 0.15) = 1.37$ m and $q_{d2} = 1.57H_2S = 1.57(5.87 \times 0.15) = 1.38$ m (4.53 ft).

Or, for comparison purposes (see Figure 10), based on the flow net, $q_{d1} = H_1N_{f1}/N_{d1} = 6.86(3)/15 = 1.37$ m and $q_{d2}/k = H_2N_{f2}/N_{d2} = 6.3(3)/14 = 1.37$ m.

Drawdown Curves

The method illustrated in example 1 was used with the data shown in Figure 9 and the chart shown in Figure 7 to determine the locations of the x_1, y_1, and x_2, y_2 coordinates of the drawdown curve. The resulting curve was then plotted as the dashed line in Figure 10. It can be seen that the agreement between this approximate curve and the more exact free-water surface generated by the flow-net solution is quite good.

SYMMETRICAL DRAWDOWN DRAINS

Calculation Method

To solve a problem such as that shown in Figure 3, the method of fragments can be used by breaking the flow domain into fragments, as shown in Figure 11. Basically, this amounts to assuming that there is a horizontal streamline existing at the level of the drain. Flow-net analyses have shown that this is not an unreasonable assumption.

The quantity of flow into the drain from fragment 1 (q_1) can be estimated by using Dupuit theory (6) to be

$$q_1 = k(H - H_0)^2/2(L - b) \quad (8)$$

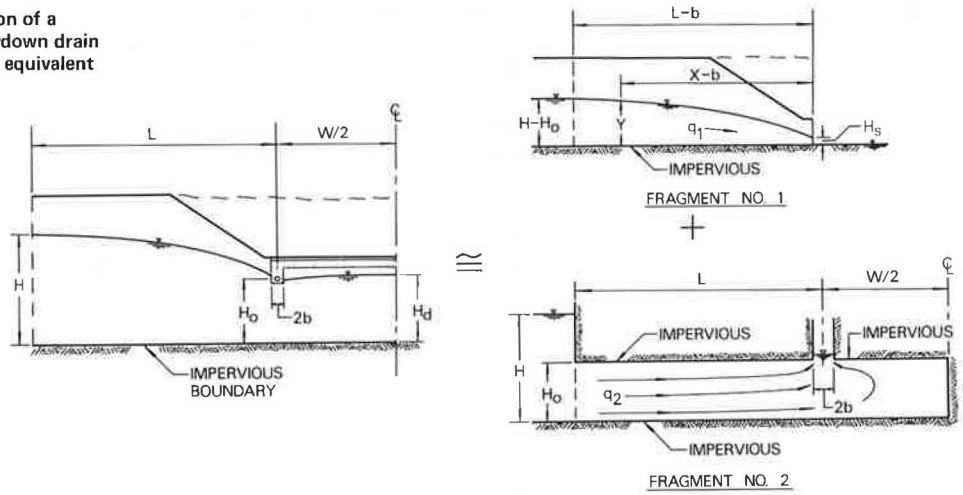

Figure 11. Division of a symmetrical drawdown drain problem into two equivalent fragments.

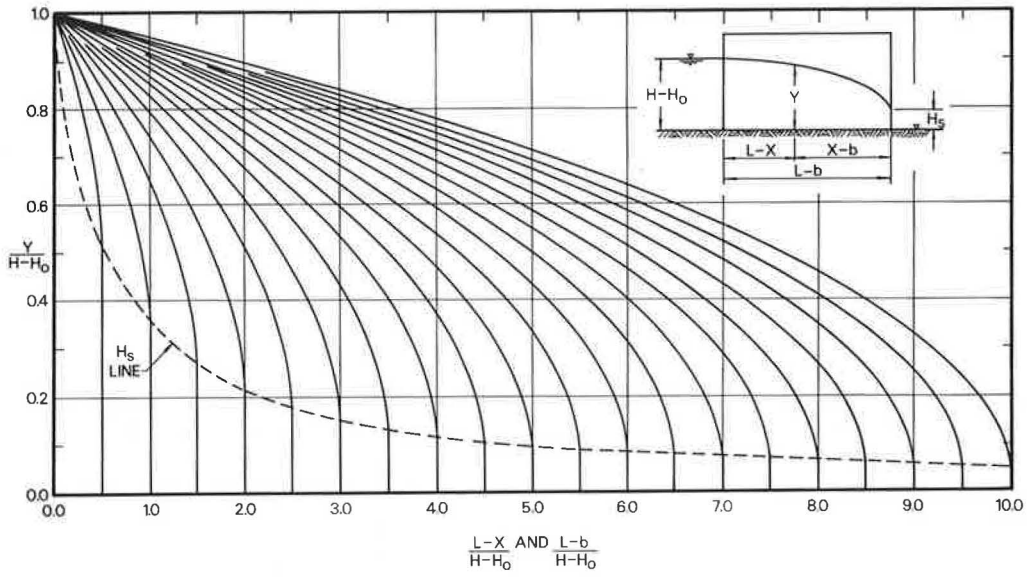

Figure 12. Free-water surfaces based on Gilboy modification of Dupuit theory.

The drawdown curve for Fragment 1 can be determined from the relationship

$$x = (L - b) + (1/2H_s m)\left[y(y^2 - H_s^2 m^2)^{1/2} - (H - H_0)[(H - H_0)^2 - H_s^2 m^2]^{1/2} - H_s^2 m^2 \ln([y + (y^2 - H_s^2 m^2)^{1/2}]/\{(H - H_0) + [(H - H_0)^2 - H_s^2 m^2]^{1/2}\})\right] \quad (9)$$

where $m = 0.43\pi$. [Equation 9 was derived by using the modification of Dupuit theory suggested by Gilboy (11).] For convenience, Equation 9 has been put into dimensionless form and solved by computer to prepare Figure 12, which can be used to determine the x and y coordinates of the drawdown curve.

The solution to the problem represented by fragment 2 in Figure 11 has been given by Aravin and Numerov (10), who showed that the flow rate (q_2) for this situation can be computed from the relationship

$$q_2 = k(H - H_0)/\{(L/H_0) - (1/\pi)\ln[(1/2)\sinh(\pi b/H_0)]\} \quad (10)$$

and that the value of the piezometric head at the roadway centerline ($H_d - H_0$) can be determined from the relationship

$$(H_d - H_0) = (q_2/\pi k)\ln[\coth(\pi b/2H_0)] \quad (11)$$

Equations 10 and 11 were solved by computer and used to prepare Figures 13 and 14, respectively. Figure 13 can be used to determine the quantity of flow (q_2) entering the drain from fragment 2 in terms of known values of H, H_0, b, and k. The total quantity of flow entering the drain (q_d) is then the sum of the flows from the two fragments, i.e.,

$$q_d = q_1 + q_2 \quad (12)$$

In the method of solution proposed here, it is assumed that the right branch of the drawdown curve can be approximated by the piezometric level along the upper boundary of fragment 2. Thus, Figure 14 can be used to estimate the location of the drawdown curve between the drain and the roadway centerline.

Example 3

Let us consider the proposed construction of a two-lane depressed roadway in an urban area, as shown in Figure 3. In connection with this proposed construction, it is desired to design a system of symmetrical longitudinal underdrains to draw the groundwater down as far as possible below the bottom of the granular base course. The detailed dimensions of the problem are

Figure 13. Chart for determining flow rate in symmetrical underdrains.

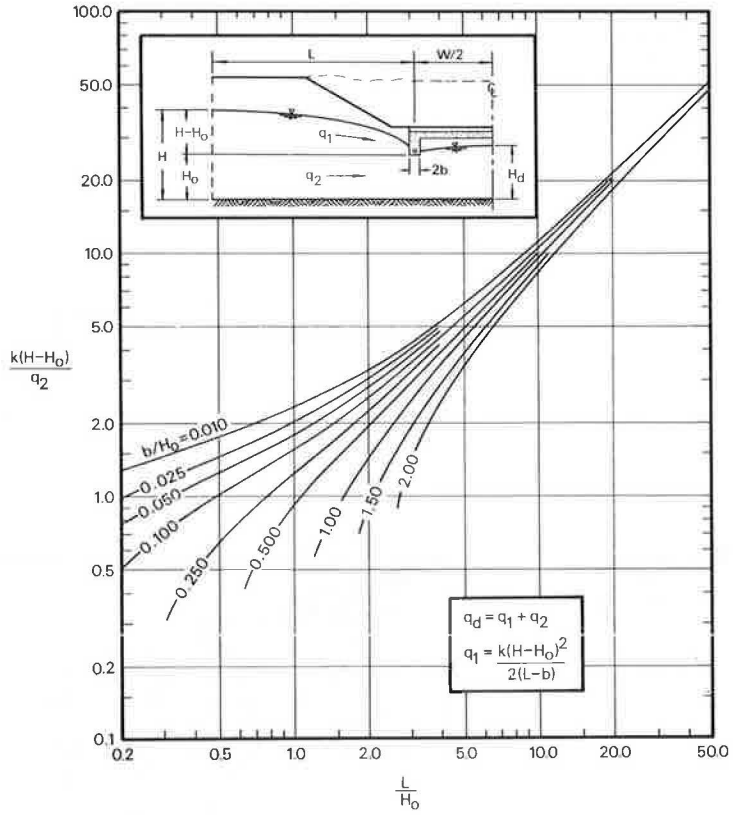

Figure 14. Chart for determining maximum height of free-water surface between symmetrical underdrains.

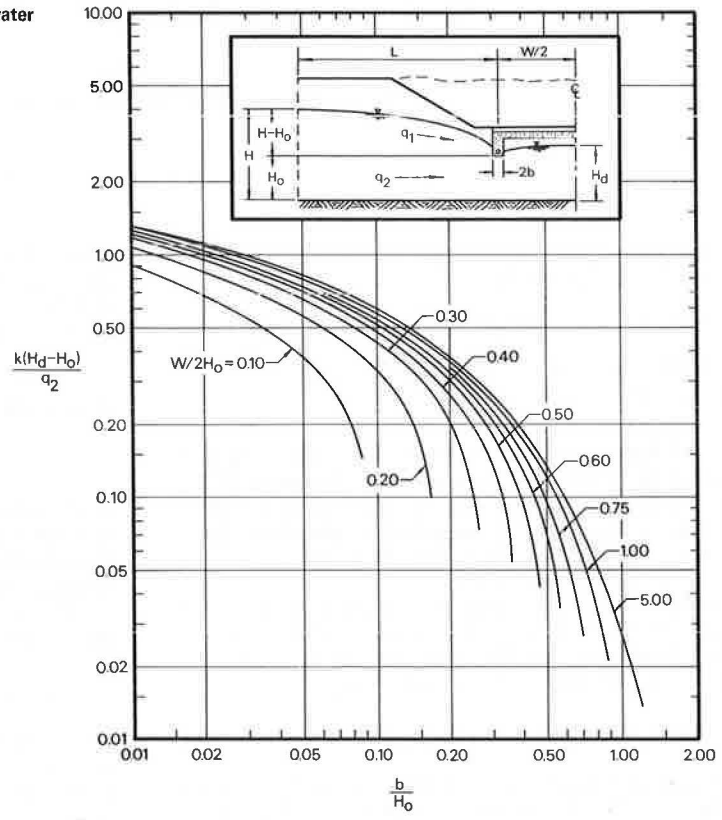

Figure 15. Example 3: flow net, dimensions, and details.

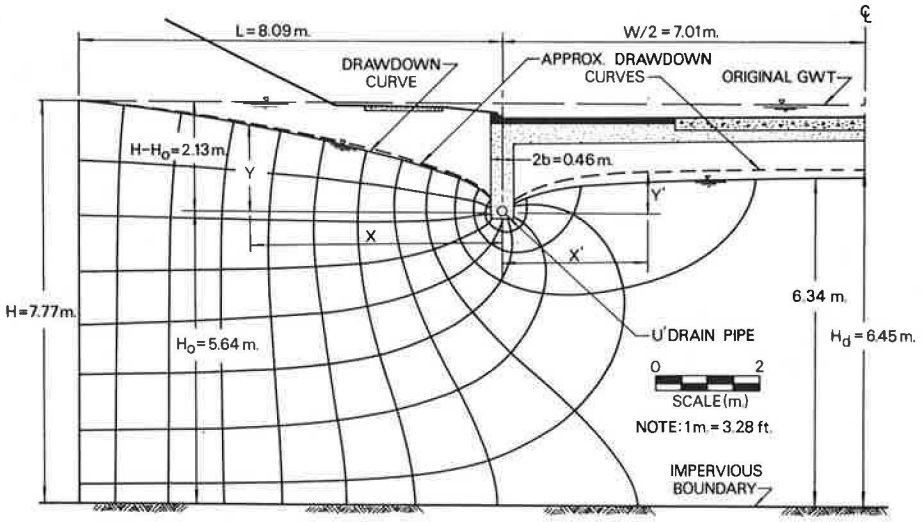

Figure 16. Chart for determining flow rate in horizontal drainage blanket.

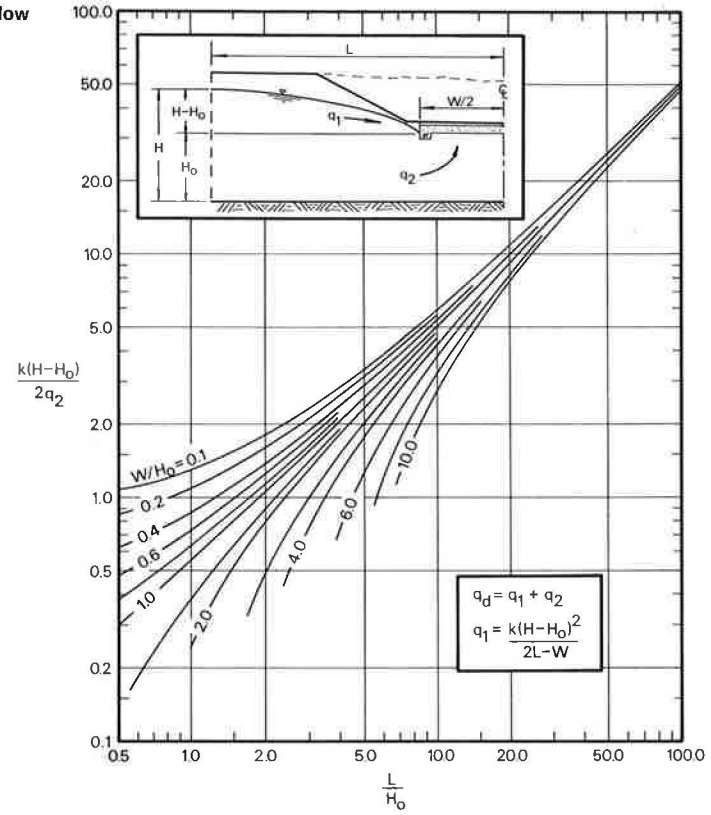

shown in Figure 15. The depth of the drains was established by trial, taking into consideration the desirability of producing the maximum drawdown without requiring excessively deep excavation (the trench depth below the bottom of roadway excavation was limited to 1.5 m).

From Equation 7, $L = 3.8(H - H_0) = 3.8(2.13) = 8.09$ m (26.5 ft).

Reduced Flow Rate

From Figure 13, for $b/H_0 = 0.23/5.64 = 0.041$ and $L/H_0 = 8.09/5.64 = 1.43$, it is found that $k(H - H_0)/q_2 = 2.30$. Thus, $q_2/k = (H - H_0)/2.30 = 2.13/2.30 = 0.926$ m (3.04 ft).

Then, from Equation 8, $q_1/k = (H - H_0)^2/2(L - b) = 2.13^2/2(8.09 - 0.23) = 0.289$ m (0.945 ft).

Therefore, the total reduced flow rate to the drain becomes, from Equation 12, $q_d/k = q_1/k + q_2/k = 0.926 + 0.289 = 1.28$ m (4.20 ft).

Or (for comparison), based on the flow net shown in Figure 15, if $\Delta H = (H - H_0) = 2.13$ m (7.0 ft), $q_d/k = \Delta H N_f/N_d = 2.13\ (7.4)/11.8 = 1.33$ m (4.38 ft).

Drawdown Curves

The right branch of the drawdown curve can be determined by taking various values of x' in Figure 15 as W/2 in Figure 14 and considering y' in Figure 15 as $(H_d - H_0)$ in Figure 14 as follows (noting that $b/H_0 =$

0.041 and $q_2/k = 0.926$ m) (1 m = 3.28 ft):

$x' = W/2$ (m)	$W/2H_0$	$k(H - H_0)/q_2$	$y' = (H_d - H_0)$ (m)
0.61	0.108	0.47	0.44
1.22	0.216	0.64	0.59
1.83	0.324	0.73	0.68
2.44	0.432	0.78	0.72
4.57	0.811	0.85	0.79
7.01	1.243	0.87	0.81

Then, from Figure 15, the left branch of the drawdown curve can be determined from Figure 12 by noting that $(L - b)/(H - H_0) = (8.09 - 0.23)/2.13 = 3.69$. Thus, for various values of y, the values of x can be determined by using Figure 12 as follows:

$y/(H - H_0)$	$(L - x)/(H - H_0)$	$(L - x)$ (m)	y (m)	x (m)
0.13	3.69	7.86	0.28	0.23
0.20	3.65	7.77	0.43	0.32
0.40	3.27	6.97	0.85	1.12
0.60	2.50	5.33	1.28	2.76
0.80	1.38	2.94	1.70	5.15
1.00	0	0	2.13	8.09

These approximate drawdown curves are shown dashed in Figure 15. It can be seen that, although this method produces a free-water surface that is slightly high, the agreement between it and the more exact free-water surface produced by flow-net analysis is reasonable.

For the special case where the underdrain cannot be placed sufficiently deep to draw down the groundwater table below the granular drainage blanket of the pavement system, the flow rate to this layer can be estimated by using Figure 16. Figure 16 was prepared by using Equation 10 with L as defined in the figure and $b = W/2$.

CONCLUSIONS

On the basis of the comparison between the solutions obtained by the approximate rational methods presented in this paper and those obtained by the use of the more-exact flow nets, it can be concluded that the proposed methods do permit the development of reasonably good practical designs for the removal and/or control of groundwater in highway applications. However, a few limitations of the proposed methods should be noted.

The solutions are based on the assumption that the soil is homogeneous and isotropic. The problems offered by layered or by anisotropic systems are difficult, although, in many instances, they can be treated approximately by the use of appropriate transformations of coordinates (6, 12).

It has been assumed that there is negligible head loss in the underdrains and that they are designed to have sufficient capacity to carry all the water that could theoretically flow into them. It should be noted in this regard that underdrains should be very carefully designed and have an appropriate filter system if their long-term performance is to be ensured.

Finally, it is necessary to know the coefficient of permeability of the soil in order to translate the reduced quantity of seepage into a meaningful flow rate that can be used in designing underdrain collection pipes and checking on capacity of the underdrain system. In many instances, this coefficient of permeability may be difficult to estimate without reliable field measurements.

ACKNOWLEDGMENT

I wish to express my gratitude to Sameh A. Mitry, whose computer analyses made the various design charts possible, and to Randy L. Moulton, who prepared the figures.

REFERENCES

1. Water in Pavements. Offices of Research, Development, Engineering, and Highway Operations, Federal Highway Administration, 1973.
2. H. R. Cedergren, J. A. Armon, and K. H. O'Brien. Guidelines for the Design of Subsurface Drainage Systems for Highway Structural Sections. Federal Highway Administration, Rept. FHWA-RD-73-14, 1973. NTIS: PB 231 173/AS.
3. H. R. Cedergren. Drainage of Highway and Airfield Pavements. Wiley, New York, 1974.
4. B. McClelland and L. E. Gregg. Methods of Analysis of Flow Problems for Highway Subdrainage. Proc., HRB, 1944, pp. 364-376.
5. W. W. Donnan. Drainage of Agricultural Lands Using Interceptor Lines. Journal of the Irrigation and Drainage Division, Proc., ASCE, Vol. 85, No. IR1, March 1959, pp. 13-23.
6. M. E. Harr. Groundwater and Seepage. McGraw-Hill, New York, 1962.
7. J. Keller and A. R. Robinson. Laboratory Research on Interceptor Drains. Journal of the Irrigation and Drainage Division, Proc., ASCE, Vol. 85, No. IR3, Sept. 1959, pp. 25-40.
8. W. Sichardt and W. Kyrieleis. Grundwasserabsenkungen bei Fundierungsarbeiten. J. Springer, Berlin, 1930.
9. C. I. Mansur and R. I. Kaufman. Dewatering. In Foundation Engineering (G. A. Leonards, ed.). McGraw-Hill, New York, 1962.
10. V. I. Aravin and S. N. Numerov. Theory of Fluid Flow in Undeformable Porous Media (A. Moscona, tr. and ed.). Israel Program for Scientific Translations, Jerusalem, 1965, 511 pp.
11. G. Gilboy. Hydraulic-Fill Dams. Proc., International Committee on Large Dams, Stockholm, Sweden, 1933.
12. H. R. Cedergren. Seepage, Drainage and Flow Nets. Wiley, New York, 1967.

Publication of this paper sponsored by Committee on Subsurface Drainage.

Swelling Characteristics of Compacted B-Horizon Oklahoma Soils

James B. Nevels, Jr., Oklahoma Department of Transportation, Oklahoma City
Joakim G. Laguros, School of Civil Engineering and Environmental Science, University of Oklahoma at Norman

One of the critical field problems of compacted clay soils used as subgrades for pavement structures is related to the deformation and swelling that result from water absorption. This paper describes the swelling characteristics of five composite B-horizon soils belonging to the Renfrow series that are encountered throughout north-central Oklahoma. Unlike the C-horizon soils in this area, the soils reported on here are sufficiently weathered and not well cemented. This was verified by the fact that neither the clay-size portion nor the plasticity index of these soils increased substantially after ultrasonic degradation. Laboratory specimens compacted to maximum dry density at optimum moisture content were tested by using the constant-volume and free-swell methods. The volume increased with the logarithm of the time; the initial phases showed higher rates of moisture uptake than did the final stages. This and the other relationships among swelling pressures, volume changes, moisture uptake, and physicochemical properties were generally characterized by a band pattern that implied the existence of upper and lower limits of swelling response. In addition, the reaction potential, which serves as a good predictor of volume changes and swelling pressures for C-horizon soils, did not have the accuracy expected. Scanning electron microscopy data indicated that swelling pressure and volume increase in direct proportion to the void cross-sectional area.

The structural damage that results from the swelling of clay soils has been documented over the years by numerous authors (1). Studies have shown that the magnitudes of swell and swelling pressure are dependent on many factors and that they are different for undisturbed and compacted soils. For compacted clays of the type reported on in this paper, examples have been given by Means and coworkers (2, 3). Poor pavement performance manifested by heaving, cracking, and lateral expansion has been reported by Haliburton (4).

To thoroughly understand swelling (volume-change) and swelling-pressure phenomena in compacted clay soils it is essential to study compaction and the structure of clay minerals, the physicochemical aspects of soil behavior, current theories of swelling, and the mechanical (or physical) factors that affect the phenomena. The expansiveness of compacted clay is a well-documented topic (5-12), but the current literature (13-16) suggests that there have been no major changes in theory development or procedures for the investigation and testing of expansive clays in the past decade.

In this investigation, the swelling potential of B-horizon soils was measured by the use of swelling pressure and percentage swell and correlated with the unconfined compressive strength, adsorbed cations, and void cross-sectional area (as determined by scanning electron microscopy).

EXPERIMENTAL PROCEDURE

Soil Characteristics

The five B-horizon soils used in this investigation were obtained from north-central Oklahoma. They are residual soils developed in place from the underlying clay shale of Permian deposition. Their engineering properties, which were determined by standard American Association of State Highway Officials (AASHO) methods, and their physicochemical properties are given in Table 1. That these soils are well weathered was verified by ultrasonic treatment [which has been successfully applied to Oklahoma shales (17)]. As shown in Table 2, the differences between the raw and the treated soils are inconsequential.

Mineralogically, the soils are predominantly illitic, as shown by their X-ray diffraction patterns, being composed of a mixture of illite (I), kaolinite (K), and mixed-layer illite-montmorillonite (ML). The relative proportions of the clay minerals were estimated by using an area-under-the-curve method. The concept of the "reaction potential" (17, 18) was then used to calculate a composite parameter (see Table 3) that can be considered indicative of the clay expansiveness.

1. The reaction potential for each individual mineral was calculated by multiplying its average cation exchange capacity (CEC) (16, p. 189) by the percentage of it present in the soils.
2. The composite reaction potential was calculated by multiplying the sum of the individual reaction potentials by the percentage of clay (<0.002 mm) in the soil and dividing by 100.

Swell and Swelling Pressures

A laboratory testing program was carried out to determine the volume change (percentage swell) and the swelling pressure at maximum dry density and optimum moisture content conditions. The swelling pressure was determined by the constant-volume (1, 14) and free-swell methods (14, 19). The data are given in Table 4, and the volume change is shown in Figure 1.

DISCUSSION OF RESULTS

The relationship between volume change on absorption of moisture and time (Figure 1) follows an S-curve pattern that appears to reach a constant value after about 7 days (or 10 000 min). The initial low volume change is believed to be due to the time lag between the absorption of moisture and the accompanying swelling. As shown in Figure 2, the free-swell method gave a slightly higher swelling pressure than did the constant-volume method. It is of interest that the pattern of the scatter of data points suggests that the relationship between moisture absorption and swelling pressure is direct but falls within a narrow fan-type range.

Similarly, when the CEC (or the amount of exchangeable sodium ions) is plotted against the swelling pressure, a fan-type or band pattern is observed (see Figure 3). Conversely, there is a straight-line relationship between swelling pressure and activity index (see Figure 4), as shown by Seed and others (12). Although the formulation of the reaction potential is based on earlier experiences with C-horizon soils in Oklahoma (18), Figure 4 indicates that, for B-horizon soils, the reaction potential is inversely proportional to swelling pressure. An explanation of this inconsistency may lie in the fact that the C-horizon soils were predominantly montmorillonitic while the B-horizon soils studied

Table 1. Properties of B-horizon soils.

Property	Soil 1	Soil 2	Soil 3	Soil 4	Soil 5
Physical[a,b]					
Location (county)	Oklahoma	Kingfisher	Blaine	Kay	Pawnee
Soil series	Renfrow	Renfrow	Renfrow	Renfrow	Renfrow
Depth (cm)	25-91	25-127	30.5-117	15-152	30.5-178
Liquid limit (%)	51	56	52	60	51
Plastic limit (%)	18	18	18	19	17
Shrinkage limit (%)	8	9	10	11	10
Plasticity index (%)	33	38	34	41	34
Textural composition (%)					
Sand (2 - 0.074 mm)	2	2	4	16	11
Silt (0.074-0.002 mm)	47	46	46	40	48
Clay (<0.002 mm)	51	52	50	44	41
(<0.001 mm)	47	47	46	40	38
Specific gravity	2.75	2.73	2.72	2.72	2.71
Activity index	0.65	0.72	0.73	0.93	0.83
Free swell (%)	65	50	60	60	50
Dry density (kg/m^3)[c]	1630.8	1632.2	1601.8	1600.2	1750.8
Optimum moisture (%)	21.9	21.5	20.0	23.0	19.3
AASHTO soil classification	A-7-6(36)	A-7-6(41)	A-7-6(35)	A-7-6(36)	A-7-6(31)
Unified soil classification	CH	CH	CH	CH	CH
Physicochemical					
pH	9	8.6	8.7	8.9	8.5
Carbonates (as $CaCO_3$) (%)	0.620	0.432	1.124	2.330	0.796
Cation exchange capacity (meq/100 g)	26.36	20.54	31.04	28.97	25.39
Exchangeable cations (meq/100 g)					
Calcium	18.71	14.97	27.94	18.96	16.74
Magnesium	4.11	3.29	4.52	4.52	2.88
Potassium	0.25	0.13	0.25	0.25	0.13
Sodium	1.74	1.30	1.96	1.74	1.55

Note: 1 cm = 0.39 in; 1 kg/m^3 = 0.062 lb/ft^3.
[a] Determined by AASHTO 1974 test procedures and specifications.
[b] Results (except for specific gravity, activity, dry density, and optimum moisture content) reported to nearest whole number.
[c] Standard Proctor density [AASHTO T 99(A)] with soil-water mix seasoned approximately four hours.

Table 2. Index properties of raw and ultrasonically treated soils.

	Type of Clay Mineral (Percentage)			Total Reaction Potential (meq/100 g)				Clay (<0.002 mm)	
Soil	I	K	ML	I	K	ML	Sum	Percentage	Reaction Potential (meq/100 g)
1	16.6	2.4	81.0	4.1	0.2	56.7	61.0	51	31.1
2	21.8	5.2	73.0	5.4	0.5	51.1	57.0	52	29.6
3	15.4	7.6	77.0	3.8	0.8	53.9	58.5	50	29.2
4	12.8	5.1	82.1	3.2	0.5	57.5	61.2	44	26.9
5	6.4	6.5	87.1	1.6	0.6	61.0	63.2	41	25.9

Table 3. Clay mineral composition and reaction potential.

	Clay (<0.002 mm) (%)		Liquid Limit (%)		Plasticity Index (%)	
Soil	Raw	Treated	Raw	Treated	Raw	Treated
1	44	51	51	58	33	37
2	52	44	56	60	38	34
3	50	53	52	54	34	30
4	44	41	60	56	41	37
5	41	37	51	48	34	32

Note: 1 mm = 0.039 in.

contain only traces of mixed-layer illite-montmorillonite. Consequently, it will be erroneous to apply the conclusions formulated for the C-horizon soils to the B-horizon soils.

Moisture absorption by soil implies, to some degree, moisture accommodation within the soil mass. Therefore, the void-domain characteristics of the soil may be important in determining the amount of moisture absorbed and the accompanying swelling or swelling pressure experienced. This question was studied in the following way: Electron microscopy was used to measure the void space per unit surface area (see Figure 5), and the unconfined compressive strength of samples molded at optimum moisture and near maximum dry density [Harvard miniature compaction at a diameter of 33.2 mm (1.31 in) and a height of 71.5 mm (2.81 in)] was determined. As shown in Figure 6, the strength increased as the void cross-sectional area decreased, and swelling pressure increased as the void area increased. Admittedly, measurements on five soils may raise questions of statistical validity and, therefore, any quantified relationships inferred may be premature. The significance, however, lies in the trend established; namely, scanning electron microscopy can be used as a time-saving predictive tool to determine the swelling of these or similar soils.

CONCLUSIONS

For the five B-horizon Oklahoma soils studied, the following conclusions can be drawn:

1. Swelling pressures increase directly with moisture absorption, but the relationship has a fan-type scatter of points.
2. Swelling pressure is directly related to activity index.
3. The reaction potential, which is a good predictive tool for C-horizon soils, does not appear to apply in the case of B-horizon soils.
4. The void cross-sectional area, which can be determined by scanning electron microscopy, shows great potential as a predictive tool for determining swelling pressures; the higher the area, the higher the swelling pressure.

Table 4. Volume changes and swelling pressures of soils at maximum dry density and optimum moisture content conditions.

Soil	Compaction Characteristics		Determination of Volume Change				Determination of Swelling Pressure			
			Moisture Content (%)				Constant-Volume Method		Free-Swell Method	
	Optimum Moisture Content (%)	Maximum Dry Density (kg/m³)	Initial	Final	Water Intake (%)	Volume Change (%)	Initial Moisture (%)	Swelling Pressure (kPa)	Initial Moisture (%)	Swelling Pressure (%)
1	21.9	1630.8	22.1	22.4	2.3	1.94	21.9	67.37	22.9	89.24
2	21.5	1632.2	20.7	24.9	4.2	2.13	22.1	72.17	20.7	128.46
3	20.0	1601.8	20.7	26.8	6.1	3.18	20.3	77.27	20.7	125.52
4	23.0	1600.2	22.1	27.1	5.0	4.21	22.0	111.50	22.1	143.17
5	19.3	1750.8	18.8	21.1	2.3	3.95	19.0	95.81	18.8	171.61

Notes: 1 kg/m³ = 0.062 lb/ft³; 1 kPa = 0.145 lbf/in².

Figure 1. Relationship between volume change and time.

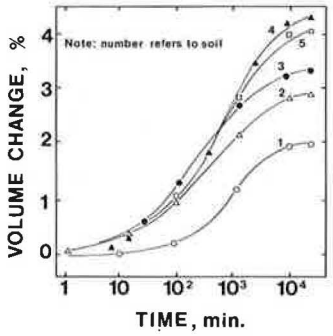

Figure 2. Relationship between moisture uptake and swelling pressure.

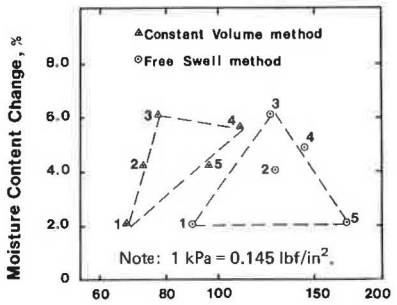

Figure 3. Effect of cations on swelling pressure.

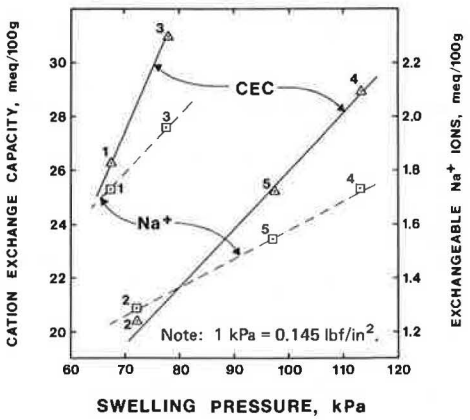

Figure 4. Effect of clay characteristics on swelling pressure.

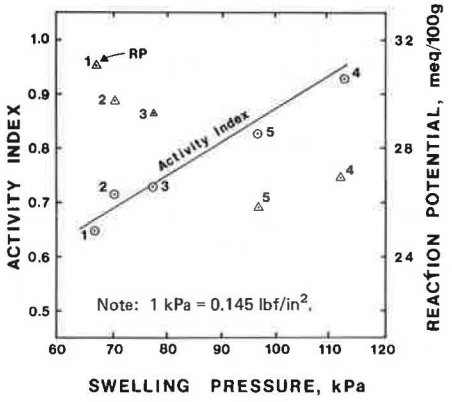

Figure 5. Schematic representation of void cross-sectional area in soil system.

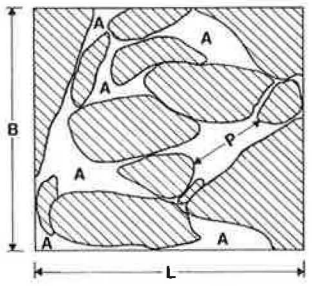

$B \times L = 6.7 \times 10^{-4}$ mm²

Void Cross-sectional Area, $V,\% = \left(\frac{\Sigma A}{B \times L}\right) \times 100$

P = Longest Pore Intercept, mm.

Note: 1 mm = 0.039 in.

Figure 6. Effect of void cross-sectional area on unconfined compressive strength and swelling pressure.

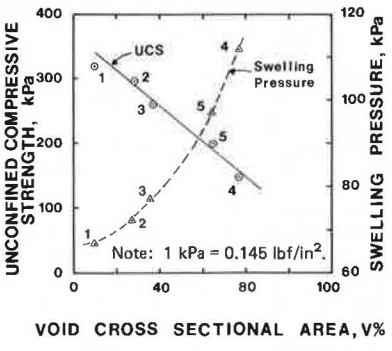

REFERENCES

1. G. Kassiff, M. Livneh, and G. Wiseman. Pavements on Expansive Clays. Academic Press, Jerusalem, Israel, 1969.
2. R. E. Means. Buildings on Expansive Clay. Colorado School of Mines Quarterly, Vol. 54, No. 4, 1959, pp. 1-31.
3. J. V. Parcher and R. E. Means. Soil Mechanics and Foundations. Charles E. Merrill Publishing Company, Columbus, Ohio, 1968, p. 573.
4. T. A. Haliburton. Final Report of the Subgrade Moisture Variations Research Project. School of Civil Engineering, Oklahoma State Univ., Stillwater, Aug. 1970.
5. T. W. Lambe. Compacted Clay: Structure. Trans., ASCE, 125, 1960, pp. 681-717.
6. T. W. Lambe. Compacted Clay: Engineering Behavior. Trans., ASCE, 125, 1960, pp. 718-756.
7. H. B. Seed and C. K. Chan. Compacted Clays: Structure and Strength Characteristics. Trans., ASCE, 126, 1961, pp. 1343-1425.
8. W. G. Holtz and H. J. Gibbs. Engineering Properties of Expansive Clays. Trans., ASCE, 121, 1956, pp. 641-663.
9. M. G. Spangler and R. L. Handy. Soil Engineering, 3rd ed. Intext Educational Publishers, New York, 1973, p. 748.
10. R. E. Grim. Clay Mineralogy, 2nd ed. McGraw-Hill, New York, 1968, p. 596.
11. C. C. Ladd. Mechanisms of Swelling by Compacted Clay. HRB, Bull. 245, 1959, pp. 10-26.
12. H. B. Seed, R. J. Woodard, and R. Lundgren. Prediction of Swelling Potential for Compacted Clays. Journal of the Soil Mechanics and Foundations Division, Proc., ASCE, Vol. 88, No. SM3, 1962, pp. 53-87.
13. J. K. Mitchell. Fundamentals of Soil Behavior. Wiley, New York, 1976, p. 422.
14. D. R. Snethen, F. C. Townsend, L. D. Johnson, and D. M. Patrick. Review of Engineering Experiences with Expansive Soils in Highway Subgrades. Federal Highway Administration, Interim Rept. FHWA RD-75-48, June 1975, p. 137. NTIS: PB 248 658/7ST.
15. G. J. Gromoko. Review of Expansive Soils. Journal of the Geotechnical Engineering Division, Proc., ASCE, Vol. 100, No. GT6, June 1974, pp. 667-694.
16. Proc., 3rd International Conference on Expansive Clay Soils, Haifa, Israel. Academic Press, Jerusalem, Aug. 1973.
17. J. G. Laguros. Predictability of Physical Changes of Clay Forming Materials in Oklahoma. Univ. of Oklahoma Research Institute, Norman, 1972.
18. J. G. Laguros, S. Kumar, and M. Annamalai. A Comparative Study of Simulated and Natural Weathering of Some Oklahoma Shales. Clays and Clay Minerals, Vol. 22, No. 1, Nov. 1974, pp. 111-115.
19. R. M. Hardy. Identification and Performance of Swelling Soil Types. Canadian Geotechnical Journal, Vol. 2, No. 2, May 1965, pp. 141-153.

Publication of this paper sponsored by Committee on Physicochemical Phenomena in Soils.

Soil Aggregates and Their Influence on Soil Compaction and Swelling

R. J. Hodek, Department of Civil Engineering, Michigan Technological University, Houghton
C. W. Lovell, Department of Civil Engineering, Purdue University, West Lafayette, Indiana

Prediction of the characteristics and properties of compacted fine-grained soils is much aided by a physical soil mechanism or model. This model should, as nearly as possible, fit the observed soil conditions during and after compaction. This paper describes an extension to existing soil compaction models and uses it to explain the behavior of kaolinite compacted in the laboratory by static pressures under conditions of no lateral strain. The experimental investigation included an examination of the kaolinite aggregations at the compaction moisture content but before compaction. This was followed by the determination of the relationship between the net energy input during compaction and the compacted unit weight. Finally, constant-volume swelling-pressure measurements were made on selected compacted samples. The swelling pressures were monitored continuously after giving the samples access to water; the results are presented as swelling pressure versus time relationships. The experimental results confirm the appropriateness of a deformable-aggregate soil model to explain the compaction of kaolinite as prepared in the laboratory and then compacted statically. The model is also appropriate for understanding the constant-volume swelling-pressure pattern that develops on wetting the compacted soil.

The objective of the research described in this paper was to develop a model and a mechanism that can adequately explain the achievement of compacted unit weight for kaolinite statically compacted in the laboratory. Such an explanation should be complete enough to explain the condition of the soil before compaction, the interactions within the soil mass during compaction, and the observed behavior of the compacted soil.

The model hypothesized was one in which the soil is made up of macroscopic aggregations of clay particles. During compaction, it is the interactions of these aggregates, their deformation characteristics, and their ability to fit together in a compact mass that determine the end result unit weight for a given type of compaction and amount of effort. It is this same compacted macrostructure—an assemblage of aggregates—that, to some extent, determines the engineering behavior of the compacted soil.

The experimental approach was to study certain of the properties of the soil aggregates before compaction, monitor the compaction effort, and then subject the

compacted samples to a test significant to engineering practice. The achievement of compaction was examined by calculating the energy required to densify the soil continuously from a low unit weight to the final unit weight achieved for each sample. The correctness of the model was determined by analysis of existing results, especially stress-strain and volumetric swelling, and from the results of constant-volume swelling-pressure determinations on the compacted samples. [The relevant literature is reviewed elsewhere (1).]

COMPACTION-MECHANISM HYPOTHESIS

This paper attempts to explain the compaction of fine-grained soils in terms of soil structure and changes in it. The explanation is based in part on the results of previous investigators, principally Lambe (2, 3) and Olson (4), and on tests on a single commercial clay (Edgar Plastic Kaolin) in a single compaction mode (static). The hypothesis states the necessity of recognizing (a) that there are a number of fabric levels and (b) that the stress history before compaction can strongly influence the compaction result. The postulated explanation for laboratory static compaction of kaolinite, from dry soil to the as-compacted state, is described below.

Initial Soil Structure

Before the addition of water to kaolinite, the layers of adsorbed water present on the particles are no more than a few molecules thick. In this state, many of the particles, each being many unit layers thick, are flocculated in face-to-face fashion due to Van der Waals' forces and, probably, hydrogen bonds (which had developed as the Van der Waals' forces brought the particles closer together). Each group of face-to-face particles can be thought of as a domain. Depending on the amount of hydrogen bonding, the adsorbed water will more likely be found on the domain surface rather than being uniformly distributed around each flocculated particle in the packet. Figure 1 presents an idealized representation of the effects of adding water to the soil. In Figure 1a, there are three air-dry domains. The relative spacing between the domains is quite variable and, for the mixing technique used in this research, is constantly changing, but the orientation and spacing of the particles within each domain is relatively constant. Each particle within a domain is many units thick (not shown), and these repeating units are permanently fixed with respect to each other in the particle.

The usual procedure is to add water to the air-dry soil, either in increments or continuously, while agitating or mixing so that the moisture is, in a gross sense, evenly distributed throughout the soil. This can be done manually or, as was done in this research, by using a mechanical blender.

As the soil domains come into contact with the water mist, external double layers begin to form and, depending on the degree of bonding within the domain, water is adsorbed between the face-to-face particles and a slight swelling of the domain may occur (see Figure 1b).

Figure 1c shows the condition as more water is added. The external double layers continue to develop, and the domains are held to one another in edge-to-face arrangement to form aggregates as they collide. This is principally due to Van der Waals' attraction and, to some extent, mutual desire for the water on the surfaces of the domains, because there is a large net water deficiency in the system. As the agitation continues, the flocculated groups of domains grow in size and decrease in number and, as the addition of water continues, the water will inevitably be unevenly distributed among the many aggregates and domains. Hence, domain-aggregate growth continues because the water-poor domains are held at the water-rich sites on the surfaces of the aggregates.

At some point during the mixing operation, the quantity of water on the surface of an aggregate may be large enough so that this water will exhibit, at least temporarily, bulk water properties. Collisions and contacts among aggregates in this state will cause the aggregates to fuse due to capillary pressures caused by the menisci developed near their points of contact; these fused aggregates will be called apparent aggregates.

By this process, the apparent aggregates continue to grow as the water content increases. However, because of the shear strains developed within these relatively large apparent aggregates as they collide with each other and the components of the mixture, they will in time lose their individual identity. Thus, the effect of the shear strains and their accompanying moisture redistribution is to cause a more-dispersed structure to occur within and among the domains.

This characterization of the soil fabric is similar to that described by Yong and Warkentin (5), who recognize the arrangement of clay particles as domains, the grouping of domains as clusters, and the arrangement of clusters in peds. Many more fabric features, primarily in naturally occurring soils, have been reported and are reviewed by Mitchell (6). However, the soil model used for this study appears to be the appropriate one for this laboratory-compacted soil.

Thus, at the end of the mixing operation, the soil batch consists of aggregates and apparent aggregates over a large size range, having a considerable range of water content and a water state that varies from almost bulk to tightly held in a thickness of only a few molecules. The water distribution within each aggregate (we will no longer differentiate between aggregates and apparent aggregates) is not at equilibrium and can be expected to change with time and the pore water pressure is negative, yet the degree of saturation of the aggregate is quite high.

Compaction Mechanism

It has been postulated that the preparation of a clay soil before compaction causes the appearance of macroscopic balls or aggregates whose intra-aggregate moisture content is at a pressure less than atmospheric but having a relatively high degree of saturation that is significantly higher than that of the uncompacted mass as a whole.

Compaction is accomplished by the reduction of the void space at a constant moisture content. That is, no water leaves the system. The increase in density is due to the reduction of air voids only.

During compaction, it is of secondary importance that the aggregates are made up of clay particles, because very little total aggregate-volume change will occur (the volume of air within the aggregates is small). Densification can occur by rearrangement of the aggregates into a denser packing even if they are individually rigid. However, at most compaction water contents, the aggregates act in a plastic manner and can deform under the compactive load to conform to the available interaggregate void space.

Schematically, this densification is illustrated in Figure 2. Figures 2a and 2b show the decrease in interaggregate void ratio (densification) that can occur with only translation and rotation. The aggregates have not changed shape or volume; they have merely been rearranged. Figure 2c shows the further de-

creases in interaggregate void space that can occur if the aggregates deform to flatten at points of contact and to conform to the shapes of available voids or if two of the aggregates experience unit-weight increases due to aggregate-volume decreases. Thus, volume a > volume b > volume c.

Laboratory compaction can be achieved by a number of different procedures—including impact, kneading, and static type loadings and partial to full coverage of the surface of the soil. The procedure used in this investigation was a nonimpact, rapid-rise-time, controlled-loading-rate type of loading with full coverage of the soil surface. At no time during compaction is the external compressive load released. It builds up rapidly to some preselected peak, is maintained at this value for a time considerably longer than that required to reach the peak, and is finally released to conclude the densification of the soil.

The densification proceeds at an ever decreasing rate from the outset of loading, due to (a) aggregate rearrangements not requiring deformation, (b) aggregate rearrangements initiated by slight yielding, (c) void-space filling as aggregates are deformed and literally flow into the necessary shape, and (d) the reduction of possible intra-aggregate air voids.

As the density increases, discrete aggregates become less and less apparent until finally they lose their individuality almost completely.

The microstructure or fabric of an individual aggregate also may change. If change does occur, it will be toward a more directional arrangement of particles, parallel to the plane of major stress increase, and be a result of intra-aggregate straining and surface smearing. Fabric reorientation increases as density increases and as the aggregate water content increases.

Figure 1. Domains and formation of aggregates: idealized representation.

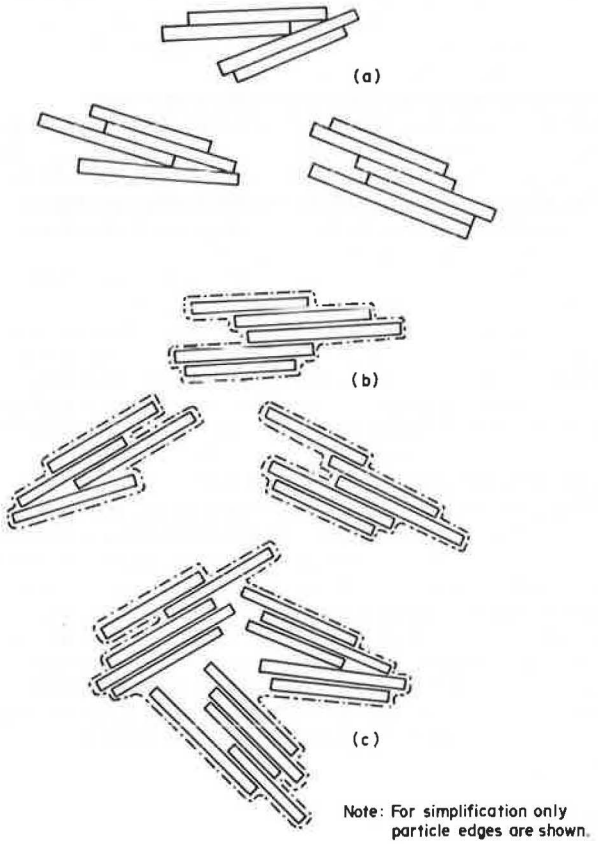

Figure 2. Aggregate compaction: idealized representation.

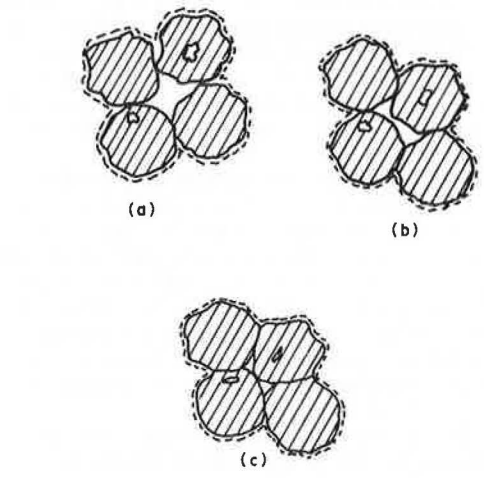

Note: The volumes are considered to be those areas bounded by the dashed lines

DESCRIPTION OF EXPERIMENTAL PROGRAM

Soil

The single raw material used for this study was a naturally occurring Florida kaolin mined commercially by the Edgar Plastic Kaolin Company and known as EPK Airfloated Kaolin.

The classification properties of this soil are given below:

Property	Value (%)
Liquid limit	58.5
Plastic limit	36.5
Specific gravity of solids	2.6
Clay fraction (< 0.002 mm)	81.0

Sample Compaction

The samples were compacted in a specially designed mold, and the effort was applied by an MTS servo-hydraulic tester. This combination, along with a Sanborn model 321 dual-channel carrier amplifier-recorder and a high-speed Brush model 16-2300 oscillograph, made it possible to monitor the sample densification in detail.

In the full-face-coverage compaction process (generally termed static), it is possible to control the rate of loading, monitor the axial deformation or compression, measure the input load, and measure the load transferred to the bottom of the mold by the sample, all as functions of time.

An extensive pilot study was made of the load-displacement characteristics of the machine-soil system. A comparison of the limitations of the system and the requirements of the research led to the following standard test procedure: a single application of a full-coverage compaction foot applied at a loading rate of 13.35 kN/s (3000 lbf/s) to a load of either 4.45 kN (1000 lbf) or 6.67 kN (1500 lbf) using effort as a variable. The maximum load of 4.45 or 6.67 kN was then maintained on the sample to allow further densification

Figure 3. Effect of moisture content on relationship between wet unit weight and energy: P6-R8 at 4:45-kN level.

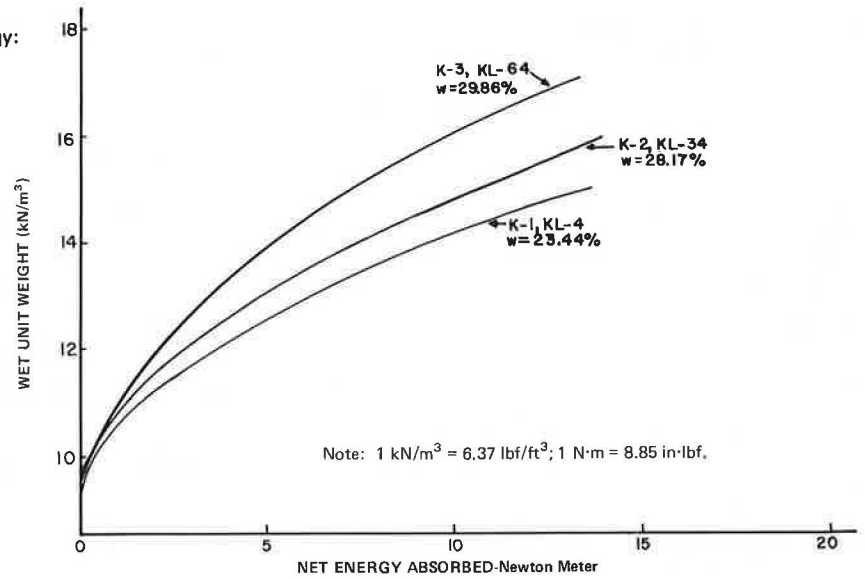

Figure 4. Results of swelling-pressure tests: K-1 at 4.45-kN level.

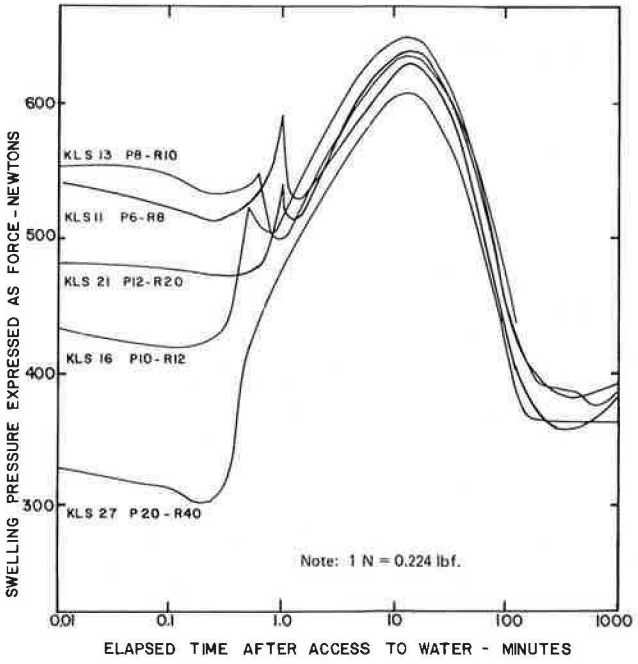

to occur for a period of 2 min.

The rapid rise time followed by the relatively long-term continuation at constant load made it possible to infer the aggregate-aggregate interaction. That there was no further compression (or increase in unit weight) of the sample after the initial load buildup indicates that there was an immediate rearrangement of the aggregates into a denser packing by aggregate movement, aggregate fracture, and elastic straining. Long-term compression, on the other hand, suggests plastic behavior of the aggregates.

Swelling-Pressure Measurements on Compacted Samples

As an aid to the determination of the macrostructure after compaction and its response to the forces generated by the addition of water, swelling pressure as a function of time was monitored for selected compacted samples. No gross volume change was permitted, and the temperature was held constant by making water available to the sample.

The apparatus used for these measurements consisted of a cell equipped with lower and upper bronze stones and an upper cap to eliminate vertical swelling, a Sanborn model 321 strip-chart recorder to monitor the vertical total stress by means of a Statham pressure transducer, and a constant temperature chamber (±0.2°C). Water was supplied to the cell from an inclined burette through a Tygon tube.

The cell was placed in the constant-temperature [29.5°C (84°F)] chamber and allowed to equilibrate. The pressure head of the water supply at the bottom stone was essentially constant and of small magnitude. The moisture movement through the soil was upward, which allowed the air to escape through the upper porous stone and perforated lucite spacer. The relationship between the constant-volume swelling pressure and time was recorded until an equilibrium pressure was reached (usually 24-48 h).

RESULTS

Some typical results are shown in Figures 3 and 4. The samples of soil batches are identified by the batch number and the aggregate-size sieve limits. For example, K-2, P8-R10 indicates batch number K-2 and aggregates that passed a 2.36-mm (no. 8) sieve and were retained on a 2.00-mm (no. 10) sieve. The moisture content of the batch increases with the batch number.

Achievement of Compacted Unit Weight

The relationship between load and deformation during the densification process was monitored for each compacted sample. This made it possible to define the relationship between the sample unit weight and the work applied to achieve that unit weight.

Figure 3 shows this relationship for the P6-R8 samples for the 4.45-kN load in terms of wet unit weight (w). The net energy absorbed was calculated by averaging the measured loads at the top and bottom of

the sample at the beginning and end of an increment of the test data, averaging the two averages, and multiplying by the net compression of the specimen during the increment. (The averaging of the loads at the top and bottom of the sample represents an attempt to take into account the side friction between the soil and the confining ring.)

In general, the results indicate that the relationship between unit weight and net energy absorbed by the soil during densification is a simple one; that is, it does not appear to be mathematically complex.

Swelling Pressure

Figure 4 shows the relationship between the swelling pressure and time; the results are expressed as a function of aggregate size, with the batch (compaction moisture content) and level of compactive effort as constants.

In general, for the samples compacted at the 4.45-kN level of effort, the maximum swelling pressure increases as the compaction water content increases. A general time versus pressure pattern is also evident. The pressure rapidly reaches a maximum value after the sample has been given access to water and there after decreases at a slower rate to some equilibrium value.

The time versus pressure pattern for the samples compacted at the 6.67-kN level showed the same general pattern. However, whereas at the 4.45-kN effort level, for each aggregate size, there was an increase in the maximum swelling pressure as the compaction moisture content increased, at the 6.67-kN effort level, all aggregate sizes, without exception, exhibited increases in their maximum swelling pressure from the low (K-1) to the intermediate (K-2) moisture content and decreases from the intermediate (K-2) to the high (K-3) moisture content.

DISCUSSION OF RESULTS

Achievement of Compacted Unit Weight

In the usual terminology, the samples were compacted at water contents dry of optimum for the static compaction involved. It is commonly known that increasing the compactive-effort input results in a higher unit weight at a constant moisture content and a lower optimum moisture content. That is, as the compactive effort increases, the curve of the moisture content versus unit weight relationship shifts upward and to the left. It is also known that, if the type of compaction and the compactor rating are held constant and only the number of blows per layer or of passes in the procedure are allowed to vary, a condition—a combination of compaction and soil variables—is reached beyond which no further densification occurs and no further net energy is transferred to the mass; i.e., the soil behaves elastically. However, a heavier roller in the field or a heavier hammer in the laboratory will cause the soil to accept additional net energy until a new plateau is reached.

This can be understood in terms of the second-order skeleton. The skeletal strength increases during densification until its shear strength is equal to the compaction shear stresses. If the compaction stresses are increased by a procedural change or a change in equipment rating, further densification will occur until a new equilibrium is reached between the skeletal shear strength and the imposed shear stress system. Beyond a certain combination of stress input and compaction moisture content (or aggregate strength), the skeleton structure is effectively destroyed.

For a given soil and type of compaction, the optimum moisture content is essentially dependent on the degree of saturation. For a given moisture content, the upper limit on the compacted unit weight is imposed by the compacted soil reaching a particular degree of saturation. As shown elsewhere (2), a marked decrease in air permeability occurs at this point, which indicates a rapid decrease in the interconnected or continuous air voids. The moisture content controls the intraggregate structure. The type of compaction and the aggregate size distribution control the degree of saturation at which the air voids become discontinuous. Once the air voids become discontinuous, very little further densification will occur, regardless of the input effort. This is shown by the fact that, as the moisture content is increased wet of optimum, a common water content versus unit weight relationship develops that is independent of input energy.

The curves relating the unit weight achieved (γ_m) to the net energy absorbed (E) (such as Figure 3) are mathematically uncomplicated and can be fitted by regression analysis to quadratic equations that adequately describe the experimental results. A few examples are shown below.

For K-1, P6-R8 at 6.67 kN:

$$\gamma_m = 10.162 + 0.57122E - 0.01378E^2 \quad (1)$$

For K-3, P12-R20 at 6.67 kN:

$$\gamma_m = 10.396 + 0.80701E - 0.02191E^2 \quad (2)$$

(where γ_m is expressed in kilonewtons per cubic meter).

Grouping the linear terms of these equations at constant moisture contents shows a definite correlation; as the aggregate size decreases, the coefficient of the linear term increases. Grouping these linear terms by aggregate size also shows a definite correlation; in general, as the moisture content increases, the coefficient of the linear term also increases.

Swelling Pressure Tests

The swelling pressure tests show two characteristics that do not appear to have been previously reported in the literature. The first is that the swelling pressure for most samples tested first increased and then decreased as a function of the elapsed time after initial access to water. The second is the temporary decrease of the swelling pressure after an elapsed time of one minute or less.

As shown by Hodek (1), both the short-term (temporary) and the long-term decrease of the swelling pressure can be explained with the aid of the compacted soil model used in this study.

According to Mitchell (6), collapse due to wetting at constant total stress requires an open, partly unstable, partly saturated fabric, a metastable structure for the particular state of stress, and sufficient strength for stability before wetting.

Although collapse is usually not associated with compacted cohesive soils, when these conditions are met, collapse at a constant boundary stress level or swelling-pressure behavior such as shown in Figure 4 at constant gross volume should be expected.

Before being given access to water, the soil skeleton is at equilibrium with the boundary restraint provided by the confining ring and the fixed end cap. On the introduction of additional water to the system, at least

three changes can occur. The aggregate skeleton may collapse due to local softening at the aggregate-aggregate contacts. Because the gross volume is fixed, this effect will be manifested as a rapid decrease in the measured swelling pressure. Also, as water becomes available, the aggregations may swell. If the soil skeleton can resist the increase in pressure due to this, there will be an increase in the boundary or confining pressure. Finally, as the moisture content of each aggregate increases due to swelling, its strength will decrease to allow plastic deformation of the soil skeleton into the previously empty skeletal voids. This effect occurring alone would result in a decrease in the measured swelling pressure.

Thus, the effects of water on this system are not additive. Because all three phenomena will occur simultaneously, the observed swelling pressure will be a reflection of the dominant mechanism occurring during some time increment. According to this explanation, the temporary decrease in the swelling pressure exhibited by most of the samples is caused by structural collapse, and the slow decrease from some peak value (as shown in Figure 4) is due to the dominance of plastic structural rearrangement over the swelling of individual aggregates.

SUMMARY AND CONCLUSIONS

In this study, a model or mechanism has been developed to explain the effects observed during the laboratory static compaction of kaolinite. The mechanism includes the influences of the precompaction soil preparation and conditioning as well as those of the soil interactions that occur during compaction.

Many of the swelling-pressure tests exhibited a temporary collapse or at least a decrease in the swelling pressure generated. This effect is also explained by the model. At the lower level of compaction, the maximum swelling pressure increased as the compaction moisture content increased. But at the higher compaction level, the maximum swelling pressure was largest at intermediate compaction moisture content. The final measured swelling pressures have the same type of relationship with the compactive load-moisture content combination.

ACKNOWLEDGMENT

The financial support of the Indiana State Highway Commission extended through the Joint Highway Research Project at Purdue University is much appreciated.

REFERENCES

1. R. J. Hodek. Mechanism for the Compaction and Response of Kaolinite. Purdue Univ., West Lafayette, IN, Ph. D. thesis, Dec. 1972, 269 pp.; Joint Highway Research Project, Rept. 36.
2. T. W. Lambe. Compacted Clay: Structure. Trans., ASCE, Vol. 125, 1960, pp. 682-717.
3. T. W. Lambe. Compacted Clay: Engineering Behavior. Trans., ASCE, Vol. 125, 1960, pp. 718-756.
4. R. E. Olson. Effective Stress Theory of Soil Compaction. Journal of the Soil Mechanics and Foundations Division, Proc., ASCE, Vol. 89, No. SM2, March 1963, pp. 27-45.
5. R. N. Yong and B. P. Warkentin. Soil Properties and Behavior. Elsevier, New York, 1975, pp. 77-86.
6. J. K. Mitchell. Fundamentals of Soil Behavior. Wiley, New York, 1976, 422 pp.

Publication of this paper sponsored by Committee on Compaction.

Evaluation of the Use of Indirect Tensile Test Results for Characterization of Asphalt-Emulsion-Treated Bases

Michael S. Mamlouk, Cairo University, Cairo, Egypt
Leonard E. Wood, Department of Civil Engineering, Purdue University, West Lafayette, Indiana

The results of a laboratory investigation of cold-mixed asphalt-emulsion-treated mixtures used for black bases are reported. The tensile properties for several mix variables and test temperatures were evaluated by the indirect tensile test. One type of asphalt emulsion and two types of aggregate were used. Two asphalt-emulsion contents and two initially added moisture contents were used. Specimens were cured at two curing conditions to represent early and long-term field curing. The relationships between load and horizontal deformation and between vertical and horizontal deformation were recorded during the test on X-Y recorders. The indirect tensile properties evaluated included indirect tensile strength, Poisson's ratio, indirect tensile stiffness, total strain at failure, and indirect tensile index. The indirect tensile index is represented by the secant modulus of the load versus horizontal deformation curve. Other parameters evaluated included compactability (unit weight after compaction), unit weight at time of testing, and percentages of retained moisture and voids at time of testing. The indirect tensile properties of the mixtures were very sensitive to the test temperature and were also affected by the other factors included in the study. In most cases, the interactions of the different factors had significant effects on the mixture properties. The indirect tensile index provided a high correlation with the asphalt-emulsion content, the type of aggregate, and the test temperature and proved to be a better mixture-characterization factor than the indirect tensile stiffness.

Emulsified-asphalt-treated mixtures are being widely accepted by engineers because of their many ecological-performance and economic advantages. Unlike asphalt cement, emulsified asphalt requires little or no heating

when mixed with aggregates, which significantly reduces energy demands and air pollution.

In recent years, emulsified asphalt bases have been used under both concrete and asphalt pavements. Emulsified asphalt provides cohesion to aggregates and minimizes segregation and blowing dust during placement. Either road-mix or plant-mix procedures can be used for preparation of emulsified asphalt mixtures.

The most critical disadvantage of asphalt-emulsion-treated materials is their relatively low strength at early ages and slow development of strength [which is limited by the rate of water loss in the mixture (1-3)]. In addition, the possibility of erosion and decrease in mixture strength, due to the presence of water in the system, before curing is completed can be important. A thorough understanding of the integral behavior of emulsified asphalt mixtures—including the effects of different components and at different curing stages and environmental conditions—does not exist at present.

The indirect tensile test was developed in 1953. In this test, cylindrical specimens are failed by applying compressive loads along a diametrical plane through two opposite loading heads. This type of loading produces a relatively uniform tensile stress that acts perpendicular to the applied load plane. The theory and stress patterns of the test have been described in previous studies (4-6). Maupin (7) has reported the following advantages of the indirect tensile test: (a) it is simple, (b) Marshall specimens may be used, (c) surface irregularities do not seriously affect the results, and (d) the coefficient of variation of the test results is low.

Several studies of asphalt concrete materials have used the indirect tensile test. A long-term project was performed at the University of Texas at Austin to evaluate the tensile properties of highway pavement materials (8, 9), and indirect tensile tests, as well as fatigue tests, have been conducted on asphalt concrete specimens by Maupin and Freeman (10), who found that the indirect tensile test can be used to predict the fatigue characteristics of bituminous concrete. However, black bases using asphalt-emulsion-treated mixes have not been studied as much as other mixture types and there is still need for a comprehensive characterization of asphalt emulsion mixtures.

In this study, the performance of emulsified-asphalt-treated mixtures at different mix variables and environmental conditions was evaluated by using the indirect tensile test. As the properties of asphalt emulsion mixtures are highly affected by curing, both early and long-term curing stages were investigated.

MATERIALS

Aggregate

Two types of aggregates were used in this study. The first was totally a mixture of sand and gravel consisting of approximately 50 percent each calcareous and siliceous pieces; 56 percent of the gravel particles retained on a 4.75-mm (no. 4) sieve had crushed faces. The second was totally crushed limestone. The aggregate gradation used followed the midspecification of the Indiana State Highway Commission 73B gradation band, which has a maximum size of 19 mm (¾ in). The aggregate gradation and properties are given below (1 mm = 0.039 in):

Sieve Size (mm)	Percentage Passing
19	100
9.52	67
4.76	47.5
2.38	38.5
1.19	29.5
0.59	21
0.295	15
0.148	9
0.074	2.5

Property	Sand and Gravel	Limestone
Apparent specific gravity	2.71	2.74
Bulk specific gravity (SSD)	2.61	2.70
Absorption (%)	1.20	1.28

Asphalt Emulsion

Indiana State Highway Commission designation AE-150 mixing-grade emulsified asphalt was used in this study. Its physical properties are given below [$t°C = (t°F - 32)/1.8$]:

Property	Value
Residue by distillation (%)	70.0
Penetration of residue after distillation (25°C, 5 s, 100 gm)	>200
Specific gravity at 25°C of residue after distillation	1.010

This type of asphalt emulsion is similar to HFMS-2S (ASTM D977).

DESIGN OF THE EXPERIMENT

Response Variables

Response variables that were measured to evaluate the performance of the mixture include the following:

1. Indirect tensile strength, which is the maximum load the specimen can resist;
2. Poisson's ratio, as determined from the relationship between the vertical and the horizontal deformations of the specimen during the loading operation;
3. Indirect tensile stiffness, as determined from the relationship between the applied load and the horizontal deformation of the specimen;
4. Total tensile strain at failure, as determined from the total horizontal deformation at failure, where failure is defined to occur at maximum load;
5. Indirect tensile index, as represented by the slope of the line between the origin and the point corresponding to 50 percent of the maximum load on the load versus horizontal deformation curve—this new parameter is a measure of the relationship between load increments and the resulting horizontal deformation and may, in addition to other conventional design parameters, provide a good characterization and design concept for asphalt emulsion mixtures;
6. Compactibility, which is the unit weight of the specimen immediately following compaction and is determined from the specimen weight and height just after compaction;
7. Wet and dry unit weights at time of testing, where wet unit weight refers to the density of the specimen including the moisture portion and dry unit weight is determined by excluding the moisture portion in the specimen;
8. Percentage of moisture retained in the specimen at time of testing, as a percentage by weight of the dry aggregate; and
9. Percentage of voids at time of testing, which in-

cludes (a) percentage of air voids and (b) percentage of total voids, i.e., the sum of the air voids and the voids filled with moisture (where both are calculated on a basis of the apparent specific gravity of the aggregate and assuming no asphalt is absorbed into the aggregate).

Figure 1. View of indirect tensile test assembly.

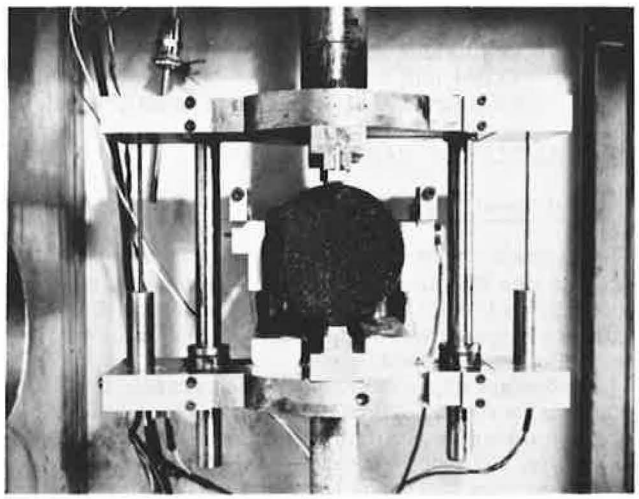

Figure 2. Relationship between load and horizontal deformation.

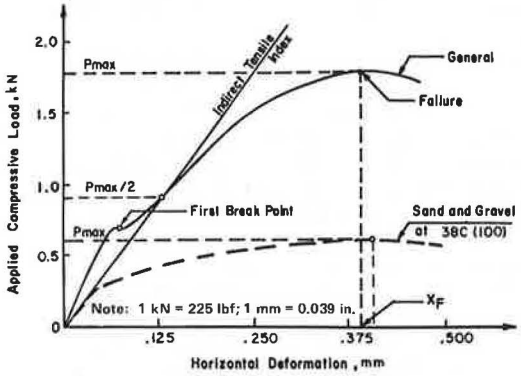

Figure 3. Relationship between vertical and horizontal deformations.

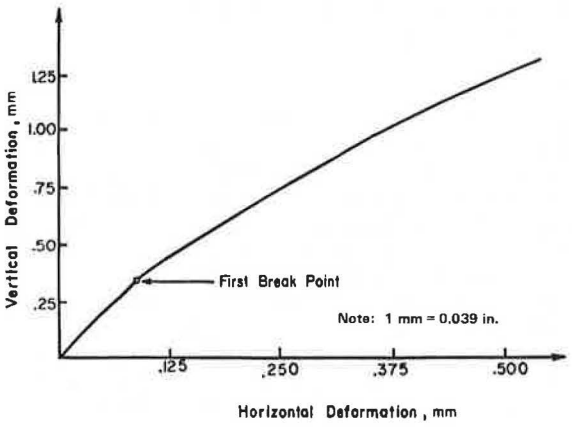

Independent Variables

The independent variables included the following:

1. Type of aggregate—sand and gravel versus crushed limestone;
2. Asphalt emulsion content—expressed as the percentage (3.25 versus 4) of asphalt emulsion residue (AER) in the mixture, based on dry weight of aggregate;
3. Initially added moisture (IAM)—expressed as percentage (3 and 4.5) of dry weight of aggregate;
4. Curing conditions—1-day air-dry versus 3-day oven-dry at 49°C (120°F) to represent early versus long term (3); and
5. Test temperature—10°C (50°F) versus 24°C (75°F) versus 38°C (100°F).

Three replicates of each combination were tested. One replicate for all combinations was performed first, then the second replicate was performed, and then the third. This method of design allows tests of all factors and interactions despite the restrictions on randomization (11).

EXPERIMENTAL PROCEDURE

Specimen Preparation

Specimens 102 mm (4 in) in diameter and 64 mm (2.5 in) in height were prepared according to the mix procedure suggested by Gadallah (3). They were compacted in a model 4C gyratory compaction machine manufactured by Engineering Developments Co., Inc., Vicksburg, Mississippi, by using a fixed roller. Twenty revolutions of the gyratory machine and 1380 kPa (200 lbf/in^2) vertical pressure were used. This compaction effort gave a specimen density almost identical to that given by applying 50 blows on each side of the specimen with the Marshall hammer. Immediately after compaction, specimen height was determined according to ASTM D3387. Specimen weight was determined while it was still in the mold to avoid damage.

After curing, the specimen height was measured again. The wet unit weight was determined according to ASTM D1188 by dusting the surface with zinc stearate rather than by coating the specimen with wax (2). Zinc stearate is easy to use and, at the same time, does not affect the moisture content of the specimen, especially when the specimen surface is smooth.

Experimental Arrangement

An MTS electrohydraulic closed-loop testing machine was used for the indirect tensile test. The machine had a temperature control chamber in which the specimens were placed for 2-4 hours after curing to reach the required test temperature. During this period, the specimens were placed in sealed plastic bags to prevent moisture loss.

The specimens were loaded by using two 12.7-mm (0.5-in) wide, curved stainless steel loading strips (see Figure 1). Load was applied at a constant rate of 51 mm/min (2 in/min). Two guide rods were used to prevent any eccentricity in loading. Vertical deformation was measured by using two identical linear variable differential transformers (LVDTs) fixed at equal distances from the specimen on both sides. Horizontal deformation was measured by an LVDT attached to a special device consisting of two arms touching the specimen across the horizontal diameter. The load was measured by a load cell connected to the

Figure 4. Indirect tensile strength as a function of type of aggregate, curing conditions, and test temperature.

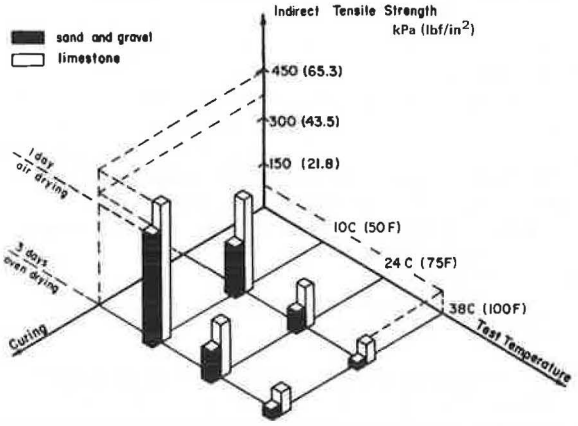

MTS machine. The outputs of the LVDTs and the load cell were calibrated and connected to two X-Y recorders. The X-Y recorders were adjusted to plot load versus horizontal deformation and vertical versus horizontal deformation (see Figures 2 and 3).

After the test was completed, the specimens were broken apart and dried in a forced-draft oven for 24 h at 110°C (230°F) and then weighed. The dry unit weight was calculated by dividing the dry weight of the crushed specimen by the difference between the specimen weights in air and in water.

ANALYSIS OF RESULTS

The general shape of the load versus horizontal deformation curve is as shown in Figure 2. At a certain load—the so-called first break point (9)—there is an increase in horizontal deformation without increase in load. For those specimens tested at 10°C, the first break load was much lower than the maximum load while, at 38°C, the first break load was closer to the maximum load. For the sand and gravel specimens at 38°C, the first break point was not clear.

The general shape of the vertical deformation versus horizontal deformation curve is as shown in Figure 3. The curve is fairly close to a straight line. At a point corresponding to the first break in the load versus horizontal deformation curve, the slope of the line is slightly changed. However, in some cases the vertical deformation versus horizontal deformation is a continuous curve.

The equations used to determine the indirect tensile parameters are given below:

$$\sigma_{IT} = 0.156\,(P_{max}/h) \quad (1)$$

$$\nu = (0.0673DR - 0.8954)/(-0.2494DR - 0.0156) \quad (2)$$

$$E_{IT} = (P/X)\,(1/h)\,(0.9976\nu + 0.2692) \quad (3)$$

$$\epsilon_T = X_T\,(0.1185\nu + 0.03896)/(0.2494\nu + 0.0673) \quad (4)$$

[these equations are valid for English units only and are restricted to 102-mm diameter specimens and a loading-strip width of 12.7 mm (9, 10)]

where

σ_{IT} = indirect tensile strength (lbf/in²);
P_{max} = maximum load at failure (lbf);
h = specimen height (in);
ν = Poisson's ratio;
DR = deformation ratio, i.e., the slope of the least-squares line of best fit between the vertical deformation and the corresponding horizontal deformation up to the first break point (for those cases where there is no first break point, the first portion of the curve is used);
E_{IT} = indirect tensile stiffness (lbf/in²);
P/X = the secant modulus at 50 percent of the first break point on the load versus horizontal deformation curve;
ϵ_T = total tensile strain at failure (in/in) [the length over which strain is estimated = 0.1 mm (0.004 in)]; and
X_T = total horizontal deformation at failure (in).

EVALUATION OF PARAMETERS

Indirect Tensile Strength

The indirect tensile strength varied between 25 and 596 kPa (3.6 and 86.4 lbf/in²). This wide range of the indirect tensile strength is due to the significant effects of type of aggregate, curing conditions, test temperature, and IAM.

In contrast to the smooth sand and gravel, the limestone had a rough surface and angular shape that increased the aggregate interparticle friction and, consequently, the tensile strength of the mixture.

Curing also increases the tensile strength of the mixture. As shown in Figure 4, the indirect tensile strength after three days of oven curing is always greater than the indirect tensile strength after one day of air-dry curing. This is due to the fact that curing breaks the asphalt emulsion, which allows water to evaporate and leaves the asphalt residue adhering to the aggregate particles.

Test temperature proved to be a major factor in determining the tensile strength of the mixture. Increasing the test temperature softens the asphalt emulsion residue and weakens the mixture.

To some extent, increasing the percentage of IAM makes the asphalt emulsion more effective in coating the aggregate particles. However, in most combinations the effect on the indirect tensile strength was greater with 3 percent IAM than with 4.5. Thus, the effect of IAM depends on its interaction with other factors.

The effects of interactions of aggregate type, curing conditions, and test temperature on the indirect tensile strength are summarized in Figure 4. The highest value of the indirect tensile strength found was that for the combination of limestone, a test temperature of 10°C, and 3-day oven curing. The lowest value was that for the combination of sand and gravel, a test temperature of 38°C, and 1-day air curing.

Poisson's Ratio

The majority of the values of Poisson's ratio found were between 0.2 and 0.45. Poisson's ratio was very sensitive to test temperature; at the higher temperatures, the Poisson's ratio values were higher. At the 10°C test temperature, a small number of the values of Poisson's ratio were negative, although most of the values found at 38°C exceeded 0.5. Thus, the asphalt emulsion mixture does not wholly meet the assumptions in the original derivation of the equations (8), and Poisson's ratio should not be determined by using the indirect tensile test, especially at high temperatures. In the remainder of this analysis, Poisson's ratio was

Figure 5. Indirect stiffness as a function of asphalt emulsion content, test temperature, and type of aggregate.

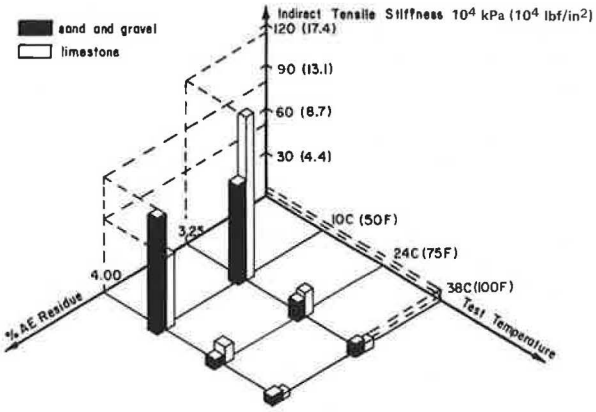

Figure 6. Total tensile strain at failure as a function of curing conditions, asphalt emulsion content, and test temperature.

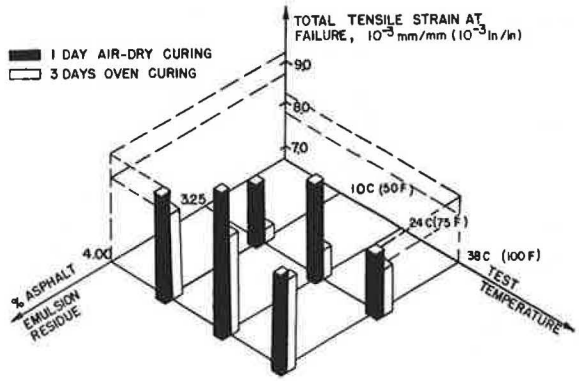

assumed to be 0.3, 0.35, and 0.4 at test temperatures of 10°C, 24°C, and 38°C, respectively.

Curing conditions had a significant effect on the values of Poisson's ratio found. Specimens air dried for 1 day were tender and, consequently, had high values of Poisson's ratio while those oven dried for 3 days had low values. Other factors did not significantly affect the values of Poisson's ratio found.

Indirect Tensile Stiffness

The indirect tensile stiffness values determined by using the experimentally found values of Poisson's ratio varied between 2.4×10^4 and 206.8×10^4 kPa (0.35×10^4 and 30×10^4 lbf/in^2). However, the stiffness values determined by using the assumed values of Poisson's ratio (i.e., 0.3, 0.35, and 0.4 at test temperatures of 10°C, 24°C, and 38°C, respectively) varied between 1.7×10^4 and 248.2×10^4 kPa (0.24×10^4 and 36×10^4 lbf/in^2).

The stiffness values found by using the assumed values of Poisson's ratio were greatly affected by temperature. As the test temperature increased, the stiffness decreased to a very small value. Stiffness was also affected by the interactions of test temperature, asphalt emulsion content, and type of aggregate. As shown in Figure 5, no trend could be found for the effects of asphalt emulsion content of type of aggregate. At some combinations, the sand and gravel mixtures had higher stiffness values than did the limestone mixtures, while at other combinations, the opposite was

Figure 7. Indirect tensile index as a function of asphalt emulsion content, test temperature, and type of aggregate.

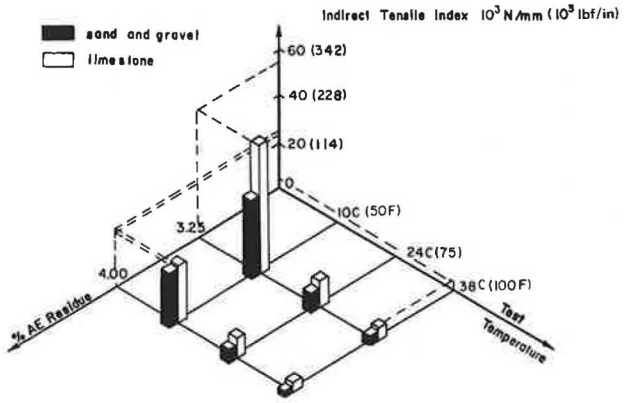

Figure 8. Effect of asphalt emulsion content, type of aggregate, and added moisture on unit weight at time of compaction.

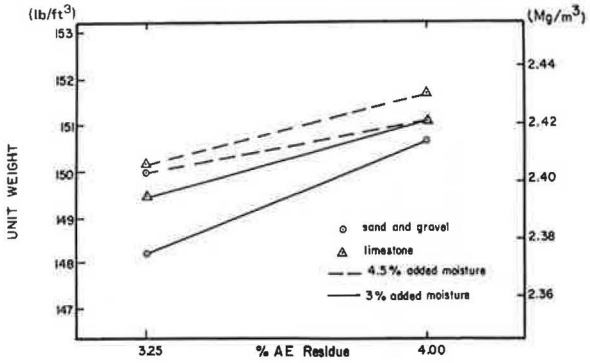

Figure 9. Effect of asphalt emulsion content, type of aggregate, and curing conditions on wet unit weight at time of testing.

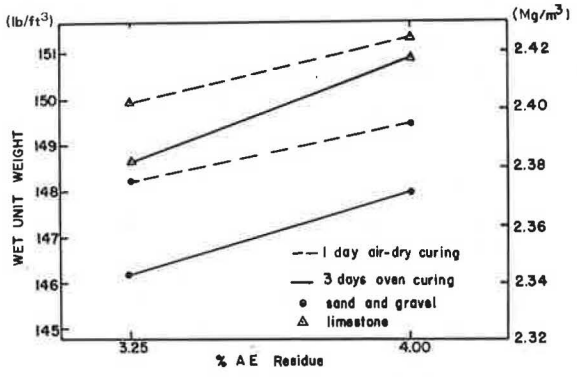

true. The significant effect of type of aggregate was apparent at a test temperature of 10°C.

The highest stiffness value was that found for the combination of limestone, 3.25 percent AER, and a test temperature of 10°C.

Total Tensile Strain at Failure

The total tensile strain at failure varied between 7.4×10^{-3} and 9.6×10^{-3} mm/mm (in/in) (calculated by using the assumed values of Poisson's ratio).

Figure 6 shows the effect of the asphalt emulsion content on the total tensile strain at failure. Asphalt emulsion acts as a lubricant between the aggregate

Figure 10. Effect of asphalt emulsion content, type of aggregate, and curing conditions on moisture retained at time of testing.

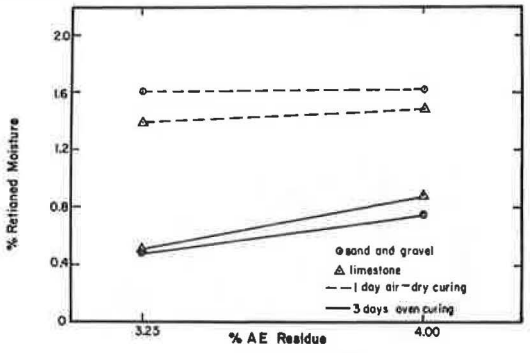

Figure 11. Percentage of air voids at time of testing as a function of curing conditions, added moisture, and type of aggregate.

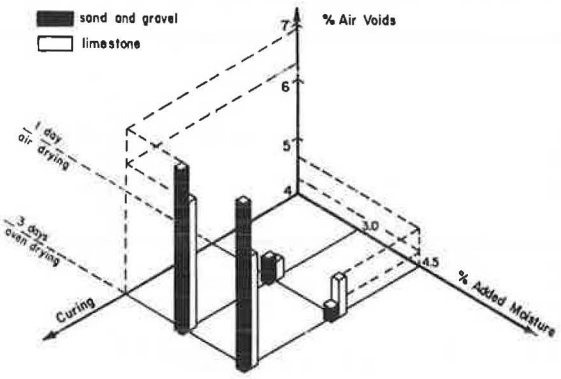

particles and, thus, the tensile strain at failure was higher at higher asphalt emulsion contents. The tensile strain at failure was also affected by curing, which increases the rigidity of the mixture and so decreases the total tensile strain at failure. The largest value of tensile strain was that found at the intermediate test temperature (i.e., 24°C).

Indirect Tensile Index

The indirect tensile index (Figure 2) varied between 0.8 and 119 kN/mm (4.5×10^3 and 680×10^3 lbf/in). The value was very sensitive to test temperature; as the test temperature increased, the value decreased significantly. In addition to test temperature, type of aggregate and asphalt emulsion content also affected the indirect tensile index. Limestone mixtures always had higher indices than did sand and gravel mixtures, and 3.25 percent AER mixtures had higher indices than did 4 percent AER mixtures (see Figure 7).

The indirect tensile index values provided a good correlation with the test temperature, the aggregate type, and the asphalt emulsion content but were independent of Poisson's ratio. This leads to the conclusion that the use of the indirect tensile index in conjunction with other parameters (such as indirect tensile strength) can provide a good characterization of an asphalt-emulsion-treated mixture.

Unit Weight at Time of Compaction

The unit weight at the time of compaction (which can be used as a measure of compactibility) varied between 2.36 and 2.44 Mg/m^3 (147.3 and 152.3 lb/ft^3). Both asphalt emulsion content and IAM affected the compactibility of the mixture. Increasing either (or both) increases the lubrication between the aggregate particles. This allows the aggregate particles to move smoothly during compaction to fill the air voids (which increases the unit weight of the mixture) and, at the same time, both asphalt emulsion and moisture fill the air voids between the aggregate particles.

The interaction of asphalt emulsion content, IAM, and type of aggregate had a significant effect on compactibility (Figure 8). The highest value found was that for the combination of limestone (because of its angular particles), 4 percent AER, and 4.5 percent IAM.

Unit Weight at Time of Testing

The wet unit weight was affected by the asphalt emulsion content, curing conditions, and type of aggregate (Figure 9). Increasing the asphalt emulsion content helps to fill the air voids in the mixture and also lubricates the mixture, which allows more compaction and increases the wet unit weight. However, increased curing allows moisture to leave the mixture and decreases the wet unit weight. Limestone, because of its angular shape, allows fewer voids in the mixture, which increases the wet unit weight.

The dry unit weight was affected only by asphalt emulsion content and type of aggregate. It was not affected by curing conditions, as expected, because, regardless of the amount of moisture that leaves the specimen during curing, the oven-dried weight and the dry unit weight of the specimen will remain the same. The effects of asphalt emulsion content and type of aggregate followed the same pattern as the case of the wet unit weight.

Percentage of Moisture Retained at Time of Testing

The percentage of moisture retained at the time of testing varied between 0.26 and 2.15 of the dry weight of aggregate. It was affected mainly by curing conditions but also by asphalt emulsion content.

As shown in Figure 10, the oven-cured specimens retained much less moisture than the air-dried specimens, and the 4 percent AER specimens retained more moisture than the 3.25 percent AER specimens. Thus the highest percentages of retained moisture were those found for the combination of 4 percent AER and air-dry curing.

Percentage of Voids at Time of Testing

The percentage of air voids at time of testing was markedly affected by asphalt emulsion content and curing conditions. The value decreased as the asphalt emulsion content increased because the asphalt emulsion can replace the air voids and thus allow greater densification. The effect of curing is to increase the percentage of air voids because curing allows water to leave the mixture.

The interaction of curing, IAM, and aggregate type was found to be significant, as shown in Figure 11.

The percentage of total voids at time of testing (including voids filled with moisture) was not affected by curing because, while curing allows water to leave the mixture, the total voids remain the same. Thus, the total voids are affected only by asphalt emulsion content.

SUMMARY AND CONCLUSIONS

Asphalt-emulsion-treated mixtures were evaluated by using the indirect tensile test. Different design parameters were evaluated at several mix variables and temperatures. Two types of aggregate, two asphalt emulsion contents, two values of initially added moisture, and two curing conditions were investigated. One type of asphalt emulsion and grade was used. The test was performed at three different temperatures. The important findings of the study are as follows:

1. Test temperature was the most important factor that affected the indirect tensile properties of the mixtures. High test temperatures increased the values of Poisson's ratio and decreased the indirect tensile strength, stiffness, and index. Test temperature also affected the total tensile strain at failure.
2. Limestone mixtures had higher indirect tensile strengths and indices than did sand and gravel mixtures. Aggregate type had a significant effect on the indirect tensile stiffness, especially at low temperature. In addition, limestone mixtures had higher unit weights and lower percentages of air voids than did sand and gravel mixtures.
3. In most cases, increasing the asphalt emulsion content decreased the indirect tensile stiffness and index and both air voids and total voids at time of testing and increased the total tensile strain at failure, compactibility, unit weight, and moisture retained at time of testing.
4. The curing conditions affected the characteristics of the specimens markedly. Oven curing increased the indirect tensile strength and the air voids and decreased the Poisson's ratio values, the total strain at failure, the wet unit weight, and the moisture retained at time of testing.
5. Increasing the initially added moisture from 3 to 4.5 percent of the dry weight of aggregate decreased the indirect tensile strength and increased the compactibility of the specimens.

Based on the results of the overall study, the following recommendations should be noted:

1. The indirect tensile test is a simple and suitable method for characterizing asphalt-emulsion-treated mixtures.
2. The indirect tensile index proved to have a good correlation with asphalt emulsion content, type of aggregate, and test temperature. The use of this index, together with other indirect tensile parameters, should provide a good characterization of an asphalt emulsion mixture.
3. It should be remembered that these results are based on the use of one emulsion system (which has rates of cure, water loss, and strength and stiffness development and electrochemical properties that are inherent to that one emulsion type and grade and are not necessarily the same for other emulsion types).

ACKNOWLEDGMENT

The contents of this report reflect our views; we are responsible for the facts and the accuracy of the data presented herein.

REFERENCES

1. Bitumen Emulsified Asphalt Base. Treatment Methods Manual 1967. Chevron Asphalt Company, San Francisco, CA.
2. L. D. Coyn. Emulsion Stabilization Mix Design. Chevron Asphalt Company, San Francisco, CA, Tech. Paper 172, Jan. 1976.
3. A. A. Gadallah, L. E. Wood, and E. J. Yoder. A Suggested Method for the Preparation and Testing of Asphalt Emulsion Treated Mixtures Using Marshall Equipment. Proc., AAPT, Vol. 46, 1977, pp. 196-227.
4. M. M. Frocht. Stresses in Circular Disks. In Photoelasticity: Volume 2, Wiley, New York, 1948, pp. 118-133.
5. G. Hondros. The Evaluation of Poisson's Ratio and Modulus of Materials of a Low Tensile Resistance by the Indirect Tensile Test. Australian Journal of Applied Science, Vol. 10, No. 3, Sept. 1959, pp. 243-268.
6. S. Timoshenko and J. N. Goodier. Stresses in a Circular Disk. In Theory of Elasticity (2nd ed.), McGraw-Hill, New York, 1951, pp. 107-111.
7. G. W. Maupin, Jr. Results of Indirect Tensile Tests Related to Asphalt Fatigue. HRB, Highway Research Record 404, 1972, pp. 1-7.
8. W. O. Hadley, W. R. Hudson, and T. W. Kennedy. A Method of Estimating Tensile Properties of Materials Tested in Indirect Tension. Center for Highway Research, Univ. of Texas at Austin, Res. Rept. 98-7, July 1970.
9. W. O. Hadley, W. R. Hudson, and T. W. Kennedy. Evaluation and Prediction of Tensile Properties of Asphalt Treated Materials. Center for Highway Research, Univ. of Texas at Austin, Res. Rept. 98-9, May 1971.
10. G. W. Maupin, Jr., and J. R. Freeman, Jr. Simple Procedure for Fatigue Characterization of Bituminous Concrete. Federal Highway Administration, Rept. FHWA-RD-76-102, June 1976. NTIS: PB 268 701/AS.
11. V. L. Anderson and R. A. McLean. Design of Experiments: A Realistic Approach. Marcel Dekker, Inc., New York, 1974.

Publication of this paper sponsored by Committee on Soil-Bituminous Stabilization.

Abridgment

Sulfur-Asphalt Mixtures as Soil Stabilizers

Nagih M. El-Rawi and Husham I. Al-Saleem, College of Engineering, University of Baghdad

In recent years, there have been several investigations of methods for reducing the amount of asphalt in bituminous mixtures by the substitution of sulfur for part of the asphalt. The use of sulfur in sand-asphalt pavements appears to be potentially valuable (1). Shell Canada, Ltd., has developed a material known as Thermopave, in which elemental sulfur is used in hot asphalt mixes (2), and sand-sulfur-asphalt mixtures made with inexpensive, poorly graded sands are reported to perform as well as or better than conventional asphalt cements made with dense-graded aggregates (3). Sulfur can be effectively used as a binder and reduce the asphalt content by 30 percent by weight (4). The addition of sulfur seems to result in lower viscosity, improved workability, and a wider permissible range of mixing and placing temperatures (4). Flexible pavements made with poorly graded beach sand and sulfur-asphalt mixtures can have properties superior to those of pavements made with dense-graded sands (5). Compared with asphalt concrete, thinner pavements are permitted for sulfur-asphalt-sand mixtures having a sulfur content of 13.5 percent by weight of the asphalt (5). The addition of sulfur to produce sulfur-bitumen emulsions tends to result in decreased viscosity, increased specific weight, and lower temperature sensitivity of the emulsion (6). There is a good possibility that river sands, dune sands, silty soils, and some types of clayey soils could be stabilized by using bituminous materials (7).

This paper reports the results of an investigation of the prospects of using sulfur-asphalt mixtures to stabilize typical Iraqi soils with locally available types of asphalts.

MATERIALS

The properties of the materials used are given below.

Soils: The gradations and properties of the four Iraqi soils used in this investigation are shown in Figure 1.

Asphalts: Two types of asphalt were used: a grade 85-100 asphalt cement and a grade MC-30 cutback asphalt, both produced at the Dora refinery in Baghdad.

Sulfur: The sulfur used was a natural sulfur of 99.9 percent purity by weight from Mishraq, Iraq.

SPECIMEN PREPARATION AND TESTS

The binder materials made with asphalt cement were prepared by separately heating the asphalt and the correct amount of sulfur to the required temperature and then mixing them thoroughly. Temperatures used were 130°C, 150°C, and 170°C (266°F, 302°F, and 338°F). Those made with cutback asphalt were prepared by heating the cutback in a closed container to 130°C and then adding the sulfur, also heated to 130°C, and mixing thoroughly. Both types of materials were allowed to cool to room temperature.

Hot mixtures: The mixtures made with soils 1 and 2 were prepared by separately heating the soil and the binder to the required temperature and then mixing them thoroughly. Each mixture was compacted by 25 standard hammer blows and static compaction at 26.7 kN (6000 lbf) for 2 min at a loading rate of 2.54 cm/min (1 in/min) to give specimens 5.1 cm (2 in) in diameter by 5.1 cm in height (ASTM D 915).

Cold mixtures: To prepare the mixtures made with soils 3 and 4, water was added to the soil and mixed in by using a mechanical mixer and then the amount of asphalt or cold asphalt-sulfur binder required to bring the fluid content to the optimum water content for modified Hubbard field compaction was added. The materials were mixed again and compacted according to the modified Hubbard field method to produce the specimens.

Curing conditions: The compacted specimens were cured in an aerated room for the required period of time.

Compressive strength tests: The compressive strengths of the specimens were determined by using a strain-controlled compression machine. The rate of loading was 0.15 cm/min (0.06 in/min). The samples were stored in a temperature-controlled oven for 2 h at the required test temperature before testing. The results reported are the average value of triplicate tests.

RESULTS

Soils 1 and 2

The amount of sulfur asphalt used was that equivalent to the amount of asphalt that produced the maximum compressive strength, i.e., 6 and 8 percent by weight for soils 1 and 2, respectively. The following results (8) were observed (see Figures 2 and 3):

1. For the binders mixed at 130°C, the addition of sulfur decreased the strength of both soils. This reduction in strength appears to be due to the reduction in net asphalt content; the strength of a sulfur-asphalt specimen was equal to that of an asphalt-only specimen having the same net asphalt content (8). Thus, at this temperature, sulfur seems to act as mineral filler.
2. For a given sulfur content, the strengths of the specimens prepared at higher mixing temperatures were higher.
3. At a mixing temperature of 170°C, where sulfur becomes very reactive, the addition of it markedly increases the strength of soil-asphalt specimens. The maximum strength was that for specimens prepared by substitution of 10 percent by weight of the asphalt cement by sulfur.
4. At a mixing temperature of 170°C, the evolution of H_2S and SO_3 gases, due to the chemical processes of dehydrogenation and polymerization, could become a major problem in the field.
5. The addition of sulfur slightly improved the temperature susceptibility of the mixture. This was particularly true at higher mixing temperatures as indicated by the slope of the strength versus temperature lines shown in Figure 3.
6. The addition of sulfur made the mixtures easier to compact and to work with (i.e., the workability of the mixture was improved).

Soils 3 and 4

For these two soils, substitution of part of the cutback asphalt by sulfur was useful. The following results were observed (Figures 2 and 3):

1. As the amount of sulfur substituted for asphalt

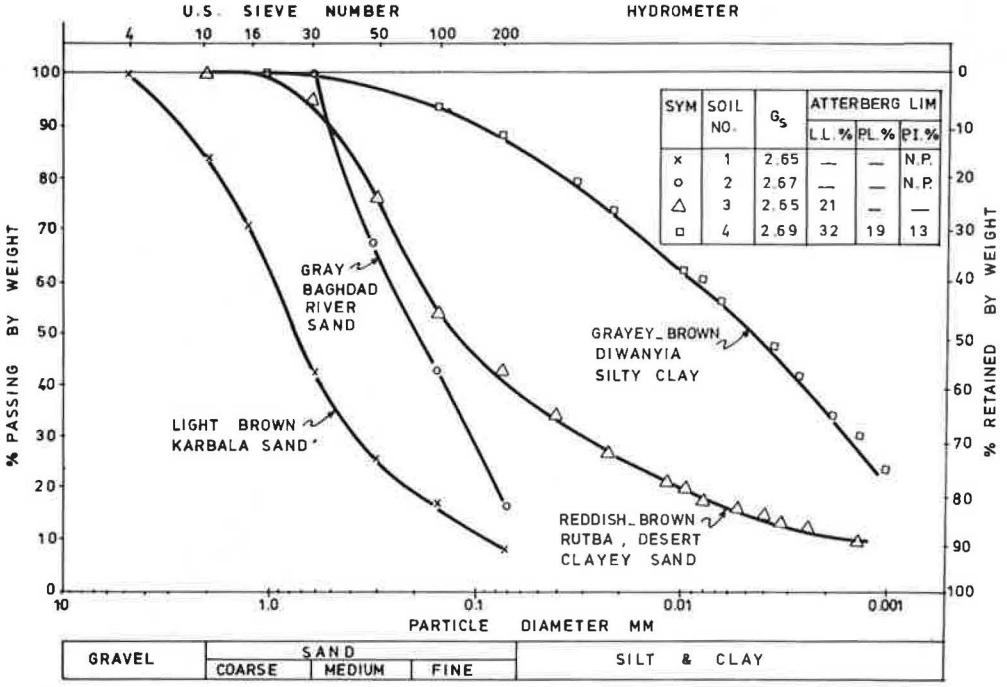

Figure 1. Gradations and properties of soils used.

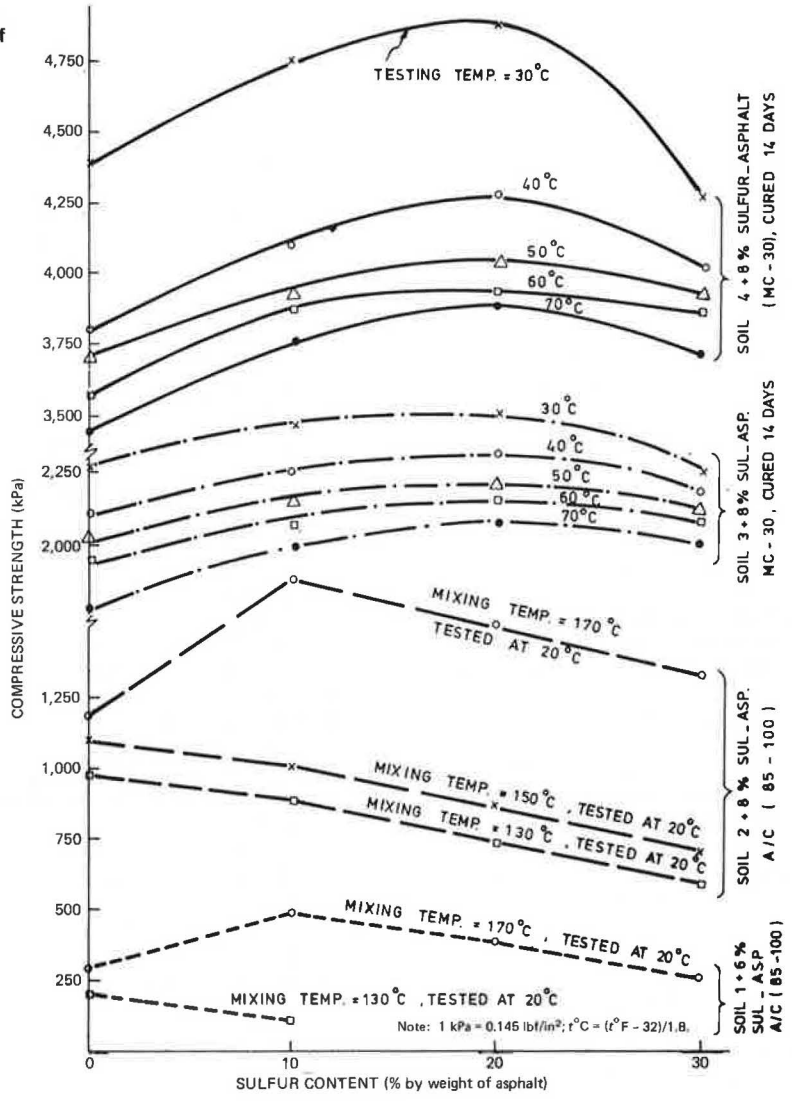

Figure 2. Effect of mixing and test temperatures on strength of sulfur-asphalt mixtures.

Figure 3. Effect of amount of sulfur substitution and mixing temperature on temperature susceptibility of sulfur-asphalt mixtures.

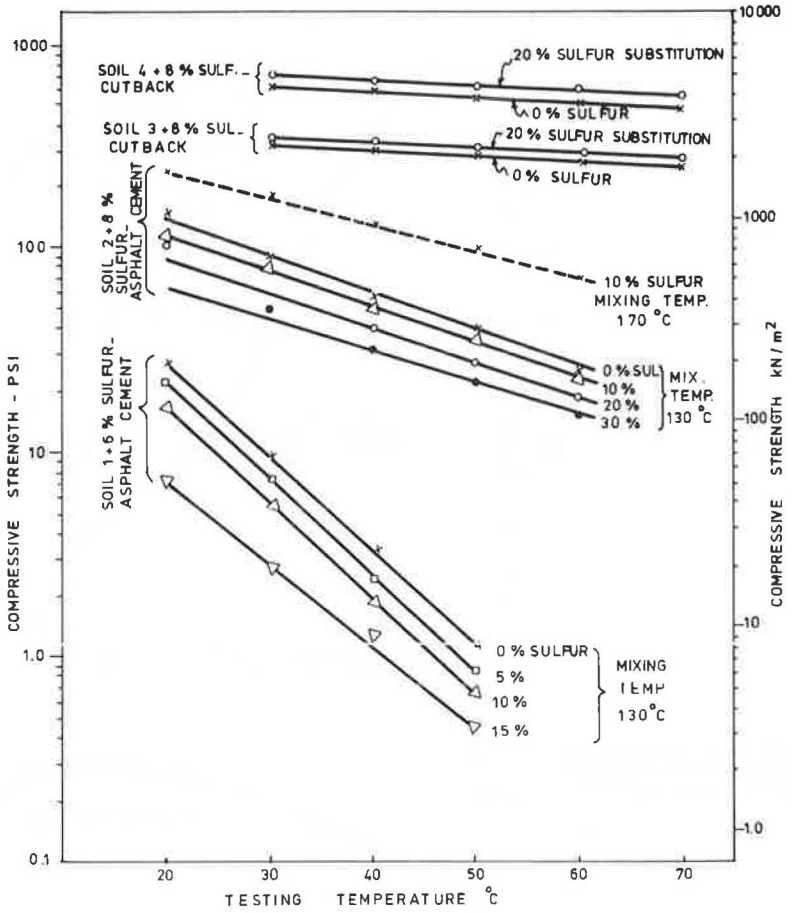

increased, the compressive strength increased to a maximum at 20 percent sulfur by weight of asphalt and then decreased. At all test temperatures, the mixtures in which sulfur had been substituted for part of the asphalt were stronger than the corresponding mixtures without sulfur.

2. The addition of sulfur to cutback asphalt at a mixing temperature of 130°C had no marked effects on the temperature susceptibility of the mixtures.

3. The addition of sulfur made the mixtures easier to compact.

CONCLUSIONS

The following conclusions may be drawn.

1. Sulfur as an additive to cutback asphalt can be used to stabilize clayey sands and silty clays. The addition of sulfur could save up to 20 percent by weight of the asphalt.

2. When sulfur is added to asphalt cement, the mixing temperature influences the strength and temperature susceptibility of the mixtures produced. Better specimens are produced at higher mixing temperatures.

3. The addition of sulfur makes soil-asphalt mixtures easier to compact.

4. At a mixing temperature of 170°C, the evolution of H_2S and SO_3 gases could become a major problem.

REFERENCES

1. R. M. Jimeson, L. W. Richardson, and T. S. Needols. Fossil Fuels and their Environmental Impact. Paper presented at Symposium on Energy and Environmental Quality, Illinois Institute of Technology, Chicago, IL, May 1974.
2. I. Deme. Basic Properties of Sand-Asphalt-Sulfur Mixes. Paper presented at 7th International Road Federation Meeting, Munich, Federal Republic of Germany, Oct. 1973.
3. B. M. Gallaway, D. Saylak, and H. Ahmad. Beneficial Use of Sulfur in Sulfur-Asphalt Pavements. Paper presented at American Chemical Society Meeting, Los Angeles, CA, April 3, 1974.
4. D. Saylak, B. M. Gallaway, and J. S. Noel. Evaluation of a Sulfur-Asphalt Emulsion Binder System for Road Building Purposes. Societe Nationale des Petroles d'Aquitaine, Paris, France, and Sulphur Institute, Washington, DC, Jan. 1976.
5. D. Saylak, B. M. Gallaway, J. A. Epps, and H. Ahmad. Sulfur-Asphalt Mixtures Using Poorly Graded Sands. Journal of the Transportation Engineering Division, Proc., ASCE, Vol. 101, No. TE1, Feb. 1975, pp. 97-113.
6. Societe Nationale des Petroles d'Aquitaine. Properties of Sulphur Bitumen Binders. Paper presented at 7th International Road Federation Meeting, Munich, Federal Republic of Germany, Oct. 1973.
7. N. M. El-Rawi. Prospects of Using Asphalt to Stabilize Iraqi Soils. Al-Muhandis, Baghdad, Iraq, Vol. 15, No. 3, Dec. 1971.
8. H. I. Al-Saleem. Use of Sulfur in Soil Bitumen Mixtures. College of Engineering, Univ. of Baghdad, Iraq, M. Sc. thesis, April 1976.

Publication of this paper sponsored by Committee on Chemical Stabilization of Soil and Rock.